Durham E-Theses

NMR studies of silicate and aluminosilicate solutions as precursors for zeolites

Maybodi, Abdolraouf Samadi

How to cite:

Use policy

NMR Studies of Silicate and Aluminosilicate Solutions as Precursors for Zeolites.

by

Abdolraouf Samadi Maybodi

A thesis submitted in partial fulfilment of the requirements for the degree of Doctor of Philosophy at the University of Durham.

Department of Chemistry

University of Durham

February, 1996

2 3 MAY 1996

ABSTRACT

The search for a detailed understanding of the mechanism of zeolite synthesis has, over the past two decades, promoted many investigations into the species present in (alumino)silicate solutions. It is generally accepted that dissolved (alumino)silicate species are involved as precursors in the nucleation of zeolites. Several techniques have been employed to understand the mechanism of formation of these complex structures. NMR spectroscopy has been shown to be a very powerful tool for the detection and characterization of (alumino)silicate species in the solutions in question.

This thesis presents a comprehensive study of certain silicate solutions employing ^{29}Si NMR which has extended the knowledge gained in previous studies. The role of structure-direction on the distribution of silicate species in silicate solutions is discussed, the results providing more understanding of this effect. The effects of pH, temperature, Si/cation ratio and silica concentration on the distribution of silicate anions were also studied.

Aluminium-27 NMR was applied to investigate the local structure about aluminium atoms in a series of aluminosilicate solutions with Si:Al mole ratios pertinent to zeolite synthesis. The kinetics of the reaction of aluminate with silicate anions have been studied by investigating the temporal evolutions of ^{27}Al NMR spectra and by 2D NMR exchange spectroscopy.

Structural analyses of two new silicate crystals were carried out by single-crystal X-ray diffraction. Liquid- and solid-state NMR spectroscopy were employed to characterize the mother liquors, the powdered polycrystalline products, and their melts.

The Zeolite SUZ-9 was characterized by application of multinuclear magnetic resonance spectroscopy : ^{29}Si, ^{27}Al, ^{13}C and ^{1}H NMR spectra of this zeolite were studied.

MEMORANDUM

The research presented in this thesis has been carried out in the Department of Chemistry, University of Durham, between October 1992 and October 1995. It is the original work of the author unless stated otherwise. None of the work has been submitted for any other degree.

ACKNOWLEDGEMENTS

Contents

^{13}C and ^{1}H NMR spectroscopy

Chapter one

Introduction

1.1. Introduction

Since zeolites were first successfully synthesized in the laboratory, researchers have been trying to understand how these microporous materials are formed from complex mixtures. In considering the mechanisms of zeolite formation, it is essential to understand that the synthesis is a crystallization process governed by many factors that differ from those applied to other chemical reactions[1].

It is generally accepted that the nucleation of a zeolite takes place in the liquid phase of the synthesis gel and that the growth also involves dissolved nutrients[2,3]. In these systems equilibria exist between (alumino)silicates which vary with different physical chemistry. There is general agreement that silicate anions in the gel play a key role in determining the final zeolitic structure[4], and that there is therefore a direct link between zeolite synthesis and the chemistry of basic (alumino)silicate solutions.

Several approaches have been taken in an attempt to understand the mechanism of formation of these complex structures. The results have been informative but not conclusive on exactly how these materials form from precrystalline materials. Barrer et al.[5] first proposed that the nucleation of zeolite formation occurs through the polymerization of aluminate and silicate ions present in the aqueous phase of the synthesis mixture.

In particular, addition of organic molecules such as amines and alkylammonium ions to zeolite synthesis gels can make new structures or framework chemical compositions. However, the exact role of the organic species and the mechanism by which it affects the formation of the product is difficult to describe in detail. Often only the templating or structure-directing role of organic cations is emphasized. This structure-directing role is commonly discussed in terms of the cation having a template function during the crystallization of the (alumino)silicate framework. However, the exact role of the organic species and the mechanisms by which it affects the formation of the product structure remain to be elucidated and other possible roles of the organic moiety may have to be considered. In the following, three possibilities are pointed out:

(i) The organic cation may exert an influence on the gel chemistry by, for example, changing dissolution rates[6,7].

(ii) The organic cation can play a stabilizing role by being incorporated in Si-rich zeolite frameworks[8].

(iii) The organic cation can influence the (alumino)silicate equilibria in the synthesis mixture and stabilize possible zeolite precursor species[5].

These observation have stimulated a desire to understand the chemistry of zeolite formation at a molecular level so that this knowledge can be used to guide the synthesis of new materials. With this objective in mind, investigations have been carried out to identify the species present in synthesis mixtures and the extent to which these species contribute to the formation of zeolites. NMR techniques have provided insight into the species present and molecular events occurring in the precrystalline mixture.

The purpose of these studies was to seek evidence for the existence of precursor species in solution by using ^{29}Si and ^{27}Al NMR spectroscopy, and to determine what effect they may have on gelation and, ultimately, zeolite crystallization. In particular ^{29}Si NMR spectroscopy has proved to be a very powerful technique for studying silicate species in solution[9-18], from the observed chemical shifts. The role of templates was particularly considered in this thesis and illustrated by employing silicon-29 NMR spectroscopy to examine different silicate solutions.

The ultimate aim of the work in this thesis is the elucidation of the mechanism of zeolite synthesis via the use of the techniques of liquid - and solid-state NMR.

1.2. Organization of this thesis

Chapter two describes the basic concepts of NMR and the principles behind the NMR experiment. The aim of this chapter is to provide the background of NMR necessary to follow the experimental results.

Chapter three contains a comprehensive study of silicate solutions by employing ^{29}Si NMR to extend the knowledge gained in previous studies. The role of templates on the distribution of silicate species in silicate solutions is discussed, the results providing more understanding of this effect. Firstly, a mixture of Na/HMBTP silicate with a variable ratio of Na:HMBTP was considered, and secondly, silicate solutions with different organic bases were studied. Also in this chapter, the effects of pH, temperature, Si/cation ratio and silica concentration on the distribution of silicate anions were studied.

Chapter Four discusses results obtained from ^{27}Al NMR. The evolution of spectra with time using a high-field spectrometer is the main concern in this chapter. Exchange processes between the aluminosilicate species were also studied by 2D EXSY Al NMR.

Chapter five will present a detailed description of two new silicate crystals. Structural analyses of these compounds were obtained by single-crystal X-ray diffraction. Liquid- and solid-state NMR spectroscopy were employed to characterize the mother liquor and the powdered polycrystalline compounds. Correlation of X-ray data and NMR results provides useful information.

Chapter six : Finally, the zeolite SUZ-9 was characterized by application of multinuclear magnetic resonance spectroscopy. ^{29}Si, ^{27}Al, ^{13}C and ^{1}H NMR spectra of this zeolite were studied.

1.3. References.

1. Sand, B. L. *Pure Appl. Chem.*, 52, 2150 (1980).

2. Perez-Pariente, J.; Martens, J. A.and Jacobs, P. A. *Zeolites,* 8, 46 (1988).

3. Moudafi, L.; Massiani, P.; Fajula, F. and Figueras, F. *Zeolites,* 7, 63 (1987).

4. Barrer, R. M. *The Hydrothermal Chemistry of Zeolites;* Academic Press: London, 1982.

5. Barrer, R. M. *Chem. Brit.* 380 (1966).

6. Lok, B. M.; Canna, T. R. and Massina, C. A. *Zeolites*, 3, 282 (1983).

7. Dewaele, N.; Gabelica, Z.; Bodart, P.; Nagy, J. B.; Giordano, G. and Derouane, E. G. *Stud. Surf. Sci. Catal.,* 37, 65 (1988).

8. Van Santen, R. A.; Keijsper, J. J.; Ooms, G. and Kortbeek, A. G. T. G. *Stud. Surf. Sci, Catal.,* 28, 169 (1986).

9. Harris, R. K. ; Knight, C.T.G. and Hull, W.E. *J. Am. Chem. Soc.* 103, 1577 (1981).

10. Harris, R. K. and Newman, R.H. *J. Chem. Soc., Faraday Trans.* 73, 1204 (1977).

11. Harris, R. K.; Jones, J.; Knight, C.T.G. and Newman, R.H. *J. Mol. Liq.* 29, 63 (1984).

12. Knight, C.T.G. ; Kirkpatrick, R.J. and Oldfield, E. *J. Am. Chem. Soc.* 109, 1632 (1987).

13. McCormick, A.V.; Bell, A.T. and Radke C.J. *Zeolites,* 7, 183 (1987).

14. McCormick, A.V. ; Bell, A.T. and Radke, C. *J. Phys. Chem.* 93, 1737 (1989).

15. Kinrade, S.D. and Swaddle, T.W. *Inorg. Chem.* 27, 4259 (1988).

16. Engelhardt, G.and Hoebbel, D. *J. Chem. Soc., Chem. Commun.* 514 (1984).

17. Mortlock, R.F. ; Bell, A.T. and Radke, C.J. *J. Phys. Chem.* 95, 7847 (1991).

18. Kinrade, S.D. and Swaddle, T.W. *Inorg. Chem.* 28, 1952 (1989).

Chapter two

NMR Fundamentals and Practice

2.1. Basic concepts of NMR

2.1.1. Principles. A strong magnetic field causes the energies of certain nuclei to be split into two or more quantized levels, due to the magnetic properties of these particles. The study of the absorption of radio-frequency radiation by nuclei when placed in a magnetic field is called *nuclear magnetic resonance*. This technique is one of the most powerful tools for determining the molecular-level structure of both organic and inorganic species.

It is assumed that nuclei rotate about an axis, thus having the property of *spin*. Since a nucleus has a charge, its spin gives rise to a magnetic field. The resultant magnetic dipole μ is oriented along the axis of spin and has a value that is characteristic for each type of nucleus.

The angular momentum of the spinning charge can be described in terms of a spin quantum number, I, for each nucleus, which is related to its mass number (table 1).

Table 1. Spin quantum numbers for various nuclei.

Number of protons	Number of neutrons	Spin quantum number	Example
Even	Even	0	^{12}C, ^{28}Si
Odd	Even	1/2	^{1}H, ^{19}F
		3/2	^{11}B
Even	Odd	1/2	^{13}C, ^{29}Si
		5/2	^{127}I
Odd	Odd	1	^{2}H, ^{14}N

The angular momentum, P, that is associated with the spin of the particles, is quantized and specified in terms of the quantum number (Eq.1)

$$P = (h/2\pi)[I(I + 1)]^{1/2} \qquad (1)$$

where h is Planck's constant.

The spin may take $2I + 1$ different orientations, that are distinguished by a quantum number, m_I

$$m_I = +I, I\text{-}1, \ldots \text{-}I \qquad (2)$$

The ratio of the magnetic moment, μ, to the angular momentum is defined as the magnetogyric ratio, γ, that is:

$$\mu = \gamma.P \qquad (3)$$

A positive value of the magnetogyric ratio implies that the magnetic moment is parallel to the angular momentum, while a negative value indicates that μ and P are anti-parallel;

for example ^{1}H and ^{29}Si have positive and negative value respectively. Using equations 1 and 3 gives:

$$\mu = \gamma(h/2\pi)[I(I + 1)]^{1/2} \qquad (4)$$

In a magnetic field B the $2I + 1$ orientations of the nucleus have different energies, and the energy is defined by equation 5.

$$E = -\mu_z.B \qquad (5)$$

where μ_z is the component of μ in the z direction. It can be shown that there are $(2I + 1)$ non-degenerate energy levels, (Eq. 6 & 7).

$$\mu_z = \gamma(h/2\pi)m_I \qquad (6)$$

$$E = -\gamma(h/2\pi)m_I B \qquad (7)$$

The energy gap between the levels are $\Delta E = \gamma(h/2\pi)\Delta m_I B$, and these energies are often expressed in terms of frequency as follows :

$$h\nu = |\gamma(h/2\pi)B\Delta m_I| \qquad (8)$$

$$\nu = |(\gamma/2\pi)B\Delta m_I| \qquad (9)$$

Since the selection rule governing transitions is $\Delta m_I = \pm 1$,

$$\nu = |(\gamma/2\pi)|B \qquad (10)$$

Therefore, the resonance frequency, ν, depends upon magnetogyric ratio, and the strength of the magnetic field.

2.1.2. Chemical shift theory

Chemical shifts arise from the secondary magnetic fields produced by the circulation of electrons in the molecule. The magnitude of the field developed is proportional to the applied external field, hence:

$$B = B_0 - \delta B \qquad (11)$$

where B_0 is the applied field and B is the effective field which determines the resonance behaviour of the nucleus.

The chemical shift is described relative to a reference standard (e.g. TMS) and its value, δ, is defined as

$$\delta = \frac{\nu_{samp} - \nu_{ref}}{\nu_{ref}} \times 10^6 \qquad (12)$$

where subscripts *ref* and *samp* relate to the reference and sample respectively.

Nuclear screening is generally expressed as the sum of local, $\sigma(local)$, intramolecular, $\sigma(intra)$, and intermolecular, $\sigma(inter)$, contributions[1].

$$\sigma = \sigma(local) + \sigma(intra) + \sigma(inter) \qquad (13)$$

Using Ramsey's terminology[2] the local contribution is separated into diamagnetic, σ_d(local), and paramagnetic, σ_p(local), terms (Eq. 14).

$$\sigma(local) = \sigma_d(local) + \sigma_p(local) \qquad (14)$$

The diamagnetic effect induces electrons to rotate about the nucleus in opposition to B_0 such that a lower frequency is necessary to cause resonance. The magnitude of σ_d(local) depends on the electron density and spherical distribution of the core electrons and can be calculated from Lamb's formula[2].

$$\sigma_d(local) = e^2\mu_0 / 3m_e \int_0^\infty r\rho(r)dr \qquad (15)$$

where ρ is the electron density, r is the distance from the nucleus and m_e is the mass of the electron. To account for the loss in nuclear shielding caused by the addition of electron density to heavy nuclei, Ramsey[2] derived a complex expression describing how valence electrons hinder the free rotation of core electrons and reduce the overall symmetry of the electron shell. He called the term (temperature-independent) paramagnetism because it serves to reinforce the external field. The local paramagnetic term is more complex than the local diamagnetic term, and it requires a detailed knowledge of excited state wave functions, which is often not available. It may be approximated by [3]:

$$\sigma_p = -(e^2h^2/6\pi^2\Delta m^2c^2) (\langle 1/r^3\rangle_p P_u + \langle 1/r^3\rangle_d D_u)$$

where P_u and D_u respect the "unbalance" of the valance electrons in the p and d orbitals centred on the atom in question. The parameters Δ, ($\langle 1/r^3\rangle_p$, $\langle 1/r^3\rangle P_u$ and $\langle 1/r^3\rangle D_u$ determine the magnitude of σ_p and of the changes in it. Of these, the average excitation energy Δ exhibits about as much variation for different chemical states of an element as for compounds of different elements. Also, Δ covers a relatively small, two- or threefold range. Therefore, the major periodicities of the chemical shift range are not due to Δ.

The numerical values of P_u and D_u depend largely upon the coordination number of the atom, the hybridization of its bonding orbitals and the ionicity of its bonds. In the spherical system closed-shell case, P_u and D_u both have their minimum value of zero, which corresponds to a free, diamagnetic ion or an inert gas. On the other hand, the maximum values of P_u and D_u correspond to the maximum "unbalance" of electron distribution[3].

The intra- and intermolecular terms in equation 13 refer to shielding processes arising from electron circulation which is not localized at the nucleus of interest. Intramolecular screening (Eq. 16) typically includes magnetic anisotropy σ_a(intra) and ring current σ_r(intra) contributions; (of course, the latter term is not relevant to silicate and aluminosilicate solutions which are the concern of this study).

$$\sigma(\text{intra}) = \sigma_a(\text{intra}) + \sigma_r(\text{intra}) + \sigma_e(\text{intra}) \qquad (16)$$

The term σ_e(intra) accounts for electron field distortions arising from intramolecular polar group interactions.

The third term in the right hand side of equation 13 arises from intermolecular solution interactions. Solute···solvent and solute···solute intermolecular dispersion (or London) forces give rise to rather complex van der Waals screening influences, σ_{vdw}(inter)[4]. Moreover, for the case of polar molecules, the dielectric strength of the solvent will further modify the electron distribution of the solute molecule, σ_e(inter).

However, for silicate solutions (which are the concern in this study), the interaction of silicate···M+, σ_M(inter). and silicate···H_2O hydrogen bonding, σ_H(inter) are more effective than other processes.

2.1.3. Quadrupole moments

An uneven distribution of positive charge at the nucleus gives rise to a electric quadrupole moment, Q. The electric quadrupole moment is only important when the nucleus is not in a spherically symmetrical environment, which will result in a finite electric field gradient at the nucleus. The charge distribution in such a case is usually ellipsoidal with two possible types. The distribution is either slightly flattened (oblate- or discus-shape) or slightly elongated (prolate-shape). Therefore quadrupole moments possess a sign (Figure 1). A prolate quadrupole is associated with a positive sign, whereas an oblate quadrupole is given a negative sign.

(a)   (b)
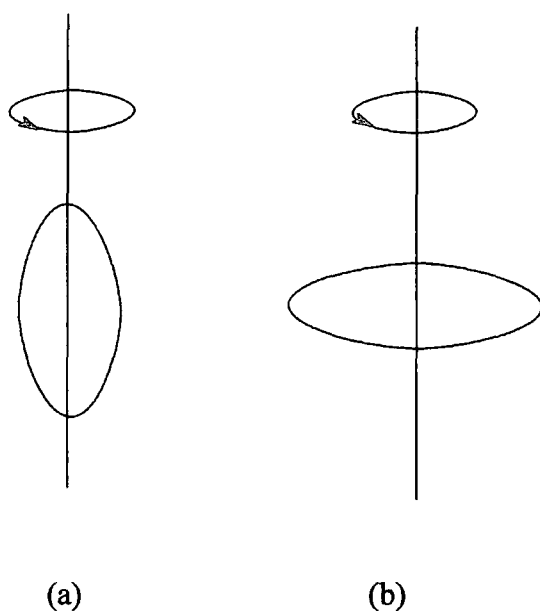
Figure 1. Charge distribution in quadrupolar systems, (a) prolate, (b) oblate.

2.1.4. Quadrupolar Nuclei. Any nucleus with a spin I greater than 1/2 has an electric quadrupole moment. Such a quadrupolar nucleus differs from spin-1/2 nuclei in that its quadrupole moment interacts with any gradient in the surrounding electric field, resulting in a quadrupolar splitting of the energy levels in addition to the Zeeman splitting created by B_0.

The practical influence of the quadrupole effect is a change in the observed NMR transition frequency. The perturbation is dependent upon the angle, θ, between the electric field gradient axis and B_0, and on which of the 2I possible transitions is being considered. The quadrupole effect is considerably averaged out by molecular tumbling motion. However, in powdered solids all possible values of the angle θ are present, resulting in a broad line. In principle, the MAS technique could result in a narrow peak, but sufficiently high spin rates can hardly be obtained. Some more effective, but also more sophisticated, techniques are available, such as spinning about two axes simultaneously.

In the present work, aluminosilicates and zeolites involve the quadrupolar nucleus ^{27}Al (I=5/2). However, in the solid state transitions other than the central $m_I = 1/2 \leftrightarrow -1/2$ are unobservable, because they partly occur at frequencies outside the excitation bandwidth of the radio frequency pulses used. The remaining central transition is unaffected by the quadrupolar interaction to first order, because the difference in energy between the $m_I = 1/2$ and $m_I = -1/2$ states does not change. Second-

order effects produce a broadening and a shift in the position of the band; neither of these effects is as great as the chemical shift difference between Al in tetrahedral and octahedral environments in zeolites. Further discussion is given elsewhere[5].

All the above discussion is at a very elementary level, where only the basics behind the NMR technique have been outlined. A more considerable and detailed study of NMR theory can be found in many text books[6-13].

2.2. The spectrometer system

The majority of the NMR spectroscopy for liquid-state NMR was performed with a Bruker AC-250 instrument in the Department of Chemistry, University of Durham. However, to achieve better resolution and signal-to-noise the former especially for ^{27}Al NMR, the Varian VXR-600 at the Department of Chemistry, University of Edinburgh (Ultra High Field NMR Service); and Bruker AMX-500 at the University of Durham were also used.

The majority of the solid-state NMR spectroscopy was performed with the Varian Unity Plus 300 spectrometr at the University of Durham Industrial Laboratories. Some solid-state NMR analyses were carried out using a Chemagnetics CMX-200 spectrometer in the Department of Chemistry, University of Durham.

Table 2 gives information of magnetic field strengths and corresponding resonance frequencies of nuclei used in this study.

Table 2. Data of magnetic field strength and resonance frequency.

Isotope	% Natural abundance	Spin	B_0=5.87 Tesla	B_0=7.05 Tesla	B_0=11.75 Tesla	B_0=14.10 Tesla
^{1}H	99.985	1/2	250.00	300.00	500.00	600.00
^{13}C	1.108	1/2	62.87	75.44	125.73	150.88
^{14}N	99.63	1	18.06	21.67	36.12	43.34
^{23}Na	100.0	3/2	66.13	79.35	132.26	158.71
^{27}Al	100.0	5/2	65.86	78.17	130.28	156.34
^{29}Si	4.70	1/2	49.70	59.60	99.32	119.19

2.3. The optimization procedure

Prior to acquisition of spectra, several procedures need to be followed to optimize and standardize the performance of the spectrometers. The experimentalist

must optimize tuning, shimming coils, set the 90° pulse and reference the chemical shift for the observed nucleus.

Shimming. The homogeneity of the field is adjusted with *shims*. Shims are small magnetic fields used to cancel out errors in the static field. A coil whose field is aligned along the vertical axis of the magnet is called a *Z* gradient, while those aligned along the two orthogonal axes are various orders of *X* and *Y* gradients. Superconducting magnets are invariably fitted with room temperature *Z* gradients up to the order Z, Z^2, Z^3 and Z^4. The adjustment of these gradients strongly affects the lineshape and linewidth obtained. On the other hand, the horizontal field is usually corrected to third order, with *X* and *Y* (first order), *XZ*, *YZ*, *XY* and X^2-Y^2 (second order) and XZ^2 and YZ^2 (third order) gradients being common[8].

The field homogeneity is independent of the nucleus under study. Therefore any nucleus can be used to shim the probe. Shimming can be achieved by means of the following:

(i) Shimming using the lock. If the sample under study contains deuterium (e.g. D_2O or $CDCl_3$), when the deuterium lock signal is found, shimming is obtained by maximizing the lock signal.

(ii) Shimming can also be achieved by optimizing the area or the length of a FID after a single transient.

To get better resolution and avoid spurious line broadening, shimming was done very carefully for each individual silicate solution study . The shimming procedure was carried out until the linewidth at half-height ($\Delta v/_{1/2}$) for the single peak of Q^0 (see notation in chapter 3) was approximately 1-2 Hz (it sometimes takes more than two hours to find the desired conditions). Such a procedure has been done for all experiments.

Tuning. The central component of the probe is simply a piece of wire, formed into a shaped coil, in which the sample sits after descending into the magnet. This is the device which receives the NMR signals; in most probes designed for use with superconducting magnets it also transmits the pulses. In order for the output of the transmitter to be properly amplified by the receiver, it is necessary for the impedance of this wire to be matched with those of the transmitter and receiver. The spectrometers were, in each case, tuned to the appropriate nucleus frequency by reducing the reflection from the tuning box to minimum. For the silicon-29 nucleus, the tuning procedure was a

relatively difficult and slow task. This problem was also faced for optimizing the conditions for performance of ^{27}Al NMR of aluminosilicate solutions, probably due to the unobservable colloidal particles (see chapter 4).

2.4. Chemical compounds used as references for the nuclei studied

Silicon-29. The chemical shifts reported in this thesis are referenced with respect to TMS. In the case of the liquid state, TMS was used as an external reference. In order to find the exact chemical shifts of signals, the spectrum was recorded by using a co-axial NMR tube, i.e. a 5 mm NMR tube containing TMS was inserted in the 10 mm NMR tube that includes the appropriate silicate solution. In the case of solid-state NMR spectra, chemical shifts are referenced with respect to TMS using tetrakis(trimethylsilyl)methane as a secondary reference material by replacement.

Aluminum-27. The ^{27}Al NMR chemical shifts are referenced with respect to Al(H$_2$O)$_6$$^{3+}$. The sharp resonance of the hexa-aqua cation is visible in all aqueous solutions of aluminum salts, and is therefore easily accessible. A 1M aqueous aluminium chloride solution was used in both cases of liquid- and solid-state NMR experiments.

Sodium-23. The ^{23}Na chemical shifts are referenced relative to the Na$^+$ ion. A 1M aqueous sodium chloride solution was used.

Nitrogen-14. The ^{14}N chemical shifts are referenced to the NH$_4$$^+$ ion of 1M aqueous ammonium chloride solution. A sharp signal can be observed from this solution.

Carbon-13. The ^{13}C NMR chemical shifts reported in this thesis are referenced with respect to TMS. In the case of liquid-state ^{13}C NMR, TMS was used as an external reference; the solid-state ^{13}C MAS NMR spectra are referenced to TMS using solid adamantane as a secondary reference.

Protons. ^{1}H chemical shifts are referenced to the signal of TMS for both liquid- and solid-state NMR experiments.

2.5. Applications of liquid-state NMR to silicate solutions

NMR is now well-established as an important and informative technique for the study of silicate and aluminosilicate solutions as well as zeolites, and it provides key information enabling their chemical structure characterization. Its principal advantages over other techniques are that it is non-destructive (ensuring that the sample is in the desired form during and after the measurement) and that it is sensitive to small, local variations. Under appropriate conditions, it is also possible to use NMR for quantitative

analysis. However, as pointed out, the experimentalist must set several parameters such as the 90° pulse, and recycle delay appropriately. The following sections deal with some parameters which were of concern in this study, especially for the performance of silicon-29 NMR spectra. Preliminary experiments were necessary to find spectral conditions and thus obtain reasonable results.

2.5.1. Calibration of B_1

An accurate determination of the pulse duration for the $\pi/2$ and π pulses is often essential to the performance of an NMR experiment. In the single-pulse experiment, the tip angle is not usually critical, but it is important to know roughly the $\pi/2$ pulse duration. However, accurate pulse duration is important for obtaining quantitative results and is also vital in many pulse sequences.

The strength of B_1 is usually reported in terms of the duration of the 90° pulse, which secures the maximum signal height obtainable from a single pulse. In fact, measurement of peak height versus τ_p should yield a sine curve. The first null point (after $\tau_p = 0$) corresponds to a 180° pulse.

However, we cannot simply look at successive FIDs on the oscilloscope while increasing the pulse duration, and then take the maximum intensity as corresponding to the $\pi/2$ pulse. First, it is possible to overshoot the actual value and determine the $3\pi/2$ pulse duration or some other odd multiple of $\pi/2$. Second, if relaxation is slow, and the delay between pulses is not long enough, the magnetization will not recover fully to equilibrium between pulses. Third, the sine function varies rather slowly near $\pi/2$ and the maximum is not well defined. A systematic approach can remove all of these potential problems.

One should start with a very short pulse, collect an FID, transform, and phase the spectrum. One then acquires a set of FIDs with adequate relaxation delays, gradually increasing the pulse duration, and plots the intensity of the resulting spectrum as a function of pulse duration. At least one complete sine wave should be plotted. The null for a π pulse is much better defined than the maximum at the $\pi/2$ pulse. Equation 17 explains how the tip angle of the magnetization depends upon the length of time (τ_p) for which the radio frequency (B_1) is applied

$$\theta = \gamma B_1 \tau_p \qquad (17)$$

where θ is the tip angle; γ the gyromagnetic ratio; B_1 the applied radio frequency field and τ_p the pulse duration.

In order to find the accurate $\pi/2$ pulse duration for silicate solutions the above experiment was carried out for a HMBTP silicate solution. Figure 2 shows the result for a set of calibration spectra for the determination of the ^{29}Si pulse duration (a single peak of Q^0 was recorded).
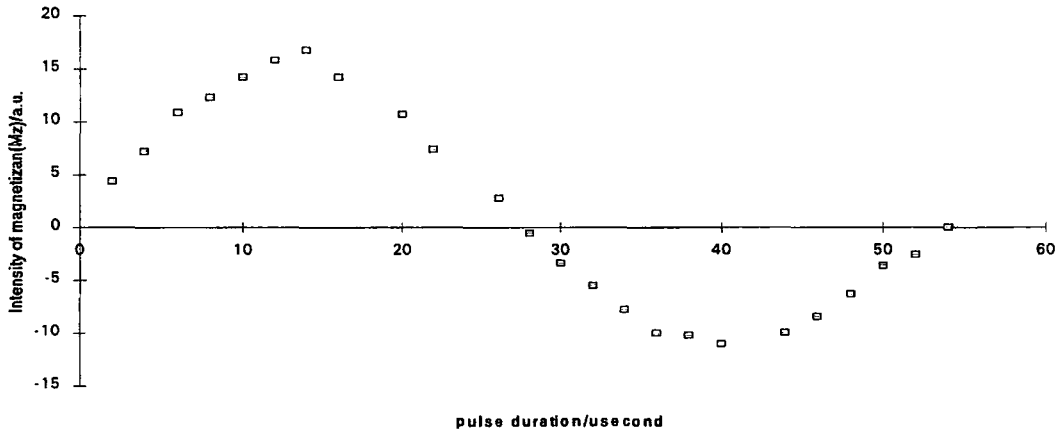
Figure.2. Typical example of B_1 calibration for ^{29}Si NMR spectra of silicate solutions (HMBTP silicate solution with (SiO$_2$/ HMBTP = 1 and wt% SiO$_2$ = 5.87 was used, see chapter 3).

Data obtained from this experiment indicate that to tip the magnetization from the z or field axis into the xy plane, i.e. $\theta = 90°$, requires 14 microseconds for the pulse duration,τ_p,. This experiment was carried out using the Bruker AC-250 spectrometer. Such a result was recorded for all silicon-29 spectra obtained with this spectrometer. An analogous procedure was considered for all cases in different spectrometers for obtaining NMR spectra of all nuclei studied.

2.5.2. Silicon-29 spin-lattice relaxation times for silicate solutions

Spin-lattice or longitudinal relaxation occurs as the nuclear magnetic moments lose energy to their surroundings and thus relax toward the z' axis with a time function $\Phi_1(t)$. In many cases $\Phi_1(t)$ is given by a single exponential $\exp(-t/T_1)$, which defines the longitudinal relaxation time T_1.

The most common method of measuring spin-lattice relaxation times is known as an inversion-recovery sequence. The pulse sequence is simple (equation 18).

$$\pi - \tau_D - \pi/2 - \textit{Acquire} \qquad\qquad (18)$$

where π is a 180° pulse, $\pi/2$ is a 90° pulse and τ_D is a delay which is under the control of the operator.

Before applying the π pulse, the sample is in thermal equilibrium and therefore has a magnetization M_0. After the π pulse the magnetization will be $-M_0$, if the pulse is assumed to be very short in comparison with both T_1 (spin-lattice relaxation) and T_2 (spin-spin relaxation). Owing to the longitudinal relaxation, the magnetization will shrink along the negative branch of the z' axis, pass through zero and then regain its equilibrium value. The instantaneous value of the longitudinal magnetization after a given time interval τ_D can be determined by applying the $\pi/2$ pulse and measuring the initial signal amplitude of the generated FID. By plotting this initial signal amplitude against the pulse separation, τ_D, the entire relaxation process can be mapped out.

By taking the Fourier transform of the FID signal and by plotting the amplitudes of the different NMR lines (e.g. different peaks for a silicate solution) versus τ_D, longitudinal relaxation times of the individual lines can be measured selectively.

To find the spin-lattice ralaxation time of silicate solutions, as a preliminary study, HMBTP silicate solution (composition of the silicate solution was the same as for Figure 2) was used to perform this experiment (HMBTP=2,3,4,5,6,7,8,9-octahydro-2,2,5,5,8,8-hexamethyl-2H-benzo(1,2-c:3,4-c':5,6-c")tripyrrolium). Results obtained from the measurement of spin-lattice relaxation times of this solution illustrate that the different species of the silicate solution involve different spin-lattice relaxation times. To ensure full recovery of magnetization, recycle delays of 50 seconds (the time between two pulses) were selected, with 16 different τ_D values (with maximum τ_D value 50 s), and 14 μs pulse duration (on the basis of the B_1 calibration, data obtained from the previous experiment). To achieve a sufficient signal-to noise ratio, the experiment took more than 50 hours.

Data obtained from this experiment are given in table 3. Figure 3 shows schematically the spin-lattice relaxation times for the above species .

Table. 3. Data for spin-lattice relaxation times of species in HMBTP silicate solution.

Species	T_1 (in seconds)
monomer ,Q^0,	6.1
dimer, Q^1_2,	3.7
liner trimer,$Q^1Q^2Q^1$,	3.9*
cyclic trimer,Q^2_Δ,	6.4
prismatic hexamer,Q^3_6,	10.4
cubic ocatamer,Q^3_8,	6.3

* value belongs to the Q^1 sites of the species.
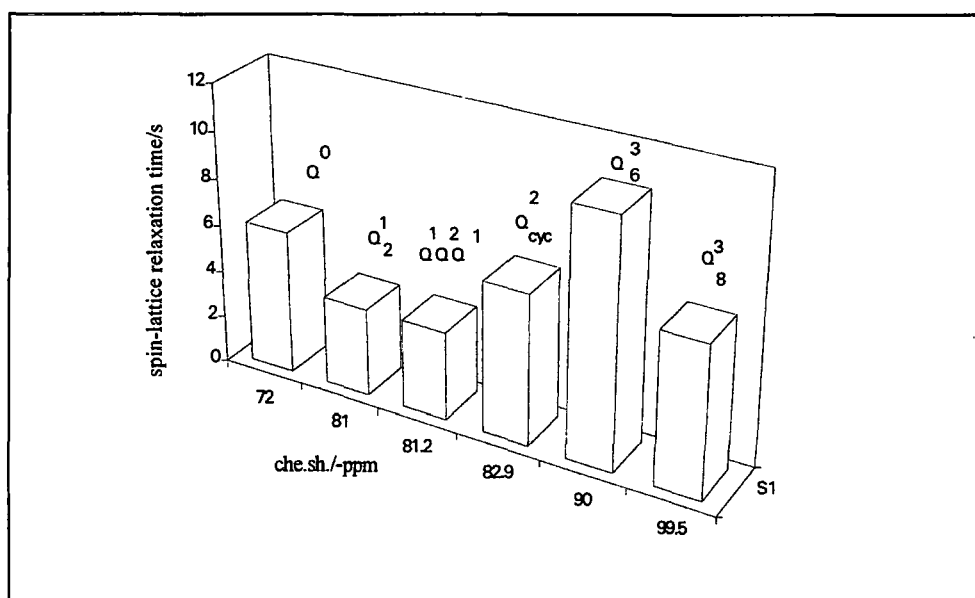
Figure 3. schematic representation of $T^1(^{29}Si)$ for the species of HMBTP silicate solution.

It should be noted that the relaxation measurements were performed under normal sample conditions and no degassing was done to remove air. The experiment was carried out with no decoupling. The results obtained indicate that for the normal situation the maximum $T_1(^{29}Si)$ of species in such silicate solution is about 10 s, and this is instructive for recording ^{29}Si NMR spectra of HMBTP silicate solutions quantitatively (i.e. recycle delay $\geq 5 \times T_1$).

A recycle delay of 50 s has been employed for most of the present work in silicate solutions Some workers have employed Ernst's procedure[14] of applying pulses of an angle less than 90° with a recycle delay shorter than $5T_1$ in order to maximize the signal intensity acquired in a given time; this practice has however not been used here

on account of the variability of the ^{29}Si T_1 values in the materials under study, and moreover to obtain quantitative results. However, for the case of solid-state experiments a short recycle delay was used with cross polarization. For other nuclei, different values of recycle delays were applied; for instance, the ^{27}Al NMR spectra were recorded with very short recycle delays (less than 1 s).

2.5.3. The Nuclear Overhauser effect (NOE)

The NOE is a change in intensity of an NMR resonance when the transition of another one is perturbed. If the normal intensity of a resonance (i.e. that observed at thermal equilibrium and without perturbing the system) is I_0; and if the intensity observed while some other related resonance is saturated (with waiting for the new equilibrium to be established) is I, the NOE (enhancement) is defined as follows:

$$\eta_A(X) = (I-I_0)/I_0 \qquad (19)$$

This expression is also often multiplied by 100 to make the figure a percentage. $\eta_A(X)$ indicates that this is the NOE for nucleus A when X is saturated[6].

Consider the relaxation properties of a heteronuclear two-spin (AX) system (Figure 4). The possible transition rates are defined in this figure. However, it is assumed that the $\alpha\beta \leftrightarrow \beta\beta$ and $\alpha\alpha \leftrightarrow \beta\alpha$ pathways are equivalent and have the same rate W_{1A} (and similarly for W_{1X}). The subscript numerals to W_0, W_1 and W_2 indicate the change in total quantum number m (m_T) involved
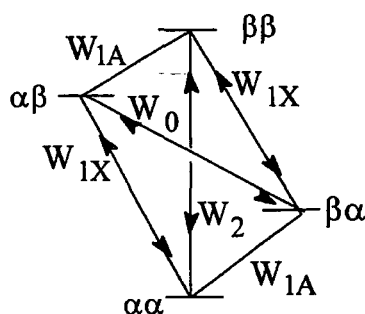
Figure 4. definition of transition rates for an AX spin system.

In terms of the relaxation pathways, the ratio of total intensity for gated decoupling (i.e. decoupling *on*), N_A to the intensity for no decoupling, N°_A is described by Eq. 20.

$$\frac{N_A}{N^{\circ}_A} = 1 + \frac{N^{\circ}_X}{N^{\circ}_A}\left(\frac{W_2-W_0}{W_2+2W_{1A}+W_0}\right) \qquad (20)$$

where N_A is the population difference for the case of decoupling on, whereas N_A° and N_X° are the population differences for nuclei A and X without decoupling respectively. The values of the population differences at equilibrium are proportional to the magnetogyric ratio, γ. Hence the ratio of signals for the decoupled case, S_A, to the coupled case, S_A°, is given by equation 21.

$$\frac{S_A}{S_A^{\circ}} = 1 + \frac{\gamma_X}{\gamma_A}\left(\frac{W_2 - W_0}{W_2 + 2W_{1A} + W_0}\right) \qquad (21)$$

This intensity change is known as the nuclear Overhauser effect (NOE), and the second term of equation 21 is sometimes called the nuclear Overhauser enhancement, η, that is,

$$\eta_A(X) = \frac{\gamma_X}{\gamma_A}\left(\frac{W_2 - W_0}{W_2 + 2W_{1A} + W_0}\right) \qquad (22)$$

Moreover, in the extreme narrowing limit, (i.e. $\omega_2 \tau_c^2 \ll 1$, where τ_c is the correlation time), and when (A, X) dipolar interactions provide the dominant relaxation mechanism, the relaxation rate ratios are as in equation 23.

$$W_0 : W_1 : W_2 = 1/6 : 1/4 : 1 \qquad (23)$$

If Eq. 23 is substituted into Eq. 21, it will give

$$S/S_A^{\circ} = 1 + 1/2(\gamma_X/\gamma_A) \qquad (24)$$

This is the maximum observable NOE, so the η_{max} is described as:

$$\eta_{max} = \gamma_X/2\gamma_A \qquad (25)$$

Therefore, as equation 25 indicates for nuclei whose magnetogyric ratio are positive, $\gamma_A > 0$, the observed A signal will be increased (i.e. the maximum NOE is given by $0.5(\gamma_X/\gamma_A)$); however, for nuclei having negative magnetogyric ratio, $\gamma_A < 0$, irradiation of protons may decrease or even invert their signals.

For example, γ_H/γ_{Si} is about -5, so the maximum NOE is about -2.5. However, if the full NOE is not realized, enhancement close to -100% may arise, leading to loss of signal ("null-signal" situation), and no signal is observed. Therefore, the usual manner of acquiring ^{29}Si NMR spectra of silicate solutions is by means of a single-pulse experiment without high ^1H decoupling. Figure 5 illustrates a typical example for a ^{29}Si
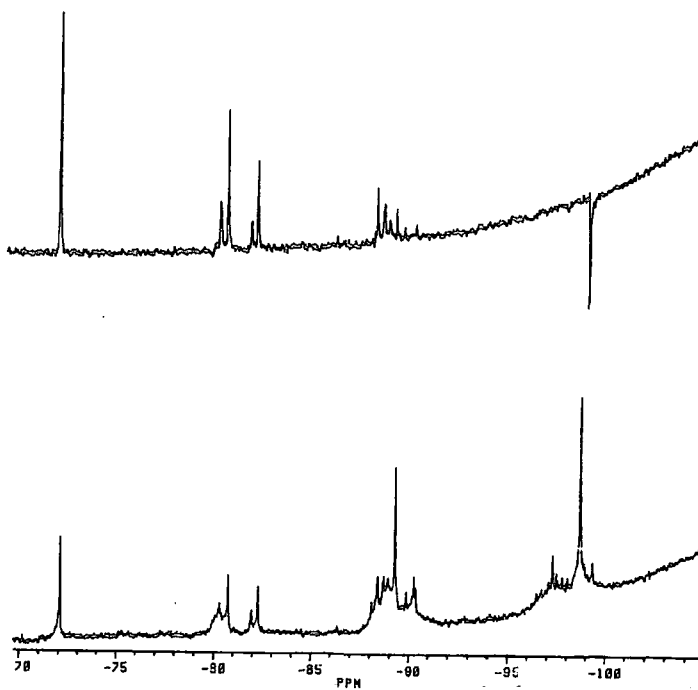
Figure 5. Typical example of the influence NOE on the silicon-29 NMR spectra.
The upper trace realise the ^{29}Si NMR spectrum of TMA silicate solution with
decoupling *on* and the lower trace shows ^{29}Si NMR spectrum of TMA silicate solution
with decoupling *off*. Both spectra carried out with AC-250.

NMR spectrum of TMA silicate solution (TMA = tetramethyl ammonium) with decoupling (upper trace) and without decoupling (lower trace). The significant negative signal at a chemical shift of ca -99 ppm (assigned to the cubic octamer, see chapter 3) clearly demonstrates this phenomenon (i.e. illustrates that for this molecule (^{29}Si, ^{1}H) dipole-dipole relaxation is the dominant mechanism).

The nuclear Overhauser effect is the subject of a book by Noggle and Schirmer[15] to which the reader is referred for a full discussion.

2.6. Preparation of samples

The preparation of the samples is explained in detail for each case in the appropriate chapter. The following sections describe the synthesis of some chemical compounds.

2.6.1. Preparation of SiO_2

Amorphous silica was prepared from the hydrolysis of silicon tetrachloride using doubly-distilled water (i.e. by dropwise addition of silicon tetrachloride in to doubly-distilled water), to give SiO_2. The solid was then filtered and washed repeatedly with doubly-distilled water to achieve an acid-free silica. Finally, the silica was dried overnight at ca. 150°C. The silica was solubilized in appropriate basic solutions. The chemical reaction is quite simple :

$$SiCl_4 + 2H_2O \rightarrow SiO_2 + 4HCl$$
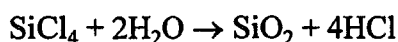
2.6.2. Making silicate solutions

The silicate solutions were prepared by dissolving the appropriate quantity of silica in doubly-distilled water and deuterium oxide (ca. 15% w/w, to provide a field/frequency lock), made alkaline by the addition of the particular base required. The dissolution of the silica was very slow, so it was assisted by heating the solution, contained in a plastic bottle, at ca. 70°C. For high concentrations of silica, solutions were not clear and it was necessary to filter or to take clear supernatant solution. Therefore, the exact concentration of silica is not clear in such circumstances.

The chemical compounds, together with their sources, which were used in this study are presented in the Table 4.

Table 4. Chemical compounds used in this study together with their sources.

Compounds	Suppliers
Deuterium oxide	Aldrich
Tetraethylammonium hydroxide	Fluka
Silicon tetrachloride	Fluka
Tetramethylammonium hydroxide, pentahydrate	Janssen chimica
Tetrapropylammonium hydroxide	Aldrich
Potassium hydroxide	Aldrich
Sodium aluminate	Fison
Aluminium chloride hexahydrate	Aldrich

The samples of HEBTP (HEBTP = 2,3,4,5,6,7,8,9-octahydro-2,2,5,5,8,8-hexaethyl-2H-benzo(1,2-c:3,4-c':5,6-c")tripyrrolium) and HPBTP (HPBTP = 2,3,4,5,6,7,8,9-octahydro-2,2,5,5,8,8-hexapropyl-2H-benzo(1,2-c:3,4-c':5,6-c")tripyrrolium) were prepared by BP (British Petroleum Co. p.l.c. Sunbury, London).

However, for the study of HMBTP (alumino)silicate solutions and the synthesis of silicate crystals as well as SUZ-9 zeolite it was necessary to synthesise HMBTP (HMBTP=2,3,4,5,6,7,8,9-octahydro-2,2,5,5,8,8-hexamethyl-2H-benzo(1,2-c:3,4-c':5,6-c")tripyrrolium). The procedure is given below.

2.6.3. Synthesis of HMBTP

The preparation of the HMBTP involves three steps, which are as follows:

(i). Preparation of hexakis (bromomethylbenzene)

Hexamethyl benzene(35 g) was dissolved in dibromoethane (775 ml). The solution was brought to reflux. Bromine (92 ml) was added dropwise to the solution over a 6 hour period. Hydrogen bromide gas was evolved, which was neutralized by sodium hydroxide solution. The reaction mixture was then heated and stirred for 2 days. The reaction was then cooled to ambient temperature (ca. 22°C) and 0.2 g of a,a'-azoisobutyronitrile (AIBN) was added. The solution was again heated for 3 hours and then allowed to cool down; 0.2 g AIBN was added. the solution was heated and stirred for a further 4 hours, and then the heating was stopped and the mixture was allowed to cool down overnight. The solid was filtered, washed repeatedly with ether, and dried at 60°C.

(ii). Preparation of HMBTP (Br form)

122 g of hexakis(bromomethylbenzene) was suspended in ethanol (275 ml). An ethanolic solution of dimethylamine was added (200 ml). The reaction mixture was heated to 70°C, and dimethylamine was slowly bubbled through the mixture until a clear solution was obtained by adding a small amount of the mixture to water. Bubbling of the gas was continued for a further three hours. The reaction mixture was left to stand overnight and was then cooled to 0°C. The solid was filtered, dissolved in the minimum of water, and crystallized from hot ethanol. The product was filtered and dried at 60°C.

(iii). Ion-exchange of HMBTP (Br form) to the hydroxide form

A column of Amberlite resin 400(OH) was washed with 10% NaOH solution and then with doubly-distilled water until the liquid emerging was pH=7. The synthesized HMBTP(Br) was dissolved in the minimum quantity of water and introduced to the column. Elution of the column was carried out by doubly-distilled water and continued until the emerging liquid had neutral pH. The resulting HMBTP hydroxide was concentrated by vaporizing water at ca. 50°C under reduced pressure.

Measurement of HMBTP hydroxide. The quantitative measurement of HMBTP hydroxide was obtained by a titration method (i.e. titration of HMBTP hydroxide solution against the standardized hydrochloric acid). The measurement of HMBTP hydroxide also was carried out by a ^{13}C NMR spectroscopy technique (using standard solutions of TPAOH and TEAOH and the unknown concentration of HMBTP hydroxide); a long recycle delay (ca. 10 s) was applied for all cases. Results were obtained by measurement of the signal intensity through integration of the ^{13}C NMR signal for the methyl group of the corresponding compounds; results from NMR were in good agreement with those of the titration method. The sources of chemical compounds which were used for the synthesis of HMBTP are given in Table 5.

Table 5. Chemical compounds together with their sources used in the synthesis of HMBTP.

compounds	suppliers
Dimethylamine	Fluka
Hexamethylbenzene	Laboratory chemicals
Bromine	Aldrich
1,2-Dibromoethane	Aldrich
Dimethylamine in abs. alcohol	Fluka
α,α'-azoisobutyronitrile	Fluka
Sodium hydroxide	Janssee Chimica
Amberlite IRA-400(OH)	Aldrich

Another compound necessary for the research work was SUZ-9 zeolite. The procedure for its synthesis is as follows:

2.6. 4. Synthesis of SUZ-9 zeolite

14.54 g of TEA hydroxide solution and 6.9 g of HMBTP hydroxide solution were mixed with 20.0 g of water and then added to 9.5 g of fumed silica. This mixture was stirred for about two hours. The resultant gel was then added to a solution which contained 3.89 g KOH and 34.98 g of sodium aluminate in 35.0 g of distilled water. The reaction mixture was stirred for a further hour. The reaction mixture had the following molar composition;

20.1 SiO_2:Al_2O_3:1.2 Na_2O:4.3 K_2O:5.0 TEAOH:0.8 HMBTP(OH):484 H_2O
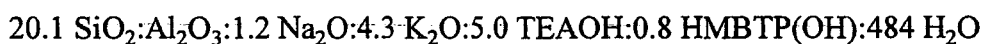
The reaction mixture was loaded into a pressure vessel of 150 cm^3 volume and heated at 135°C for 70 hours. At the end of this period the pressure vessel was cooled to room temperature and the contents filtered. The solid product was washed with distilled water and dried at 100°C.

2.7. References

1. Pople, J.A. *Discuss. Faraday Soc.* **32**, 7 (1962).

2. Ramsey, N.F. *Phys. Rev.* **78**, 699 (1950)

3. Jameson, C. J. and Gutowsky, H. S. *J. Chem. Phys.* **40**, 1714 (1964).

4. Rummens, F. H. A. *NMR* **10**, 1 (1975).

5. Engelhardt, G. and Michel, D. *High-Resolution Solid-State NMR of Silicates and Zeolites*, Wiley , New York, 1987.

6. Harris, R. K. *NMR Spectroscopy*, Longman Scientific & Technical, Essex, 1986.

7. Mason, J., *Multinuclear NMR*, Plenum Press, New York, 1987

8. Derome, A. E. *Modern NMR Techniques for Chemistry Research*, Pergamon Press, Oxford, 1987

9. Fukushima E. and Roeder, S. B. W. *Experimental Pulse NMR - A Nuts and Bolts Approach*, Addison - Wesley Publishing Co., London, 1981.

10. Akitt, J. W. *NMR and Chemistry - An Introduction to Modern NMR Spectroscopy*, Chapman and Hall, 3rd ed., London, 1992.

11. Gunther, H. *NMR Spectroscopy : An Introduction*, Wiley, New York, 1980.

12. Abraham, R. J.; Fisher, J. and Loftus, P. *Introduction to NMR Spectroscopy A Guide for Chemistry*, 2nd. ed., Wiley, New York, 1988.

13. Sanders, J. K. M. and Hunter, B. K. *Modern NMR Spectroscopy*, Oxford University Press, Oxford, 1987

14. Ernst, R. R. Anderson, W. A. *Rev. Sci. Instrum.* **37**, 93 (1966).

15. Noggle, J. H. and Schirmer, R. E. *The Nuclear Overhauser Effect, Chemical Applications*, Acad. Press, New York, 1971.

Chapter three

The Chemistry of Silicate Solutions as Precursors of Zeolites

3.1. Introduction

The structures of the silicate anions present in aqueous alkaline silicate solutions have long been the subject of debate[1]. Techniques of chemical analysis such as trimethylsilylation and reaction with molybdic acid[2] have provided the bulk of the information available. Raman spectra of aqueous silicate solutions are not very well-defined but suggest that the observed distribution of silicate species is independent of both the solution history[3] and the alkali-metal cation used[4]. It is generally accepted now that a dynamic equilibrium exists in silicate solutions between a range of silicate anions of varying degrees of condensation and molecular weight which can not be chemically separated owing to their rapid exchange rates. Although useful information can be obtained from the methods mentioned above, e.g. trimethylsilylation, silicomolybdate formation and paper chromatography, it is possible that the technique itself may perturb the labile equilibria involving the silicate oligomers. Nevertheless, valuable information on the complex nature of silicate solutions has been obtained by these methods, especially after some modifications of the experimental procedures had been introduced which take into account the above-mentioned complications.

^{29}Si NMR spectroscopy has been shown to be a very powerful tool for the study of silicate anion species and the structural units present in silicate solutions. ^{29}Si NMR can directly and non destructively probe such solutions, providing information as to the number, concentration and structures of the constituent species[5-9].

3.2. Silicate solutions

The solubility of silica in water is not simple and it depends markedly on the particle size and form of the solid (quartz, cristobalite, tridymite, vitreous, *etc.*) and the degree of polymerization of the solute, and increases with increasing alkalinity, temperature, and pressure[10]. For example, the solubility of quartz in pure water at 25°C and 0.1 MPa may be taken to be 11 mg kg^{-1} and that of amorphous silica to be 60-200 mg kg^{-1}. Sjöberg et al.[11] found the pKa for acid ionization of monomeric silicic acid $Si(OH)_4$ and $(HO)_3SiO^-$ to be 9.47 and 12.65 respectively , at 25°C and ionic strength 0.6 mol l^{-1}, with various values for silicate oligomers [e.g. for $(HO)_3 SiOSi(OH)_2O^-$, 10.25].

Stable solutions containing significant amounts of silica exist only at high pH. Figure 1 summarizes silicate solutions in terms of pH and concentration[12]. The boundaries between the regions have been shaded where they are not well determined.

Solutions in the instability region sooner or later precipitate solids. For the silicate solutions there are two types of equilibria governing the species found, an acid-base equilibrium:

$$(HO)_3Si\text{-}OH + OH^- = (HO)_3Si\text{-}O^- + H_2O \qquad (1)$$
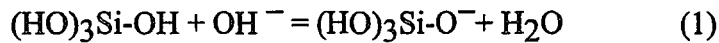
and a polymerization-depolymerization equilibrium:

$$(HO)_3Si\text{-}OH + HO\text{-}Si(OH)_3 = (HO)_3Si\text{-}O\text{-}Si(OH)_3 + H_2O \quad (2)$$
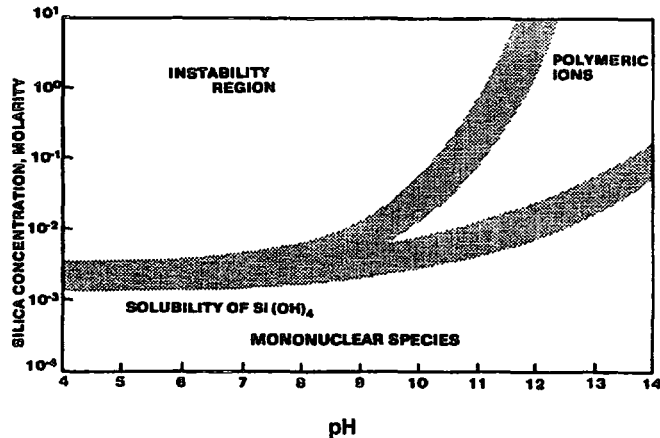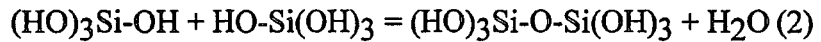
Figure 1. Silicate solutions summarized in terms of pH and concentration[12].

The term "polymerization" here is defined as the mutual condensation of SiOH fragments to give molecularly coherent units of increasing size. No distinction is made as to whether these species contain rings of increasing diameter or branched chains of an increasing number of silicate units. Acidity is coupled with polymerization, as it is known that the greater the number of siloxane linkages and the fewer the OH groups on a silicon atom, the stronger the acidity:

$$Si(OH)_4 < \text{-}Si\text{-}O\text{-}Si(OH)_3 < (\text{-}Si\text{-}O)_2Si(OH)_2 < (\text{-}Si\text{-}O)_3Si(OH)$$

least acidic   most acidic
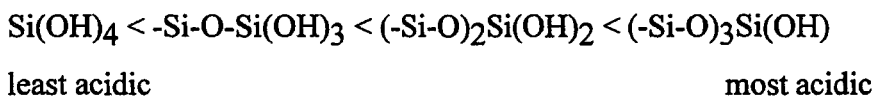
In this way polymerization-depolymerization and base-acid properties of these silicate species are tied together. In general, decreasing concentration and increasing pH both favour the formation of less condensed species. Except in the instability region, equilibrium re-establishes itself rapidly after a change in conditions. Within the instability region adjustment may be relatively slow and solutions are metastable[12].

3.3. Chemistry of dissolved silicate species

The presence of individual silicate anions in alkaline solutions of SiO_2 was first established from measurement of pH and through the use of

trimethylsilation/chromatography and the reaction of silicate anions with molybdic acid. These studies demonstrated the existence not only of monomeric anions but of oligomers differing in both molecular weight and extent of ionization. However, the structural characterisation of individual anions and quantitative measurements of the distribution of silicate anions has become possible only within the past two decades through application of ^{29}Si NMR spectroscopy.

^{29}Si NMR spectroscopy has proved to be a particularly useful method for characterizing the structure and chemistry of soluble silicate species. In an early application of this technique, Marsmann[13] showed that ^{29}Si NMR spectroscopy could distinguish Si atoms with different connectivities, whilst Engelhardt et al.[14] demonstrated that the alkali : silicate ratio has a significant influence on the condensation of the silicate oligomers in solutions used for faujasite synthesis. In an elegant series of studies , Harris et al.[15-17] reported that high-resolution NMR spectroscopy could be used to identify spectral features attributable to individual silicate anions. With this technique, these authors were able to make peak assignments for 19 anionic structures in potassium silicate solutions prepared with ^{29}Si-enriched SiO_2. More recently Knight[18], using the technique of two-dimensional homonuclear correlation spectroscopy (COSY), has confirmed the structural assignments proposed by Harris et al.[15-17] and has identified four new silicate species.

3.4. Q-units

To simplify writing of the various silicate species that can occur in solution, an abbreviated notation has been utilized to describe these silicate structures. The use of "Q-units" was first proposed by Engelhardt[14,19], and they have been used by most investigators in later studies. In this notation, Q represents a silicon atom bonded to four oxygen atoms forming a tetrahedron. The superscript i indicates the connectivity, i.e. the number of other Q units attached to the SiO_4 tetrahedron under study. Thus Q^0 denotes the monomeric orthosilicate anion SiO_4^{4-}, Q^1 end-groups of chains, Q^2 middle groups in chains or cycles, Q^3 chain-branching sites and Q^4 three-dimensionally cross-linked groups. Also in this representation the subscript j tells you how many Si(Q-units) there are in the species. With this notation the extent of ionization is ignored; therefore, the full structure corresponding to a given abbreviated notation may be either completely ionized or entirely as the protonated form, or at any stage in between. Thus the linear trinuclear silicate species would be represented as:

$$Q^1 Q^2 Q^1 = \begin{matrix} OH & OH & OH \\ \backslash & \backslash & \backslash \\ HO-Si-O-Si-O-Si-OH \\ / & / & / \\ OH & OH & OH \end{matrix} = \left[\begin{matrix} {}^-O & {}^-O & {}^-O \\ \backslash & \backslash & \backslash \\ O-Si-O-Si-O-Si-O \\ / & / & / \\ {}^-O & {}^-O & {}^-O \end{matrix} \right]^{-8}$$
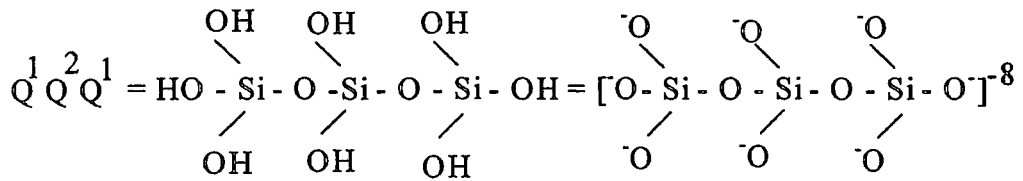
The term 'species' is used to denote a given silicic acid or any ion derived from it, that is, to refer to the Si-O skeleton only. The term ' n-mer ' and ' n-membered ' are used in reference to species containing n "Q" sites, as in the linear ' trimer ' or the three-membered ' ring. It must be noted, however, that a ring containing three "Q" sites is in fact a six-atom ring. When considering heavily-condensed species and zeolites it is useful to define secondary building units (SBU) with two types of structure: single-ring (SR) and double-ring (DR). The former is two-dimensional and the latter has three dimensions. For instance, S4R and S5R are the single four ring and single five ring respectively, and D4R and D5R are double four and double five rings. It should be noticed that D3R, D4R, D5R are contained in $Q^3{}_6$, $Q^3{}_8$ and $Q^3{}_{10}$ species respectively. The chemical structures of silicate species identified by silicon-29 NMR[15-18] are provided in the Figure 2.

Q^1 — Q^1

I

Q^1 Q^2 Q^1

II

Q^1 Q^2 Q^1

III

Q^2

IV

Q

Q^2 Q^3 Q^1

V

Q^2

VI

Q^2_a Q^3 Q^1 Q^2_b Q^2_a

VII

Q^2 Q^3

VIII

Q^3 Q^2

IX

Q^2_a Q^3 Q^2_b

X

Q^2 Q^3_c Q^3_b Q^3_a

XI

Q^2

XII

Q^3 Q^2

XIII

Q^3

XIV

Q^3_b Q^2 Q^3_a

XV

Q^3 Q^2

XVI

Q^3 Q^2

XVII

Q^2 Q^3

XVIII

Q^3

XIX

Q^3_b Q^2_b Q^2_a Q^3_a

XX

Q^3_a Q^2_b Q^3_b Q^2

XXI

Q^3_a Q^3_c Q^3_b

XXII

Q^3

XXIII
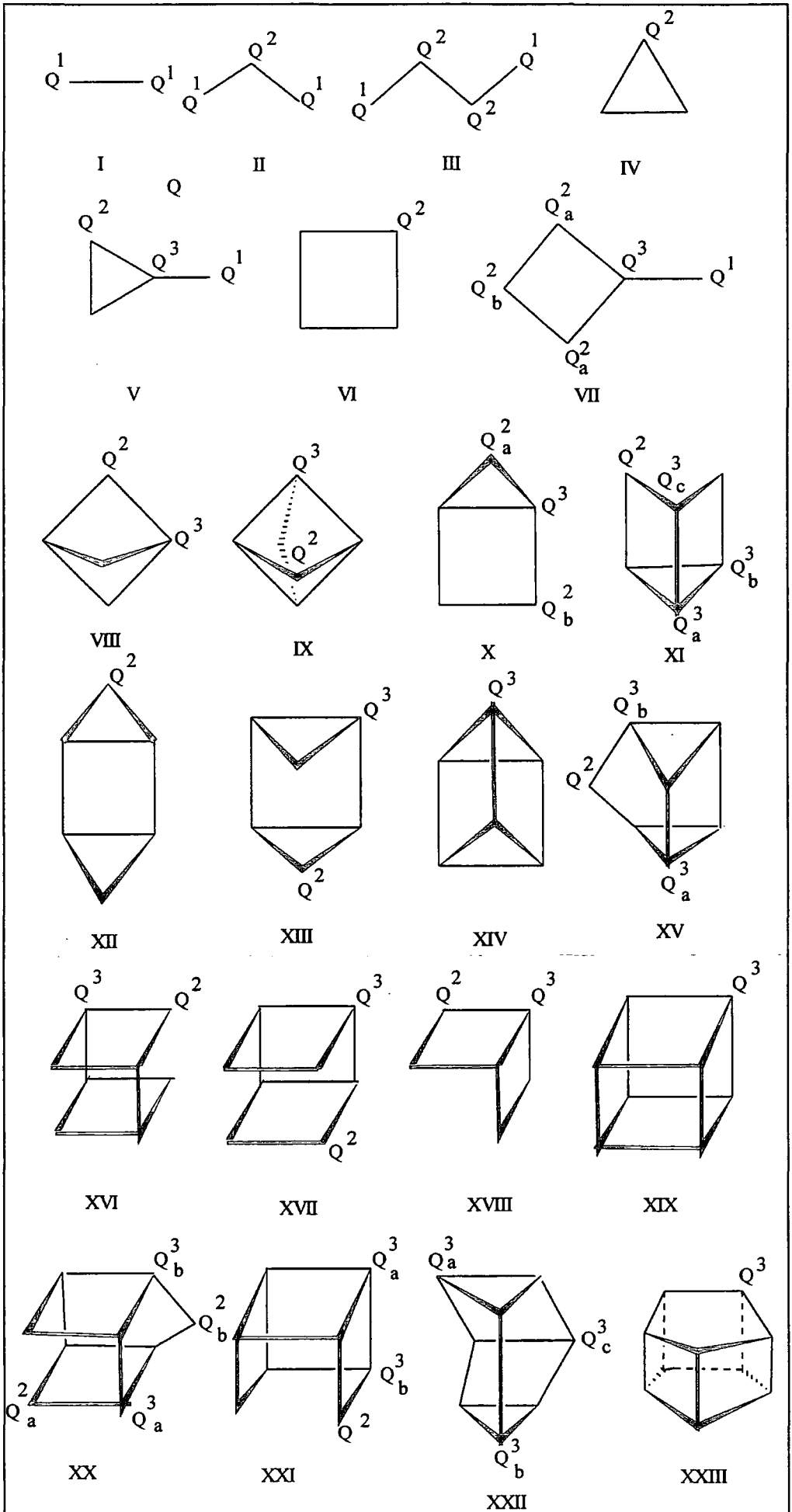
Figure 2. Silicate structures that have been detected by ^{29}Si NMR in alkaline aqueous media. Each line represents a SiOSi linkage.

I:dimer, II:linear trimer, III:linear tetramer, IV:cyclic trimer, V:monosubstituted cyclic trimer, VI:cyclic tetramer, VII: monosubstituted cyclic tetramer, VIII:bridged cyclic tetramer, IX:doubly bridged cyclic tetramer, X:bicyclic pentamer, XI:tricyclic hexamer a, XII:tricyclic hexamer b (transoid), XIII:tricyclic hexamer c (sisoid), XIV:prismatic hexamer, XV:pentacyclic heptamer, XVI:bicyclic octamer, XVII:tricyclic octamer, XVIII:bicyclic hexamer, XIX:cubic octamer, XX:tetracyclic nonamer, XXI:tetracyclic octamer, XXII:hexacyclic octamer, XXIII:prismatic decamer

3.5. Chemical shifts of species in silicate solutions

In the following discussion the chemical shifts of species in silicate solutions are given. The total range of ^{29}Si chemical shifts observed in the ^{29}Si NMR spectra of silicate and silicic acid solutions extends from about -60 to about -120 ppm (TMS reference), i.e. about 60 ppm. Within this range, five well-separated subdivisions have been found which correspond to the five possible Q^i building units.

The peak of the monomeric silicate anions, Q^0, appears at the high-frequency side of the spectrum followed in a regular sequence by the Q^1 to Q^4 units shifted by about 10 ppm to low frequency for each newly formed Si-O-Si bond. The relative concentration of the Q units can be obtained directly from the integrated peak area and may be used to estimate the mean degree of condensation of the SiO_4 tetrahedra in the solution. A short review on the structural interpretation of the spectra is described in the following:

At the highest frequency, about -66 to -73 ppm, the signal of monomeric silicate Q^0 is observed. In the range of about -76 to -83 ppm two groups of signals may be present. The first group, centred at about -76 to -80 ppm, contains the peak of Q^1 units in dimeric silicate anions and the slightly shifted peaks of Q^1 end-groups of chains or Q^1 groups connected with Q^3 or Q^4 units.

The second group of peaks, centred at about -81 to -83 ppm, includes Q^2 groups in trimeric cyclosilicates. A sharp singlet is observed for the cyclotrisilicate anion $Si_3O_9^{6-}$ which is near to signals of Q^2 groups on mono or disubstituted trimeric rings

e.g. $Q^2{}_2Q^3Q^1$. Q^2 groups in four- and higher membered rings and chains give rise to the group of signals in the range of about -86 to -90 ppm.

In contrast with the other Q^3 units, Q^3 units in trimeric ring structures are shifted by only about 8 ppm relative to the corresponding Q^2 units. Consequently, the peaks of the prismatic hexamer, $Q^3{}_6$, and other Q^3 units which are located in substituted trimeric rings appear in the low frequency side of the Q^2 shift range. The signals of other branching Q^3 appear in the shift range of about -95 to -101 ppm.

3.6. Silicon-29 NMR spectroscopy of silicate solution

The first ^{29}Si NMR spectrum of a sodium silicate solution was published in 1973[20], followed by three independent papers on this topic in 1974[13,19,21]. These studies clearly demonstrated that ^{29}Si NMR might contribute greatly to the knowledge of the complex nature of aqueous silicate solutions owing to two fundamental features of the spectra: (i) characteristic and mostly well-separated signals for SiO_4 groups in different structural surroundings may be observed; (ii) from the peak hights the relative concentrations of the different specific structures can be estimated.

Although the ^{29}Si NMR is a valuable tool for the study of aqueous silicate solutions there are some difficulties which are noted below:

⊚ The *low sensitivity* of the method due to the rare-spin character (4.7% natural abundance) of ^{29}Si, that restricted its early application to silicate solutions.

⊚ Also, silicate solutions contain a large number of species, even when differences in protonation are ignored, giving rise to complicated ^{29}Si spectra. *Spectral overlap* is therefore a considerable problem.

⊚ Additionally, because ^{29}Si is a 'rare spin' each chemically distinguishable silicon site gives rise to a single resonance, no (Si, Si) *spin-coupling* effects being visible.

⊚ Furthermore, proton exchange is rapid on the NMR time-scale, so that no (Si,H), *multiplet structure* is observed in the spectra.

Thus there is no obvious method of even demonstrating which resonances belong to the same ionic species. The assignment of individual resonances to definite chemical sites has therefore required special techniques.

i) Use of the highest feasible applied magnetic field to achieve maximum dispersion and improvement of resolution or prevention of spectral overlap.

ii) Use of samples enriched in ^{29}Si. This not only improves the signal-to-noise ratio, S/N, but also introduces splittings in the spectra for many silicon environments due to (Si,Si) spin-spin coupling.

iii) Homonoclear Si-{Si} decoupling that enables bands due to nuclei in the same chemical species to be located.

3.7. Silicate anions in the presence of organic amine cations

In the synthesis of zeolites the nature of both the inorganic alkali and the amine cation influence the final zeolite structure obtained from crystallization of aluminosilicate gels. The term "template" has been used on a macroscopic scale to describe their role in directing structure formation. With knowledge of the effect the organic cation has on the components of the reaction mixture, a better understanding might be gained of the "template" mechanism and its effect on product formation in actual zeolite synthesis. Use of different quaternary amine cations in zeolites has led to the discovery of numerous new molecular sieve structures. The way that these species interact with the (alumino)silicate ions in solution to cause crystallization of specific structures has been open to much speculation and conjecture, but only recently to direct examination.

Following the pioneering work of Barre and Denny[22] and Kerr and Kokotailo[23] in the early sixties, organic bases have found wide application in the synthesis of zeolites. Numerous variations on this theme have resulted in the syntheses of both silicon-rich forms of known zeolites and new , even aluminium-free, frameworks[24]. The cation of the base is considered to play a structure-directing role, an interesting but as yet poorly understood phenomenon. However, the importance of the solution (gel) chemistry for the specific zeolite structure that is being formed has long been recognised[24,25]. Therefore, the question arises whether the organic species already exerts a structure-directing influence in solution via the stabilization of a particular (alumino)silicate or even via the formation of an (alumino)silicate. Such a pre-selected silicate in solution may then act as a building unit for the germ nuclei.

These consideration have led us to institute a systematic study of the influence of organic molecules on the occurrence of specific (alumino)silicates in solutions from which zeolites may be crystallised. The organic cation used in this study is HMBTP (Fig. 3), where HMBTP is: (2,3,4,5,,6,7,8,9-octahydro-2,2,5,5,8,8-hexamethyl-2H-benzo(1,2-c:3,4-c':5,6-c-")tripyrrolium^{+++}).

R = CH₃
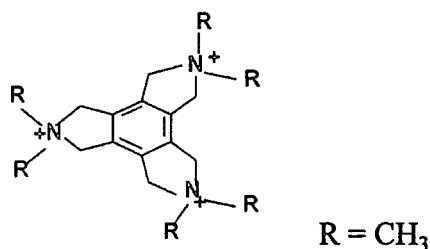
Figure 3. Chemical structure of the 2,3,4,5,6,7,8,9-octahydro-2,2,5,5,8,8-hexamethyl-2H-benzo(1,2-c:3,4-c':5,6-c'')tripyrrolium cation (HMBTP)

3.8. Characterisation and structural studies of HMBTP/Na silicate solutions

Although the most commonly encountered silicate solutions are those involving sodium (commercially available 'water glass' is a sodium silicate solution) equivalent solutions may be readily prepared using any similar metal hydroxide as the base oxide. Indeed, since silica dissolves above about pH 7-11 silicates may be prepared with organic bases having dissociation constants greater than about 10^{-3}. This section deals with the study of HMBTP silicate solutions by ^{29}Si NMR spectroscopy and compares then with Na silicate solutions under the same conditions. Also in this experiment, HMBTP/Na silicate solutions with various HMBTP/Na ratios are studied by silicon-29 NMR to obtain information on the extent to which the successive replacement of HMBTP against Na affects the structural composition of the silicate anions present.

3.9. Experimental

Six aqueous HMBTP/Na silicate solutions with constant silica concentrations of 1.6M and constant Si/cation mole ratios of 1.0, but different HMBTP/Na ratios of 1.0:0.0, 0.8:0.2, 0.6:0.4, 0.4:0.6, 0.2:0.8 and 0.0:1.0, were prepared. It should be pointed out that in this series of experiments the ratio of silica to cation is concerned, (i.e. Si/cation = 1), so the hydroxide concentration can be varied in different silicate solutions because each HMBTP cation carries three OH⁻ ions but the Na cation carries one OH⁻ ion.

All six silicate solutions were prepared by adding the appropriate amount of silica, obtained by hydrolysis of silicon tetrachloride, to the appropriate mixture of base solutions. The resulting composition was shaken vigorously and heated at 60°C for one

week. HMBTP was synthesised as explained in the experimental chapter. The silicate solutions were stored in a plastic bottle between NMR experiments .

Prolonged contact with glass surfaces was avoided, the samples being stored in plastic bottles when NMR spectra were not being recorded, as this has been held responsible for paramagnetic contamination[26]. Silicon tetrachloride was hydrolysed with high purity distilled water to yield silica, which was washed with high purity distilled water and dried overnight at ca. 130°C. Individual samples were prepared by mixing the appropriate quantity of silica and alkali metal hydroxide pellets or organic base (i.e. tetraalkylammonium hydroxide or HMBTP hydroxide solutions) with ca. 15% deuterium oxide solution. This either occurred in a plastic bottle, immediately prior to placing the solution in the sample tube, or else solutions were made up to volume in a glass volumetric flask and then placed in plastic bottles. Contact of either the sample or any of its constituents with any metal implements was avoided.

All ^{29}Si NMR measurements were carried out at the highest magnetic field available, namely with a 14.1 T (Varian VXR-600) spectrometer operating at 119.9 MHz for silicon-29, in the Fourier transform mode at ambient temperature (ca. 20°C). Due to the nuclear Overhauser effect (silicon-29 has a negative gyromagnetic ratio), spectra were recorded without decoupling. Also, to achieve accurate measurement of signal intensity, all spectra were obtained with a long-enough recycle delay (i.e. with full recovery of magnetisation) of ca. 50 s. To improve the signal-to-noise (S/N) ratio each spectrum was acquired over more than 14 hours in a 10 mm NMR tube.

In order to find the exact chemical shifts of signals, TMS was used as an external reference. In this case the spectrum was recorded by using a co-axial NMR tube, i.e. a 5 mm NMR tube containing TMS was inserted in the 10 mm NMR tube that includes the appropriate silicate solution. However for the best resolution, spectra were then obtained without the 5 mm insert tube. All the spectra were recorded at ambient temperature and the same conditions. It should be noted that the spectra were printed out in absolute intensity mode (to compare signal intensity quantitatively), with the same apodization.

Ultra-high field spectrometer systems. In any spectrometer system, it is imperative that the magnetic field be as high as possible, extremely stable and homogenous over the sample volume. The use of superconducting magnets not only fulfils these conditions, but also allows the generation of very strong magnetic fields without excessive heat

release. Field strengths attained in superconducting spectrometer systems range from 5.85 T to 14.1 T. The use of such systems in the study of aqueous silicate solutions offers two distinct advantages. The intensity of an NMR signal depends upon the square of the applied magnetic field, B_0, whereas the r.m.s. noise is proportional to the square root of B_0. Overall, the signal-to-noise ratio depends on B_0 to a power of 3/2. Thus, by increasing B_0 from 5.85 T to 14.1 T (ca. 250 MHz to 600 MHz for ^1H) the sensitivity will increase by a factor of ca. 3.74.

The second advantage associated with a large magnetic field is that of the improved chemical shift dispersion obtained. Since the resonance frequency of any nucleus is directly related to the applied field, the separation, in Hz, between any two resonances will increase proportionally to the field (the separation as measured in ppm will, by definition , remain unchanged). Provided that the linewidths are unaffected, the advantages in improved dispersion are obvious.

3.10. Results and discussion

3.10.1. Ultra-high field ^{29}Si NMR studies of pure HMBTP and sodium silicate solutions

Unlike alkali metal cations, the HMBTP cation may exert specific structure-forming effects on the silicate anions present in aqueous HMBTP silicate solution. This is clearly demonstrated by the ^{29}Si NMR spectra of HMBTP and Na silicate solutions shown in Figure 4. Although the silica concentrations and cation-to-silicon ratios of both solutions are equivalent, a broad distribution of silicate anions is observed in the Na silicate solution but a significantly different distribution is observed in the HMBTP silicate solution. In the latter, the signals attributed to the prismatic hexamer, Q^3_6, and the cubic octamer, Q^3_8, dominate. Therefore the number of species is decreased by using the specific cation. In other words cage-like species are favoured in the presence of the organic base. This phenomenon was observed previously by using tetraalkyammonium (TAA) cations, especially tetramethylammonium (TMA)[27-29].

Further evidence of the structure-forming role of the HMBTP cation has been obtained by an ^{29}Si NMR study of mixed sodium-HMBTP silicate solutions of constant silica concentration and cation-Si ratio of 1 , but different sodium-to-HMBTP ratios, which are presented in the following section.

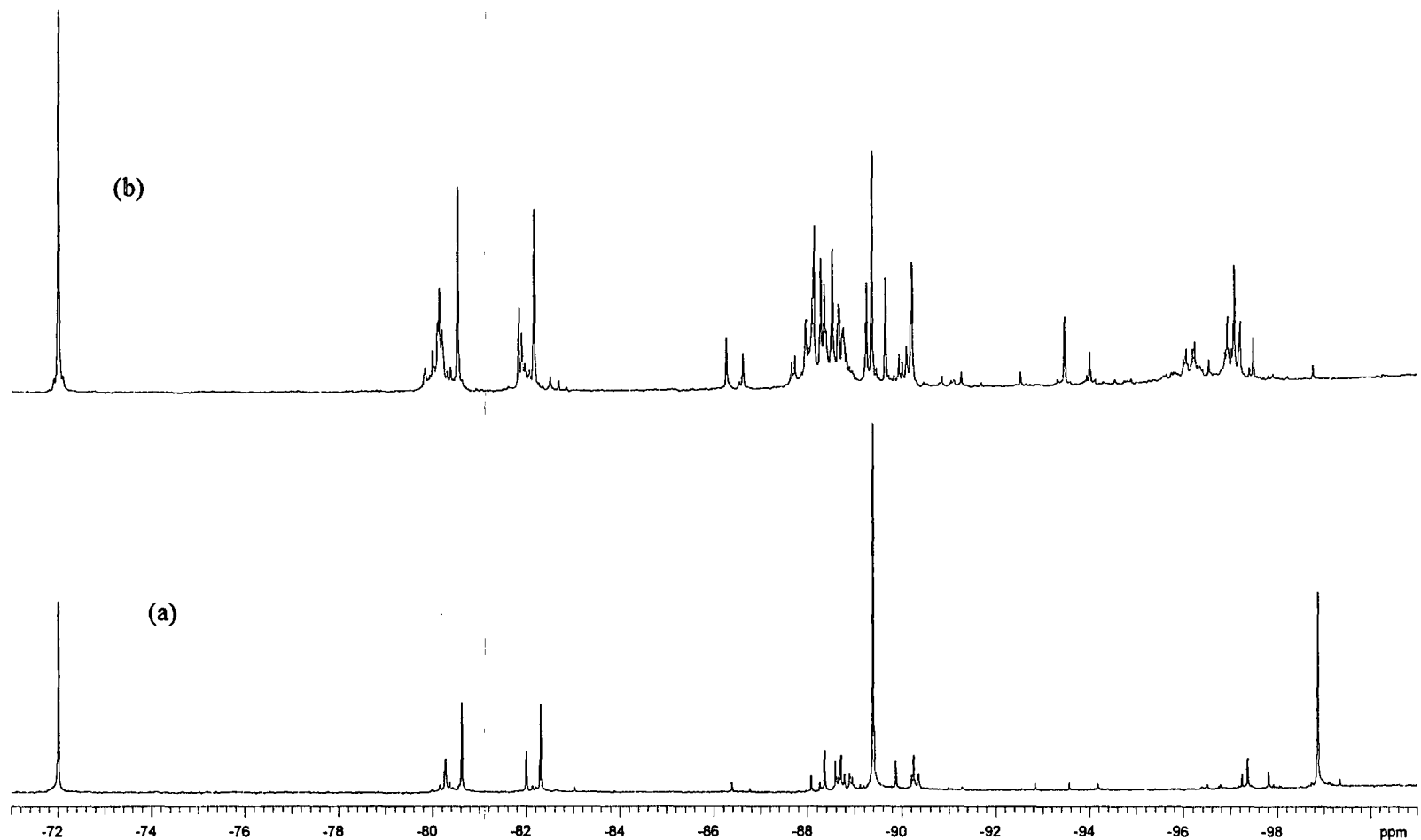Figure 4. 119.2 MHz ^{29}Si NMR spectrum of silicate solutions. (a) HMBTP silicate, Si/HMBTP =1 and (b) Na silicate, Si/Na=1. The two solutions are for the same concentration of silica of 5.78 wt%. Spectral parameters: 50 s recycle delay; 11965.3 Hz total spectral width; 1 s acquisition time and 1000 transients for each spectrum. All spectra were carried out at ambient probe temperature (ca. 25°C).

3.10.2. Structural studies of mixed HMBTP/Na silicate solutions by ultra-high resolution ^{29}Si NMR spectroscopy

Many silicon-rich zeolites crystallize from solutions containing an organic base (such as TMA or HMBTP) or alkali hydroxide. So far, it has not been possible to predict which template is required for a given structure and composition[30]. In selecting possible templates, however, one has to bear in mind some general criteria regarding the template potential for zeolitization, such as solubility in the solution, stability under synthesis conditions, and possible framework stabilization.

Among the structure-directing species, cations occupy an important position in zeolite synthesis as these not only function as structure and composition directing agents but also influence the rate of zeolite synthesis[25].

Therefore, we have investigated the fate of the distribution of silicate anions particularly for the cage-like species (such as the prismatic hexamer, Q^3_6, and cubic octamer, Q^3_8) in HMBTP-containing solutions upon addition of NaOH, a base combination present in some zeolite syntheses such as those for ZSM-18[41,42] and SUZ-9[43].

3.10.2.1. Assignments

Besides the general conclusion on the structure-forming role of the cations in the silicate solutions, information on the presence of certain silicate anions in those solutions can be derived from the ^{29}Si NMR spectra obtained from the various HMBTP/Na silicate solutions with different HMBTP/Na ratios.

The structural assignments determined for HMBTP/Na silicate solutions are based on the fact that similar structures have been observed for sodium, potassium and tetraalkylammonium silicate solutions. It is noted, however, that the exact value of the Si chemical shift in a given anion is sensitive to the specific cation as well as to the concentration. Consequently, similarity of chemical shift is sometimes an insufficient basis for establishing a firm peak assignment. In such cases, attention is paid to the peaks for well defined species (e.g. Q^1, Q^2_Δ, Q^2_4, Q^3_6 and Q^3_8) by careful comparison of previous studies[6-9,15-18]. Figures 5-10 show the ^{29}Si NMR spectra obtained from different HMBTP/Na silicate solutions with the same concentration of silica and constant ratio Si/cation of 1 but different ratios of HMBTP/Na.

As the first stage, we study the variation of the main species in the different HMBTP/Na silicate solutions.

Figure 5. 119.2 MHz ^{29}Si NMR spectrum of a HMBTP silicate solution with Si/ HMBTP=1, HMBTP:Na=1:0 and a concentration of silica of 5.78 wt%. The computer expansion of the $Q^2/Q^3{}_\Delta$ region is shown at the left-hand side of the upper trace and a computer expansion of the cubic octamer region is shown at the right-hand side of the upper trace. Spectral parameters: 50 s recycle delay; 11965.3 Hz total spectral width; 1 s acquisition time and 1000 transients. The spectrum was carried out at ambient probe temperature (ca. 25°C).
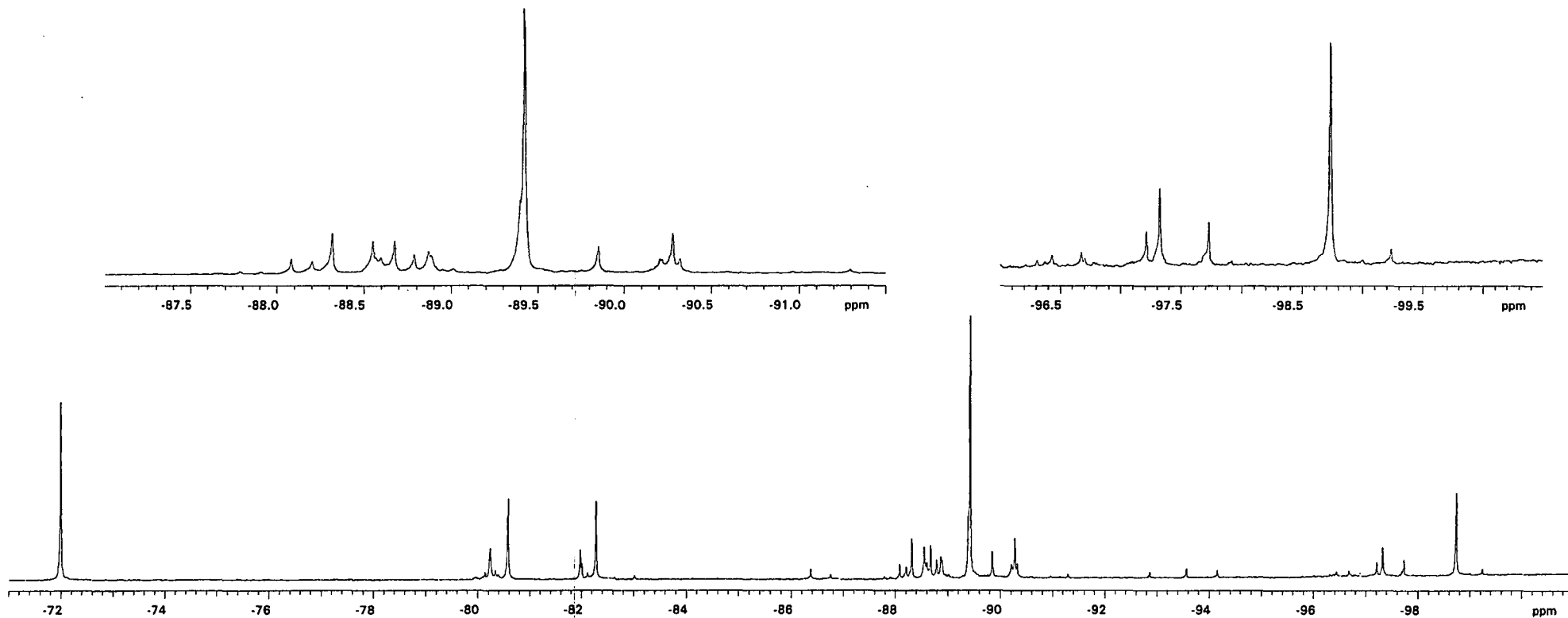
Figure 6. 119.2 MHz ^{29}Si NMR spectrum of a HMBTP/Na silicate solution with Si/cation =1, HMBTP:Na=0.8:0.2 and a concentration of silica of 5.78 wt%. The computer expanstion of the $Q^2/Q^3{}_\Delta$ region is shown at the left-hand side of the upper trace and a computer expansion of the cubic octamer region is shown at the right-hand side of the upper trace. Spectral parameters: 50 s recycle delay; 11965.3 Hz total spectral width; 1 s acquisition time and 1000 transients. The spectrum was carried out at ambient probe temperature (ca. 25°C).
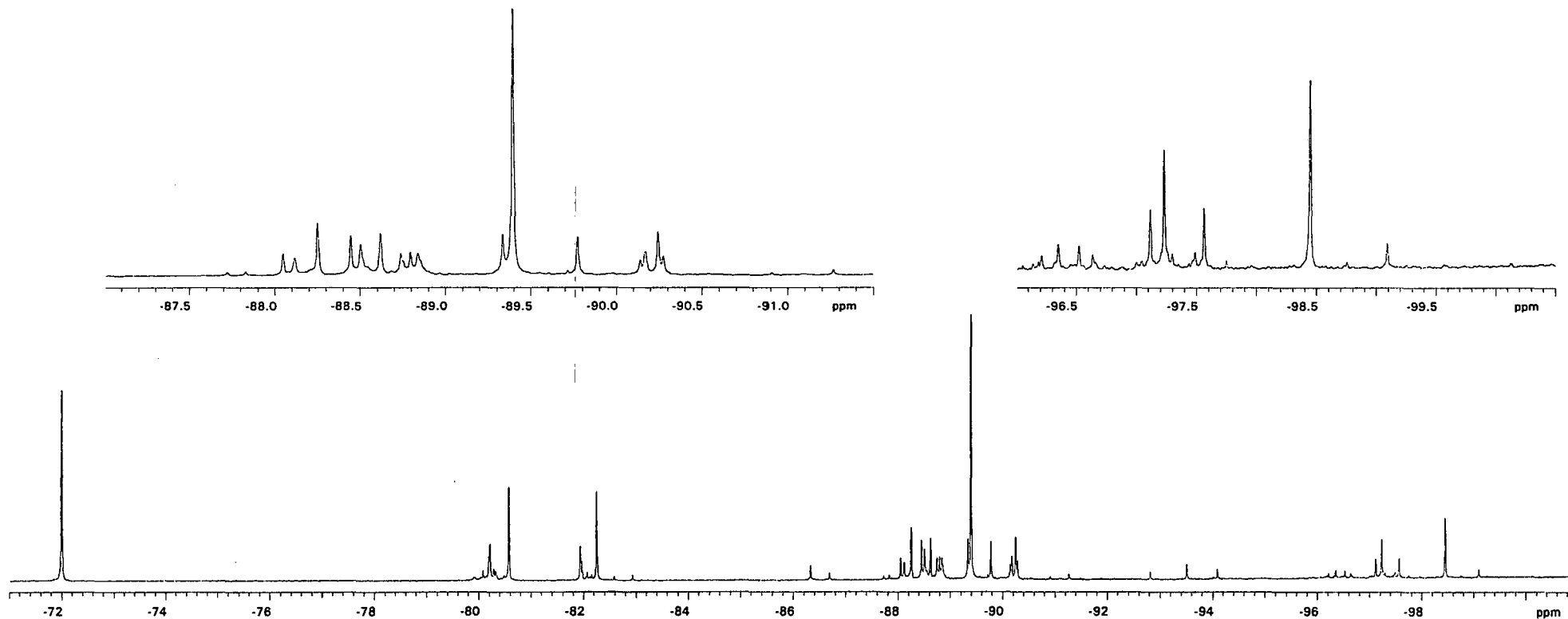
Figure 7. 119.2 MHz ^{29}Si NMR spectrum of a HMBTP/Na silicate solution with Si/cation =1, HMBTP:Na=0.6:0.4 and a concentration of silica of 5.78 wt%. The computer expanstion of the $Q^2/Q^3{}_\Delta$ region is shown at the left-hand side of the upper trace and a computer expansion of the cubic octamer region is shown at the right-hand side of the upper trace. Spectral parameters: 50 s recycle delay; 11965.3 Hz total spectral width; 1 s acquisition time and 1000 transients. The spectrum was carried out at ambient probe temperature (ca. 25°C).

Figure 8. 119.2 MHz ^{29}Si NMR spectrum of a HMBTP/Na silicate solution with Si/cation =1, HMBTP:Na=0.4:0.6 and a concentration of silica of 5.78 wt%. The computer expanstion of the Q^2/Q^3_Δ region is shown at the left-hand side of the upper trace and a computer expansion of the cubic octamer region is shown at the right-hand side of the upper trace. Spectral parameters: 50 s recycle delay; 11965.3 Hz total spectral width; 1 s acquisition time and 1000 transients. The spectrum was carried out at ambient probe temperature (ca. 25°C).

Figure 9. 119.2 MHz ^{29}Si NMR spectrum of a HMBTP/Na silicate solution with Si/cation =1, HMBTP:Na=0.2:0.8 and a concentration of silica of 5.78 wt%. The computer expanstion of the Q^2/Q^3_Δ region is shown at the left-hand side of the upper trace and a computer expansion of the cubic octamer region is shown at the right-hand side of the upper trace. Spectral parameters: 50 s recycle delay; 11965.3 Hz total spectral width; 1 s acquisition time and 1000 transients. The spectrum was carried out at ambient probe temperature (ca. 25°C).
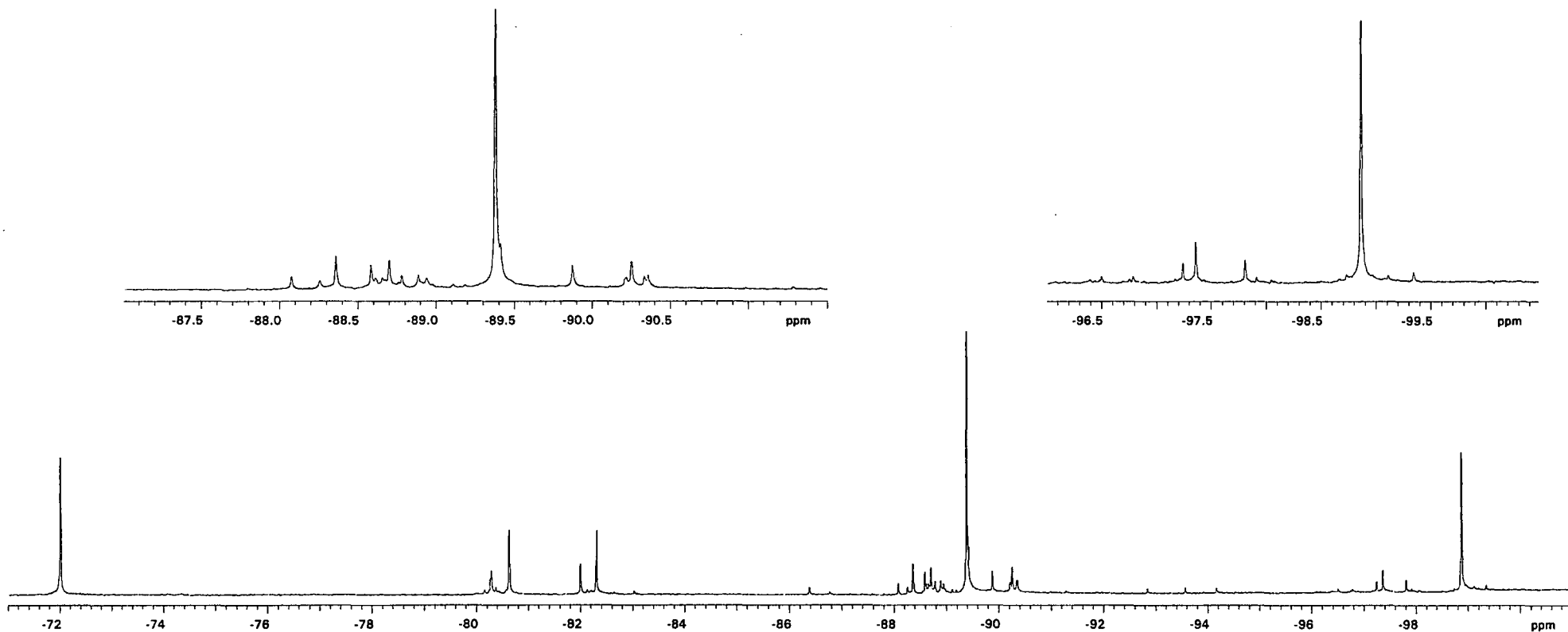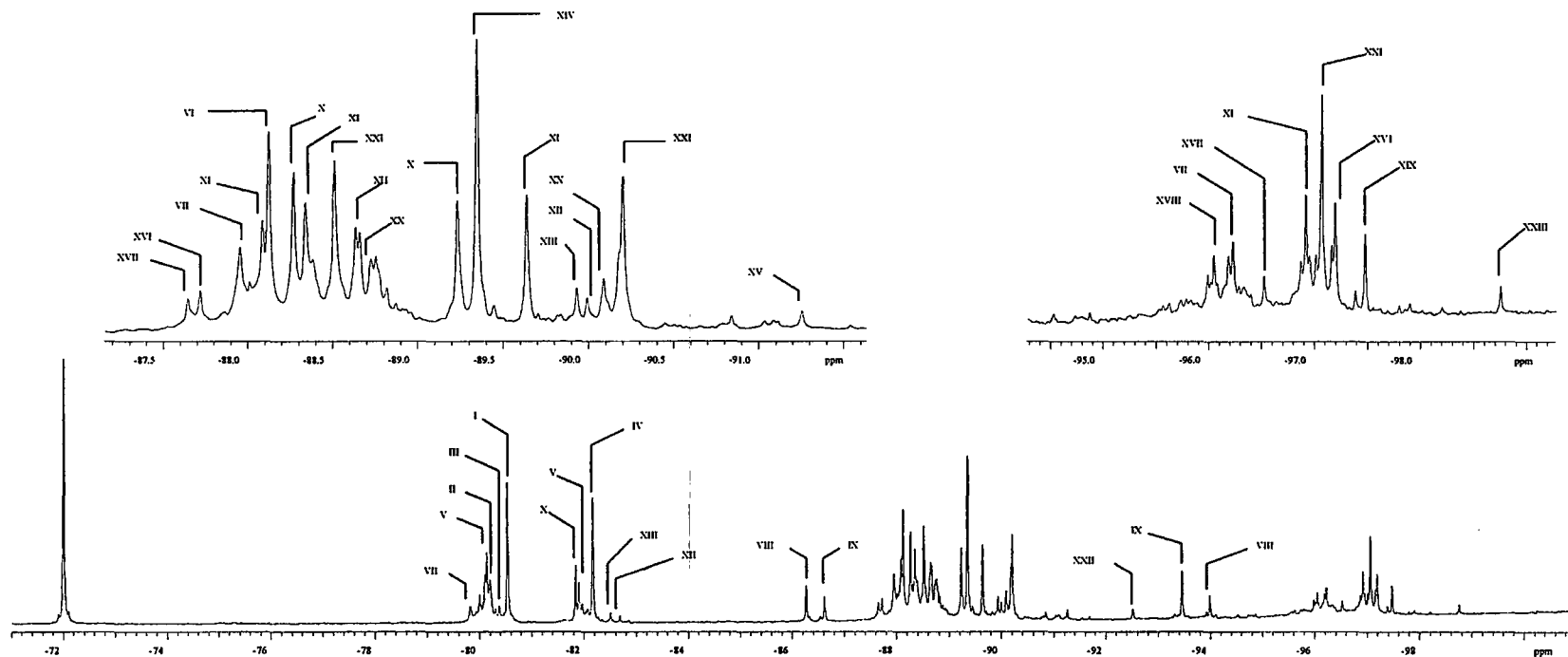
Figure 10. 119.2 MHz ^{29}Si NMR spectrum of a Na silicate solution with Si/cation =1, HMBTP:Na=0.0:1.0 and a concentration of silica of 5.78 wt%. The computer expanstion of the Q^2/Q^3_Δ region is shown at the left-hand side of the upper trace and a computer expansion of the cubic octamer region is shown at the right-hand side of the upper trace. Spectral parameters: 50 s recycle delay; 11965.3 Hz total spectral width; 1 s acquisition time and 1000 transients. The spectrum was carried out at a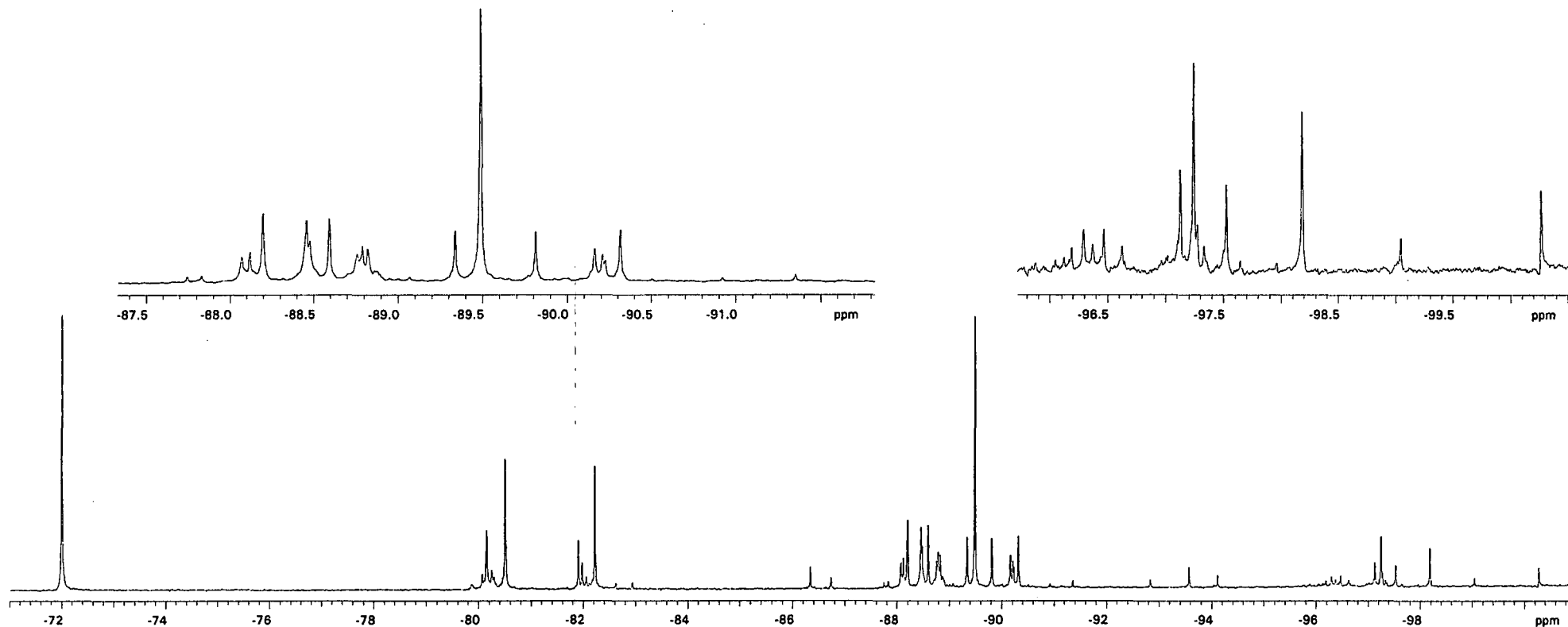mbient probe temperature (ca. 25°C). Assignment of peaks is quoted on the top of each peak [15-17]. The number refers to the structures presented in Figure 2.

3.10.2. 2. Assignment of species containing a single silicon site

There are some anion species in the silicate solution which show a single peak in the ^{29}Si NMR spectrum even using isotopic enrichment of silicon-29. These are the anions in which all the silicon sites are chemically (symmetrically) equivalent. Such species include the monomer, Q^0, dimer, Q^2, unsubstituted cyclics, e.g. $Q^2{}_\Delta$, or $Q^2{}_4$ and regular cage anions, e.g. $Q^3{}_6$, or $Q^3{}_8$. The assignment of such species has been already well defined. Therefore we can attribute the lines denoted to the corresponding species unambiguously. The variation of the intensity as well as the chemical shifts of these silicate anions are presented as follows:

Here we consider the signals lying at approximate chemical shifts (relative to the momomer) of 0, 9,11,16, 17 and 27 ppm, which are assigned to Q^0, Q^1, $Q^2{}_\Delta$, $Q^2{}_4$, $Q^3{}_6$ and $Q^3{}_8$ species respectively. Figures 11a-11f show a schematic representation of the intensity dependence of those species as a function of HMBTP concentration (a.u. indicates arbitrary units for intensity). Figure 5 shows that in the HMBTP silicate (i.e. without sodium hydroxide) the prismatic hexamer, $Q^3{}_6$, and cubic octamer, $Q^3{}_8$, dominate. However Figures 6-10 prove that those species drop sharply in concentration with decreasing HMBTP/Na ratio. In lower concentrations of the HMBTP cation, a complex and non-uniform distribution of different silicate anions is found, visible by the increasing number and intensity of the NMR signals for various $Q^i{}_j$ units.

(a)

(b)

(c)

(d)

(e)   (f)
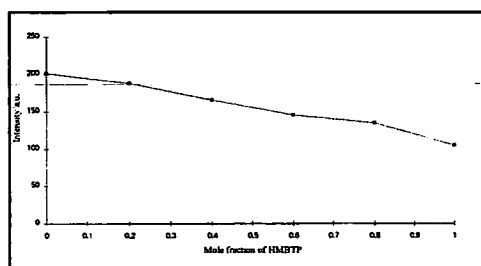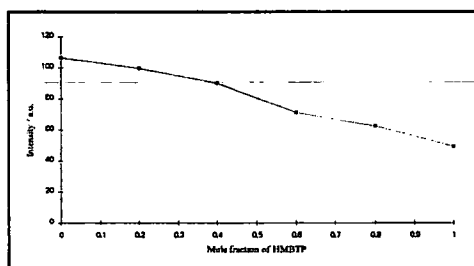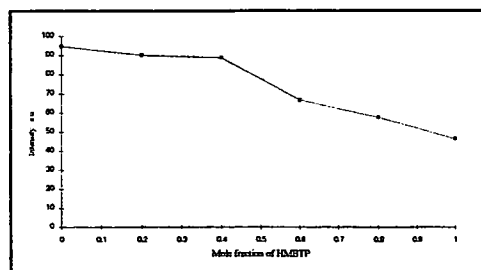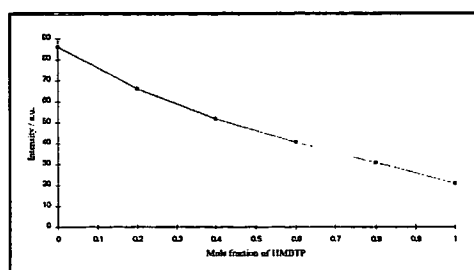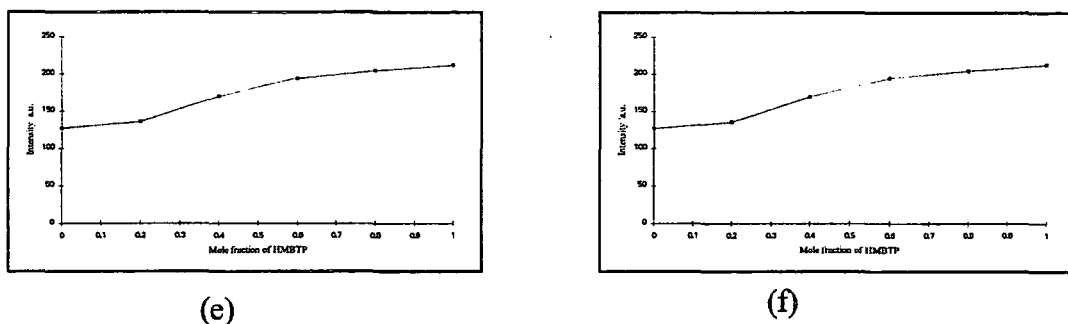
Figure 11. Intensity dependence of the single silicon sites as a function of HMBTP concentration. (a) monomer, Q^0, (b) dimer, Q^1_2, (c) cyclic trimer, Q^2_Δ, (d) cyclic tetramer, Q^2_4, (e) prismatic hexamer, Q^3_6, and (f) cubic octamer, Q^3_8.

Figure 11 illustrates the role of the structure-forming HMBTP cation very clearly. The peak heights related to the prismatic hexamer, Q^3_6 and cubic octamer are enhanced with the increasing concentration of the HMBTP cation. However, when the concentration of HMBTP is increased, the small silicate anions decrease in intensity quite significantly. Therefore in the presence of the HMBTP cation the silicate species are polymerised to make the cage-like species such as Q^3_6 or Q^3_8.

From the results discussed above, it can be concluded that the existence of stable silicate anions (i.e. Q^3_6, Q^3_8) in the presence of the HMBTP cation has been positively proved by ^{29}Si NMR studies, but the conditions of their formation and stability are far from being fully understood. Information of this type is, however, of fundamental interest for a better understanding of mechanisms governing the synthesis of zeolite and other crystalline aluminosilicates. Further evidence of the structure-forming power of organic cations has been provided from the ^{29}Si NMR studies of sodium/tetramethyl ammonium silicate solutions by Engelhardt et al.[29].

It is worth pointing out that the the line widths of the signals do not change substantially by variation of HMBTP/Na ratio. For example the line-widths measured with computer program for the Q^0 signals in different HMBTP/Na silicate solutions are listed in table 1.

Table 1. Line widths of the Q^0 signal in HMBTP/Na silicate solution.

HMBTP/Na ratio	Line-width (Hz)
1.0	0.93
0.8	0.89
0.6	0.97
0.4	0.85
0.2	0.91
0.0	0.94

Therefore it can be concluded that, using ^{29}Si NMR spectroscopy, the concentration of 21 silicate anions can be determined quantitatively in HMBTP/Na silicate solutions suitable for the synthesis of ZSM-18[41,41] and SUZ-9[43] zeolites. The equilibrium distribution of these anionic species is a sensitive function of HMBTP/Na ratio. With increasing ratio, the mole fraction of individual anions decreases monotonically for the monomer, dimer, cyclic trimer and cyclic tetramer but increases monotonically for the prismatic hexamer and cubic octamer. In general, the maximum $Q^3{}_6$ and $Q^3{}_8$ concentration is found to occur in the pure HMBTP silicate solution (i.e. HMBTP/Na = ∞).

Summarising the results, it can be concluded that with increasing replacement of Na by HMBTP in silicate solutions the structure-forming effect of HMBTP is increased, and consequently cage-like species are dominant.

3.10.2.3. The prismatic hexamer and related structures

Perhaps the most obvious feature to emerge from these studies is the apparent predilection of the silicate system to form cage-like species. Of these cages, the prismatic hexamer and species related to it appear to be the most abundant and consequently may be assumed to be the most stable. This fact has important implications. Large species have occasionally been proposed as major components in aqueous silicate solutions. The study of the quantitative distribution of such species as a function of HMBTP/Na ratio in HMBTP/ Na silicate solutions gives another insight to the structure-directing effect of the organic cation (i.e. HMBTP).

The left-hand sides of the upper traces of Figures 5-10 show the expanded-scale spectra of HMBTP/Na silicate solutions in that region. It is apparent that the number of signals decreases with increasing concentration of HMBTP (i.e. in higher ratios of

HMBTP/Na), that is HMBTP influences the extent of condensation of the silicate species.

Fig. 12 gives a schematic representation of the ^{29}Si NMR spectra of HMBTP/Na silicate solutions in the shift range -87 to -91.5 ppm. The intensities (measured as a peak height) as well as chemical shifts of the signals are normalized, i.e. the intensity and chemical shift of the main peak in this region, $Q^3{}_6$, was set to 100 and 0.0 ppm respectively. The nature of the HMBTP cation appears, to a certain extent, to affect the stability of individual silicate structures. This is best illustrated by considering a specific structure, a good example being the prismatic hexamer.
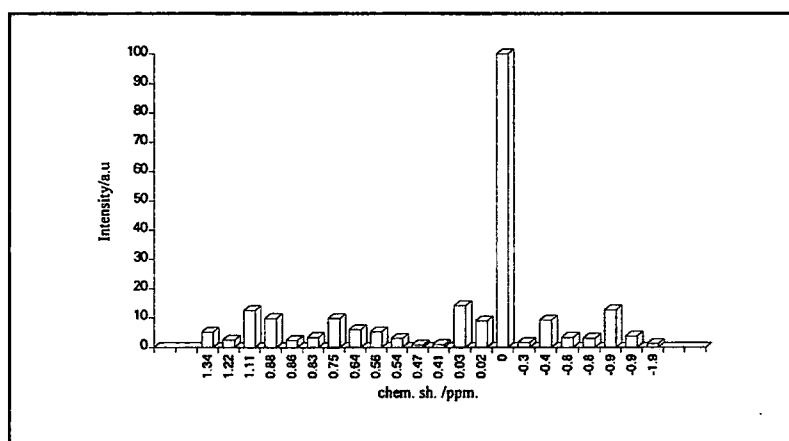
(a)
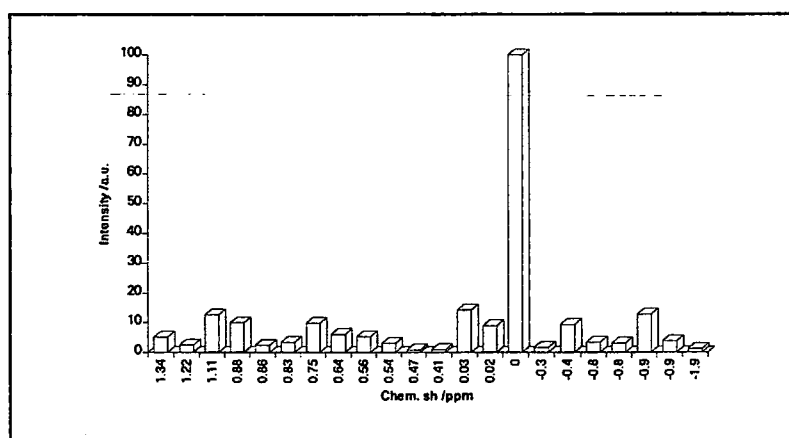
(b)
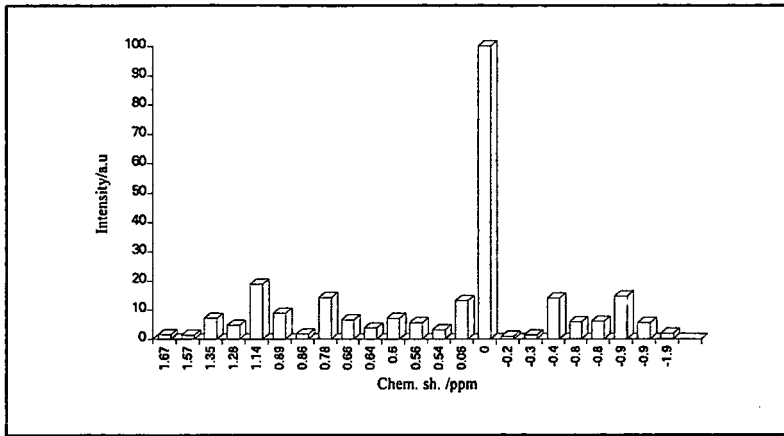
(c)
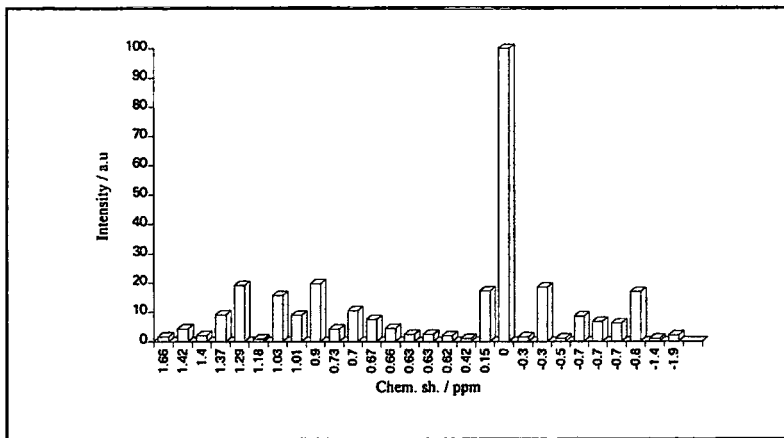
(d)
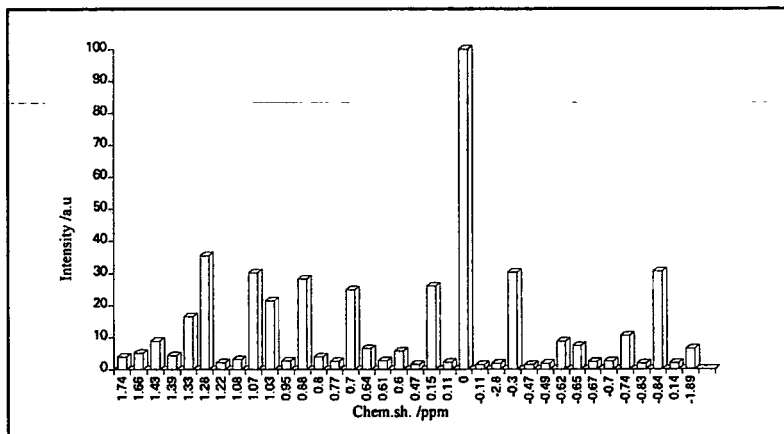
(e)
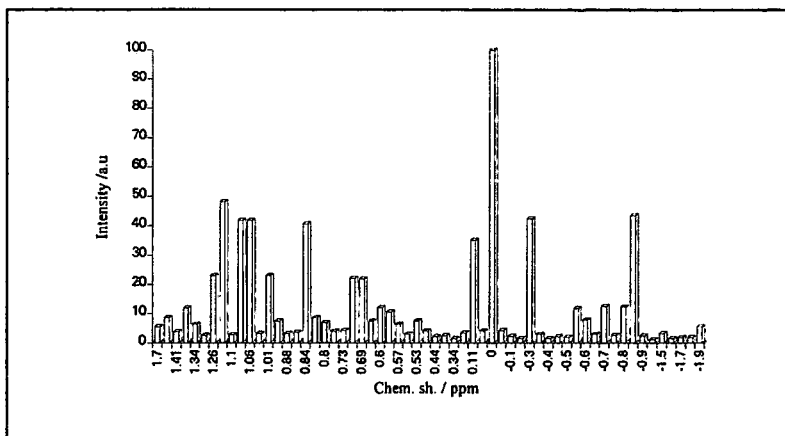
(f)

Figure 12. Schematic representation of the Q^2/Q^3_Δ region for HMBTP/Na silicate solutions. (a) HMBTP : Na = 1.0 : 0.0, (b) HMBTP : Na = 0.8 : 0.2, (c) HMBTP : Na = 0.6 : 0.4, (d) HMBTP : Na = 0.4 : 0.6, (e) HMBTP : Na = 0.2 : 0.8, and (f) HMBTP : Na = 0.0 : 1.0

The number of lines shown in the $Q^2/Q^3\Delta$ region decreases with increasing concentration of HMBTP. Some signals in this region are related to the species shown in Figure 13 which were identified by Harris et al.[15-17] and Engelhardt et al.[34]. They represent stages in the formation of the prismatic hexamer.
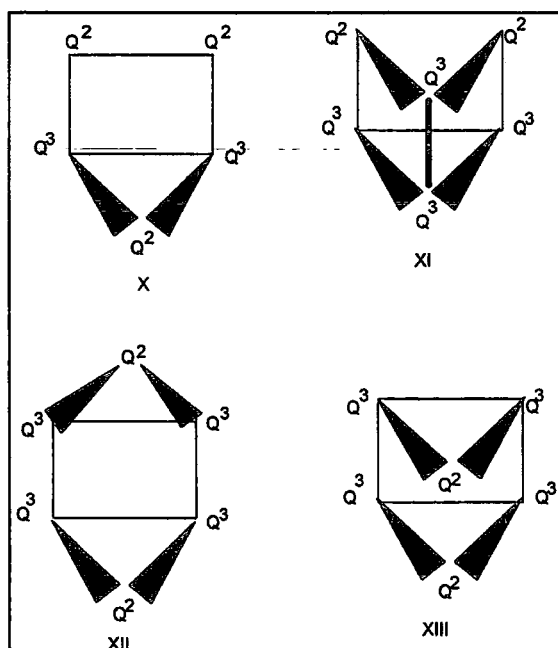
Figure 13 The proposed species related to the prismatic hexamer.

Thus by replacing Na by HMBTP, i.e. increasing the HMBTP :Na mole ratio, the open-ring species (Figure 13) are converted to the prismatic hexamer, $Q^3{}_6$, or more polymerized species. Fig. 14 shows a schematic representation of the variation of the intensity of species associated with prismatic hexamer. Figure 14 demonstrates that the abundance of the silicate anions associated with the prismatic hexamer decreases with increasing concentration of HMBTP cation, although the signal attributed to $Q^3{}_6$ is enhanced. Therefore the structure directing effect of the HMBTP cation can be defined in terms of increasing the prismatic hexamer .

(a)   (b)

(c)   (d)
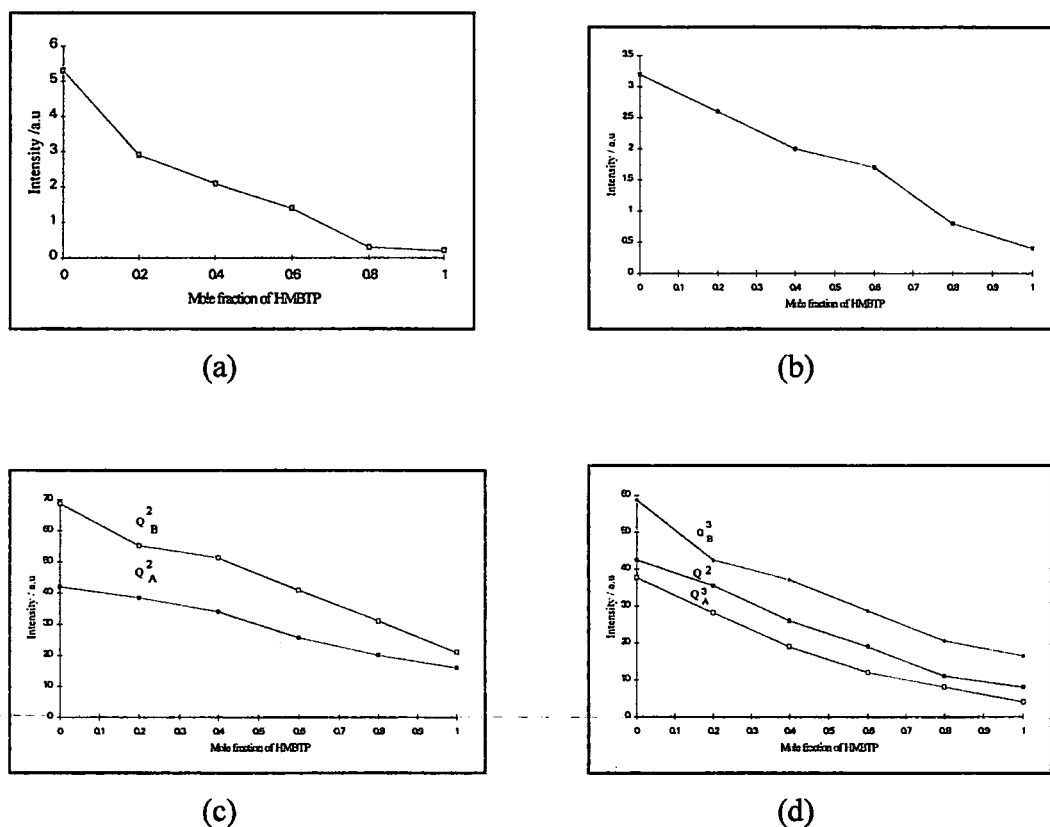
Figure 14. Normalized concentration of species associated with the prismatic hexamer as a function of mole fraction of HMBTP in HMBTP/Na silicate solutions. (a) tricyclic hexamer (cisoid) (XIII), (b) tricyclic hexamer (transoid) (XII), (c) bicyclic pentamer (X), and (d) tricyclic hexamer(XI). The number in parentheses refers to the structures presented in Figure 2.

3.10.2.4. On the assignment of bands due to the bridged cyclic tetramer and doubly bridged cyclic tetramer.

Two species VIII and IX (Figure 15) were identified as giving signals in the shift ranges of about -86.3 and -86.7 ppm as well as -93.4 and -94.1 ppm, which refer to the Q^2 and Q^3 sites respectively.

VIII   IX
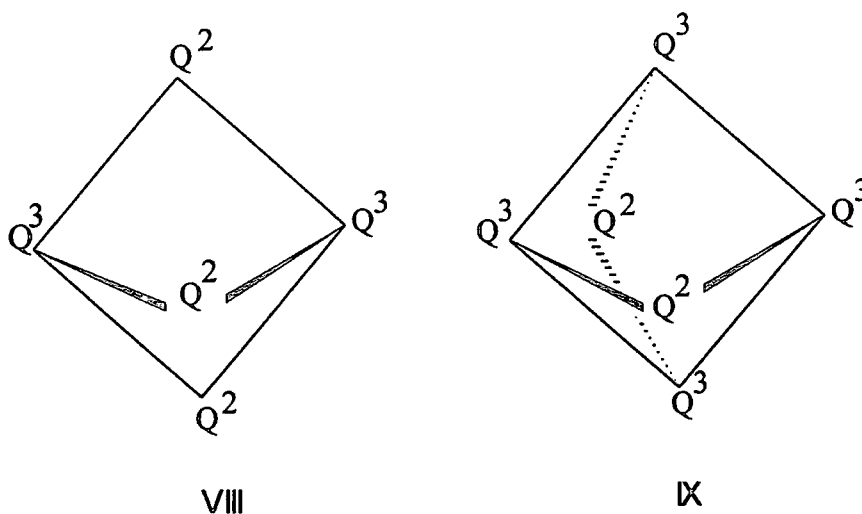
Figure 15. Chemical structure of silicate anions of the bridged cyclic tetramer (VIII) and the doubly bridged cyclic tetramer (IX).

The signals with chemical shifts of about -86.3 (caused by Q^2 sites) and -93.4 ppm (related to Q^3) belong to structure VIII (bridged cyclic tetramer), while signals at about -86.7 ppm (Q^2 site) and -94.1 ppm (Q^3 site) arise from species IX (doubly bridged cyclic tetramer). Figures 5-10 show the significantly changing intensity of these species in various HMBTP/Na silicate solutions. Schematic representations of this phenomenon are given in Figure 16. As can be seen, signals related to species VIII & IX decrease in intensity with increasing HMBTP /Na mole ratio. Both silicate anions are no longer readily detected in HMBTP silicate solution. It is supposed that these species may act as precursors for the cubic octamer, $Q^3{}_8$, and consequently that they may be converted to cubic octamer by the templating effect of HMBTP. This realisation becomes clear when we consider the variation in intensity of species VIII & IX and that the cubic octameric anion is stabilised in HMBTP silicate solution.

(a)   (b)
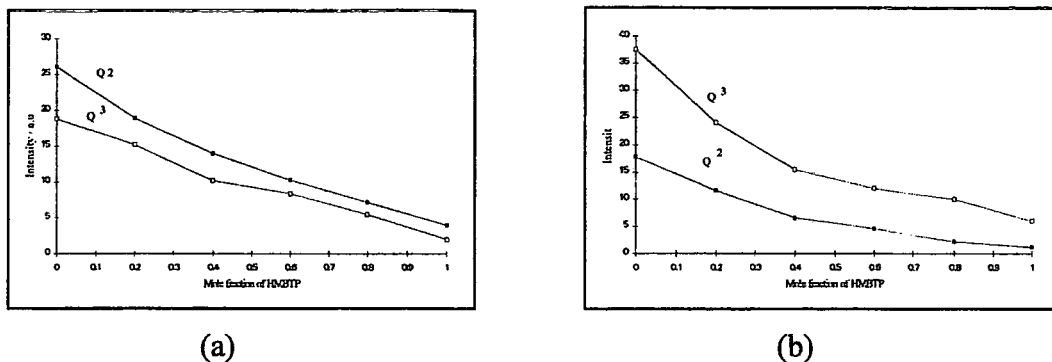
Figure 16. Variation of the intensity of the bridged cyclic tetramer (VIII) (a) and double bridged cyclic tetramer (IX) (b) as a function of the concentration of HMBTP in HMBTP/Na silicate solutions.

3.10.2.5. Variation in the distribution of species in the region of the cubic octamer

It is interesting to point out the distribution of signals in the range of about -96 to -99.5 ppm. Here also a similar situation to that of Q^3_6 exists with the cubic octamer, which appears to be most stable in HMBTP silicate solution. The cubic octamer, Q^3_8, is believed to give rise to the peak at a shift about -99 ppm (with respect to the signal for TMS).

Computer expansions of this portion of the ^{29}Si NMR spectra of HMBTP/Na silicate solutions are presented in the right-hand sides of the upper traces of spectra presented in Figures 5-10. The chemical shifts and related intensity considerations allow assignments to be made by analogy to the more familiar shift range of the prismatic hexamer discussed earlier. It seems that, moving to higher concentrations of HMBTP (i.e. high HMBTP/Na ratio), signals in this region collapsed to that of Q^3_8.

Evidence for the assignment of the peaks lying in this area has been presented by some authors. Knight et al.[18], using the technique of two-dimensional homonuclear correlation spectroscopy (COSY) , have identified four new silicate species (Figure 17).
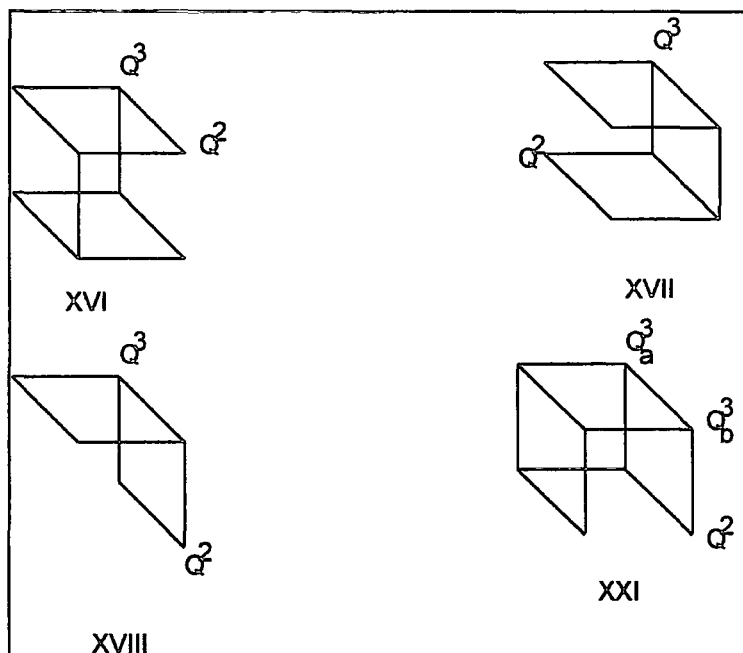
Figure 17. Illustration of silicate structures identified from ^{29}Si NMR
COSY experiments[18]. The number refers to the structures presented in Figure 2.

Figures 18a-18f show the distribution of species as affected by the replacement of Na against HMBTP. The species proposed in Figure 18 are mostly changed to the cubic octamer which is stabilised at high HMBTP : Na ratio in HMBTP/Na silicate solutions. All peak hights and chemical shifts are extracted from the ^{29}Si NMR spectra of HMBTP/Na silicate solutions with different mole ratios of HMBTP/Na. In this case the chemical shifts are given with respect to the signal for TMS (using TMS as an external reference for each silicate solution separately).
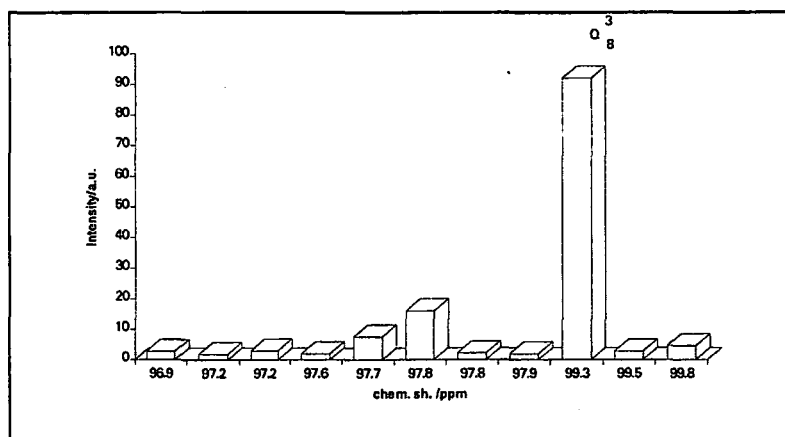
(a)
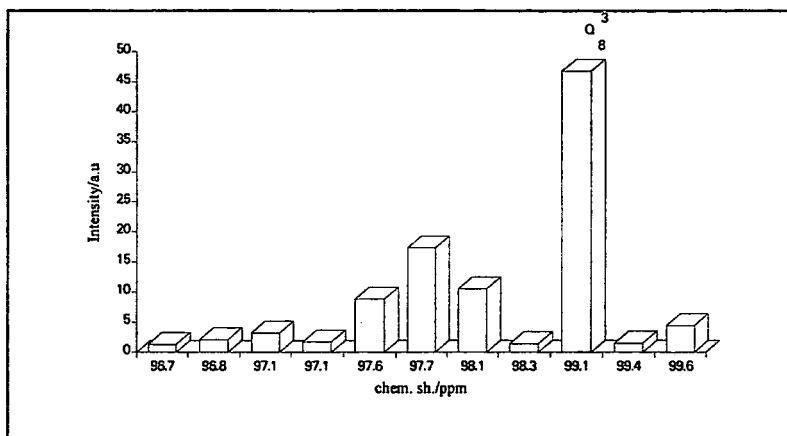
(b)
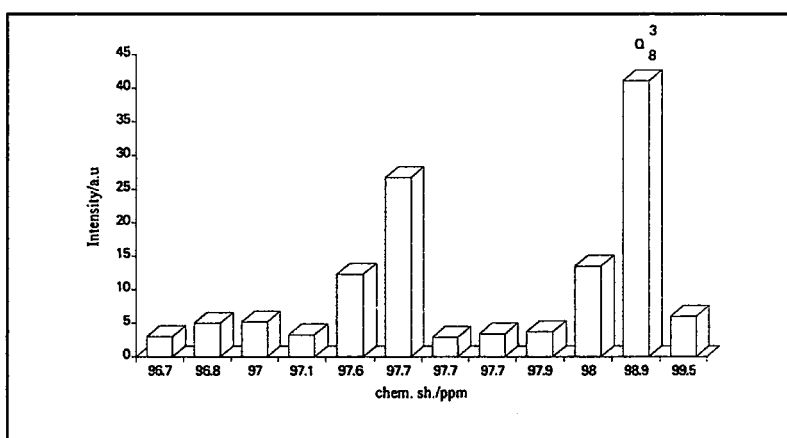
(c)
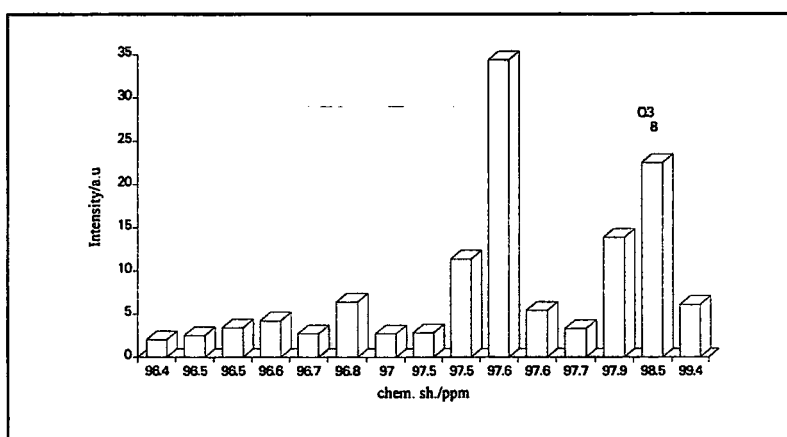
(d)
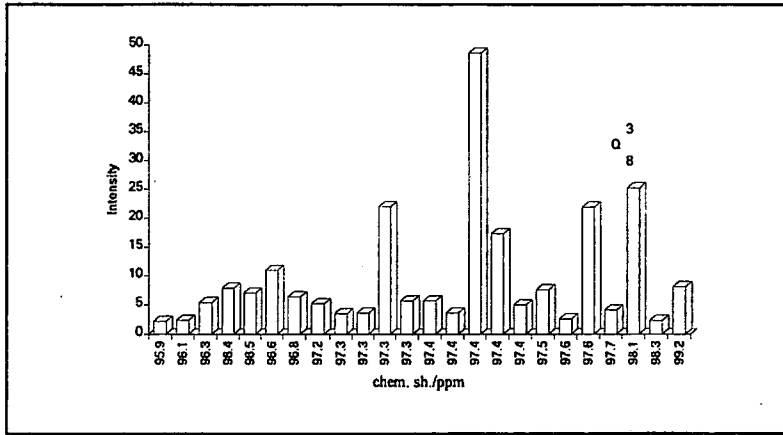
(e)
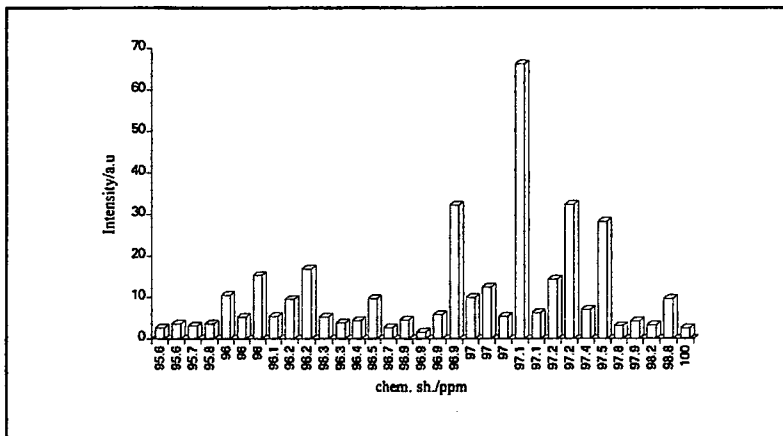
(f)

Figure 18. Schematic representation of the distribution of silicate species giving signals in the cubic octamer region. The chemical shifts are referenced to external TMS. (a) HMBTP : Na = 1.0 : 0.0, (b) HMBTP : Na = 0.8 : 0.2, (c) HMBTP : Na = 0.6 : 0.4, (d) HMBTP : Na = 0.4 : 0.6, (e) HMBTP : Na = 0.2 : 0.8, (f) HMBTP : Na = 0.0 : 1.0.

Going from low concentration of HMBTP to higher, the intensity of the line assigned to $Q^3{}_8$ is enhanced. Also, the number of lines (i.e. silicate species) displayed in this region decreases with increasing mole ratio of HMBTP/Na. As a result, the role of structure direction of HMBTP can be clearly demonstrated by this phenomenon. Decreasing the number of lines in the spectra can be explained by polymerization of the silicate anions, which leads to the formation of cage-like species containing more silicon atoms, in this case the cubic octatmeric anion, $Q^3{}_8$. This observation is consistent with the mechanism of structure direction proposed by Hoebbel et al.[28,32]. They also observed the preferred formation of cage-like silicate anions in tetramethylammonium (TMA) and tetraethylammonium (TEA) silicate solutions.

Hoebbel at al. ascribe the occurrence of cage-like silicates to the formation of 'clathrate water' structures in concentrated TMA^+ and TEA^+ solutions, which would then stabilise the cage-like silicates. As explained, we have found that the HMBTP cation behaves qualitatively the same (i.e. more concentration of HMBTP gives more cage-like species, e.g. Q^3_8). It can be deduced that a simple electrostatic picture can be used to describe the general trend towards cage-like silicates upon replacing sodium by HMBTP cation. At a given degree of silicate condensation the cation with the higher charge density, favours the formation of the oligomer with the tight ion pairs through optimizing of the electrostatic attraction. Increasing the radius of the cation by replacing sodium by HMBTP may not reduce the attraction since HMBTP carries three positive charges rather than one as for sodium. Apparently, the formation of cage-like silicates becomes favourable.

At the end of this section it is pertinent to notice the integration values for the regions of Q^1, Q^2/Q^2_A, Q^2/Q^3_A and Q^3, which are listed in table 2. These values were obtained from Si-29 NMR spectra of HMBTP/Na silicate solutions after computer subtraction of the spectra. From data of Table 2, it can be realised that the HMBTP silicate has the largest value in Q^2/Q^3_A and Q^3, but this solution has a minimum value in the Q^1/Q^2_A region. However, integration values do not change dramatically with variation of the HMBTP/Na mole ratio.

Table 2 Data of integration values for different regions of HMBTP/Na silicate solution.

HMBTP/Na mole ratio	Q^1/Q^2_A (-79 to -89 ppm)	Q^2/Q^3_A (-87 to -92 ppm)	Q^3 (-95 to -99 ppm)
1.0	28.85	65.01	19.52
0.8	31.22	64.16	17.44
0.6	32.48	63.07	16.80
0.4	33.24	62.41	15.94
0.2	34.37	60.81	15.98
0.0	33.21	60.96	15.90

In conclusion, the HMBTP cation changes distribution of species and stabilises cage-like anions.

3.10.2.6. Variation of the chemical shifts of silicate anions in different HMBTP/Na silicate solutions

The chemical shifts of the silicate anions change for the different HMBTP/Na mole ratios of silicate solutions. The ^{29}Si chemical shift information reported here was derived from spectra of HMBTP/Na silicate solutions having Si : cation = 1 with a natural isotopic abundance of ^{29}Si. Figures 19a-19p present schematically the variation of the chemical shifts (on the y axes) associated with different silicate anions in various HMBTP/Na silicate solutions.

The zero values on the y-axes are chosen arbitrarily for each site so as to emphasise the variations. The true values of the zeroes, with respect to the signals for TMS, are given in Table 3.

Table 3 The true values for the zeroes, with respect to the signal for TMS.

Graph	Species, Q-site	Shift at scale zero
(a)	(II), Q^1	80
(b)	(V), Q^1	80
(c)	(VII), Q^1	79
	(VII), Q^2	78
(d)	(IV), Q^2	82
(e)	(XIII), Q^2	82
(f)	(XII), Q^2	82
(g)	(VIII), Q^2	86
	(VIII), Q^3	93
(h)	(IX), Q^2	86
	(IX), Q^3	93
(i)	(XVII), Q^2	87
(j)	(XI), Q^2	88
	(XI), Q^3a	88
	(XI), Q^3b	89
	(XI), Q^3c	97
(k)	(XVI), Q^2	87
	(XVI), Q^3	97
(l)	(VI), Q^2	88
(m)	(X), Q^2a	81
	(X), Q^2b	88
(n)	(XX), Q^2	88
	(XX), Q^3a	90

| (o) | (XIV), Q^3 | 89 |
| (p) | (XIX), Q^3 | 97 |
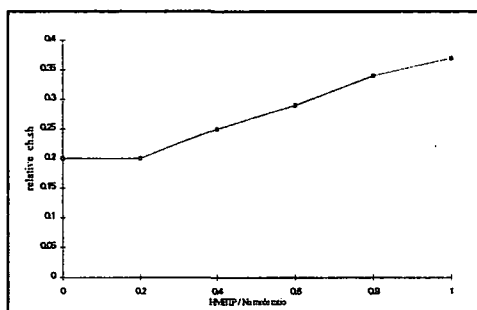
(a)
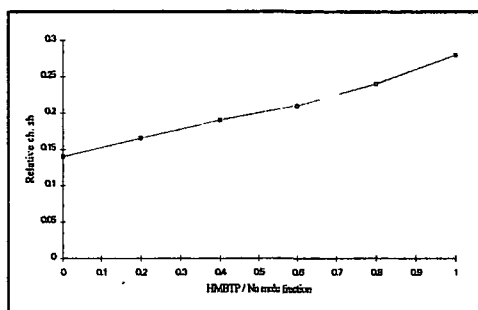
(b)
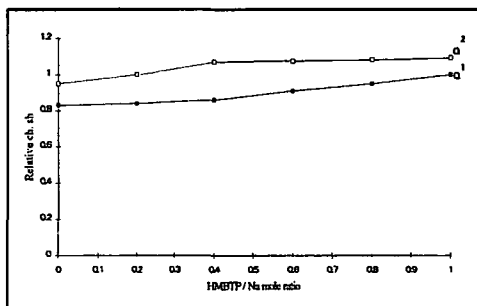
(c)
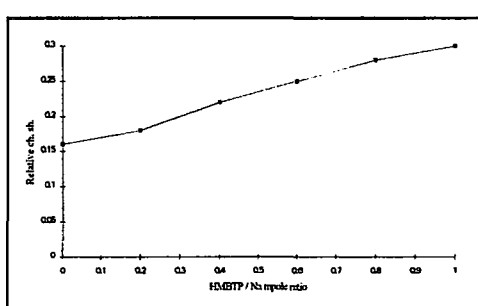
(d)
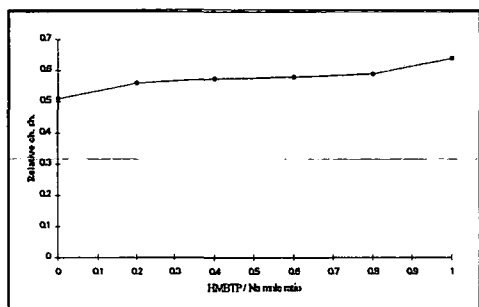
(e)
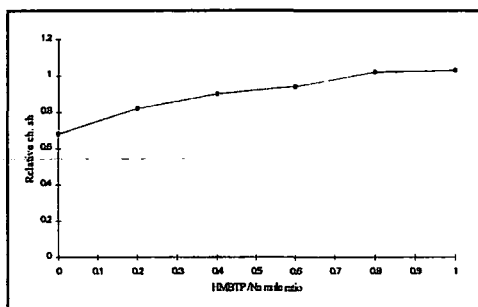
(f)
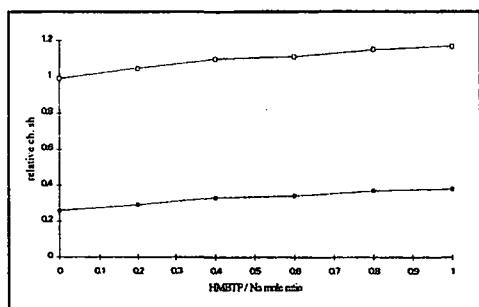
(g)
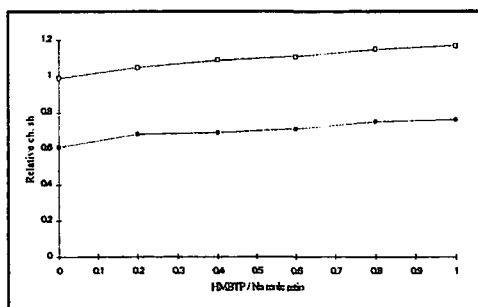
(h)
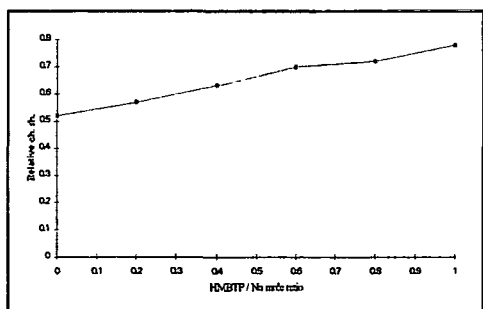
(i)
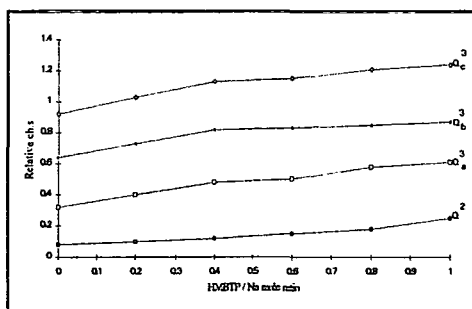
(j)
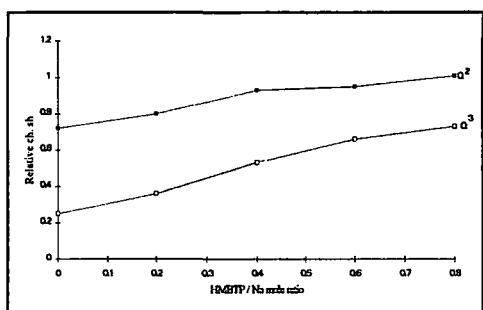
(k)
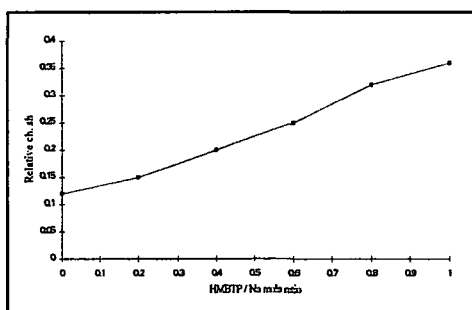
(l)
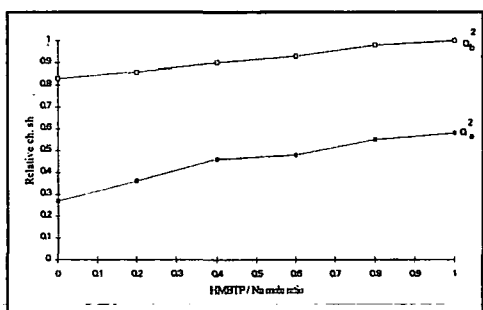
(m)
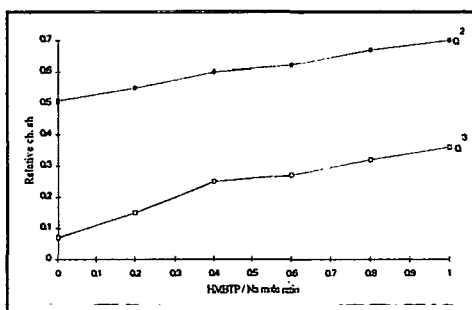
(n)
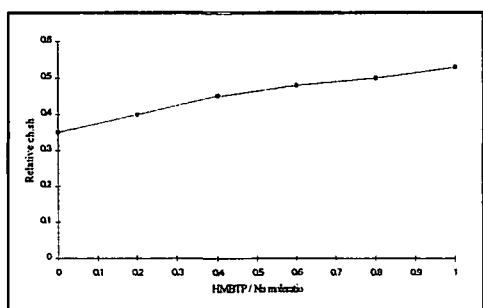
(o)
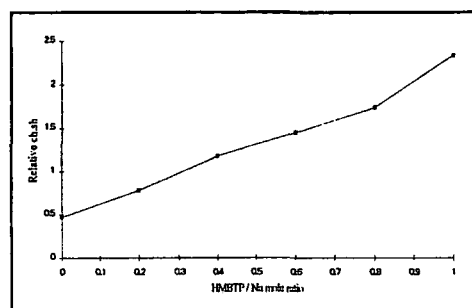
(p)

Figure 19. Chemical shift dependence for the silicate anions as a function of the concentration of HMBTP in HMBTP/Na silicate solutions. (a) Linear trimer(II), (b) branched cyclic trimer (V), (c) branched cyclic tetramer (VII), (d) cyclic trimer (IV), (e)

tricyclic hexamer (cisoid) (XIII), (f) tricyclic hexamer (transoid) (XII), (g) bridged cyclic tetramer (VIII), (h) doubly bridged cyclic tetramer (IX), (i) tricyclic octamer (XVII), (j) tricyclic hexamer (XI), (k) bicyclic octamer (XVI), (l) cyclic tetramer (VI), (m) bicyclic pentamer (X), (n) tetracyclic octamer (XXI), (o) prismatic hexamer (XIV) and (p) cubic octamer (XIX). The number in parentheses refers to the structures presented in Figure 2.

Although there is no clear evidence for the direct interaction of the silicate anions and the cations (i.e. HMBTP and Na), it can be seen that the chemical shifts of the species present in the silicate solution are influenced by changing the HMBTP/Na mole ratio. The chemical shifts versus the HMBTP/Na mole ratio for the species have different slopes. The clear example is the cubic octamer. This fact suggests that there might be some interaction between cations and anions in silicate solutions, since this particular species, cubic octamer, is highly affected by variation of the HMBTP concentration .

The results described here provide additional evidence for structure direction by the organic base. Thus, the detection of interaction between the organic structure-directing agent and silicate species has broad implications for the design and synthesis of new zeolites. The structural features of the product can perhaps be controlled through the judicious choice of an organic species that can interact with the silicate anions in a specific manner as determined by optimizing electrostatic interactions.

3.10.2.7. NMR studies of nuclei other than silicon-29

Hitherto we discussed anions in silicate solutions through the interpretation of ^{29}Si NMR spectra. Although it is anticipated that the chemical shifts of nuclei which come from the cations will not change substantially, it is pertinent to study the NMR of relevent nuclei.

^{1}H NMR studies of silicate solutions. Hydrogen atoms are present in HMBTP/Na silicate solutions either in the cations (i.e. HMBTP) or as H_2O. Also, hydrogen atoms may be present in SiOH sites but the exchange rate of hydrogen in this form (with water) is rapid on the NMR time scale.

The ^{1}H NMR spectrum of HMBTP/Na silicate solution is shown in Figure 20. From the chemical structure of HMBTP, two peaks can be expected, which arise from CH_3 and CH_2 groups. Clearly the large peak at 4.8 ppm is assigned to protons in water
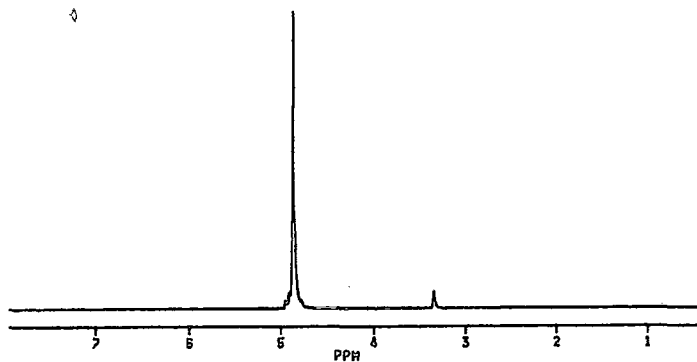
Figure 20. 250 MHz ^{1}H NMR spectrum of the HMBTP/Na silicate solution (HMBTP:Na = 0.6:0.4) at a Si/cation ratio of 1.0 with SiO_2 concentration of 5.78 wt% at ambient probe temperature (ca. 24°C).
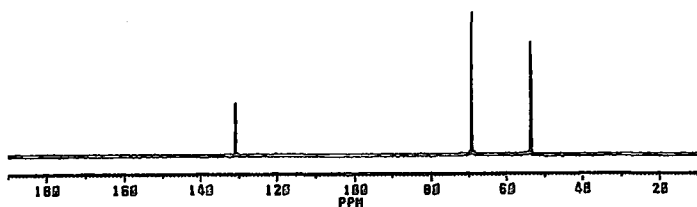
Figure 21. 62.85 MHz ^{13}C NMR spectrum of the HMBTP/Na silicate solution (HMBTP:Na = 0.6:0.4) at a Si/cation ratio of 1.0 with SiO_2 concentration of 5.78 wt% at ambient probe temperature (ca. 24°C).

molecules, overlapped by the CH_2 proton resonance (there are six equivalent CH_2 groups as well as six equivalent CH_3 groups in the HMBTP cation).

Obviously, the chemical shift of ^1H in CH_2 does not change in different HMBTP/Na silicate solutions, from which it can be realised that no direct interaction occurrs between HMBTP cations and anionic silicate species. Of course, the intensity of the signals increases with increasing HMBTP : Na mole ratios.

^{13}C *NMR studies of HMBTP/Na silicate solutions.* The ^{13}C chemical shift is sensitive to the environment of the carbon nucleus, and ^{13}C NMR spectra in general display narrow and well-resolved lines for each kind of distinct carbon atom of the organic species in silicate solutions. Using the HMBTP cation this particular matter has been studied.

Figure 21 shows a typical ^{13}C NMR spectrum of an HMBTP/Na silicate solution. The same spectrum was observed with different HMBTP : Na ratios. Comparison of ^{13}C NMR spectra for these solutions reveals no difference in carbon chemical shifts (as can be seen, there are three signals at shifts ca. 131.8, 69.1 and 53.2 ppm that are assigned to quaternary, CH_2 and CH_3 carbons respectively), but as expected the signal to noise improves with increasing HMBTP:Na mole ratio.

However, comparison of ^{13}C NMR spectra for HMBTP/Na silicate solutions with the parent HMBTP cation (hydroxide form, i.e. $HMBTP(OH)_3$) reveals a slight difference in chemical shifts, i.e. quaternary, CH_2, and CH_3 carbons shift to high frequency by as much as 0.66, 0.71 and 0.72 ppm respectively.

These results also indicate that there is no substantial interaction between HMBTP cations and silicate anions present in the silicate solution. The difference in chemical shifts of the carbons in HMBTP hydroxide and HMBTP/Na silicate solutions can come from the different solution media.

^{23}Na *NMR studies.* The ^{23}Na NMR nucleus has spin I=3/2, a large quadrupole moment and 100% natural abundance. In solution, rapid isotropic molecular tumbling averages the quadrupolar interaction. Consequently, only a single NMR absorption is usually seen. However, in many cases, the averaging is not sufficient to give a sharp NMR line.

In this case, as expected, the chemical shift of the sodium cation does not change visibly with the HMBTP/Na ratio. ^{23}Na NMR spectra were carried out at ambient temperature (ca. 24°C), and a typical ^{23}Na NMR spectrum is shown in Fig. 22.
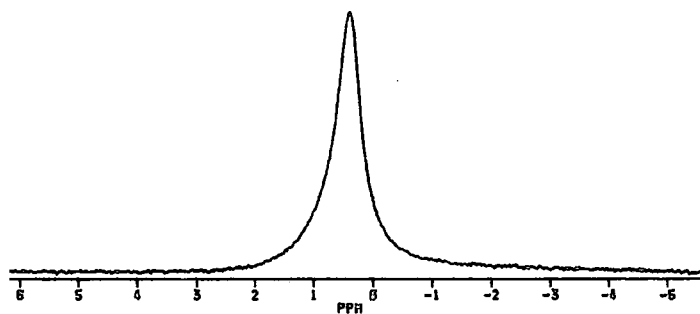
Figure 22. 66.13 MHz ^{23}Na NMR spectrum of the HMBTP/Na silicate solution (HMBTP:Na = 0.6:0.4) at a Si/cation ratio of 1.0 with SiO_2 concentration of 5.78 wt% at ambient probe temperature (ca. 24°C).Chemical shifts are referenced to 1M NaCl solution.

3.10.3. Effect of cation-to-Si ratio and silica concentration on silicate anion distribution in HMBTP silicate solutions

3.10.3.1. *Characterisation of the HMBTP silicate solutions at constant cation concentration*

It was found that the degree of polymerisation of silicate anions present in silicate solutions increases with decreasing cation-to-Si ratio and increasing silica concentration.

In this experiment three aqueous HMBTP silicate solutions with different SiO_2/HMBTP mole ratios (no sodium hydroxide was added) were studied. In all of the solutions the concentration of HMBTP was held constant (Table 4). To make silicate solutions with different ratios of Si/HMBTP the concentration of silica was increased. Preparation with a high concentration of silica needed heating at ca. 45°C for about one week to dissolve the SiO_2 completely and to obtain a clear solution. Figures 23a-23c show the ^{29}Si NMR spectra of solutions with SiO_2/HMBTP = 1, 3 and 4 respectively.

Table 4. Data for the HMBTP silicate solutions (constant cation concentration)*

Si/HMBTP	wt% SiO_2
1	5.8
3	7.5
4	8.1

* All solutions contain 19 wt% of HMBTP and ca. 20 wt% of D_2O.

Comparison of integration between two regions, Q^3_6 (prismatic hexamer and related compounds) and Q^3_8 (cubic octamer and related compounds), reveals that with increased SiO_2/HMBTP ratio, the intensity of the latter becomes larger than that of the former. Therefore it can be concluded that at higher SiO_2/HMBTP mole ratios i.e. SiO_2/HMBTP=4, the degree of polymerisation is increased and Q^3_8 becomes more stable than the other species.

3.10.3.2. *Study of ^{29}Si NMR spectra for different Si/HMBTP ratios at constant silica concentration*

In this experiment HMBTP silicate solutions with different Si/HMBTP mole ratios were studied, but with constant concentration of silica (ca. 6 %wt silica). The ^{29}Si NMR spectra are shown in Figures 24a-24d. The number of species in the silicate
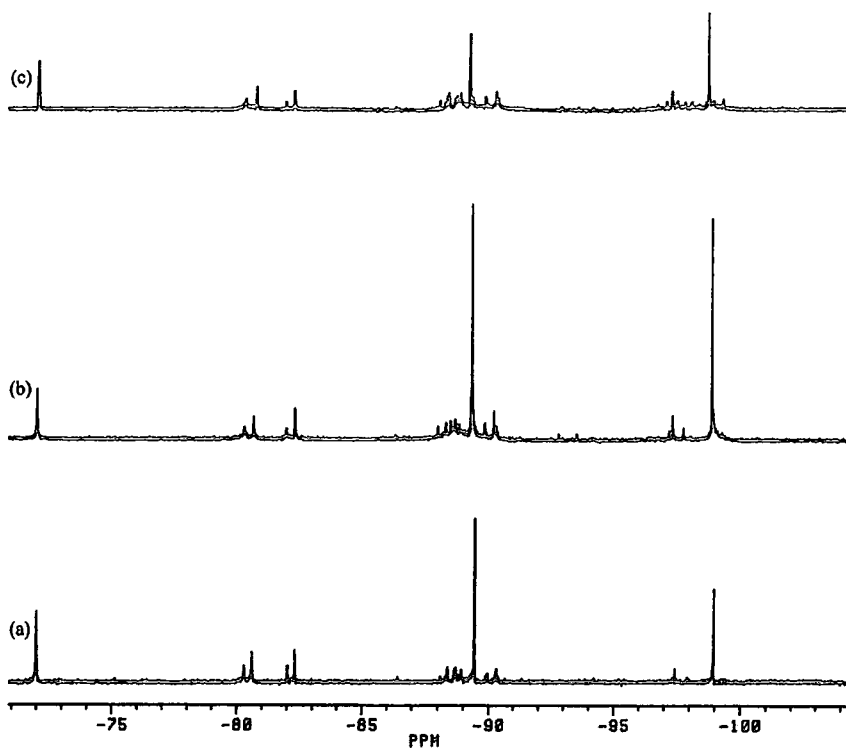
Figure 23. 49.50 MHz ^{29}Si NMR spectra of HMBTP silicate solutions with different ratios Si/HMBTP at constant concentration of the HMBTP cation (19 wt%HMBTP). (a) Si/HMBTP=1, (b) Si/HMBTP=3 and (c) Si/HMBTP=4. All spectra were carried out at ambient probe temperature of ca. 24 °C. The samples were prepared with ca. 15 wt% of D_2O to provide a (^{2}H) lock signal. Spectral parametrs: 50 s recycle delay; 4950 Hz total spectral width; 16384 data points; 1000 transients for each spectrum. All spectra plotted on the same scale and absolute intensity.

solutions increases with increasing Si/ HMBTP mole ratio, i.e. with decreasing HMBTP concentration. The most important observation is a relative decrease in the intensity of the signals assigned to the prismatic hexamer, $Q^3{}_6$, and cubic octamer, $Q^3{}_8$. However, it seems that the number of signals in the prismatic hexamer and cubic octamer regions is considerably increased with increasing Si/HMBTP mole ratio (i.e. decreasing HMBTP concentration). The narrow lines, especially for Q^0 show that exchange between silicate anions is slow on the NMR time scale, so therefore broad peaks in the $Q^2/Q^3{}_\Delta$ and Q^3 regions can be ascribed to an increase of the number of signals. This phenomenon indicates that the $Q^3{}_6$ and $Q^3{}_8$ are breaking up, the fragments being still associated to the prismatic and cubic octamer regions of the spectrum. As a conclusion, it can be said that the broad peaks arise from the appearance of a number of signals which cannot be resolved separately, not from exchange processes .

This observation once again strongly supports the role of the structure-directing HMBTP cation, which demonstrates that in low concentration of the HMBTP cation the silicate anions are not directed to the cage-like species $Q^3{}_6$ and $Q^3{}_8$, but to broken cages and small oligomeric anions.

However, it should be noticed that the pH of the silicate solutions decreases with increasing Si/HMBTP ratio (Table 5), i.e. the solutions become less basic. This is a critical parameter, since a study of the effect of pH on the distribution of silicate anions shows a similar situation (see below).

Table 5. Data for the HMBTP silicate solutions*.

Silica/HMBTP	pH	wt% HMBTP
3	12.3	13.25
4	12	9.53
5	11.8	8.14
6	11.7	6.28

* All solutions contain 6 wt% of SiO_2 and ca. 20 wt% of D_2O.

3.10.4. Effect of temperature

The characterisation of solutions at room temperature, as explained in the preceding section, is only a first step when one wants to investigate stages of zeolite formation. This synthesis process takes place at elevated temperatures, and therefore the
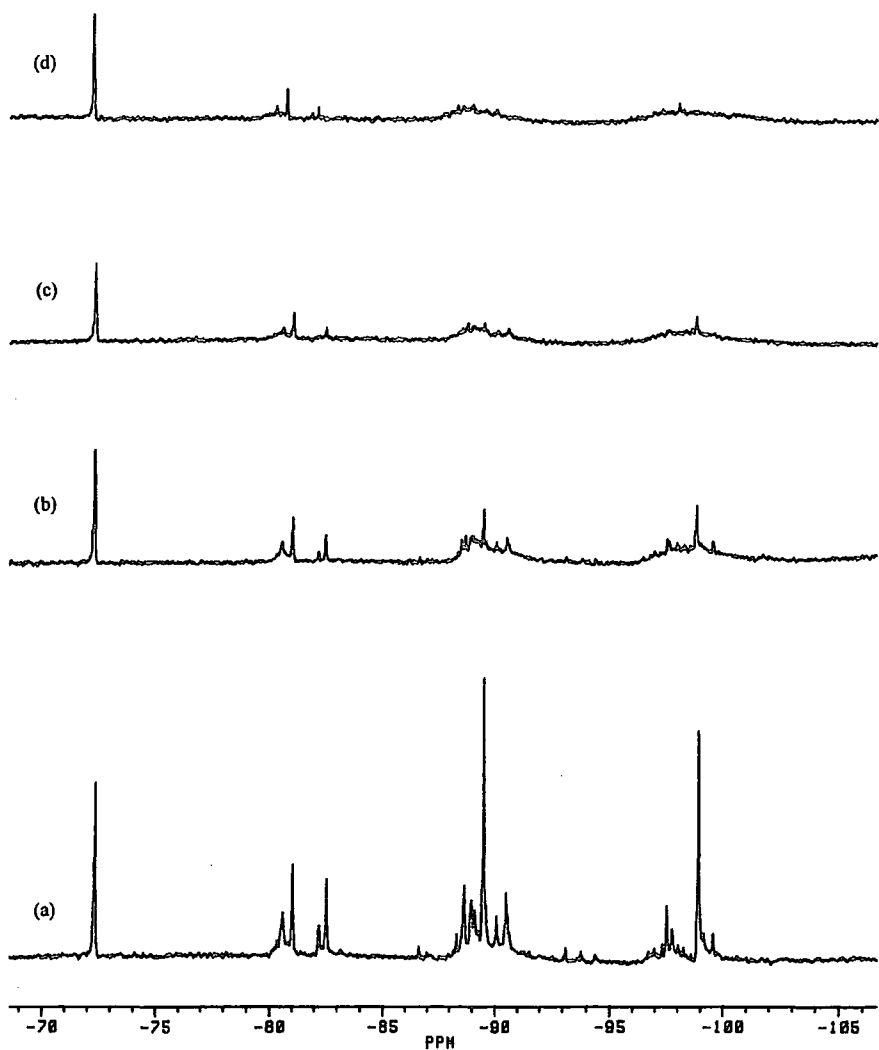
Figure 24. 49.50 MHz ^{29}Si NMR spectra of HMBTP silicate solutions with different ratios Si/HMBTP at constant concentration of silica. (6 wt%SiO$_2$). (a) Si/HMBTP=3, (b) Si/HMBTP=4, (c) Si/HMBTP=5 and (d) Si/HMBTP=6. All spectra were carried out at ambient probe temperature of ca. 24 °C. The samples were prepared with ca. 15 wt% of D$_2$O to provide a (^{2}H) lock signal. Spectral parametrs: 50 s recycle delay; 4950 Hz total spectral width; 16384 data points; 1000 (a), 1100(b), 1120(c) and (d) 1450 transients. All spectra are drawn on the same scale and with absolute intensity.

solution studies were extended to higher temperatures. ^{29}Si NMR spectra were examined at elevated temperature for HMBTP silicate solutions, particularly with high Si/cation ratio or high concentration of silica. The probe temperature was calibrated by using 100% of ethylene glycol in the range of temperature from 25 to 85 °C.

An aqueous HMBTP silicate solution with Si/cation = 4 (wt% SiO_2 = 8.1) was followed at different temperatures by ^{29}Si NMR spectra. Since an increase in temperature causes a lowering of signal-to-noise, it is necessary to carry out more transients to achieve a good quality of spectrum. However, due to the restrictions on time for using the spectrometer, it was not feasible to entirely compensate. Figures 25a-25d show the ^{29}Si NMR spectra of HMBTP silicate solutions at 25, 50, 65 and 80°C respectively. To achieve better signal-to-noise the number of transients, and consequently the experimental time for each spectrum was increased with rising temperature. Data for this series of experiments are shown in Table 6.

Table 6. Data for variable temperature experiments*.

Temperature (°C)	Number of transients	Exp. time (hours)
25	1000	14
50	1300	18.5
65	1400	20
82	1777	25

* All solutions contain the same ratio of Si/HMBTP=4 and a similar

concentration of silica (i.e. 8.1 wt%), together with ca. 20 wt% of D_2O.

The changes in the silicate solution with temperature are found to be fully reversible. As a result, it is possible to use exclusively the same HMBTP silicate solution for all temperatures. The ^{13}C NMR spectra of the silicate solutions proved that no change is involved in the chemical structure for HMBTP at elevated temperatures. The ^{13}C NMR spectrum of HMBTP silicate obtained at the end of this series of experiments indicates no difference from the ^{13}C NMR spectrum (Figure21) before doing variable temperature experiments.

Upon a temperature increase, the silicate solution (Si/HMBTP =4) showed a general trend towards the formation of silicate anions of lower molecular weight. The ^{29}Si NMR spectra of HMBTP silicate solutions illustrate that at difference temperatures
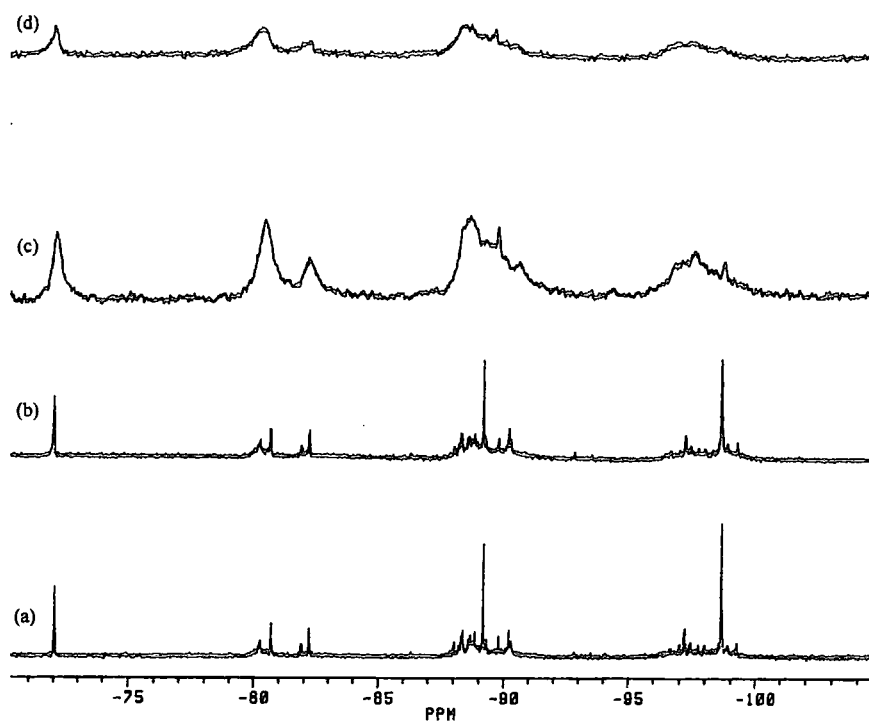
Figure 25. 49.50 MHz ^{29}Si NMR spectra of the HMBTP silicate solutions at variable temperature with the Si/HMBTP ratio of 4 and 8.1 wt% of silica. (a) 24°C, (b) 52°C, (c) 65°C and (d) 80°C. The samples were prepared with ca. 15 wt% of D_2O to provide a (^{2}H) lock signal. Spectral parametrs: 50 s recycle delay; 4950 Hz total spectral width; 16384 data points; 1000 (a), 1300 (b), 1400 (c) and 1777 (d) transients. All spectra are plotted the same scale and absolute intensity.

the fraction of silicates present as cage-like species, Q^3_6, Q^3_8, diminishes for temperature $\geq 65°C$ (Figures 25c & 25d), but even at 82°C there are still some Q^3_6 and Q^3_8 left. Apparently, the disappearance of Q^3_6 and Q^3_8 is accompanied by the formation of more silicates of lower molecular weight : monomer, Q^0, dimer, Q^1_2, linear trimer, $Q^1Q^2Q^1$, and cyclic trimer, Q^2_Δ.

At the lowest temperature, 25°C (Figure 25a), five narrow peaks originating from Q^0, Q^1, Q^2_Δ, Q^3_6 and Q^3_8 are seen. With increasing temperature considerable line broadening , especially of Q^0, Q^1, Q^2_Δ peaks, is clearly visible. It is concluded, therefore, that a dynamic exchange of SiO_4^{4-}, i.e. Q^0, takes place between monomeric, dimeric and oligomeric chain silicates (preferably trimeric and tetrameric species), the rate of which increases with increasing temperature. The exchange equilibria may be described schematically by the following reactions.

$$2Q^0 \Leftrightarrow Q^1_2 \qquad\qquad (3)$$

$$Q^0 + Q^1_2 \Leftrightarrow Q^1 Q^2 Q^1 \qquad\qquad (4)$$

$$Q^0 + Q^1 Q^2 Q^1 \Leftrightarrow Q^1 Q^2 Q^2 Q^1 \qquad\qquad (5)$$
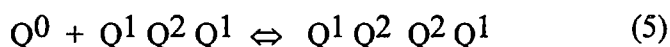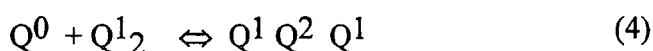
Knight et al.[33], by using ^{29}Si 2D chemical exchange (EXSY) NMR experiments on potassium silicate solutions showed that both inter- and intra-molecular exchange processes occur in solution. For example, some of the exchange processes are presented in scheme 1[33].

$$Q^0 + Q^0 \rightleftharpoons Q^1 Q^1 \tag{6}$$

$$\text{Q}^1\!\diagdown\!\text{Q}^2\!\diagup\!\text{Q}^1 \rightleftharpoons \triangle\,(Q^2,\,Q^2\text{—}Q^2) \tag{7}$$

$$Q^1\text{—}Q^2\!\diagup\!{}^{*1}\!Q \rightleftharpoons {}^{*2}\!Q\ (Q^2\text{—}Q^2) \rightleftharpoons Q^2\!\diagdown\!{}^{*1}\!Q / Q^1 \tag{8}$$

$$\Updownarrow\ {}^{*2}\!Q\!\diagup\!Q^1\ \diagdown Q^1$$

$$Q^0 + {}^{*2}\!Q\,(Q^2\text{—}Q^2) \rightleftharpoons Q^1\text{—}{}^{*3}\!Q\ (Q^2,\ Q^2) \tag{9}$$
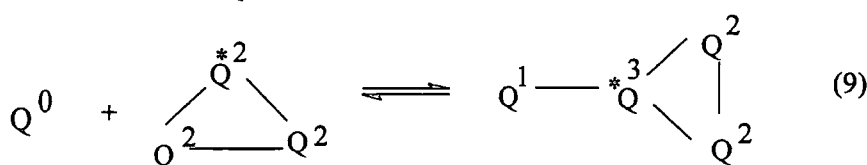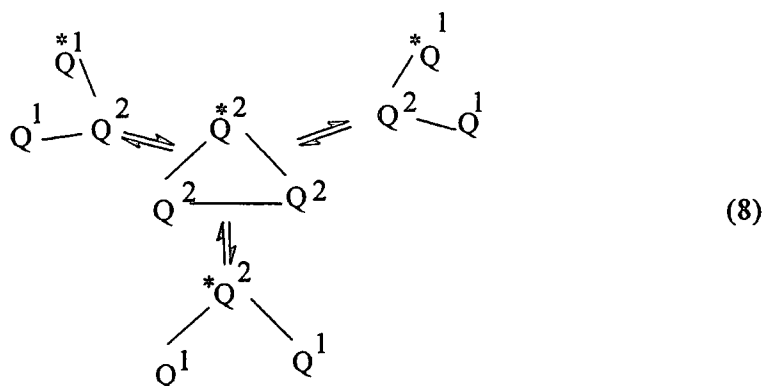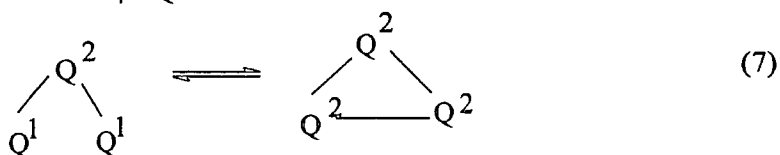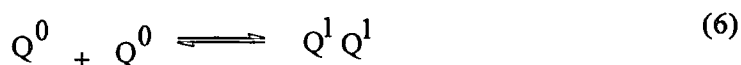
Scheme 1. Schematic representation of some of the exchange processes among the silicate species[33].

The peaks of the prismatic hexamer and cubic octamer are comparatively less broadened, which indicates that these species show slower exchange rates than the others. This is perhaps to be expected, since any exchange process involving cyclic species requires ring opening and closure. However, as mentioned above , upon a temperature increase, HMBTP solution shows a general trend towards the formation of silicate anions of lower molecular weight. Therefore, it can be realised that the $Q^3{}_6$ and $Q^3{}_8$ species might be converted to the species which are related to the prismatic hexamer and cubic octamer respectively (e.g. species X-XIII & XVI-XVIII) or (and finally) to the smaller species (e.g. Q^0 and Q^1). As a result, the HMBTP silicate solution loses the stability of $Q^3{}_6$ and $Q^3{}_8$ as the temperature is increased.

Qualitatively, the various observation of the distribution of cage-like species with varying temperature may be rationalized in terms of the depolymerization equilibria in solution. As shown above, the HMBTP silicate solutions with different Si/HMBTP mole ratios all showed the same effect. In addition, the drastic decrease in

the amount of a particular cage-like species essentially occurred only at temperatures above about 60°C.

The changes in the silicate distribution with temperature found at a particular temperature are established within a few hours at most. After heating at 80°C for 2 days and cooling to room temperature the NMR spectrum is indistinguishable from that taken before the heating.

As regards the cage-like silicates, their amount decreases in favour of low-molecular-weight species. However, Q^3_8 proves to be the most sensitive to a temperature increase. This fact can be observed in figure 25d , which is the HMBTP silicate solution recorded at 80°C. It can be said, in those cases where temperature-dependent line-broadening is observed, its primary cause must be chemical exchange.

3.10.5. Characterisation by silicon-29 NMR of HMBTP silicate solutions at different pH

It has been established above that HMBTP silicate solutions containing different Si/HMBTP ratios behave in a similar manner with respect to the occurrence of the various cage-like silicates as a function of the Si/HMBTP ratio. However, it remains to be seen whether it is the Si/HMBTP or the pH of the solution which plays a decisive role. Several HMBTP silicate solutions were made with the same Si/HMBTP ratio and silica concentration but with different pH, i.e. from pH=13.4 to pH=11.8. The pH of these solutions was adjusted by the addition of a few drops of HCl. The change in concentration of silicon was minimised by using concentrated acid, which was added in a thin stream to the vigorously-stirred solutions. Samples were withdrawn for recording ^{29}Si NMR spectra at intervals of about 0.5 pH units. However, making a silicate solution with a pH of 11.5 was not successful due to precipitation of silica, and the lowest pH for which clear solution was achieved after adding acid (and indeed shaking the solution vigorously) was found to be pH=11.8. Figure 26 shows the ^{29}Si NMR spectra obtained at different pH values from HMBTP silicate solutions with 5.7 wt% SiO_2 and a Si/HMBTP ratio of 1 at ambient temperature (ca. 24 °C).

With increasing pH considerable change occurs in the characteristics of the silicon-29 NMR spectra. Figures 26a-26e clearly illustrate that by decreasing the pH (i.e. in less basic solutions) the signals associated with the cubic octamer, Q^3_8, and prismatic hexamer, Q^3_6, are decreased. This phenomenon indicates that such cage-like species are destabilized at the lower pH. However it is noted that there is an increase in
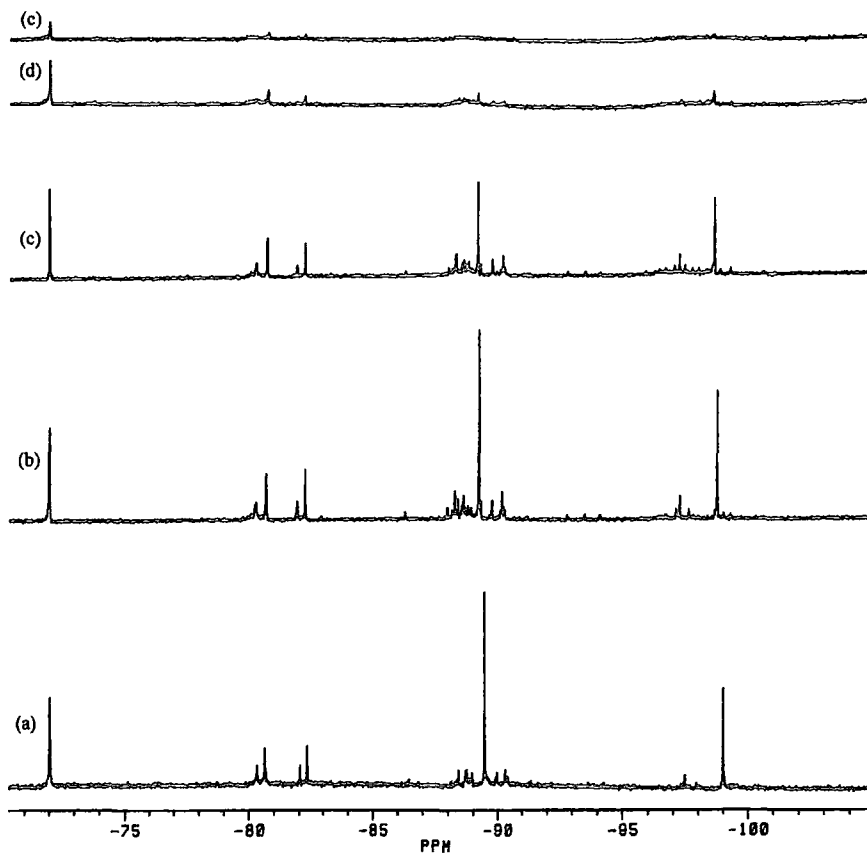
Figure 26. 49.50 MHz ^{29}Si NMR spectra of the HMBTP silicate solution at different pH, with a Si/HMBTP ratio of 1 and 5.87 wt% of ailica. (a) pH=13.4, (b) pH=13.0, (c) pH=12.5, (d) pH=12.0 and (e) pH=11.8. The samples were prepared with ca.15 wt% of D_2O to provide a (^{2}H) lock signal. Spectral parameters: 50 s recycle delay; 4950 Hz total spectral width; 16384 data points; 1000 (a), 1000 (b) 1415 (c), 1203 (d) and 1518 (e) transients. All spectra were carried out at ambient probe temperature (ca. 24°C). They are plotted on the same scale and absolute intensity.

the number of lines in the prismatic hexamer (ca. -87 to -91.5 ppm) and cubic octamer (ca. -97 to -99.5 ppm) regions at a pH of 13 and 12.5 (Figures 26b &26c respectively). It can be deduced from the appearance of these signals that there is partial depolymerization of the Q^3_6 and Q^3_8 species to smaller fragments. Breaking up the Q^3_8 and Q^3_6 species also proceeds in lower pH, so that at the lowest pH (pH=11.8, Fig. 26e) not enough Q^3_6 and Q^3_8 exist to observe their signals. An analogous situation might be occurring for Q^1_2 and Q^2_Δ. At the lowest pH (11.8) only a small peak ascribed to Q^0 and a very small peak associated with Q^1 and Q^2_Δ can be observed. It is very important to note that the peaks ascribed to Q^0 , Q^1_2, Q^2_Δ, Q^3_6 and Q^3_8 show narrow lines in varied pH, even at the lowest pH at which signals are observable. This fact shows that the exchange process between the silicate species is slow on the NMR timescale. However, monomer remains the most abundant species at the lowest pH, but the main mass of silica is found in progressively more and more highly polymerised form as the pH falls. There are a number of silicate species with small mole fractions and different chemical shifts (but very close to each other, i.e. in the regions of Q^1, Q^2_Δ , Q^2/Q^3_Δ and Q^3_8), which makes it impossible to observe separate signals.

Qualitatively, the variation observed in the distribution of silicate species with varying pH may be rationalized in terms of the polymerization equilibria in solution, which can be described schematically by the following exchanges[34].

$$2\,HO\underset{O_-}{\overset{O^-}{\underset{|}{\overset{|}{Si}}}}OH \;+2\,H^+ \rightleftharpoons HO\underset{OH}{\overset{O^-}{\underset{|}{\overset{|}{Si}}}}O\underset{OH}{\overset{O^-}{\underset{|}{\overset{|}{Si}}}}OH \;+H_2O \qquad (10)$$

$$HO\underset{O_-}{\overset{O^-}{\underset{|}{\overset{|}{Si}}}}OH \;+\; HO\underset{O_-}{\overset{O^-}{\underset{|}{\overset{|}{Si}}}}O\underset{O_-}{\overset{OH}{\underset{|}{\overset{|}{Si}}}}O\underset{O_-}{\overset{OH}{\underset{|}{\overset{|}{Si}}}}O\cdots +2H^+ \rightleftharpoons HO\underset{O_-}{\overset{OH}{\underset{|}{\overset{|}{Si}}}}O\underset{O_-}{\overset{OH}{\underset{|}{\overset{|}{Si}}}}O\underset{O_-}{\overset{OH}{\underset{|}{\overset{|}{Si}}}}O\underset{O_-}{\overset{OH}{\underset{|}{\overset{|}{Si}}}}O\cdots +H_2O \quad (11)$$
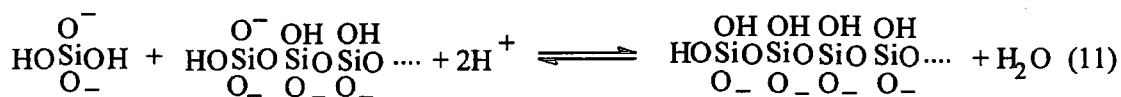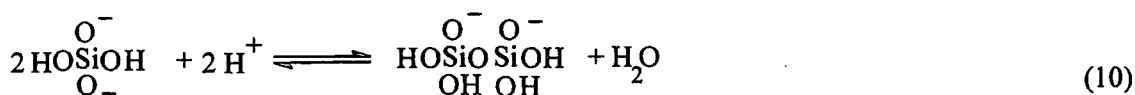
Equations 10 & 11 show that at lower pH the oligomerization is favoured. Therefore it can be realized that decrease of the signal assigned to Q^0 (SiO_4^{4-}) can arise from the involvement of this silicate anion in the above equilibria, i.e. conversion of monomer to the polymeric species.

Meanwhile, it should be mentioned that the ^{29}Si spectrum obtained from the lowest pH by the inverse-gated method (i.e. decoupling on during acquisition time and off during recycle delay, because silicon has a negative gyromagnetic ratio) gave no improvement in line broadening. However, the protonation-deprotonation process might be happening in lower pH (i.e. more acidic solution), but the rate of this process is out

side the NMR time in relation to coupling between ^1H to ^{29}Si nuclei so as to cause line broadening. In this connection, Swaddle et al.[35] suggested a modified symbol $^xQ^y$ to denote a Si centre with y co-ordinated bridging oxygen atoms and (4-y) terminal hydroxyls of which x are deprotonated. For example the following equation denotes deprotonation of $^1Q^0$ to give $^2Q^0$.

$$^1Q^0 + OH^- \leftrightarrow {}^2Q^0 + H_2O \ . \tag{13}$$
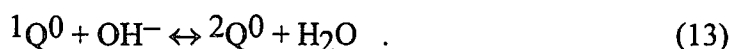
It is supposed that the polymerization could proceed by electrophilic attack of $Si(OH)_4$ on the $-O^-$ ligands of the various Si^{IV} centres. General experience[36-38] suggests expansion of the coordination number of $Si(OH)_4$ (associative attack on O in - O-Si≡), followed by elimination of H_2O or OH^-, as the most likely pathway[39]:

$$(HO)_4Si + {}^-OSi\equiv \leftrightarrow {}^-(HO)_4Si\text{-}O\text{-}Si\equiv \leftrightarrow {}^-O(HO)_2Si\text{-}O\text{-}Si\equiv + H_2O \tag{14}$$
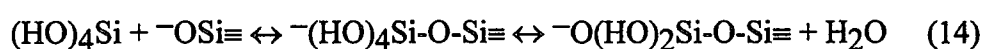
3.10.6. Characterisation by ^{29}Si NMR spectra of hexaalkylbenzotripyrrolium silicate solutions

This section deals with the study of three hexaalkylbenzotripyrrolium silicate solutions. The chemical structure of these compounds is shown in Figure 27, the only difference in the formulae being in the alkyl chain. ^{13}C NMR spectra of these compounds are shown in Figure 28.
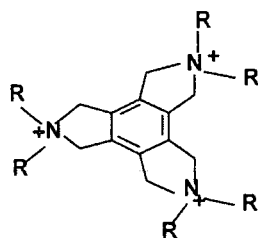
Fig. 27. Chemical structure of hexaalkylbenzotripyrrolium hydroxide, (methyl, R= CH_3; ethyl, R =CH_2CH_3; n-propyl; R = $CH_2CH_2CH_3$).

Three silicate solutions with the same silica concentration were made using (2,3,4,5,6,7,8,9-octahydro-2,2,5,5,8,8-hexamethyl-2H-benzo(1,2-c:3,4-c':5,6-c")tripyrrolium)$^{+++}$(HMBTP); 2,3,4,5,6,7,8,9-octahydro-2,2,5,5,8,8-hexaethyl-2H-benzo(1,2-c:3,4-c':5,6-c")tripyrrolium)$^{+++}$(HEBTP); 2,3,4,5,6,7,8,9-octahydro-2,2,5,5,8,8-hexpropyl-2H-benzo(1,2-c:3,4-c':5,6-c")tripyrrolium)$^{+++}$(HPBTP).
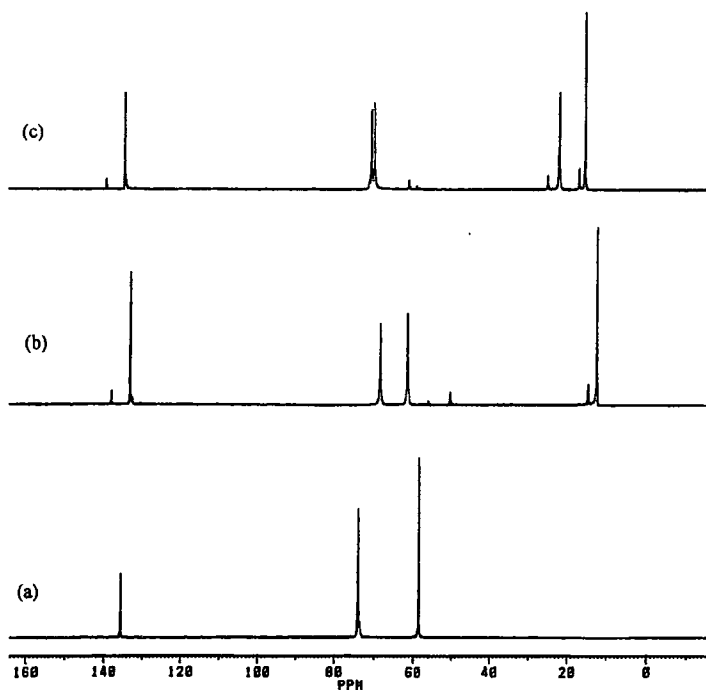
Figure 28. 62.85 MHz ^{13}C NMR spectrum of the HABTP.(a) HMBTP, (b) HEBTP and (c) HPBTP. Spectral parameters: 10 s recycle delay; 19230 Hz total spectral width; 16384 datapoints; 100 transients for each spectrum. All spectra were carried out at the ambient probe temperature (ca. 24°C). They are plotted on the same scale and absolute intensity.

Si/cation mole ratios and silica concentrations of all solutions were held constant (Si/cation = 1 and %wt SiO_2 = 5.78) and the pH values of these solutions were to be adjusted the same.

In figures 29a-29c are shown the ^{29}Si NMR spectra of HMBTP, HEBTP and HPBTP silicate solutions respectively. Assignments of the signals were discussed in previous sections. The structure-directing property is clearly demonstrated by these spectra. Although the silica concentrations, cation-to-Si ratios, and pH values of the solutions are equivalent, a broad distribution of silicate anions is observed in the Q^3_8 region for the ^{29}Si NMR spectra of HEBTP and HPBTP silicate solutions in contrast to the intense signal due to Q^3_8 in the ^{29}Si NMR of HMBTP silicate, i.e. HMBTP stabilises the cubic octamer more than HEBTP and HPBTP. Figure 29c indicates that the distribution of signals in the Q^3_6 region for the ^{29}Si NMR of HPBTP silicate is totally different from that of HMBTP silicate. It is interesting to notice for the HPBTP silicate solution the presence of the bridged cyclic tetrameric and doubly bridged cyclic tetrameric anions (structure VIII & IX respectively), which give rise to sharp and intense peaks at -86.3 & -86.7 ppm (Q^2-sites) and -93.4 & -94.1 ppm (Q^3-sites) in the ^{29}Si NMR spectrum. Neither species is detectable in the ^{29}Si NMR spectrum of HMBTP silicate solution. The existence of these species and other intense signals in the Q^3_6 & Q^3_8 regions illustrates that, under the same circumstances, HPBTP does not stabilise Q^3_6 & Q^3_8 species as much as HMBTP. The analogous situation to that of HPBTP can be seen by comparison of the ^{29}Si NMR spectra of HEBTP silicate and HMBTP silicate solutions. However, the spectra of HEBTP and HPBTP solutions show a number of lines in the Q^3 region (i.e. -95.5 to -99 ppm), indicating that, although those cations do not stabilize the cubic octamer, the polymerization of silicate anion is favoured by their presence.

The extent to which cage-like silicates become formed depends on the solvation of the HABTP/cage-like cluster. In water one may expect the solvation to become more difficult the longer the hydrophobic alkyl chain, and this may very well explain the finding that cage-like silicates are far less abundant in aqueous HEBTP and HPBTP silicate solutions than in HMBTP silicate solution. Groenen et al.[44] also found a similar situation by a study of TAA silicate solutions. They explained that, upon addition of DMSO, the fraction of cage-like silicates increases in all TAA silicate solutions, and
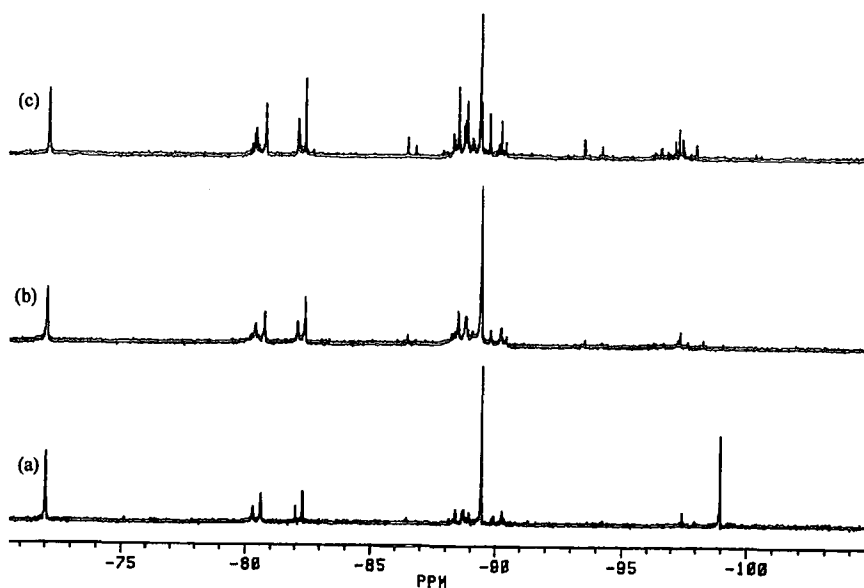
Figure 29. 49.50 MHz ^{29}Si NMR spectra of HABTP silicate solutions with similar compositions of Si/cation=1 and the same pH value. (a) 2,3,4,5,6,7,8,9-octahydro-2,2,5,5,8,8-hexamethyl-2H-benzo(1,2-c:3,4-c′:5,6-c″)tripyrrolium (HMBTP) silicate (b) 2,3,4,5,6,7,8,9-octahydro-2,2,5,5,8,8-hexaethyl-2H-benzo(1,2-c:3,4-c′:5,6-c″)tripyrrolium (HEBTP) silicate and (c) 2,3,4,5,6,7,8,9-octahydro-2,2,5,5,8,8-hexapropyl-2H-benzo(1,2-c:3,4-c′:5,6-c″)tripyrrolium (HPBTP) silicate solution. The samples were prepared with ca. 15 wt% of D_2O to provide a (^{2}H) lock signal. Spectral parameters: 50 s recycle delay; 4950 Hz total spectral width; 16384 data points; 1000 transients for each spectrum. All spectra were carried out at ambient probe temperature (ca. 24°C). They are plotted on the same scale and absolute intensity.

apparently the solvation improves so much that cage-like silicates become abundant in TPA and TBA silicate solutions as well.

Therefore it can be realised that an additional (-CH$_2$-) group in the hydrocarbon chain has a marked influence upon the species present in hexaalkylbenzotripyrrolium silicate solutions.

3.10.7. Comparison of hexaalkylbenzotripyrrolium(HABTP) and tetraalkylammonium (TAA) silicate solutions

It is pertinent to consider and compare the ^{29}Si NMR spectra of HABTP silicate and TAA silicate solutions. Six silicate solutions were prepared at constant Si/cation mole ratio and silica concentration with HPBTP, HEBTP, HMBTP, tetrapropylammonium (TPA), tetraethylammonium (TEA) and tetramethylammonium (TMA) hydroxide as templates. All spectra were recorded under the same conditions and at ambient temperature.

3.10.7.1. Comparison of the ^{29}Si NMR spectra of TPA and HPBTP silicate solutions

Figure 30 shows the ^{29}Si NMR spectrum of TPA and HPBTP silicate solutions with the same Si/cation ratio and silica concentration. The pH of TPA silicate solution was adjusted to be equal to that of the HPBTP silicate solution. It should be noted that it was necessary to change the pH of the TPA silicate solution by only 0.1 unit of pH, which is not expected to affect the distribution of species. To prove this, the ^{29}Si spectrum of the TPA silicate solution was recorded before changing the pH. The result obtained from this experiment indicated no substantial difference from the spectrum shown in Figure 30 (lower trace). Figure 30 shows that the ^{29}Si NMR spectrum of TPA is almost precisely the same as that of HPBTP.

This indicates that the structure-forming power of TPA is entirely the same as HPBTP, and consequently the distribution of species is the same for both kinds of template. The distribution of peaks in the $Q^3{}_6$ and $Q^3{}_8$ regions reveal that both templates hinder the formation of the cage species themselves.

3.10.7.2. Comparison of the ^{29}Si NMR spectra of TEA and HEBTP silicate solutions

The analogous situation to that of Figure 30 can be seen by comparison of the ^{29}Si NMR spectra of TEA & HEBTP silicate solutions. This observation also shows that the two templates TEA and HEBTP have a closely similar influence on the distribution of the silicate species. Here also, although there are a number of lines in the $Q^3{}_8$ region, none of them shows a substantial signal for $Q^3{}_8$ itself indicating that
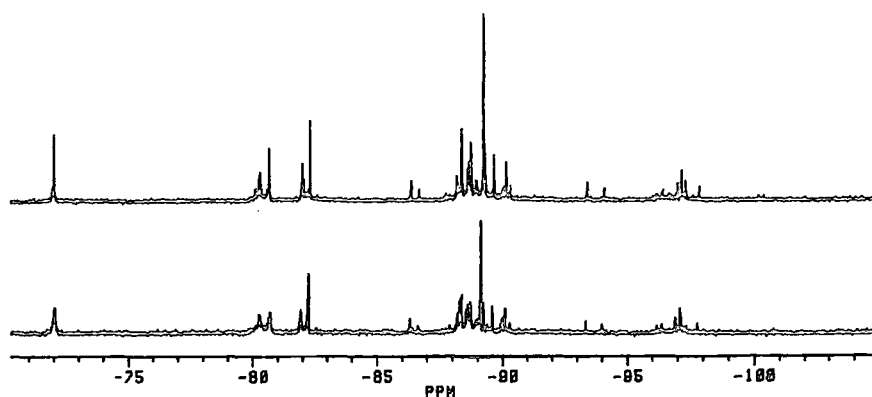
Figure 30. 49.50 MHz ^{29}Si NMR spectra of HABTP and TAA silicate solutions with the same composition of Si/cation=1 and silica concentration as well as a similar pH value. The upper trace shows the spectrum of 2,3,4,5,6,7,8,9-octahydro-2,2,5,5,8,8-hexapropyl-2H-benzo(1,2-c:3,4-c':5,6-c″)tripyrrolium (HPBTP) silicate. The lower trace shows that of the tetrapropyl ammonium (TPA) silicate solution. The samples were prepared with ca. 15 wt% of D$_2$O to provide a (^{2}H) lock signal. Both spectra were recorded at the ambient probe temperature (ca. 24 °C) and similar spectral conditions which were as follows: 50 s recycle delay; 4950 Hz total spectral width; 16384 data points; 1000 transients for each spectrum. All spectra were recorded at ambient probe temperature (ca. 24°C). They are plotted at the same scale and absolute intensity.
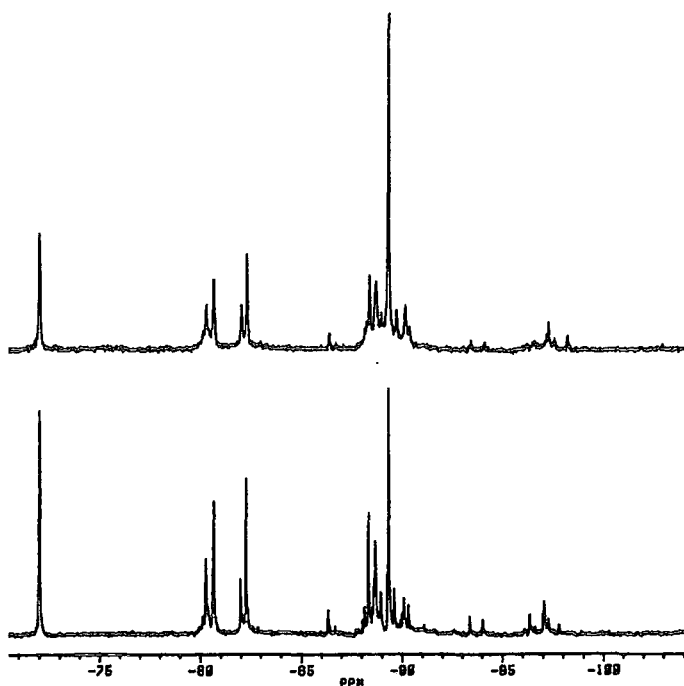
Figure 31. 49.50 MHz ^{29}Si NMR spectra of HABTP and TAA silicate solutions with the same composition of Si/cation=1 and silica concentration as well as a similar pH value. The upper trace shows the spectrum of 2,3,4,5,6,7,8,9-octahydro-2,2,5,5,8,8-hexaethyl-2H-benzo(1,2-C:3,4-C′:5,6-C″)tripyrrolium (HEBTP) silicate. The lower trace shows the teteraethyl ammonium (TEA) silicate solution. The samples were prepared with ca. 15 wt% of D$_2$O to provide a (^{2}H) lock sgnal. Both spectra were recorded at the ambient probe temperature (ca. 24 °C) and similar spectral conditions which were as follows: 50 s recycle delay; 4950 Hz total spectral width; 16384 data points; 1000 transients for each spectrum.All spectra were recorded at ambient probe temperature (ca. 24°C). They are plotted at the same scale and absolute intensity.

neither templates stabilises the cubic octamer very well. However, it seems that the HEBTP cation stabilises the $Q^3{}_6$ more than does TEA.

3.10.7.3. Comparison of the ^{29}Si NMR spectra of TMA and HMBTP silicate solutions

Figure 32 shows the ^{29}Si NMR spectra of TMA and HMBTP silicate solutions for the same conditions, i.e. Si/cation ratio of 1, silica concentration of 5.78 wt% and similar pH in the lower and upper trace respectively. In the same way as discussed in the previous section, the ^{29}Si NMR spectrum of TMA silicate solution looks very similar to that of HMBTP silicate solution. Although in general the two spectra show a very similar distribution of signals, and both templates significantly stabilise the cage-like species such as $Q^3{}_6$ and $Q^3{}_8$, nonetheless there are some differences in the distribution in the prismatic hexamer and cubic octamer regions. The intense peak of $Q^3{}_8$ in the ^{29}Si NMR spectrum of TMA silicate (Figure 32, lower trace) illustrates that the tetramethyl ammonium cation (TMA) tends mainly to stabilise cubic octamer, whereas on the other hand the considerable signal due to $Q^3{}_6$ in the ^{29}Si NMR spectrum of HMBTP silicate solution shows the stabilisation of prismatic hexamer by methyltrisquat.

3.10.7.4. Study of ^{14}N NMR spectra of HABTP and TAA hydroxides and corresponding silicate solutions

At the end of this study the ^{14}N NMR spectra of the templates were obtained to find a better understanding of the situation of templates.

The ^{14}N NMR nucleus has spin I=1, a large quadrupole moment and a 99.63% natural abundance. In solutions, rapid isotropic molecular tumbling averages the quadrupolar interaction. Consequently, only a single NMR absorption is usually seen. However, in many cases, the averaging is not sufficient to give a sharp NMR line.

The HABTP and TAA cations were studied by ^{14}N NMR in the hydroxide as well as the silicate forms.[1] All chemical shifts are referenced to 1M ammonium chloride as an external reference. The spectra were recorded using the Bruker AC250 operating at 18.6 MHz on ^{14}N NMR resonance. As can be seen all spectra show a signal at a shift of ca. 29 ppm. This signal is also observed in the blank solution (i.e. only H_2O/D_2O solution), therefore it might come from the electronic in the NMR equipment.

Figures 33 & 34 display ^{14}N NMR spectra of hydroxide and silicate forms of the TAA and HABTP cations respectively. Table 7 gives data for chemical shifts as well
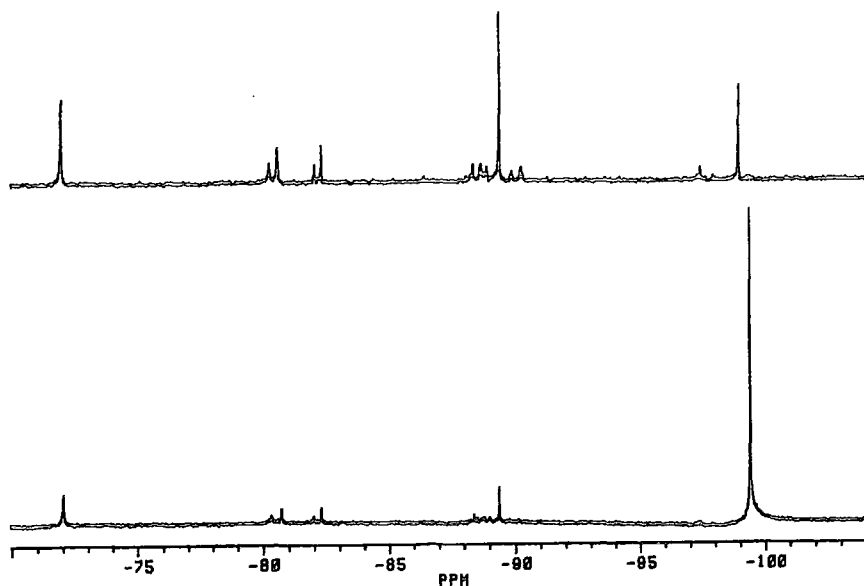
Figure 32. 49.50 MHz ^{29}Si NMR spectra of HABTP and TAA silicate solutions with the same composition of Si/cation=1 and silica concentration as well as a similar pH value. The upper trace shows the spectrum of 2,3,4,5,6,7,8,9-octahydro-2,2,5,5,8,8-hexametyl-2H-benzo(1,2-c:3,4-c':5,6-c″)tripyrrolium (HMBTP) silicate. The lower trace shows the tetramethyl ammonium (TMA) silicate solution. The samples were prepared with ca. 15 wt% of D$_2$O to provide a (2H) lock sgnal. Both spectra were recorded at the ambient probe temperature (ca. 24 °C) and similar spectral conditions which were as follows: 50 s recycle delay; 4950 Hz total spectral width; 16384 data points; 1000 transients for each spectrum. All spectra were recorded at ambient probe temperature (ca. 24°C). They are plotted at the same scale and absolute intensity.

as linewidths ($\Delta v_{1/2}$). Data were extracted from each individual ^{14}N NMR spectrum, with $\Delta v_{1/2}$ values obtained from a computer program.

Table 7. Chemical shifts and linwidths of ^{14}N for the HABTP and TAA cations in hydroxide and silicate solutions.

Sample	Chemical shift (ppm)	Linewidth ($\Delta v_{1/2}$) (Hz)
TMAOH	21	8.1
TEAOH	41	7.8
TPAOH	44	8
HMBTP(OH)3	44	ca. 34
HEBTP(OH)3	56	ca. 55
HPBTP(OH)3	60	ca. 58
TMA silicate	21	2
TEA Silicate	41	4.1
TPA Silicate	44	6.1
HMBTP Silicate	44	ca. 35
HEBTP Silicate	59	ca. 58
HPBTP Silicate	59	ca. 60

By comparison of the chemical shifts of the corresponding hydroxides and silicates it can be seen that there is no substantial difference between two solutions. This seems to indicate that there is no direct interaction between template and silicate species to change the chemical environment of nitrogen atoms. However, each particular template has a different chemical shift. For both HABTP and TAA cations the addition of the -CH$_2$ group causes the resonance line to shift to higher frequency.

Measurement of linewidths of the ^{14}N NMR spectra (figure 33) obtained from TAA hydroxide and silicate solutions reveals narrow lines (i.e. less than 8 Hz) in spite of the quadrupolar ^{14}N nucleus. However, due to the characteristics of the HABTP hydroxide and silicate solutions, which are rather viscous, they show substantially broadened peaks (Figure 34). The diluted corresponding solutions (i.e. two times) shown less broadening. A brief study of this effect was carried out using a series of TMAOH solutions made with different concentrations of the cation. The linewidth of the ^{14}N NMR signal decreases with decreasing TMA$^+$ cation concentration. However, the large size of HABTP cations is the cause of the lower mobility of these cations and consequently, the increase in line broadening.
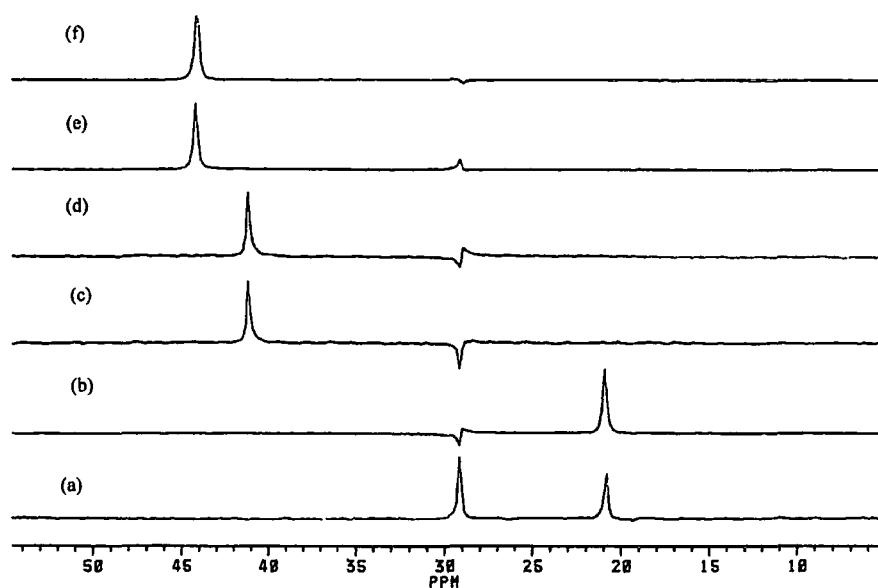
Figure 33. 18.6 MHz ^{14}N NMR spectra of TAA hydroxide and TAA silicate solutions. The percentage of the cation is the same for both hydroxide and corresponding silicate solutions. The concentration of silica is the same for all TAA silicate solutions (5.78 wt%). (a) TMA hydroxide, (b) TMA silicate (c) TEA hydroxide (d) TEA silicate (e) TPA hydroxide (f) TPA silicate solution. Spectral parameters: 1 s recycle delay; 5434.7 Hz total spectral width; 16384 data points; 100 transients for each spectrum. All spectra were recorded at ambient probe temperature (ca. 24°C). They are recorded at the same scale and absolute intensity
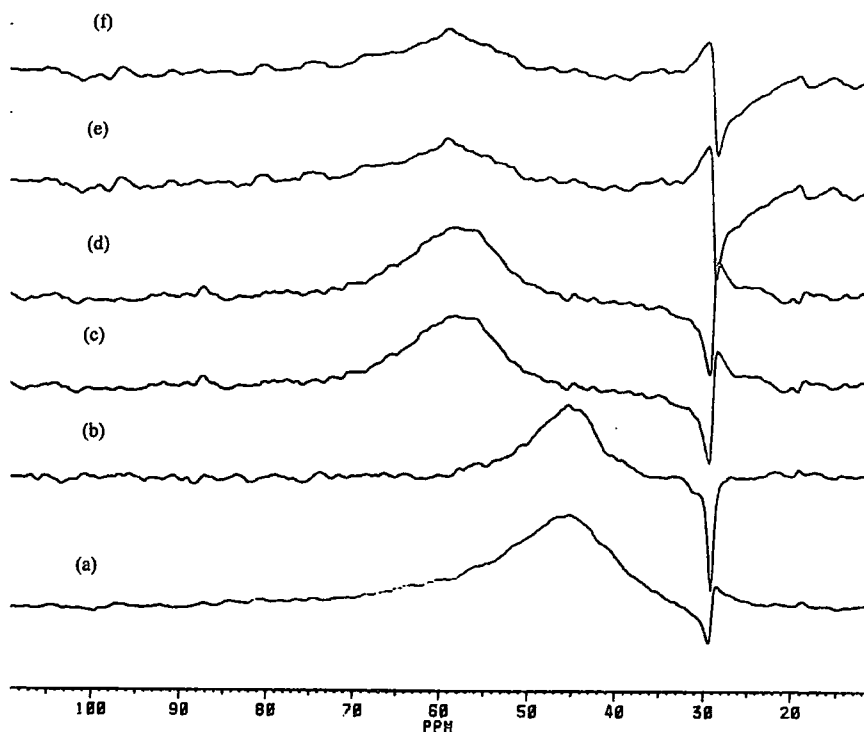
Figure 34. 18.6 MHz ^{14}N NMR spectra of HABTP hydroxide and HABTP silicate solutions. The percentage of the cation is the same for both hydroxide and corresponding silicate solutions. The concentration of silica is the same for all HABTP silicate solutions (5.78 wt%). (a) HMBTP hydroxide, (b) HMBTP silicate (c) HEBTP hydroxide (d) HEBTP silicate (e) HPBTP hydroxide (f) HPBTP silicate solution. Spectral parameters: 1 s recycle delay; 5434.7 Hz total spectral width; 16384 data-points; 100 transients for each spectrum. All spectra were carried out at ambient probe temperature (ca. 24°C). They are recorded at the same scale and absolute intensity.

3.10.8. Study of silicate solutions with other templates

It is known that the various kind of cation affect in different ways the distribution of species in silicate solutions. In this section we introduce one further kind of silicate solution.

3.10.8.1. Study of a silicate solution with KOH

It is known that double-membered rings are stabilised by alkali cations which have a large cation size. In this experiment we used KOH to make appropriate silicate solutions.

The silicate solutions were made with Si/cation = 1 with the same silica concentration as for previous cases (i.e. wt% SiO_2 = 5.78). It is worth comparing the sodium, potassium and HMBTP silicate solutions with the same composition (i.e. Si/cation ratio, wt% SiO_2 and the same pH). Figures 35a-35c show the ^{29}Si NMR spectra of the Na, K and HMBTP silicate solutions respectively. As can be seen ^{29}Si NMR spectra of both alkali (Na & K) silicate solutions (Figure 35a & 35b) show similar features and only small differences in the distribution of signals can be observed in the cubic octameric region. Thus, in similar circumstances, Na and K cations behave similarly for the distribution of the silicate species. However Figure 35c. shows a dramatic change between the alkaline (i.e. Na & K) and HMBTP silicate solutions, because of the structure directing of HMBTP, i.e. increase in the Q^3_6 and Q^3_8 concentration dramatically.

Another silicate solution was made with Si/cation =1 and mole ratio of HMBTP: K = 0.8:0.2 with the same silica concentration as for previous ones (i.e. 5.78 wt% SiO_2). Due to limitation in the time for use of the spectrometer (as mentioned, it is necessary to occupy 14 hours to get a good quality spectrum), and also because HMBTP hydroxide was not sufficiently available to make a series of silicate solutions, only one kind of HMBTP/K silicate solution was studied. Figures 36a-36b show the ^{29}Si NMR spectra of K/HMBTP and Na/HMBTP silicate solutions with the same conditions (i.e. Si/cation ratio of 1, 5.78 wt% SiO_2 and the ratios HMBTP:K and HMBTP:Na of 0.8:0.2). As can be seen, in an overall view, the distribution of signals is the same for spectra involving Na rather than K as the second cation. Interestingly, Figure 36a shows a significant signal assigned to Q^3_8, which indicates that the silicate solution is highly dominated by the cubic octamer and the signal related to Q^3_6 shows a considerable intensity. Therefore, from this point of view the ^{29}Si NMR spectra of K/HMBTP and
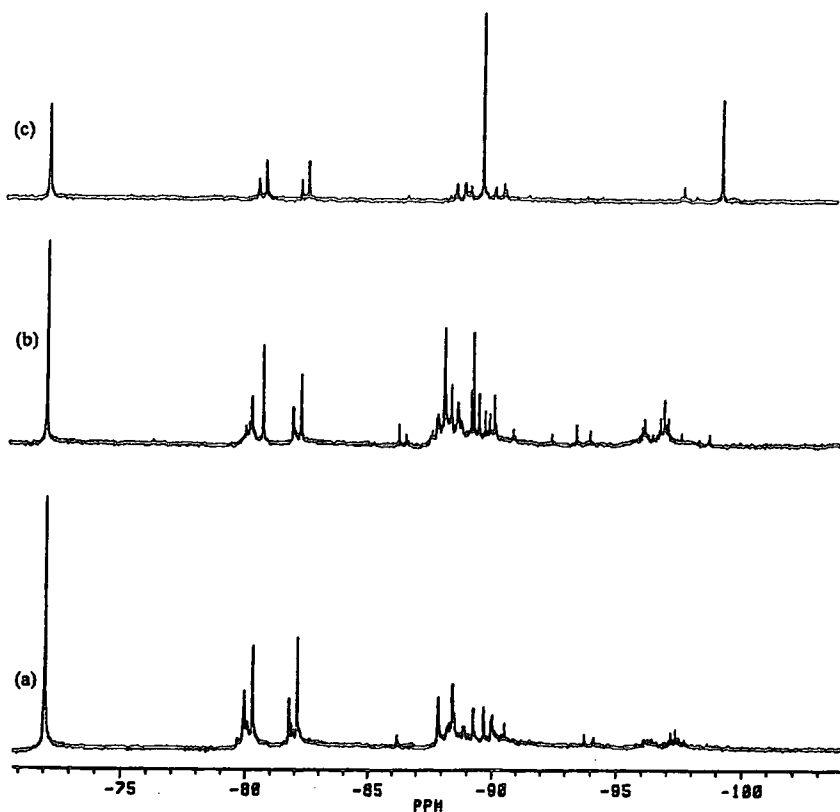
Figure 35. 49.50 MHz ^{29}Si NMR spectra of silicate solutions with the ratio Si/cation of 1 and constant concentration of the silica. (5.78 wt%SiO$_2$). The pH of the solutions are the same (ca. 13.4). (a) Na silicate, (b) K silicate, (c) HMBTP silicate solution. All spectra were obtained at ambient probe temperature of ca. 24 °C. The samples were prepared with ca. 15 wt% of D$_2$O to provide a (^{2}H) lock signal. Spectral parameters: 50 s recycle delay; 4950 Hz total spectral width; 16384 data points; 1000 transients for each spectrum. The spectra are plotted at the same scale and absolute intensity.
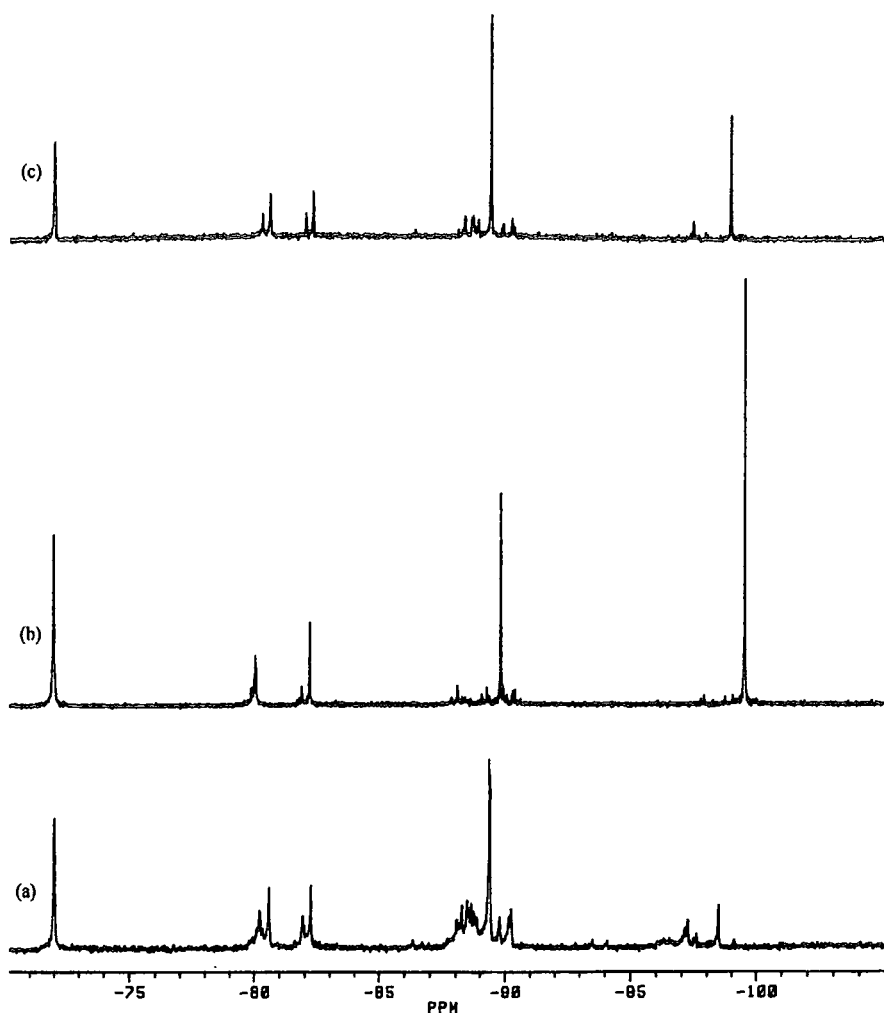
Figure 36. 49.50 MHz ^{29}Si NMR spectra of silicate solutions with the ratio Si/cation of 1 at a constant concentration of the silica.(5.78 wt%). The pH of the solutions are the same (ca. 13.4). (a) HMBTP/K silicate with ratio HMBTP:K = 0.8 :0.2, (b) HMBTP/Na silicate with ratio HMBTP:Na =0.8 :0.2 and (c) HMBTP silicate solution. All spectra were obtained at probe ambient temperature of ca. 24 °C. The samples were prepared with ca. 15 wt% of D_2O to provide a (^{2}H) lock signal. Spectral parameters: 50 s recycle delay; 4950 Hz total spectral width; 16384 data points; 1000 transients for each spectrum. The spectra are plotted at the same scale and absolute intensity.

from Na/HMBTP silicate solutions differ. Comparison of the ^{29}Si NMR spectrum of HMBTP silicate solution (Figure 36c) with the spectrum of K/HMBTP silicate solution shows that the prismatic hexamer is more stable in the former than in the latter, whereas the cubic octamer is more stabilised in K/HMBTP silicate than in HMBTP silicate solution. It seems likely that the potassium accompanied by HMBTP stabilises the double membered-rings, especially Q^3_8, and this effect can be related to the size of the cation (i.e. potassium).

As a result, the oligomerisation behaviour of silicates in HMBTP silicate solutions strongly differs from that in alkali hydroxide solutions. Alkali silicate solutions in general contain many different silicate anions, ranging from monomeric to highly branched polymeric ones, which are in mutual equilibrium[20,40,41]. Apart from minor amounts of the Q^3_6 and Q^3_8 observed in Na and K silicate solutions, cage-like species have not been found in alkali silicate solutions. Clearly in the HMBTP silicate solutions Q^3_6 and Q^3_8 are significantly dominant.

3.11. Conclusion

In conclusion, on the basis of the silicate work, the use of bulky organic bases, i.e. hexaalkylbenzotripyrrolium(HABTP), and tetraalkylammonium (TAA), instead of alkali cations, i.e. Na and K, clearly shifts the silicate equilibria to the cage-like species, and there may be a large amount of polymeric species present in silicate solutions. This is true especially at high Si/cation ratios or high Si concentration.

3.12. References

1. See for example, Vail, J.G. 'Soluble Silicates. Their Properties and Uses,' Reinhold, New York, 1952, vols. 1 and 2; Eitel, W. 'The Physical Chemistry of the Silicates,' University of Chicago Press, Chicago, 1954; Barby, D.; Griffiths, T.; Jacques, A.R. and Pawson, D. in 'The Modern Inorganic Chemicals Industry,' ed. R. Thompson, The Chemical Society, London, 1977.

2. Hoebbel, D. and Wieker, W. *Z. Anorg. Allg. Chem.*, 400, 146 (1973).

3. Freund, E. *Bull. Soc. Chim. Fr.* 2238, 2244 (1973).

4. Dutta, P.K. and Shieh, D.C. *Zeolites*, 5, 135 (1985).

5. Williams, E.A. and Cargioli, J.D. *'Annual Reports on NMR Spectroscopy'*, (Ed.G.A. Webb) Acad. Press (London), 9, 221 (1979).

6. Harris, R.K.; Knight, C.T.G. and Hull, W.E. *J. Am. Chem. Soc.*, 103, 1577 (1981).

7. Harris, R.K.; Knight, C.T.G. and Smith, D.N. *J.Chem. Soc. Chem. Commun.*, 726 (1980).

8. Harris,R.K.; Jones, J.; Knight, C.T.G. and Pawson, D.*J. Mol. Struct.*, 69, 95 (1980).

9. Harris, R.K. and Newman, R.H. .*J. Chem. Soc. Faraday Trans. 2*, 73, 1204 (1977).

10. Iler, R.K. *'The Chemistry of Silica'* Wilery-Interscience, New York, 1979.

11. Svensson, I.L.; Sjöberg, S. and Öhman, L.O. *J. Chem. Soc. Faraday Trans. 1*, 82, 3635 (1986).

12. Stumm, W.; Huper, H. and Champlin, R.I. *Enviro. Sci. Technol.*, 1, 221 (1967).

13. Marsmann, H.C., *Z. Naturforsch. B.*, 29, 495 (1974).

14. Engelhardt, G. Zeigan, D.; Jancke, H.; Hoebble, D. and Wieker, W. *Z. Anorg. Allg. Chem.*, 418, 17, (1975).

15. Harris, R.K. and Knight, C.T.G. *J. Chem. Soc. Faraday Trans. 2*, 79, 1525 (1983).

16. Harris, R.K. and Knight,C.T.G. *J. Chem. Soc. Faraday Trans. 2*, 79, 1539 (1983).

17. Harris, R.K.; O'Connor, M.J.; Curzon, E.H. and Howarth, O.W. *J. Magn. Reson.*, 57, 115 (1984).

18. Knight, C.T.G. *J.Chem. Soc., Dalton Trans.*, 1457 (1988).

19. Engelhardt, G.; Jancke, H.; Hoebbel, D. and Wieker, W. *Z. Chem.*, 14, 109, (1974).

20. Marsmann, H.C. *Chem. Ztg.*, 97, 128 (1973).

21. Gould.R.O.; Lowe, B.M. and McGilp, N.A. *J. Chem. Soc. Chem. Commun.*, 720 (1974).

22. Barrer, R.M. and Denny, P.J. *J. Chem. Soc.*, 971 (1961).

23. Kerr, G.T. and Kokotailo, G. *J. Am. Chem. Soc.*, 83, 4675 (1961).

24. Lok, B.M.; Cannan, T.R. and Messina, C.A. *Zeolites*, 3, 282 (1983).

25. Barrer, R.M. '*The hydrothermal chemistry of zeolites*' Academic Press London, UK, 1982. p.157.

26. Harris, R.K. and Newman R.H. *J. Chem. Soc. Faraday Trans. 2* 73, 1204 (1984).

27. Harris, R.K. and Knight, C.T.G. *J. Mol. Struct.* 78, 273 (1982).

28. Hoebbel, D; Garzo, G.; Engelhardt, G. and Vargha, *Z. Anorg. Allg.Chem.*, 494, 31 (1982).

29. Engelhardt, G. and Rademacher, O. *J. Mol. Liq.* 27, 125 (1984).

30. McCormick A.V. and Bell A.T. *Catal. Rev. Sci. Eng.* 31(1&2), 97 (1989).

31. Harris, R.K.; Knight, C.T.G and Hull, W.E. *ACS Symp.* 194, 79 (1982).

32. Hoebbel, D; Garzo, G.; Engelhardt, G.; Ebert, R.; Lippmaa, E. and Alla, M. *Z. Anorg. Allg.Chem.*,465, 15 (1980).

33. Knight, C.T.G.; Kirkpatrick, R.J. and Oldfield, E. *J. Mag. Res.*, 78, 31 (1988).

34. Engelhardt, G. and Hoebbel, D. *J. Chem. Soc. Chem. Commun.*, 514 (1984).

35. Kinrade, S.D.and Swaddle, T.W. *J. Chem. Soc. Chem. Commun.*, 120 (1986).

36.Corriu, R.J.P; Guérin, C.; Moreau, J. J.E. *Top. Stereochem.* 15, 43 (1986).

37. Holmes, R.R.; Day, R.O.; Chandrasekhr, V.; Harland, J.J.; Holmes, J.M. *Inorg. Chem.*, 24, 2016 (1984).

38. Liebau, F. *Inorg. Chim. Acta* 89, 1 (1984).

39. Kinrade, S.D. and Swaddle, T.W., *Inorg. Chem.*, 27, 4259 (1988).

40. Dent Glasser, L.S.; Lachowski, E.E. and Cameron, G.G. *J. Appl. Chem. Biotechnol.*, 27, 39 (1977).

41. J. Ciric, US Pat. 4850496 (1976).

42. F.X. Ryan, US Pat. 4851200 (1989)

43. W.J. Smith, Eur. Pat. 0 526 252 A1 (1993).

44. Greonen, E.J.J.; Kortbeek, A.G.T.G; Mackay, M. and Sudmeijer , O. *Zeolites*, 6, 403 (1986).

Chapter four

Application of ^{27}Al NMR to the Determination of the Incorporation of Aluminium into Silicate Anions in HMBTP Aluminosilicate Solutions

4.1. Introduction

It is proposed that nucleation for zeolite formation and crystal growth occurs through the co-polymerization of aluminate and silicate ions in a solution mixture. The question of whether dissolved aluminosilicate species are involved as precursors in the hydrothemal formation of natural or synthetic zeolites has been investigated by a number of authors for some years[1-5]. In principle, NMR spectroscopy is uniquely capable of detecting and characterising aluminium- and silicon-containing species in aqueous solutions; accordingly, a number of investigations have been carried out to address the structure of ions present in silicate[6-13] and aluminosilicate solutions.[14-17]

Kinrade et al. identified ^{29}Si NMR peaks due to low molecular weight aluminosilicate anions of sodium aluminate solutions by ^{29}Si NMR spectroscopy[15]. Using similar methods, Mortlock et al. investigated tetrapropylammonium (TPA) aluminosilicate solutions[18]. In a more recent study[19], the correlation between the partial charge on Si atoms and the ^{29}Si chemical shift was used to confirm the assignment of ^{29}Si NMR peaks due to cage species containing double-ring species, such as Q^3_6 and Q^3_8, i.e. the prismatic hexamer and cubic octamer, with some Al replacement. Mortlock et al.[14] studied TMA aluminosilicate solutions and assigned the ^{29}Si NMR spectra. They explained that when aluminium is added to a silicate solution, two distinct peaks appear in the ^{29}Si NMR spectra which are assigned to $Q^3_8(1Al)$.

The nature of the aluminosilicate ions and of their reactions in solution is still of considerable current interest. One central problem has been the nature of the aluminium co-ordination in aluminosilicate solutions. In the present study, we have used ^{27}Al NMR to investigate the local structure about the Al in a series of aluminosilicate solutions with Si:Al mole ratios pertinent to zeolite synthesis. Also, we have considered the kinetics of the reaction of aluminate with silicate anions by investigating the temporal evolution of ^{27}Al NMR spectra and by 2D NMR exchange spectroscopy.

4.2. Experimental

HMBTP silicate solutions were prepared by dissolving SiO_2 (made by the hydrolysis of $SiCl_4$) in appropriate amounts of 48% aqueous HMBTP hydroxide, (HMBTP=2,3,4,5,6,7,8,9-octahydro-2,2,5,5,8,8-hexamethyl-1H-benzo[1,2-c:3,4,-c':5,6-c"]tripyrrolium (Fig. 1), which was synthesized on the basis of reference 20), deionized

water and D$_2$O in polyethylene bottles. Dissolution of the silica required between one and two weeks at a temperature of 60°C, yielding clear solutions. Aluminate solutions were made by dissolving suitable amounts of sodium aluminate (61.3 wt% of Al$_2$O$_3$) in doubly distilled water. Fresh aluminate solution was added to the silicate solution to achieve the desired Si/Al molar ratio. After mixing, the solutions were allowed to equilibrate for no less than 1 week at room temperature (ca. 21°C).

Spectra were measured using a Varian VXR600 spectrometer, operating at 156.3 MHz for ^{27}Al NMR. Aluminium-27 NMR spectra were obtained by applying 90° pulses (34 μs pulse duration), the time elapsing between pulses being sufficient to allow a complete return of the magnetization to equilibrium, i.e. the recycle delay was 0.1 s. The T$_1$ measurements for the ^{27}Al NMR spectra were determined by the inversion-recovery method: no spin-lattice relaxation times in excess of 10 ms were found for the observed peaks. The standard Lorentz-Gauss transformation was applied to all ^{27}Al FIDs for resolution enhancement. Chemical shifts are reported in ppm from the signal for external 1M aqueous aluminium chloride hexahydrate, AlCl$_3$. 6H$_2$O.

R = CH$_3$
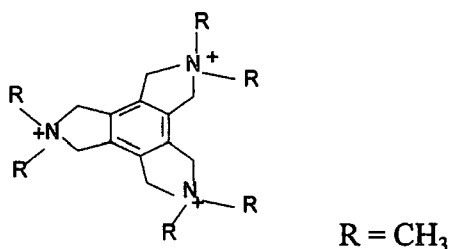
Figure 1. Chemical structure of the 2,3,4,5,6,7,8,9-octahydro-2,2,5,5,8,8-hexamethyl-2H-benzo(1,2-c:3,4-c':5,6-c")tripyrrolium cation (HMBTP)

4.3. High-resolution ^{27}Al NMR of aluminosilicate solutions

4.3.1. Principles

Aluminum-27 NMR can provide structural information about the environment of Al nuclei for aluminosilicate solutions through use of both chemical shifts and intensities of the signals. The striking extent of the range of chemical shifts for AlO$_4$$^{5-}$ terahedra from ca. 50 ppm up to ca. 80 ppm suggests that there are, beyond the immediate Al co-ordination with oxygen atoms, more subtle structural influences on the Al shielding. In particular, in addition to the directly bonded oxygen atoms, the nuclei of the second coordination sphere (i.e. Si in the case discussed herein) contribute to the

shielding of the aluminum. Corresponding ^{29}Si NMR investigations of silicates and aluminosilicates[21-23] have shown that such possible influences are: effect of atoms in the second co-ordination sphere, cation effects, bond distances and angles, and the degree of condensation of the tetrahedral groups under consideration.

A few of these structural influences have been investigated for ^{27}Al chemical shifts[24]. In contrast to the well-known dependence of ^{29}Si chemical shifts on the degree of condensation of SiO_4 tetrahedra in silicates, knowledge of the behaviour of ^{27}Al chemical shifts for corresponding condensed aluminate anions is as yet lacking. For aluminosilicates the number of AlO_4 environments is reduced by Loewenstein's rule[25], which excludes Al-O-Al bonds.

Since aluminium is a quadrupolar nucleus there are some experimental difficulties. These are critical for the investigation of condensation effects, since, particularly in the interesting cases of aluminosilicate species, the different resonances are close to each other and difficult to resolve. Hence the requirement for a very-high-field spectrometer.

4.3.2. Notation

To simplify writing of the various (alumino)silicate species that can occur in solution, an abbreviated notation has been utilised to described these (alumino)silicate structures. The use of "Q-units" was first proposed by Engelhardt[26], and they have been used by most investigators in later studies. In this notation, Q represents a silicon atom bonded to four oxygen atoms forming a tetrahedron. The superscript i indicates the connectivity, i.e. the number of other Q units attached to the SiO_4 tetrahedron under study. Thus Q^0 denotes the monomeric orthosilicate anion SiO_4^{4-}, Q^1 end-groups of chains, Q^2 middle groups in chains or cycles, Q^3 chain-branching sites and Q^4 three-dimensionally cross-linked groups.

When considering heavily-condensed species and zeolites it is useful to define secondary building units (SBU) with two types of structure: single-ring (SR) and double-ring (DR). The former is two-dimensional and the latter has three dimensions. For instance, S4R and S5R mean single four-ring and single five-ring systems respectively. Likewise D4R and D5R are double-four and double-five rings. It should be noticed that D3R, D4R and D5R are contained in the Q^3_6 , Q^3_8 and Q^3_{10} species respectively.

For aluminosilicate solutions similar notation can be introduced which deals with species containing aluminium as well as silicon. The notation dealing with the silicate sites is the same as above (i.e. for silicate solutions). The only difference is in the way the number of aluminiums involved in the species in question is indicated. For instance: the prismatic hexamer with one aluminium, $Q^3_6(1Al)$, contains a SBU denoted $D_3R(1Al)$ (that means a double three-membered ring with one aluminium), or for example the cubic octamer with two aluminium sites, $Q^3_8(2Al)$, contains $D_4R(2Al)$, i.e. a double four-membered ring with two aluminiums. For individual silicon sites the number of bridges to aluminium is similarly indicated, e.g. $Q^2(1Al)$, $Q^3(2Al)$ etc.

In the case of individual aluminium sites there is a special notation which is similar to the silicon one. An aluminium site is presented as " q " (rather than Q for the silicon sites). For such a site, linkage to one siloxane bridge is denoted q^1. In the same way, if it links to 2, 3 and 4 siloxane bridges it is indicated as q^2, q^3 and q^4 respectively. Indeed if aluminium has no siloxane bridge, as for the aluminate anion, AlO_4^{5-}, it is represented as q^0. Therefore q^0, q^1, q^2, q^3 and q^4 are Al(0OSi), Al(1OSi), Al(2OSi), Al(3OSi) and Al(4OSi) respectively. Under Loewenstein's rule, it is unnecessary to introduce a notation for aluminium sites with aluminoxy bridges.

Hereafter we use in general the simple notation for the individual silicon and aluminium sites, introduced above (Q^n and q^n respectively).

It should be remembered that the ^{29}Si signal for each Q-unit is shifted by ca. 10 ppm to lower frequency when the number of siloxane bridges is increased by one, but in the case of q-units (i.e. aluminium sites) the ^{27}Al resonance is shifted by ca. 5 ppm to lower frequency, e.g. from q^0 to q^1 the chemical shift is moved by ca. 5 ppm to lower frequency.

4.3.3. Assignment

The isotropic ^{27}Al chemical shifts of aluminosilicate species are primarily determined by the coordination number of the aluminium atoms. The shift ranges observed are about +50 to +80 ppm for the AlO_4, about -10 to +20 ppm for AlO_6, while about +30 to +40 ppm has been proposed for the relatively rare AlO_5 unit [from the signal for $Al(H_2O)_6^{3+}$ in an aqueous $Al(NO_3)_3$ solution]. In general, these well-separated shift ranges permit the coordination number of the AlO_n polyhedra present in the aluminosilicate samples to be determined unambiguously for the ^{27}Al NMR spectra, even from relatively broad lines.

For a broad range of AlO_4 tetrahedra present in aluminates, aluminosilicates and aluminophosphates, Muller et al.[27] observed distinct ^{27}Al chemical shift ranges for the AlO_4 units linked to different neighbouring TO_4 tetrahedra (T=Al, Si, P) and AlO_6 octahedra. However, there is some controversy for the assignment of aluminium sites in aluminosilicates by the various workers. Muller et al.[27] assigned the chemical shifts of 79.5, 74.3 69.5 and 64.2 ppm (from $Al(H_2O)_6^{3+}$) to q^0, q^1, q^2 and q^3 respectively, using TMA aluminosilicate solutions. Dent Glasser and Harvey[46], using potassium aluminosilicate solutions, found several bands in the ^{27}Al NMR spectrum lying at shifts range of 80, 70-72, 66, 61 and 58 ppm and assigned them to q^0, q^1, q^2, q^3 and q^4 respectively. Kinrade and Swaddle[12], observed different signals in ^{27}Al NMR using sodium aluminosilicate solutions. They assigned shifts of 80, 75, 70 and 65 ppm to q^0, q^1, q^2 and q^3 respectively. On the other hand, Mortlock et al.[14,18] using tetraalkyl ammonium aluminosilicate solutions, assigned the signals located at the 74-77, 69-72, 64-67 and 58-61 ppm to q^0, q^1, q^2 and q^3, respectively.

It should be mention that in our studies, the ^{27}Al NMR peak assignments of HMBTP aluminosilicate solution species are based on the assignment of similar peaks that appear in TMA aluminosilicate proposed by Muller et al[28]., i.e. the shift ranges of ca. 80, 75, 70, 65 and 60 ppm are ascribed to the species of q^0, q^1, q^2, q^3 and q^4 respectively.

4.3.4. Aluminum background correction

Figure 2 shows the background resonance signal which was recorded by using an aluminium-free silicate solution. As can be seen, it exhibits a very broad peak from ca. 30 to 70 ppm. The peak maximum is located at ca. 56 ppm . This must be eliminated from the spectra of interest since it lies in the shift range of ^{27}Al NMR for aluminosilicate solutions.

Semeral et al.[29] reported that they found three probe components to contribute to the ^{27}Al NMR background: borosilicate glass in the probe Dewars, insert, and coil mounts; sapphire dielectric materials in probe electronic components; and fibreglass mounts of the electrical circuits in the probe. In addition they found that borosilicate glass NMR tubes account for about one quarter of the background.

In order to eliminate the background resonance, the background spectrum was obtained by using a blank solution, i.e. an aluminium-free silicate solution with exactly

Figure 2. Representative ^{27}Al NMR spectrum at 156.3 MHz for an aluminium-free HMBTP silicate solution as a background. The broad line comes from the probe (see text). ^{27}Al spectral frequencies are referenced to the signal for octahedral Al^{3+} ion in an $AlCl_3$ aqueous solution.

the same conditions as for the aluminosilicate solution of interest. Spectra were subtracted digitally from the background spectrum.

4.4. Results and discussion

Figure 3 displays the ^{27}Al NMR spectrum of a sodium aluminate solution before addition of HMBTP silicate solution. The concentration of aluminium is the same as for the aluminosilicate solution discussed in the following sections. This spectrum indicates that the tetrahedral aluminium site of $AlO4^{5-}$ resonates at 80.45 ppm. The chemical shift is referenced to the signal for the octahedral aluminium site of 1M $AlCl_3$ aqueous solution as 0.0 ppm. The sharp peak illustrates that the aluminate site in the aluminate anion is highly symmetric. It should be noted that the ^{27}Al NMR spectrum obtained from dissolution of metal aluminium in HMBTP hydroxide shows a signal at the same position as sodium aluminate.

Figure 4 displays the ^{27}Al NMR spectrum for a solution with Si/Al mole ratio of 5 and 0.875 molar SiO_2, which was recorded at 25°C. The spectrum was recorded at the highest available field, namely 14.1 T operating at 156.3 MHz for ^{27}Al NMR resonance. The spectrum shown in Figure 4 illustrates that we have molecular species present which contain aluminium in tetrahedral environments with a variety of structural differences. Figure 4 is characterised by at least four distinct bands. The bands appearing at 73-77, 68-71, 64-66, and 57-62 ppm are assigned to q^1, q^2, q^3 and q^4 respectively. It is clear from the ^{27}Al NMR spectra of HMBTP aluminosilicate solution that the peak assigned to q^4 shows the highest intensity, which tells us that the aluminosilicate solutions are dominated by q^4 environments. This phenomenon can be expected since the corresponding HMBTP silicate solution is dominated by cage-like species, especially the prismatic hexamer and cubic octamer which can be seen in the silicon-29 NMR spectra (formation of q^4 is shown in Figure 12). Moreover it can be said that the cage-like species such as Q^3_6 and Q^3_8 might contain Al atoms replacing more than one Si atom , e.g. $Q^3_6(2Al)$ or $Q^3_8(2Al)$, without violation of Loewenstein's rule[25], with consequent enhancement of the band assigned to q^4. Although the spectrum exhibits at least four different sites of Al in aluminosilicate solutions, this does not mean there are only four kinds of anions. Because of the loss of regular symmetry around the aluminium in aluminosilicate anions and the quadrupolar property of Al nuclei, there is an increased line width. The overlap in the ^{27}Al NMR spectra suggests to us that the quadrupole coupling constants for the tetrahedral aluminium sites in the

Figure 3. Representative ^{27}Al NMR spectrum at 156.3 MHz for a sodium aluminate before mixing HMBTP silicate solution. The chemical shift of the tetrahedral site of the aluminate ion is placed at 80.45 ppm. ^{27}Al spectral frequencies are referenced to the signal octahedral Al^{3+} ions in an AlCl$_3$ aqueous solution.

Figure 4. High-resolution ^{27}Al NMR spectrum at 156.3 MHz of HMBTP aluminosilicate solution with the ratio Si/Al = 5 at 25°C. Spectrum was taken one week after mixing. ^{27}Al spectral frequencies are referenced to the signal for octahedral Al^{3+} ions in an $AlCl_3$ aqueous solution.

Spectrum conditions:

Spectral width : 46729.0 Hz.   Acquisition time : 0.2 s.
Relaxation delay : 0.100 s.   Pulse width : 45.0 us.
Number of transients : 10000

aluminosilicate anions are large. Consequently, to resolve a separate resonance line for each aluminium site seems to be impossible. However the spectra from the ultra-high-resolution 600 MHz NMR spectrometer, operating at 156.325 MHz for aluminium, are able to resolve one more resonance line at 67.4 ppm. Although it seems to be difficult to say exactly which kind of aluminate species corresponds to that signal (67.4 ppm), on the basis of shielding arguments we tentatively assigned it to Al atoms in anions involving cyclic trimeric rings. However it should be mentioned that resolution of this band (67.4 ppm) is a direct consequence of using the Lorentz-Gauss transformation[27], since such a peak has not been observed in previous aluminosilicate spectra which were not resolution-enhanced[30].

4.4.1. The effect of the aluminium concentration on the ^{27}Al NMR spectra

Figure 5 presents the ^{27}Al NMR spectra of a series of aluminosilicate solutions for which the [SiO_2] = 0.875M but with different concentrations of aluminium. Data for the compositions of these solutions are presented in Table 1.

Table 1 : Data for the composition of the HMBTP aluminosilicate solutions:

Si/Al	C_{SiO_2} / M	C_{Al} / M	pH
50	0.875	0.017	13.28
20	0.875	0.045	13.27
10	0.875	0.090	13.26
7.5	0.875	0.116	13.25
5	0.875	0.185	13.24

It is apparent that, as the mole percent of Al increases, the signal-to-noise ratio improves, but the features of the spectra do not change substantially. As a result, the ^{27}Al NMR spectra show that the distribution of Al in aluminosilicate solutions is not a strong function of the Si/Al mole ratio. For example, only negligible differences occur between the spectra for Si/Al = 50 and Si/Al = 20. Thus, the distribution of Al environments remains the same as the Al concentration increases even in the solution with lowest concentration of aluminium, i.e. Si/Al = 100, which shows the contribution of the aluminium in the number of silicate species. Therefore the distribution of Al connectivities is not influenced substantially by the concentration of dissolved Al. This result is consistent with previous reports published by Mortlock et al.[14,18]

Figure 5. 156.3 MHz ^{27}Al spectrum of an HMBTP aluminosilicate solution at 25°C of the composition 0.875 molar SiO_2 a) Si/Al (molar ratio) = 50, (b) Si/Al = 20, (c) Si/Al = 10, (d) Si/Al = 7.5 and (e) Si/Al = 5. ^{27}Al spectral frequencies are referenced to the signal for octahedral Al^{3+} ion in an $AlCl_3$ aqueous solution.

It is pertinent to notice that the position of the band at highest frequency seems to increase as the Si/Al mole ratio decreases, i.e. with increasing aluminate concentration. This phenomenon might be due to an increasing proportion of the $AlO_4{}^{5-}$, q^0, anion in the solution, which is in rapid exchange with q^1, causing the averaged peak position to move to higher frequency. This process is discussed later.

Meanwhile, due to the broad bands in the ^{27}Al NMR spectra shown in Figure 5, it seems to be difficult to say which kind of aluminosilicate species dominate when the concentration of aluminate is increased. However one can expect that cage-like species such as $Q^3{}_6(1Al)$ or $Q^3{}_8(1Al)$ might be dominant due to the stability of corresponding silicate anions in HMBTP silicate solution.

4.4.2. Study of aluminium-27 NMR spectroscopy at variable temperature

There are many chemical processes that occur at rates which are comparable with the appropriate chemical shift differences. This can lead to exchange broadening which, depending on the circumstances, may be a difficulty to be tolerated or may be highly informative.

The condition for slow exchange on the NMR timescale between two species is, in effect, that the exchange rate must be slower than the difference in NMR absorption frequency between the two sites. If the difference in frequencies expressed in hertz is Δv, then the transition from slow to fast exchange takes place when

$$k_{ex} = \pi \Delta v / \sqrt{2} = 2.22 \Delta v. \qquad (1)$$

For chemical exchange processes occurring at rates comparable with the appropriate chemical shift differences, the spectrum at low temperature will be at the slow-exchange limit, and at high temperature it will be in the fast-exchange limit. The temperature at which the lines just merge is the coalescence temperature, T_c. The following section explores in detail the interesting question of the behaviour of the exchange processes among the aluminosilicate species at variable temperature.

Figure 6 illustrates ^{27}Al NMR spectra taken at progressively higher temperatures for the HMBTP aluminosilicate solution with SiO_2/Al_2O_3 molar ratio 10.0, prepared from HMBTP silicate solution with Si/HMBTP = 2 and sodium aluminate. This solution was made one week before recording the spectra (to complete the reaction of the aluminate and silicate and subsequently to achieve an equilibrium state). Spectra were carried out over the range of 10 to 70°C, with the temperature raised

Figure 6. Temperature-dependent 156.3 MHz ^{27}Al spectrum of a HMBTP aluminosilicate solution of composition 0.875 molar SiO_2 and Si/ Al = 5 molar ratio taken at (a) 1, (b) 20, (c) 50, (d) 60 and (e) 70°C. ^{27}Al spectra frequencies are referenced to the signal for octahedral Al^{3+} ions in an $AlCl_3$ aqueous solution.

by 10 degrees for each step. For each temperature a sufficient time was allowed to elapse for a new equilibrium state to be reached. It is well known that, if a solution containing quadrupolar nuclei (i.e. aluminium-27) is heated then the rate of quadrupole relaxation is decreased and consequently broad resonances will tend to sharpen. In spite of that, no significantly better resolution was obtained by increasing the temperature, probably because the rates of exchange are increased with increasing temperature. Figure 6 reveals no significant changes happened for the ^{27}Al NMR spectra recorded in the range of 1°C to 50°C. Those spectra exhibit four distinct bands which lie in the shift ranges 75, 70, 65 and 60 ppm, ascribed to the q^0/q^1, q^2, q^3 and q^4 respectively. Therefore, although the aluminosilicate anions are being exchanged (see ^{27}Al 2-D NMR EXSY), the exchange rates are slow enough on the NMR time scale for separate bands to be observed (except for distinguishing q^0 and q^1).

As the temperature is raised, due to chemical exchange processes some of the ^{27}Al NMR peaks in Figure 6 broaden. The peak for q^1 broadens and shifts to higher frequency while the q^2 peak in turn broadens slightly and shifts to lower frequency. This trend can be attributed to an exchange of Al between environments in which Al is bonded to one and two OSi groups. The spectrum recorded at 70°C shows a single broad exchange-coalesced peak due to the q^1 and q^2 anions i.e. the corresponding aluminosilicate species undergo rapid chemical exchange. As the temperature increases, the q^3 peak shifts to high frequency slightly, probably as a result of incipient exchange. However, the q^4 peak does not shift with increasing temperature.

It should be noted that the peaks belonging to the q^3 and q^4 ions are well resolved at all accessible temperatures. Accordingly, it can be concluded that q^3, which for example can be ascribed to the cubic octamer with one or two aluminium sites (i.e. $Q^3{}_8(1Al)$ or $Q^3{}_8(2Al)$) are relatively stable on the NMR timescale even at high temperature. It can be hypothesised that the aluminium which is trapped in the cubic octamer and manifested as a $Q^3{}_8(1Al)$, is less labile than Al in the aluminosilicate species for which the aluminium is placed in the end group, or middle group i.e. q^1 and q^2 respectively.

As a check, spectra were recorded at room temperature both before heating and after heating. They indicate that no permanent change was effected with temperature on the character of the solutions. Therefore the changes observed at elevated temperature are reversible.

4.4.3. Investigation of the siloxanization process of the aluminate ion using the evolution with time of high-field aluminium-27 NMR spectra

The aim in this section is to provide some insight into the effects that aluminate/silicate replacement processes have on the appearance of ^{27}Al spectra, and to show how these effects may be exploited in assigning structures and determining reaction mechanisms.

The aluminosilicate solution was made by adding HMBTP silicate solution to the freshly-prepared sodium aluminate solution to achieve the ratio Si/Al of 5. To study evolution of the spectra with time, four different protocols were used at a temperature of 25°C :

i) Recording ^{27}Al NMR spectrum soon after mixing the solutions

ii) The first hour after mixing: recording ^{27}Al NMR spectra for 2 minutes each, without any interval of time between the spectra.

iii) The second and the third hours of mixing time: ^{27}Al NMR spectra recorded for five minutes each (1000 transients) with no interval of time between the spectra.

iv) An overnight run: recording the ^{27}Al NMR spectra for 5 minutes each (1000 transients) with 30 minutes interval of time between each spectrum.

The ^{27}Al NMR spectrum immediately following mixing of sodium aluminate and HMBTP silicate solution at 25°C is shown in Fig. 7. The major peak, at δAl = 79.0 ppm may be assigned primarily to free aluminate (the value for aqueous sodium aluminate is 80.46 ppm (Fig. 3)). However, peaks at 70.8 and 65.9 ppm represent q^2 and q^3 enviroments, which are clearly present very quickly after mixing.

The evolution of the aluminium-27 NMR spectra following the mixing of aluminate and silicate solutions is presented in Figures 8-10, obtained within 16 hours after the mixing. The top trace of each figure displays all of the spectra carried out in the time frame specified, while the bottom ones exhibit the first and the last spectra of that particular time interval. Spectra for each specific time were exclusively scaled to the tallest peak in that spectrum. Therefore, the peaks that are highest for the different formats of time cannot be compared quantitatively. All spectra were carried out with background subtraction by the method described earlier.

The spectra obtained during the evolution time imply that several things happen when the silicate and aluminate solutions are mixed. This evidence visualises the

Figure 7. 156.3 MHz ^{27}Al spectrum of a HMBTP aluminosilicate solution of composition 0.875 molar SiO_2 and Si/ Al = 5 molar ratio taken at 25°C soon after mixing the HMBTP silicate and aluminate solutions. ^{27}Al spectra chemical shifts are referenced to the signal for octahedral Al^{3+} ions in an $AlCl_3$ aqueous solution.

phenomena that occur soon after the mixing of solutions and proceed up to about 16 hours after mixing, which may be categorised as follows :

i) The growth of intensity in the bands located at the shifts ca. 70 and 65 ppm, whilst the band at the highest frequency decreases in intensity. This process is very slow and is not complete even 16 hours after mixing.

ii) A band at ca. 60 ppm, assigned to q^4 environments, which is scarcely visible immediately after mixing, also increases in intensity with time.

iii) The variation of the chemical shift associated with the first band (at the highest frequency), which changes from ca. 79.0 to ca. 75 ppm. This point is discussed in more detail below.

iv) There appear to be small low-frequency shifts, ca. 0.2 ppm, for the rest of the observed peaks within 16 hours of mixing. Clearly, the distribution of Al changes progressively from small oligomeric aluminosilicate species towards the cage-like ones, e.g. involving q^3 as time progresses.

By considering the development of the features of the aluminium-27 NMR spectra resulting from the evolution with time, one can imagine that the formation of the siloxane linkage is not necessarily step by step. In other words, building up the aluminium environments q^1, q^2, q^3 and q^4 might occur simultaneously. Indeed, this process can be expected, since, when the aluminate ions are introduced to the silicate solution, they are presented to a number of pre-existing silicate species[6-9], for instance, monomer (Q^0), dimer (Q^1), cyclic trimer (Q^2_3), linear trimer ($Q^1Q^2Q^1$), prismatic hexamer (Q^3_6) and cubic octamer (Q^3_8). The silicate solution used for this particular experiment was made one week before it was utilised, and, since it was kept in an oven at 60°C, it is supposed that it had already reached equilibrium. Subsequently it is likely that the aluminate ions can react with a number of silicate species at the same time, though the mode of reaction is a matter of speculation. Nevertheless, as pointed out earlier, the signal intensities corresponding to the different aluminosilicate environments vary with time, so that the signal at highest frequency is highly dominant during the first hour after mixing, whilst the signal assigned to q^3, i.e. Al(3OSi), is substantial at the end of the evolution time (i.e. after 16 hours). This suggests that the aluminate anions react with the silicate anions in different ways depending on the individual silicate species involved.

Figure 8. The evolution with time of the 156.3 MHz ^{27}Al spectrum of an aluminosilicate solution prepared by rapid mixing of fresh sodium aluminate and aged HMBTP silicate solutions taken at 25°C and with a final composition of 0.875 molar SiO_2 and Si/ Al = 5. Spectra were taken every 2 minutes under the same conditions (but only every alternate spectrum is displayed). Spectrometer conditions are as follows: Recycle delay : 0.1 s ; acquisition time : 0.2 s ; number of transients : 384 ; spectral width : 46729.0 Hz ; pulse duration for a 90° flip angle : 45 μs.

Top trace : The ^{27}Al NMR spectra obtained during the first hour after mixing. The spectra were scaled to the tallest peak. Bottom traces : (a) The first spectrum of the top trace, i.e. 2 minutes after mixing ; (b) the last spectrum of the top trace, i.e. 60 minutes after mixing.

Figure 9.The evolution with time of the 156.3 MHz ^{27}Al spectrum of an aluminosilicate solution prepared by rapid mixing of fresh sodium aluminate and aged HMBTP silicate solution, taken at 25°C and with final composition of 0.875 molar SiO_2 and Si/ Al = 5. Spectra were taken every 5 minutes under the same conditions. Spectrometer conditions are as follows:

Recycle delay : 0.1 s ; acquisition time : 0.2 s ; number of transients : 960; spectral width : 46729.0 Hz ; pulse duration for a 90° flip angle : 45 µs.

a: The ^{27}Al NMR spectra obtained during the second hour after mixing (but only every alternative spectrum is displayed). . a' : the first spectrum of the the second hour after mixing, i.e. obtained 65 minutes after mixing. b : The ^{27}Al NMR spectra obtained during the third hour after mixing (but only every alternate spectrum is displayed) b': the last spectrum of the third hour after mixing, i.e. obtained 180 min after mixing. All spectra were plotted on the same scale in absolute intensity mode.

Figure 10. The evolution with time of the 156.3 MHz ^{27}Al spectrum of an aluminosilicate solution prepared by rapid mixing of fresh sodium aluminate and aged HMBTP silicate solution, taken at 25°C and with a final composition of 0.875 molar SiO$_2$ and Si/ Al = 5. Spectra were taken every 5 minutes under the same conditions separated by 30 minutes interval of time (but only every alternate spectrum is displayed). Spectrometer conditions are as follows:

Recycle delay : 0.1 s ; acquisition time : 0.2 s ; number of transients : 960 ; spectral width : 46729.0 Hz ; pulse duration for a 90° flip angle : 45 μs.

Top trace : The ^{27}Al NMR spectra obtained between 3 and 16 hours (i.e. carrying out ^{27}Al NMR overnight) after mixing. The spectra were scaled to the tallest peak. Bottom trace : (a) The first spectrum of the top trace, i.e. 3.5 hours after mixing ; (b) the last spectrum of top trace, i.e. 16 hours after mixing of solutions.

One should remember that, under full ionization, the silicate species contain different negative charges as well as molecular sizes. Consequently, the repulsion forces between aluminate anions and different silicate anions should not be the same. Fig. 11 presents a schematic diagram for the reaction of aluminate ions with silicate ions.

Fig. 11. Schematic representation of the interaction of aluminate with various silicate anions. It is supposed that the aluminate ions (q^0) can react with the silicate species (Q^n) simultaneously, and produce different aluminosilicate species (q^n).

A question arising from the aluminium-27 NMR spectra obtained as a function of time after mixing silicate and aluminate solutions is why the aluminate ions should react to give large silicate species immediately after mixing (observation of peaks for q^2 and q^3 immediately after mixing), whereas other processes occur much more slowly.

Obviously, reaction of $Al(OH)_4^-$, q^0 with different silicate species can occur at different rates. Moreover, re-equilibration among the silicate ions also shows a range of rates, depending on the species concerned. The probability of the reaction of the aluminate with an individual silicate species depends upon the size and the charge of the latter. Clearly the silicate anions contain different amounts of negative charge (depending on the degree of ionisation and therefore on pK_a and pH). The larger ions carry more negative charge. A monomeric (Q^0) ion could theoretically carry a charge up

to -4. Dimer, and other Q^1 units, can carry a maximum of three negative charges per silicon, but Q^2 and Q^3 silicon can carry at most two and one negative charges respectively. As a result, the larger the silicate species, the smaller its average negative charge per silicon, and the easier it will be for it to be approached by a negatively charged q^0 group.

In the following discussion some ways are speculatively suggested whereby aluminate anions may react with silicate species:

i) Addition: in this case the aluminate ion can be added to any silicate ion to produce an aluminosilicate species with one aluminium q^1 site (eq. 2).

$$q^0 + Q^n \rightarrow q^1 Q^{n+1} \qquad (n < 4) \qquad (2)$$

ii) Substitution: in this way one silicon is replaced by aluminium, which can lead in principle to q^n with any value of n (eq. 3).

$$q^0 + Q^n\text{-}(Q)n \rightarrow q^n\text{-}(Q)n + Q^0 \qquad (3)$$

e.g.:

In the above reaction the transition states are ignored

iii) Chelation: This would imply ring or cage formation (eq. 4 and 5).

e.g.:

$$(4)$$

A

or

$$(5)$$

B

Direct substitution seems unlikely (except, perhaps, replacement of Q^1 by q^1), but chelation would be expected to lead to relatively stable products since it is known that Si-O-Al bonds are difficult to break[31]. Because cage-like silicate species are favoured in HMBTP silicate solutions it can be expected that analogous species also dominate in the corresponding aluminosilicate solutions. Reactions such as given by equations 4 and 5 would appear to be particularly favourable and may account for the rapid appearance of q^2 and q^3 groups immediately after mixing. However, the concentrations of species such as A and B in HMBTP silicate solutions are low, so after some initial formation of q^2 and q^3 by this route, further development requires re-equilibration among silicate species to form more A and B, which might be slow. After the initial formation of aluminosilicate ions, these can presumably further equilibrate (though without necessarily breaking the Al-O-Si bridge).

The formation of q^4 sites is more speculative. Aluminosilicate ions can react, without breaking Si-O-Si bonds, in a manner consistent with the observation of Hoebbel et al.[32] on the formation of double-four-ring aluminosilicates in the TMA aluminosilicate solution. They suggested that q^4 forms through linkage of Al-O-Si units (without breaking Loewenstein's rule), shown as follows:

Fig. 12 Schematic representation of the formation of q^4 sites. Closed circles represent silicon atoms and open ones indicate aluminium atoms.

This process (formation of q^4) can occur slowly as is observed in the time-evolution experiments. It should be noted that q^4 sites in zeolites are the positions active for catalysis since they are of Brönsted acid nature [33,34], i.e.:

$$\begin{array}{c} H \\ | \, + \\ O \end{array}$$

(chemical structure diagram: Si — O(H)(+) — Al(−) bonded to additional O — Si groups and two lower O — Si groups)

4.4.3.1. Variation of the chemical shift for the band at highest frequency during the evolution time

When the rate of exchange is fast in comparison with the shift difference v_a-v_b between the two sites, instead of the expected resonances v_a and v_b, we observe only a single coalesced line at Ω, the weighted mean frequency or 'centre of gravity' of the spectrum (eq. 6).

$$\Omega = \frac{v_a P_a + v_b P_b}{P_a + P_b} \qquad (6)$$

where P_a and P_b are the population of the sites a and b respectively.

In a fast-exchange system, the relative populations might be changing, causing the coalesced line to shift dramatically within the spectrum. For example, in a two-site problem, if site a becomes more highly populated than site b, the coalesced line moves towards the chemical shift of site a, the 'centre of gravity' having been shifted according to eq. 6. A good example is provided by the ^{27}Al NMR spectra obtained during the evolution time, when q^0 and q^1 are exchanging very rapidly and the peak position is moving.

The evolution of the ^{27}Al NMR spectra for HMBTP aluminosilicate solutions with time shows that only the band at highest frequency markedly changes in chemical shift, moving about 5 ppm to lower frequency over the 16 hours after mixing the solutions. It is located at ca. 79.1 ppm soon after mixing (Fig. 7) but reaches ca. 75.9 ppm 16 hours later (Figure 10).

Figure 13 depicts the movement of the chemical shift with time. However, it should be noted that no substantial changes occurred in the shifts of the other bands in the spectra.

Figure 13. Plot of the chemical shift for the band at highest frequency with time after mixing the aluminate and silicate solutions. The ^{27}Al NMR frequencies are referenced to the signal for octahedral Al^{3+} ions in an AlCl$_3$ aqueous solution.

To confirm that the signal ascribed to Al(OH)$_4^-$ and its various ionised states appears at ca. 80.45 ppm independent of pH, the ^{27}Al NMR spectrum of sodium aluminate solution was obtained for variable pH (ca. pH 13.6 to pH 12.0). Results obtained from this series of experiments indicate that the chemical shift for such aluminate solutions is always 80.4 ± 0.1 ppm (referenced to the signal for the octahedral Al^{3+} ions in an AlCl$_3$ aqueous solution), and no new resonances can be observed over the range of studies. Consequently, the chemical shift is insensitive to any pH alteration which may occur in the aluminosilicate solutions. Additional experiments were performed for different concentrations of aluminate. The ^{27}Al NMR spectra once again showed no significant change in chemical shift. As a result the movement of the band at highest frequency must arise from the shielding effect of a change in the co-ordination sphere by bonding to silicate sites i.e. by *siloxanization* of the aluminate tetrahedra, leading to ions such as AlO$_3$(OSi)$^{5-}$, i.e. q^1.

However it should be noticed that the rate of exchange between the q^0 and q^1 sites must be fast on the NMR time scale, so that separate signals from q^0 and q^1 cannot be observed. An attempt was made to resolve two signals from those species, but this was unsuccessful, even though the experiment was carried out at 0°C (see aluminium-27 NMR spectra at variable temperature).

4.4.3.2. Variation of the ratio q^1/q^0 with time

As already discussed, the first band in the aluminium-27 NMR spectra is assigned to both q^0 and q^1. Accordingly, any variation influencing that band can be related to both species. By regarding the variation of the chemical shift over time, approximate calculations were made to find quantitative values for q^1 and q^0 concentrations. It is assumed that the shift for Al nuclei in aluminosilicate species with one siloxane bridge, q^1, is located at 75 ppm and that for Al in aluminate species without any siloxane linkage, q^0, is at 80 ppm. On the basis of this assumption the simple equations 7 and 8 were applied to achieve quantitative values for the q^0 and q^1 concentrations.

$$\alpha X + \beta Y = Z \qquad (7)$$

$$\alpha + \beta = 1 \qquad (8)$$

where X = 80 and Y = 75 (X and Y are ascribed to the chemical shift values of q^0 and q^1 respectively); α and β are the fractional populations of q^0 and q^1 at any time, t, during aging, respectively; and Z is the chemical shift value of the averaged band at time t. Thus:

$$\alpha = Z/5 - 15 \qquad (9)$$

By substitution of the value of Z the corresponding values of q^1 and q^0 can be obtained. Fig. 14 exhibits the profile of the ratio q^1/q^0 during evolution.
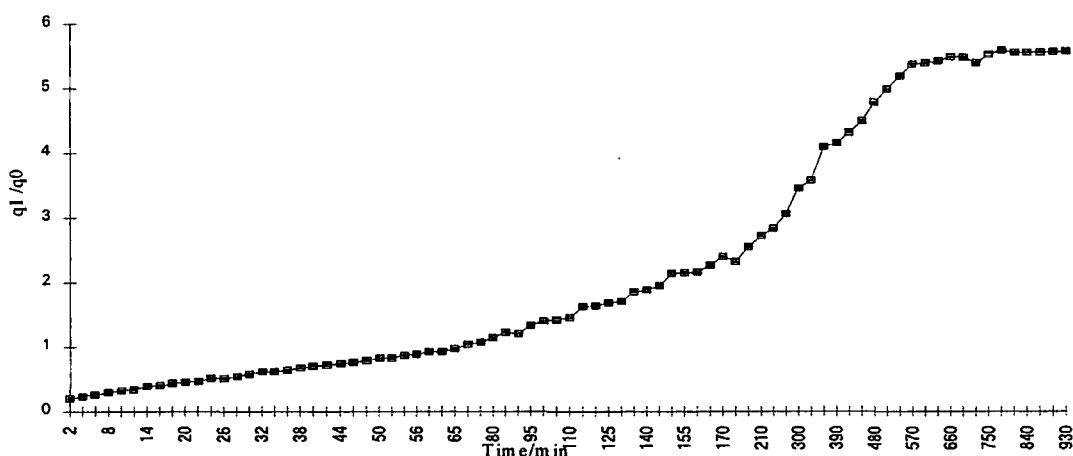
Fig. 14 Variation of the ratio of q^1/q^0 during evolution. The q^1 and q^0 values were obtained by using equation 9 (see text).

These results (Figure 14) illustrate the displacement of the band caused by the creation of q^1 and decrease of q^0. It is supposed that the siloxanization of the aluminate

ion builds up progressively with time, producing q^1. However, on the basis of the assumptions, the spectrum obtained soon after mixing indicates the presence of some amount of the q^1, i.e. the chemical shift immediately after mixing is not 80.45 ppm (Fig. 3). Likewise the spectrum recorded after 16 hours mixing could contain some q^0, i.e. the chemical shift chosen (75 ppm) is somewhat arbitrary. Clearly, however, the rate of build-up of q^1 is much slower than the rapid exchange $q^0 \leftrightarrow q^1$, which must be faster than the q^0/q^1 shift difference, i.e. ca. 780 s^{-1}. However, as mentioned earlier, it should be noticed that the conversion of q^0 to q^1 is not the only process occurring. At the same time, aluminosilicates with more than one siloxane bridge are created. The reaction of the aluminate ions with a number of silicate units leads to q^2 or q^3. Nonetheless, data obtained from the aluminium-27 NMR spectra carried out during aging did not show any substantial change of chemical shift for the rest of the bands, though they do become considerably enhanced in intensity. This supports the idea that the movement of the chemical shift involved for the first band is due to the siloxanization of q^0 to q^1, with exchange averaging.

In the above discussion it was assumed that the q^0 and q^1 resonance are located at shifts of 75 and 80 ppm respectively. However, an alternative assumption is that the band at highest frequency for the first spectrum recorded after the mixing of the silicate and aluminosilicate solutions, which has a shift of 79.01 ppm, is associated only with q^0, i.e. it is supposed that there is no q^1 at that time, and likewise that the band at highest frequency in the spectrum recorded 16 hours after mixing, located at ca. 75.9 ppm, belongs to q^1 only, i.e. no q^0 exists any longer. On this basis and by using the same equation ($\alpha X + \beta Y = Z$ where now X = 79.01 and Y = 75.9) the mole fractions of q^0 and q^1 were calculated from the equation $\alpha = Z / 3.4 - 22.2823$, where α is the proportion of q^0. The data are given in Table 2, and the profile of the mole fraction of q^1 versus time is shown in Figure 15.

Table 2: Data for chemical shifts for the band at highest frequency, extracted from spectra obtained from the evolution with time of the 156.3 MHz ^{27}Al NMR spectra of HMBTP aluminosilicate solution at 25°C.

Time (min)	Chemical shifts of the first band (ppm)	Value of q^1	Value of q^0	Mole fraction of q^1
2	79.16	0	1	0
4	79.05	0.03	0.97	0.03
6	78.96	0.06	0.94	0.06
8	78.87	0.09	0.91	0.09
10	78.76	0.12	0.88	0.12
12	78.71	0.13	0.87	0.13
14	78.59	0.17	0.83	0.17
16	78.57	0.17	0.83	0.17
18	78.48	0.20	0.80	0.20
20	78.43	0.21	0.79	0.21
22	78.40	0.22	0.78	0.22
24	78.29	0.26	0.74	0.26
26	78.29	0.26	0.74	0.26
28	78.23	0.27	0.73	0.27
30	78.15	0.30	0.70	0.30
32	78.09	0.31	0.69	0.31
34	78.09	0.31	0.69	0.31
36	78.04	0.33	0.67	0.33
38	77.98	0.35	0.65	0.35
40	77.93	0.36	0.64	0.36
42	77.90	0.37	0.63	0.37
44	77.87	0.38	0.62	0.38
46	77.84	0.39	0.61	0.39
48	77.79	0.40	0.60	0.40
50	77.73	0.42	0.58	0.42
52	77.73	0.42	0.58	0.42
54	77.67	0.44	0.56	0.44
56	77.65	0.44	0.56	0.44
58	77.59	0.45	0.55	0.45
60	77.59	0.45	0.55	0.45
65	77.53	0.48	0.52	0.48
70	77.45	0.49	0.51	0.49
75	77.41	0.51	0.49	0.51
80	77.33	0.54	0.46	0.54
85	77.24	0.56	0.44	0.56
90	77.26	0.56	0.44	0.56
95	77.14	0.59	0.41	0.59
100	77.08	0.61	0.39	0.61
105	77.06	0.62	0.38	0.62

110	77.03	0.63	0.37	0.63
115	77.90	0.66	0.34	0.66
120	76.89	0.67	0.33	0.67
125	76.86	0.68	0.32	0.68
130	76.84	0.68	0.32	0.68
135	76.75	0.71	0.29	0.71
140	76.68	0.73	0.27	0.73
145	76.59	0.73	0.27	0.73
150	76.59	0.76	0.24	0.76
155	76.58	0.76	0.24	0.76
160	76.53	0.77	0.23	0.77
165	76.46	0.79	0.21	0.79
170	76.50	0.78	0.22	0.78
180	76.48	0.79	0.21	0.79
210	76.34	0.83	0.17	0.83
240	76.30	0.84	0.16	0.84
270	76.23	0.86	0.14	0.86
300	76.12	0.89	0.11	0.89
330	76.09	0.90	0.10	0.90
360	76.98	0.94	0.06	0.94
390	76.01	0.93	0.07	0.93
420	75.94	0.95	0.05	0.95
450	75.98	0.94	0.06	0.94
480	75.98	0.93	0.07	0.93
510	75.87	0.97	0.03	0.97
540	75.83	0.98	0.02	0.98
570	75.87	0.97	0.03	0.97
600	75.76	0.99	0.01	0.99
630	75.76	0.99	0.01	0.99
660	75.79	1.0	0.0	1.0
690	75.76	0.99	0.01	0.99
720	75.76	0.99	0.01	0.99
750	75.78	1.0	0.0	1.0
780	75.72	1.0	0.0	1.0
810	75.76	1.0	0.0	1.0
840	75.76	0.99	0.01	0.99
870	75.76	1.0	0.0	1.0
900	75.68	1.0	0.0	1.0
930	75.76	1.0	0.0	1.0

The plot is, to a good approximation exponential, and yields a rate constant for the process (half-life ca. 80 min.). Of course, this procedure ignores the rest of the kinetics involving q^2, q^3 and q^4.
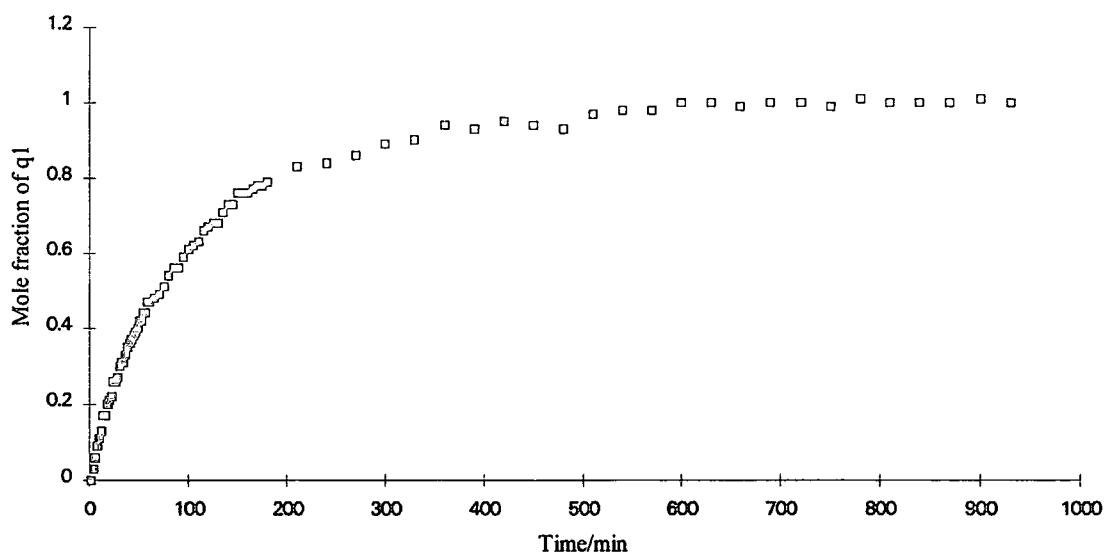
Figure 15. The mole fraction (relative to $q^0 + q^1$) of q^1 versus time · The graph was obtained by assuming the mole fraction of q^1 is 0 for the spectrum recorded soon after mixing the aluminate and silicate solutions, and that there is no q^0 16 hours afterwards. The q^1 values were obtained by the equation shown in the text.

4.4.3.3. Variation of the signal intensity with time

So far we have discussed the transformation of the chemical shifts for the observed bands in the ^{27}Al NMR spectra obtained as a function of time. However, it is pertinent also to note the variation of the signal intensity with time. Figure 8 displays ^{27}Al NMR spectra recorded within the first hour after mixing. This picture illustrates a considerable shrinkage of the intensity of the band at highest frequency. Although it might be supposed that the depletion of the signal intensity for the first band would be accompanied by a build up of the other resonances (i.e. Al(nOSi); n=2, 3 and 4), data from integration reveal that dramatic changes occur over the whole range of the observed bands (i.e. more than 130 ppm). This fact is plotted as a graph in Figure 16. Integration over the full 130 ppm produces values which decrease considerably within the first few hours after mixing. However, the spectra which were recorded overnight (i.e. starting three hours after mixing of aluminate and silicate solutions and carrying on until 16 hours) indicate that the integrated intensity during this time does not change substantially. It is possible that the small increase after 2 hours is an artefact of the spectrometer.
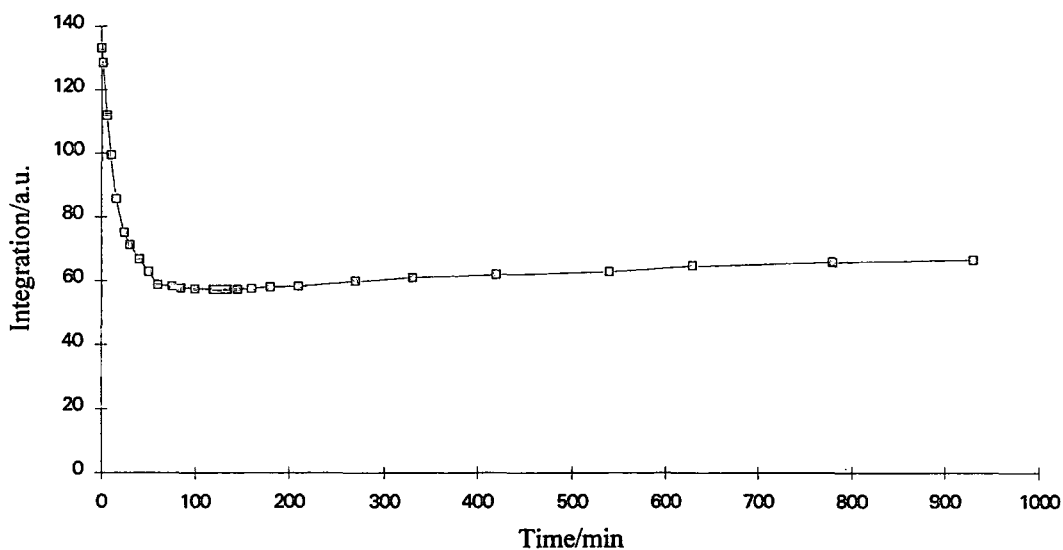
Figure 16. Variation of ^{27}Al integrated intensity as a function of time. The integrations were applied over 130 ppm in absolute intensity mode, with the same apodizing function for all the spectra.

The results do not allow us to advance in understanding the nature of the species formed. Nevertheless, it should be noticed that the measurement of spin-lattice relaxation times for the observed bands showed no more than 10 ms for T_1 (due to significant electric field gradients at the nuclei which lead to efficient quadrupolar relaxation). Since the ^{27}Al NMR spectra were collected with 100 ms recycle delays, the loss of intensity should not come from any lack of recovery of magnetisation between pulses. It is worth noting that in the case of a quadrupolar nucleus, where the chemical environment may be such as to provoke rapid quadrupole relaxation, it is possible that a proportion of the nuclei present may not be observable in a given sample, the so-called *missing intensity* problem[35]. It may be argued[36] that if the line width is comparable with the width of the spectrometer window then intensity is lost, effectively because it cannot be distinguished from the baseline [37]. However, it should be noticed that the limiting factor is not the electronic bandwidth of the instrument. Spectra obtained in the present work involved a large spectral width, so that the line intensities should not be perturbed by this factor.

In this connection, it should be mentioned that for aluminate solutions, it is possible to have the tridecameric cation $Al_{13}O_4(OH)_{24}(H_2O)_{12}^{7+}$, the structure of which was characterised by Akitt et al.[38-41] It is actually possible to detect only

tetrahedrally co-ordinated aluminium nuclei in this complex because the signals from the octahedral nuclei are too broad. The four-co-ordinated aluminium atom is presumed to be located at the centre of a structure with a symmetrical environment so that the electric field gradient at its position is very low. The 12 octahedral aluminium sites are presumed not to have a symmetrical environment. The electric field gradient at them is therefore relatively high, and the octahedron is distorted[42]. The AlO_4 unit of this cation, whose structure is known[43], gives a sharp ^{27}Al resonance at 62.5 ppm while the resonance of the octahedral aluminium is very broad and cannot be detected at high resolution[40]. Nevertheless, we may state unambiguously that at various ratios of SiO_2/Al_2O_3 there is effectively no tetrahedral aluminium present to support any evidence for the existence of the tridecameric cation, i.e. the appearance of a sharp peak at ca. 62 ppm. Moreover, ^1H NMR spectra obtained from the different aluminosilicate solutions showed no signal which can be assigned to that cation[41].

Nevertheless, to figure out that no polymerisation is involved among the aluminate species for the aluminosilicate solutions, an ageing experiment was carried out using sodium aluminate with a similar pH and temperature as well as the same concentration of aluminate. The result obtained from this experiment reveals that no decrease in intensity occurred for the aluminum-27 spectra over substantial times, i.e.^{27}Al NMR spectra showed only one resonance at ca. 80.45 ppm, with constant intensity. Accordingly, a build-up of the tridecameric cation in the aluminosilicate solution seems to be unlikely. However, it should be noted that the sample neither solidified nor gelled during the course of the experiment on the aluminosilicate solutions. Since apparenly not all the aluminium present gives rise to an ^{27}Al NMR resonance, the inference is that the nuclei concerned are present in highly distorted environments and/or large polymeric ions. Consequently, it can be hypothesised that there must be some other aluminosilicate species formed in the solution for which the already wide lines will be broadened beyond the band width limit of the high-resolution instrument.

4.4.3.4. Study of ^{27}Al NMR with time evolution at variable temperature

In order to realise the influence of the temperature on the reaction of the aluminate anion with silicate species, ^{27}Al NMR spectra of aluminosilicate solutions were carried out within the first hour after mixing of aluminate and silicate solutions at the temperatures of 0, 10, 17, 25 and 55°C. The characteristic ^{27}Al NMR spectra which

were obtained with time at these different temperatures are displayed in Figures 17- 20. These spectra were taken with the same solution for which ^{27}Al NMR spectra were carried out at 25°C as discussed above, i.e. mole ratio Si/Al of 5 and 0.875 molar SiO_2 . All spectra were recorded under similar spectroscopic conditions (e.g. recycle delay, number of transients and spectral width). No time interval was inserted between spectra, i.e. spectra were recorded every two minutes continuously. All solutions contain ca. 20% of D_2O in order to obtain field-frequency locking. All chemical shifts are referenced to the signal for external 1M $AlCl_3$ solution

It should be mentioned that in the case of 0°C, before mixing the silicate and aluminate solutions, both solutions were kept in an ice bath to equilibrate their temperatures, and the mixing of the solutions was performed at that temperate. The FIDs were accumulated for the ^{27}Al NMR spectra at 0°C immediately after preparation of the solution. Also, for the spectra which were obtained at 10 and 17°C the preparation of the aluminosilicate solutions was executed at low temperature (ca. 5°C) and the ^{27}Al NMR spectra carried out at the appropriate temperature soon after making the solutions. For the spectra which were recorded at 25°C and 55°C, the solutions were prepared at room temperature (ca. 25°C).

Figure 17 depicts the ^{27}Al NMR spectra carried out with time during the first hour after mixing solutions at the temperature of 0°C. In comparison to the spectra which were carried out under the same conditions but at 25°C (Fig. 8), the former illustrate only slight changes in intensity of the band at highest frequency. The resonance is located at 79.85 ppm (which is very closed to the 80.45 ppm ascribed to the aluminate ion free of silica, i.e. $Al(OH)_4^-$). Essentially, at 0°C there is a large number of q^0 ions in the solution during the first hour after mixing. It is nevertheless clear that we require supplementary data for this system and that the other bands in the ^{27}Al NMR might be informative. Spectra taken at 0°C display (Figure 17) other bands at the shift ranges of ca. 70 and 65 ppm, which reveals that reaction of aluminate with different silicate species can happen even at 0°C, i.e. creation of aluminosilicate species with more than one siloxane bridge. The evidence from ^{27}Al NMR spectra carried out at 10 and 17°C as a function of time (figures 18 and 19 respectively, obtained using a Bruker AMX 500 spectrometer) indicates that no dramatic differences occur in their characteristics. By considering the band at highest frequency, it can be seen that in both cases no substantial variation occurs in the intensity. Nonetheless, comparison of these

Figure 17. Illustration of the temperature-dependence of the reaction between aluminate and silicate anions. The evolution with time of the 156.3 MHz [27]Al spectrum of an aluminosilicate solution prepared by rapid mixing of fresh sodium aluminate and aged HMBTP silicate solutions, taken at 0°C and with a final composition of 0.875 molar SiO_2; and Si/ Al = 5. Before mixing, both solutions were kept in an ice bath and the mixing was done at that temperature. Immediately following mixing, a sample of the solution was placed in the NMR spectrometer and the [27]Al spectrum measured as a function of time at 0°C. Spectra are taken under the same conditions separated by no time interval. The spectra were recorded for 4 hours, i.e. the first spectrum was obtained 5 min after mixing and the last one 240 min. Spectrum conditions were as follows:

Recycle delay : 0.1 s ; acquisition time : 0.2 s ; number of transients : 960 ; spectral width : 46729.0 Hz ; pulse duration for a 90° flip angle : 45 μs.
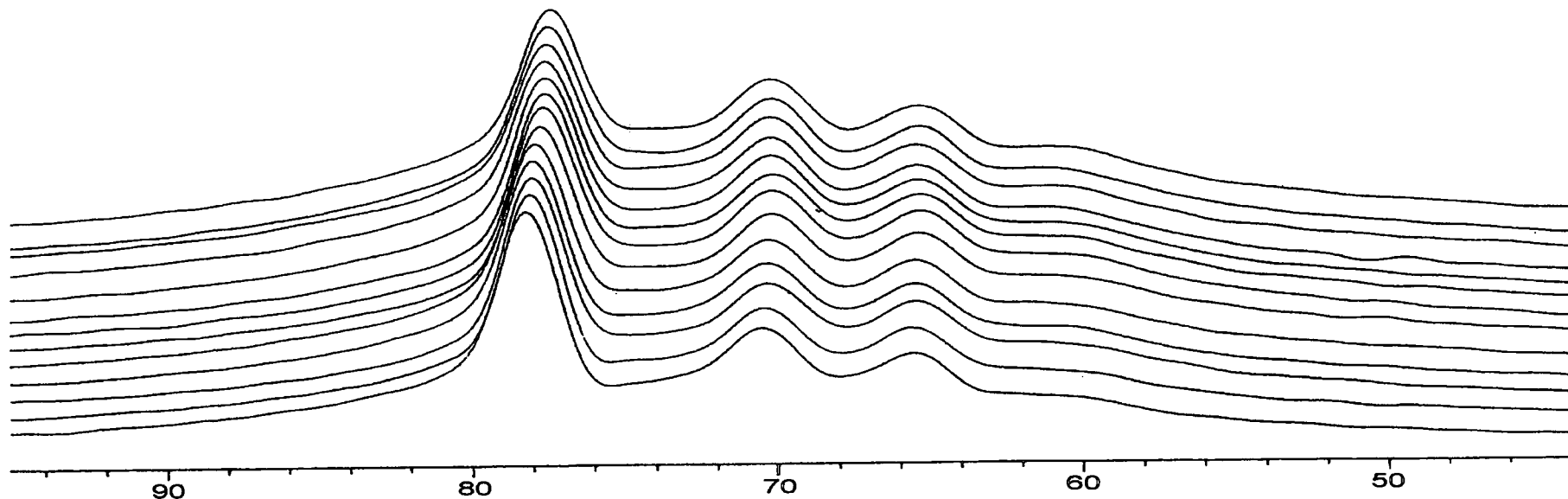
Figure 18. Illustration of the temperature-dependence of the reaction between aluminate and silicate anions. The evolution with time of the 130.3 MHz ^{27}Al spectrum of an aluminosilicate solution prepared by rapid mixing of fresh sodium aluminate and aged HMBTP silicate solutions taken at 10°C and with a final composition of 0.875 molar SiO_2 and Si/ Al = 5. Before mixing, both solutions were kept at low temperature, ca. 5°C, and mixing was done at that temperature. Immediately following mixing, a sample of the solution was placed in the NMR spectrometer and the ^{27}Al spectrum measured as a function of time at 10°C. Spectra are taken under the same conditions separated by no time interval. The spectra were recorded for 2 hours, i.e. the first spectrum was obtained 5 min after mixing and the last one taken after 120 min. Spectrum conditions were as follows: Recycle delay : 0.1 s ; acquisition time : 0.2 s ; number of transients : 960 ; spectral width : 46729.0 Hz ; pulse duration for a 90° flip angle : 45 μs.
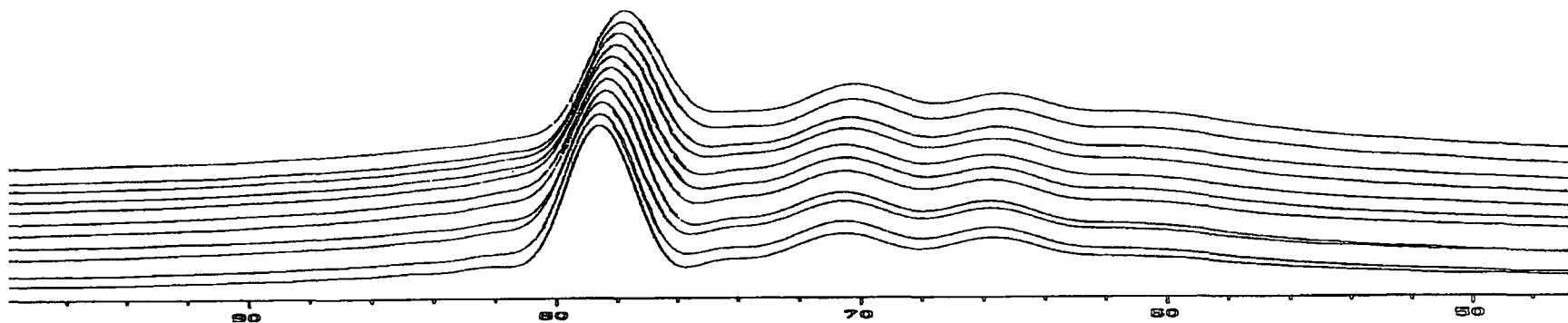
Figure 19. Illustration of the temperature-dependence of the reaction between aluminate and silicate anions. The evolution with time of the 130.3 MHz ^{27}Al spectrum of an aluminosilicate solution prepared by rapid mixing of fresh sodium aluminate and aged HMBTP silicate solution, taken at 17°C and with a final composition 0.875 molar SiO_2 and Si/ Al = 5. Before mixing, both solutions were kept at low temperature, ca. 5°C, and mixing was done at that temperature. Immediately following mixing, a sample of the solution was placed in an NMR spectrometer and the ^{27}Al spectrum measured as a function of time at 17°C. Spectra are taken under the same conditions separated by no time interval . Spectra were recorded for 2 hours, i.e. the first spectrum was obtained 5 min after mixing and the last one 120 min. Spectrum conditions were as follows:

Recycle delay : 0.1 s ; acquisition time : 0.2 s ; number of transients : 960 ; spectral width : 46729.0 Hz ; pulse duration for a 90° flip angle : 45 µs.
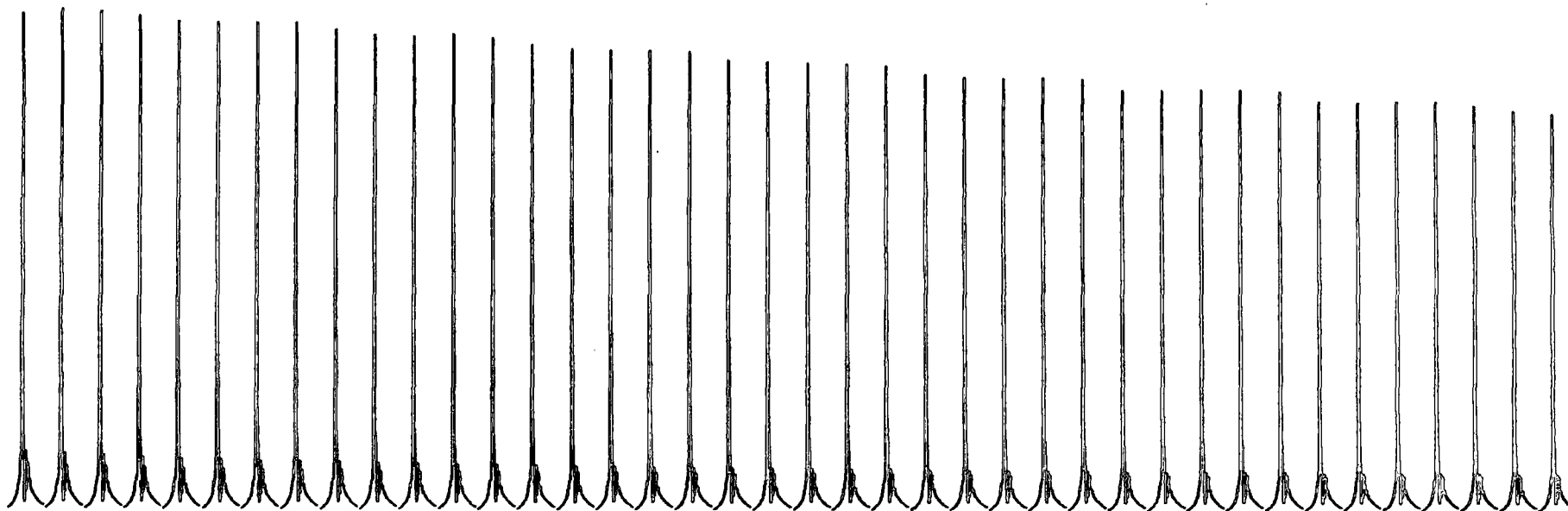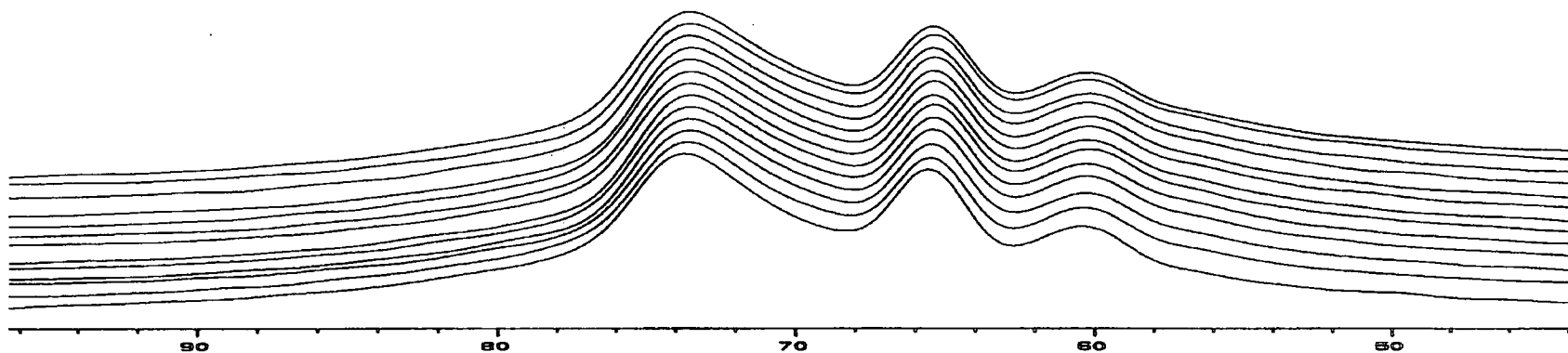
Figure 20. Illustration of the temperature-dependence of the reaction between aluminate and silicate anions. The evolution with time of the 130.3 Mhz [27]Al spectrum of an aluminosilicate solution prepared by rapid mixing of fresh sodium aluminate and aged HMBTP silicate solutions, taken at 55°C and with a final composition of 0.875 molar SiO_2; and Si/ Al = 5 molar. Before mixing both solutions were kept at room temperature, ca. 25° C, and mixing was done at that temperature. Immediately following mixing, a sample of the solution was placed in the NMR spectrometer and the [27]Al spectrum measured as a function of time at 55°C. Spectra are taken under same conditions separated by no time interval . Spectra were recorded for 2 hours (i.e. the first spectrum was obtained after 5 min and the last one after 120 min of mixing), Spectrum conditions were as follows:

Recycle delay : 0.1 s ; Acquisition time : 0.2 s ; Number of transients : 960 ; Spectral width : 46729.0 Hz ; Pulse duration for a 90° flip angle : 45 µs.

experiments with that carried out at 0°C indicates a small decrease of the intensity, more visible than that for the 0°C experiment. Likewise, the development of the characteristic ^{27}Al NMR spectra recorded during the first hour of mixing at 0°C is more insignificant than in the 10 and 17°C cases. Naturally, the reaction rates of aluminate and silicate depend upon the temperature of the solution. As was described earlier, the ^{27}Al NMR spectra taken at 25°C illustrate that it needed about 16 hours for the aluminosilicate solution to reach an equilibrium state. Accordingly, one can expect a very considerable time to be needed for aluminosilicate solutions to reach equilibrium at lower temperatures (i.e. 0, 10 and 17°C).

Another point worth noting is the variation of the chemical shift for the band at highest frequency occurring for the different temperatures within the first hour after mixing. This parameter is also highly sensitive to the temperature of the solution.

Figure 21 plots the variation of the chemical shifts of the ^{27}Al band at highest frequency versus time with variable temperature. Data were extracted from the spectra recorded during the first hour after mixing of the aluminate and silicate solutions. The spectra carried out at 0, 10, 17 and 25°C exhibit the band at highest frequency placed in the shift ranges 79.85, 79.5-78.94, 79.17-78.29 and 79.1-77.55 ppm respectively, which can be ascribed to the coalesced peaks of q^0 and q^1. However, at 55°C this band is located at ca. 73.5 ppm, which therefore must be assigned to the average over the three species q^0, q^1 and q^2.
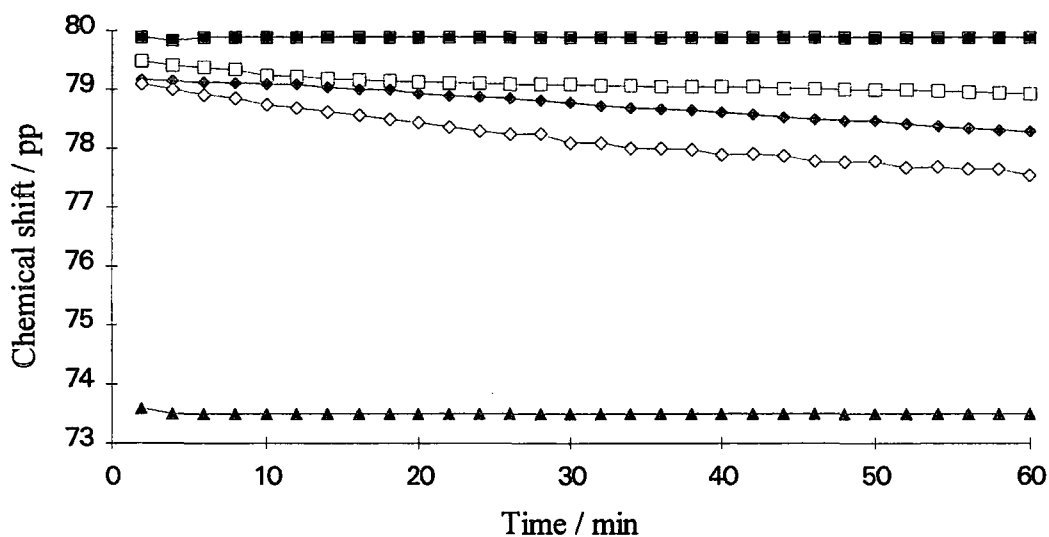
Figure 21. Schematic plots of the observed chemical shift, δ, for the first band of the ^{27}Al NMR spectra as a function of time, obtained at variable temperature. The chemical shifts were obtained from recording the aluminium-27 NMR within the first hour after mixing the silicate and aluminate solutions; (■) 0°C, (□) 10°C, (◆) 17°, C (◇) 25°C, (▲) 55°C.

Clearly the variation of the chemical shift with time is influenced by the temperature in the range between 0 and 25°C. Increasing temperature causes the variation of the shift of the first band to increase. As mentioned earlier the transformation of the chemical shift can be associated with enhancement of the proportion of q^1. Nonetheless it is quite obvious from Figure 21 that the chemical shift associated with the first band is constant as a function of time at the temperature of 55° C, at least after the first two minutes. However, the shift in this case is located at ca. 73.5 ppm. Thus at this temperature the aluminate ions react very quickly with the silicate ions, leading to a considerable amount of q^2 and q^1. within a few minutes. However, the rapid exchange of q^1 and q^2 as well as q^0 leads to a coalesced peak at 73.5 ppm.

4.4.4. Two-dimensional ^{27}Al NMR exchange spectroscopy

Nuclear magnetic resonance is an important technique for investigation of the kinetics of chemical-exchange processes. The unique ability to resolve and assign the separate signals due to nuclei in different chemical environments makes NMR especially powerful for such studies. The application of the resultant spectral changes to

the study of kinetics is often called dynamic NMR (DNMR)[44]. Several DNMR techniques have been developed that evaluate rates associated with chemically exchanging systems. Most commonly used are the classic line-shape analysis and more recent magnetization-transfer methods.

Magnetization transfer (saturation transfer, inversion transfer) is a method that has been used to study a variety of dynamic processes. Selective irradiation saturation or inversion of one or more resonances of an exchanging system, followed by examination of the effect of that perturbation on the remaining sites, allows determination of the exchange pathways and rate constants.

Two-dimensional exchange spectroscopy, based on the transfer of magnetization such as occurs in chemical exchange processes, is known as EXSY. There is a related two-dimentional experiment known as NOESY, which corresponds to the nuclear Overhauser effect. The purpose of this study is to show how 2D EXSY can be applied to problems in chemical-exchange kinetics of aluminate groups present in aluminosilicate solutions.

4.4.4.1. The Pulse Sequence for 2D Exchange Spectroscopy (EXSY)

The pulse sequence is shown in Fig. 22. The first $90°_x$ pulse produces transverse magnetization that precesses during the evolution period in the xy-plane. A second $90°_x$ pulse is followed by the mixing time t_m. The third $90°_x$ pulse transforms the resulting z-magnetization into transverse magnetization, which is measured during the detection phase. The acquisition time t_2 is the same as the acquisition time t in 1D NMR. The transverse magnetization M (subscript xy now omitted) is measured as a function of t_2. Although time is a continuous variable, measurements are made at regularly spaced, discrete values of t_2. The labelling time t_1, evolution time, is also variable. By regularly incrementing t_1 at each successive pulse sequence, t_1 becomes a second discrete variable just like t_2. The mixing time is the time during which chemical exchange occurs which is monitored by the 2D experiment. This time is of the order of the spin-lattice relaxation time or the inverse rate constant of chemical exchange processes. The measured magnetization is then a function of both t_1 and t_2 (eq. 10). Double Fourier transformation of this time-domain function then converts to a 2D spectrum (eq. 11), where the sums over discrete times are written as integrals, that is a function of the two frequency variables ω_1 and ω_2.

$$M = M(t_1, t_2) \tag{10}$$

$$S(\omega_1,\omega_2) = \iint M(t_1,t_2)e^{-i\omega_1 t_1}e^{-i\omega_2 t_2}\, dt_1\, dt_2 \qquad (11)$$
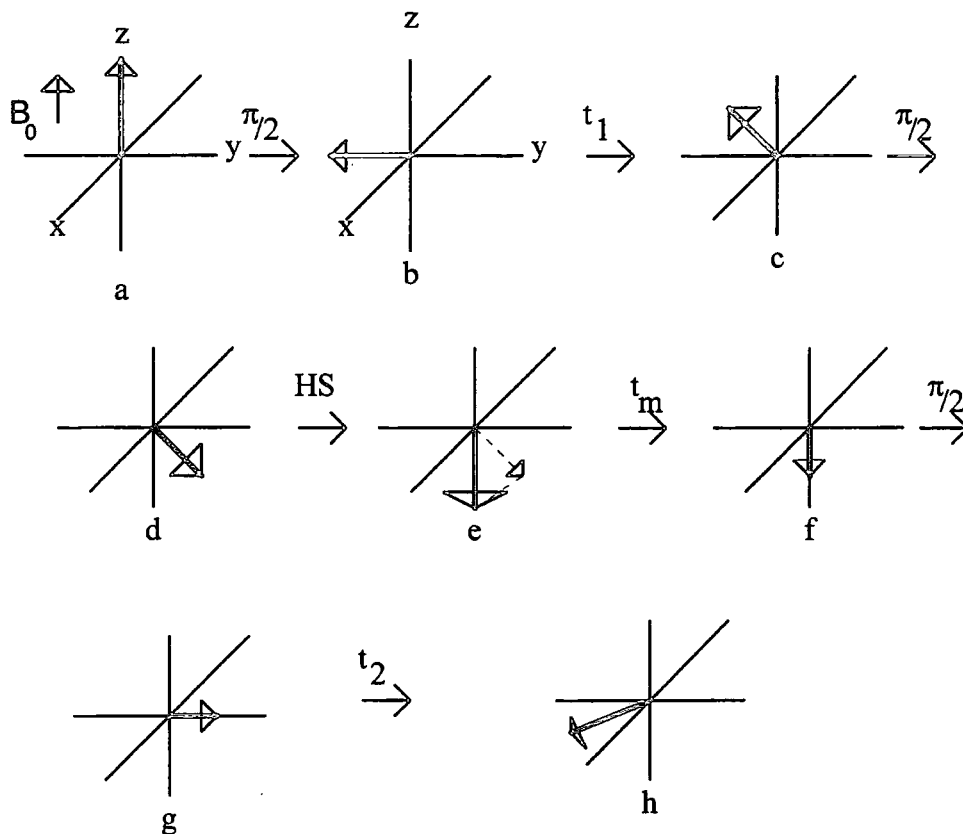
Fig. 22. Vector representation of the 2D NMR experiment: a) The magnetization is initially aligned along B_0. b) A 90 $°_x$ pulse rotates the magnetization into the xy plane where it (c) evolves for a time t_1. d) A second 90° pulse rotates the magnetization into the xz plane. Following a homospoil pulse (e), only the z component is obtained. During the mixing time this z magnetization undergoes relaxation and exchange (f). Following a third 90° pulse (g) the net magnetization (h) is detected during t_2.

Each site produces a two-dimensional peak at its own frequency along both axes, i.e. along the diagonal of the 2D spectrum. During the t_1 period, nuclei that are in site A will contribute a component $\exp(i\omega_A t_1)$ to $M(t_1,t_2)$. If during the mixing period, t_m, some of those nuclei (i.e. A) exchange to site B, they will precess at frequency ω_B during the acquisition period and thus will contribute a component $\exp(i\omega_B t_2)$ to $M(t_1,t_2)$. Double Fourier transformation will produce a peak at $\omega_1=\omega_A$ along the first frequency co-ordinate and at $\omega_2 = \omega_B$ along the second frequency co-ordinate. Those nuclei that do not exchange during t_m contribute $\exp(\omega_A t_1)$ $\exp(i\omega_A t_2)$ to the magnetization, so they produce a peak at $\omega_1 = \omega_A$, $\omega_2 = \omega_A$. Likewise nuclei that start in

site B and remain there or exchange to site A during t_m produce peaks at $\omega_1 = \omega_B$, $\omega_2 = \omega_B$ or at $\omega_1 = \omega_B$, $\omega_2 = \omega_A$, respectively.

4.4.4.2. Study of exchange processes in the aluminosilicate solutions by ^{27}Al NMR 2D-EXSY.

As mentioned above, NMR spectroscopy is unique in the range of exchange processes that it can usefully probe because it can, without perturbing the system, provide detailed mechanistic and kinetic information about reactions that are occurring in equilibrium mixtures.

The exchange process of the aluminosilicate ions present in the aluminosilicate solutions may be confirmed by the observation of the connectivities for each anion, determined with the help of two-dimensional ^{27}Al NMR exchange spectroscopy. Figure 23 shows the ^{27}Al 2D NMR EXSY taken at 25°C (for the aged aluminosilicate solution with Si/Al = 5 and 0.875 molar SiO_2). Strong cross peaks appear between q^1 and q^2, leaving no doubt that they arise from exchange between those sites. However, the EXSY experiment indicates that no exchange is involved among the other species. Therefore it can be said that q^3 and q^4 sites are more stable than q^1 and q^2. It can be supposed that aluminate sites which are trapped by more than two siloxane bridges are stabilized. i.e. q^3 or q^4.

4.4.4.3. 2-D NMR Exchange spectroscopy at variable temperature

Aluminium-27 2-D NMR EXSY experiments were carried out with the same aluminosilicate solution (the aged solution with Si/Al = 5 and 0.875 molar in SiO_2) at several temperatures. It is well known that the exchange rate among the species in (alumino)silicate solutions increase with increasing temperature[45]. In order to realise the relative stability of the aluminosilicate species at different temperatures and to understand the exchange process among the various species, ^{27}Al 2-D EXSY NMR was carried out at temperatures between 0°C and 75°C in 10°C steps. Figures 24a -24f present the ^{27}Al 2-D EXSY NMR of the aged HMBTP aluminosilicate solution. All spectra were obtained under similar conditions, e.g. mixing time, number of transients and recycle delay. As we know, cross-peaks in the spectrum illustrate the corresponding nuclei which exchange from one site to another. Figures 24a-24d indicate that no essential difference can be observed in the temperature range 10°C to 45°C, so that the 2-D spectra exhibit only one pair of cross peaks (off-diagonal) which corresponding to two species located at shifts of ca. 75 and 70 ppm, ascribed to the q^1 and q^2 sites. It is
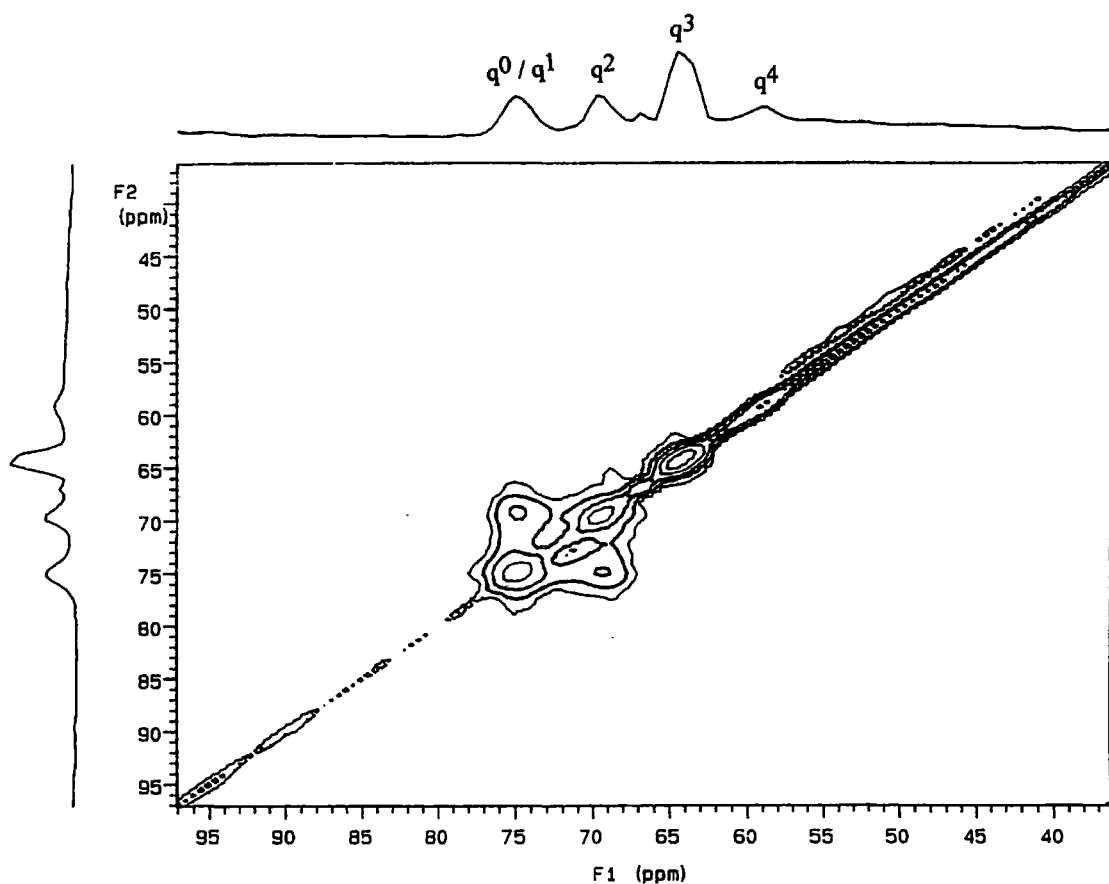
Figure 23 ^{27}Al 2D exchange NMR spectra for a HMBTP aluminosilicate solution of composition 0.875 molar SiO_2 and Si/ Al = 5 molar ratio taken at 25°. The mixing time was optimized 1 ms. The horizontal axis (F_1 dimension) as well as the vertical axis (F_2 dimension) show the [27]Al resonances. Data were collected as follows:

Recycle delay : 0.05 s ; acquisition time : 0.01 s ;spectral width 9498 Hz ; number of transients : 32 ; Number of FIDs : 64

Figure 24. Temperature-dependence of the exchange process for the aluminosilicate solution. 156.3 MHz ^{27}Al 2-D EXSY NMR spectra (contour plots) of a HMBTP aluminosilicate solution of composition 0.875 molar SiO_2; Si/HMBTP = 2 and Si/ Al = 5 molar ratio taken at variable temperature; cross peaks indicate the exchange is occurring among the aluminosilicate sites, and their position depends upon the temperature of the solution. It is illustrated that at the elevated temperature this process happens among different aluminosilicate species. Relaxation delay between two transients 0.05 s, acquisition time 0.01 s, spectral width in f_2 and f_1 axis 9498 Hz, 128 transients accumulated for each 64 increments of t_1, mixing time 1 ms, FID data matrix 256 × 256, 2D spectrum matrix 512 512; projection spectra are shown in both horizontal and vertical axes; (a) 10, (b) 25, (c) 35, (d) 45, (e) 55 and (f) 75°C.

(c)

F2 (ppm)

F1 (ppm)

(d)

F2 (ppm)

F₁ ppm
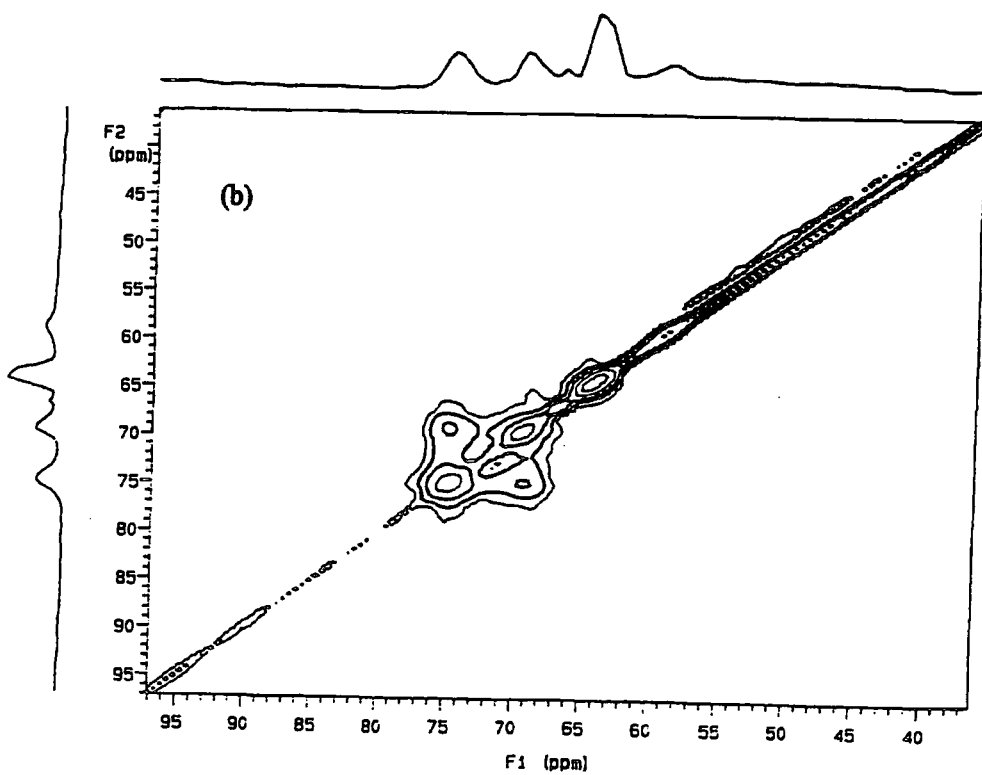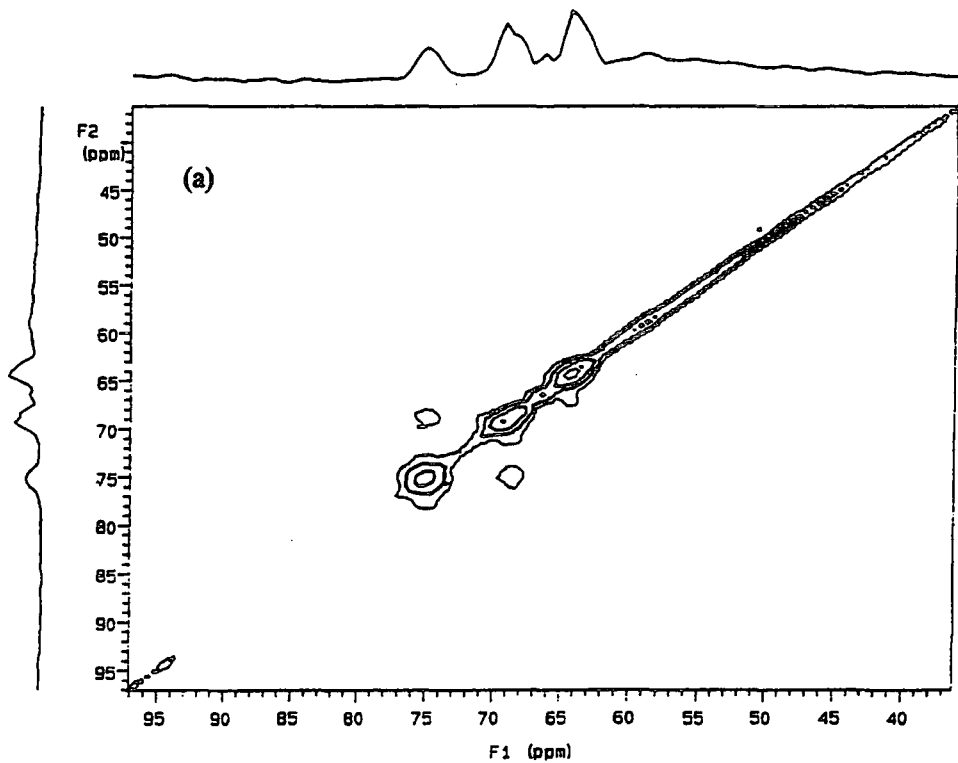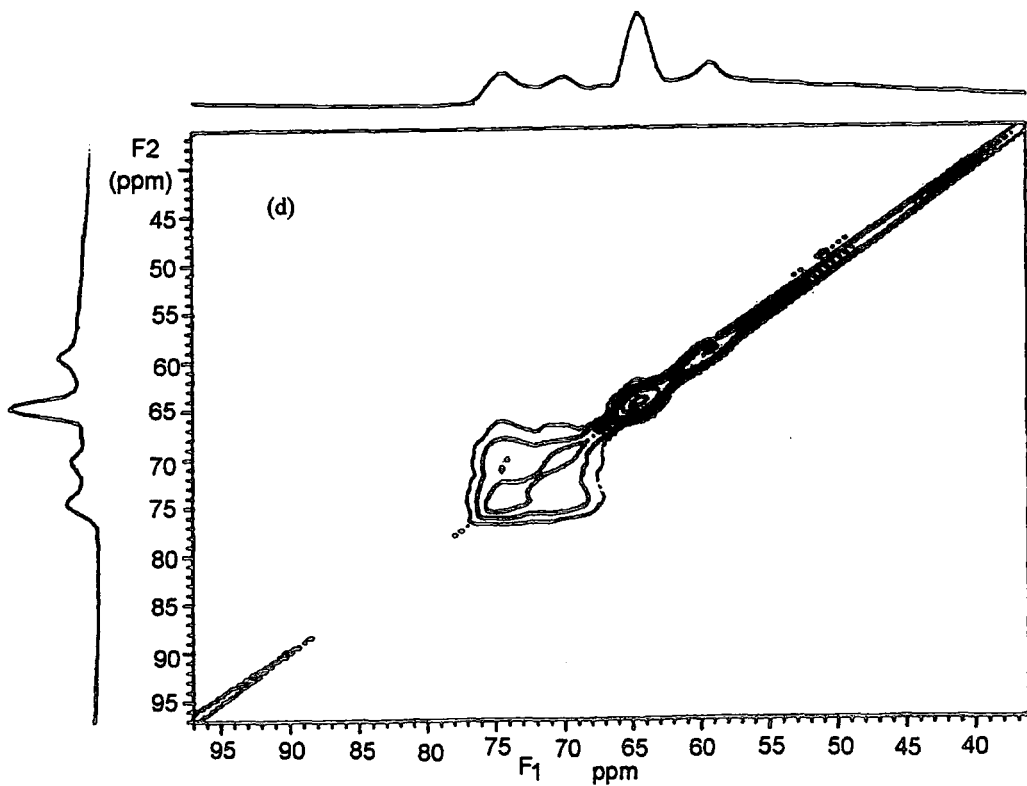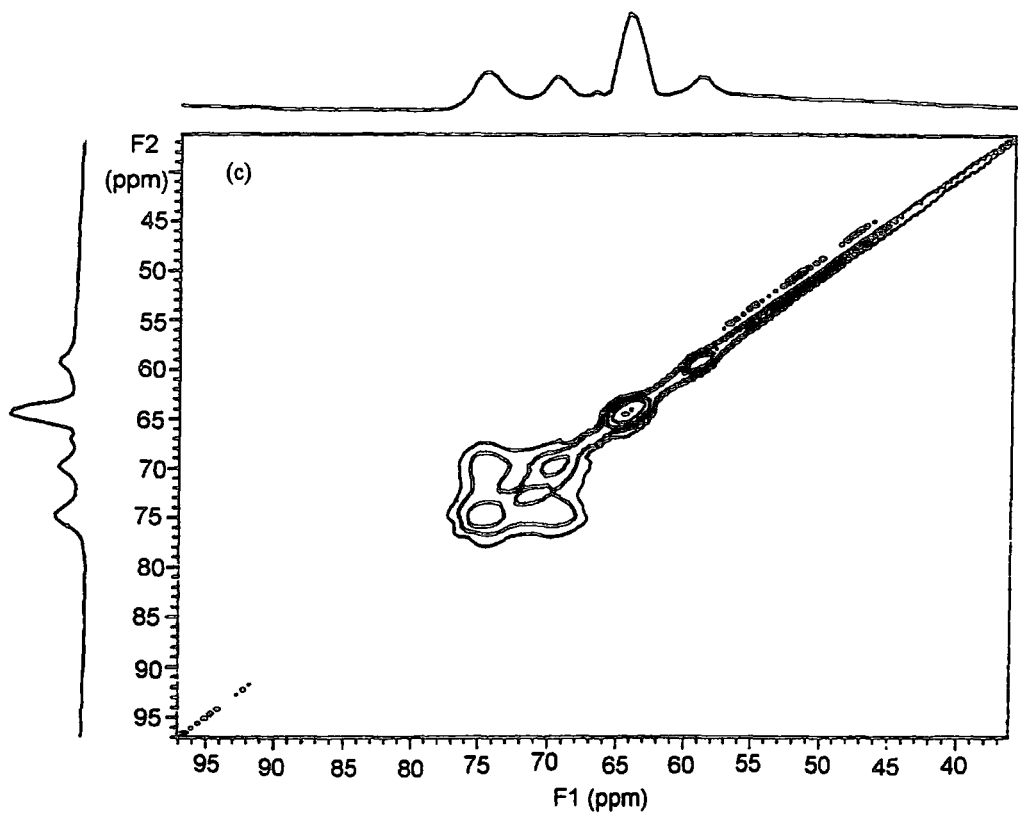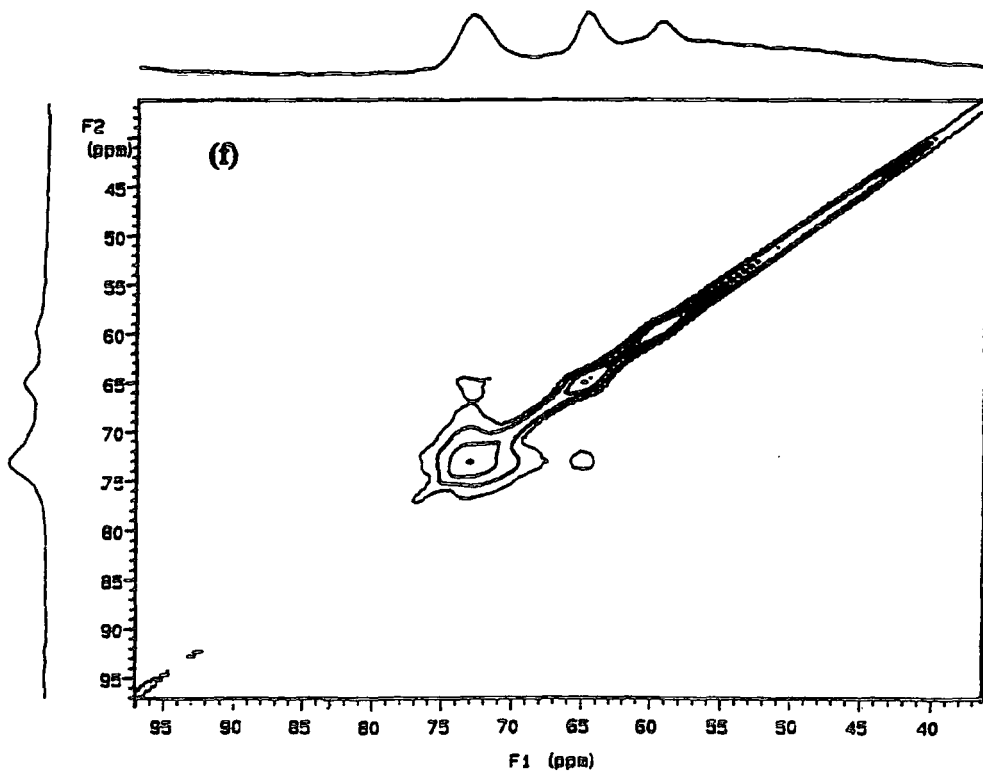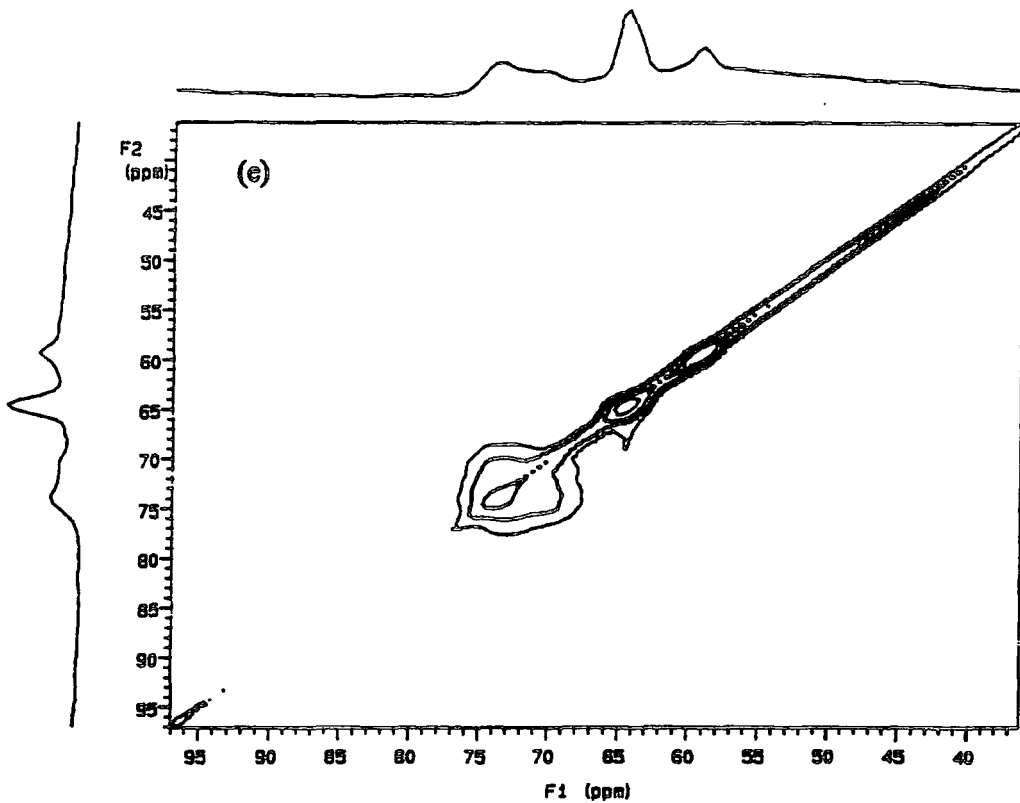
supposed that if any q^0 exists in the solution it is also involved in the exchange. Figures 24a-24d illustrate that the cross-peak in the 2D-EXSY becomes more prominent with increasing temperature up to 45°C, in other words the rate of exchange increases as expected. Figure 24a shows that the aluminium-27 2-D EXSY NMR recorded at 10°C already exhibits one pair of cross-peaks for the mixing time of 1 ms, so that exchange is already established at this temperature.

At the temperature of 55°C (fig. 24e), the signals assigned to q^1 and q^2 are almost entirely coalesced (see ^{27}Al NMR 1-D spectra recorded at variable temperature, Figure 6). As can be seen, the cross peaks are spread over the shift range between 70 and 75 ppm due to the fast exchange between the two sites (i.e. q^1 and q^2). However no evidence indicates that q^3 is also involved in the exchange process at that temperature on the timescale of 1 ms, which shows that species belonging to q^3 and q^4 are stable at 55°C.

The ^{27}Al 2-D EXSY NMR spectrum at 75°C (Fig. 24f) reveals that a cross-peak occurs at a new position, located between the shift ranges of ca. 65 and ca. 73 ppm, which shows that the exchange process now occurs among q^1, q^2 and q^3. Accordingly, it can be realised that at the temperature of 75°C the aluminosilicate species of the cage-like units such as prismatic hexamer (Q^3_6) and cubic octamer (Q^3_8) may be involved. However, it should be noted from the ^{27}Al 2-D EXSY NMR spectra shown in Figure 24f that no exchange can be deduced for the peak assigned to q^4, located at a shift of 60 ppm, which demonstrates the stability of this particular aluminium environment even at elevated temperature. Thus at 75°C most of the aluminosilicate species are involved in the exchange process, including the double-ring species. Nonetheless the exchange rate for q^3 is slow enough at the NMR timescale to give a distinct signal (i.e. the band at 65 ppm is still resolved).

4.5. Conclusions

The present study convincingly shows the formation of aluminosilicate anions through the reaction of aluminate and silicate anions. ^{27}Al NMR spectra reveal evidence for Al bound to zero, one, two, three and four Si atoms through oxygen atoms. The production of Si and Al sites present in aluminosilicate species is affected by the ratio of Si/Al. It can be concluded that most of the anions present in HMBPT aluminosilicate solutions at 25°C do not reach dynamic equilibrium rapidly. However it should be noted that anion

rearrangement of q^0 and q^1 is sufficiently fast to allow NMR experiments to resolve two separate resonance line during the evolution time. The observed spectra and behaviour as a function of time of aluminosilicate silicates are consistent with the presence of q^4 to give the line at ca. 60 ppm. The bands located at shifts of about 80, 75, 70, 65 and 60 ppm are assigned to the Al(0OSi), Al(1OSi), Al(2OSi), Al(3OSi), Al(4OSi) respectively.

4.6. References

1. Barrer R.M. , *Chem. Brit.*, 380 (1966)

2. Barrer R.M. *The Hydrothermal Chemistry of Zeolites; Academic Press: London* 1982.

3. Roozeboom, F. ; Robson H. E. and Chan S.S. *Zeolites* **3**, 321 (1983).

4. Barrer R.M. and Sieber w. *J. Chem. Soc. , Dalton,* 1020 (1977)

5. Derouane E.G. ; Detrmmerie S. ; Gabelica Z. and Blom N. *Appl. Catal.* **1**, 201 (1981).

6. Harris, R.K. ; Knight, C.T.G. ; Hull, W.E. *J.Am. Chem. Soc.* **103**, 1577 (1981).

7. Harris, R.K. ; Newman, R.H. *J. Chem.Soc., Faraday Trans.* **73**, 1204 (1977).

8. Harris, R.K.; Jones, J. ; Knight, C.T.G. ; Newman, R.H. *J.Mol. Liq.* **29**, 63 (1984).

9. Knight, C.T.G. ; Kirkpatrick, R.J. ; Oldfield, E. *J. Am. Chem. Soc.* **109**, 1632 (1987).

10. McCormick, A.V. ; Bell, A.T. ; Radke, C.J. *Zeolites,* **7**, 183 (1987).

11. McCormick, A.V. ; Bell, A.T. ; Radke, C. *J. Phys. Chem.* **93**, 1737 (1989).

12. Kinrade, S.D. and Swaddle, T.W. *Inorg.Chem.* **27**, 4259 (1988).

13. Engelhardt, G.; Hoebbel, D. *J. Chem. Soc., Chem. Commun.* 514 (1984).

14. Mortlock, R.F. ; Bell, A.T. and Radke, C.J. *J. Phys. Chem.* **95**, 7847 (1991).

15. Kinrade, S.D. and Swaddle, T.W. *Inorg.Chem.* **28**, 1952 (1989).

16. McCormick, A.V. ; Bell, A.T. and Radke, C.J. *J. Phys.Chem.* **93**, 1741 (1989).

17. Dent Glasser, L.S. ; Harvey, G. *J Chem. Soc., Chem. Commun.* 1250 (1984).

18. Mortlock, R.F. ; Bell, A.T. and Radke, C.J. *J. Phys. Chem.* **95**, 372 (1991).

19. Mortlock, R.F. ; Bell, A.T. Chakraborty, A.K. and Radke, C.J. *J. Phys. Chem.* **95**, 4501 (1991).

20. Ciric, J ; Lawton S.L. ; Kokotailo, G. T. and Griffin, G.W. *J. Am. Chem. Soc.* **100**, 2173 (1978).

21. Lippmaa, E. ; Mägi, M. ; Samoson, A. ; Engelhardt, G. and Grimmer, A-R. *J. Am. Chem. Soc.,* **102**, 4889, (1980).

22. Mägi, M. ; Lippmaa, E. ; Samoson, A. ; Engelhardt, G. and Grimmer, A-R. *J. Phys. Chem.,* **88**, 1518, (1984).

23. Smith, K.A. ; Kirkpatrick,R.J. ; Oldfield, E. and Henderson, D.M. *Am. Mineral.,* **68**, 1206 (1983).

24. Müller, D. ; Gessner, W. ; Scheler, G. *Polyhedron* **2**, 1195 (1983).

25. Loewenstein, W. *Am. Mineral.,* **39**, 92 (1954).

26. Engelhardt, G; Jancke, H. Hoebbel, D. and Wieker,W. *Z. Chem.* **14,** 109 (1974).

27. Muller, D.; Gessner,W; Samoson, A.; Lippmaa,E. and Scheler, G. *J. Chem. Soc., Dalton Trans.,* 1277 (1986).

28. Müller, D. ; Hoebbel, D. ; Gessner, W. *Chem Phys. Lett.* **84**, 25, (1981).

29. Simeral, L.S. ; Zens, T. and Finnegan, J. *App. Spec.* 47,No. 11, 1954

30. Ferrige, A. G. ; Lindon , J. C. *J. Magn. Reson.* **31**, 337 (1978).

31. Engelhardt, G. and Michel D. " High-resolution solid-state NMR of silicates and zeolites", Wiley , New York, 1987.

32. Hoebbel, D.; Garzo, G.; Ujszaszi, K.; Engelhardt, G. Fahlke,B. and Vargha,A. *Z.Anorg. Allg. Chem.,* **484**, 7 (1982).

33. Jacobs, P.A. and Uytterhoeven J.B. *J. Chem. Soc. Faraday* **69**, 359 (1973).

34. Gill, B.; Brooclawik, E. ; Datka, J and Klinowski, J. *J. Phys. Chem.* **98**, 930 (1994).

35. Akitt, J.W. *Progress.in NMR Spect.,* edited by Emsley, J. W.; Feeney, J. and Sutcliffe, L., Pergamon press, Oxford, 1988.

36. Akitt, J.W. *Prog. Nucl. Magn. Reson. Spectrosc.,* **21**, 1 (1989).

37. Akitt, J.W.; Elders, J.E. ; Fontaine, X.L.R. and Kundu, A.K. *J. Chem.Soc. Dalton,* 1889 (1989).

38. Akitt, J. W. and Farthing, A. *J. Chem. Soc. Dalton*, 1624 (1981).

39. Akitt, J.W. and Farthing, A. *J. Magn. Reson.* **32**, 345 (1978).

40. Akitt, J. W. and Mann, B.E. *J. Magn. Reson.* **44**, 584 (1981).

41. Akitt, J.W. and Elders, J.M. *J. Chem. Soc. Dalton,* 1347 (1988).

42. Bottero, J.Y. ; Cases, J.M. ; Fiessinger, F. and Poirier, *J. Phys. Chem.* **86,** 2933 (1980).

43. Johannson, G. *Ark. Kemi.,* **20**, 305 (1963).

44. Johnson, C.S. *Adv. Magn. Reson.*1, 33 (1965).

45. Engelhardt, G. and Hoebbel, D. *J. Chem. Soc., Chem. Commun.* 514 (1984).

46. Dent Glasser, L.S.; Harvey, G. *Proceeding of the sixth International Zeolite Conference,*; Olson, D., Bision, A., Eds.; Butterworths: London, 925-938 (1984).

Chapter five

Structural Analysis of Silicate Crystals by Solid-State High-Resolution NMR and X-ray Diffraction

5.1. Introduction

The atomic-scale mechanisms of formation of zeolites and related microporous host-guest materials are very complex. A detailed understanding of the molecular processes that occur during zeolite crystallisation has not been attained so far, in spite of many investigations in this field.

The search for a detailed understanding of the mechanism of zeolite synthesis has, over the past two decades, promoted many investigations into the species present in silicate solutions (with and without aluminate) and solids obtained therefrom. The vital role played by nitrogen-containing cations as templates in hydrothermal zeolite synthesis has focused attention on systems including these components. It is well-known that such cations stabilise cage-like silicate anions, for instance the so-called prismatic hexamer $Si_6O_{15}^{6-}$ and cubic octamer $Si_8O_{20}^{8-}$ (and their various protonated forms). From such solutions a variety of crystalline hydrates can be obtained. Recently these have been shown to have network topologies involving host-guest situations, i.e. they are clathrates. The host structures of these materials are three-dimensional tetrahedral networks. The frameworks involve either covalent bonding (Si-O-Si) or hydrogen bonding (Si-O-H···O-Si, HOH···O-Si and HOH···OH$_2$). Parallels are being suggested between these clathrates and zeolites. In particular, a series of papers by Wiebcke and co-workers has established the crystal structures of five systems involving the cubic octamer, namely:

$[NMe_4]_8[Si_8O_{20}].65H_2O$	(I)[1,2]
$[NMe_4]_{16}[Si_8O_{20}][OH]_8.116H_2O$	(II)[3]
$[DMPI]_6[Si_8O_{18}(OH)_2].48.5H_2O$	(III)[4]
$[TMPA]_4[Si_8O_{20}].34H_2O$	(IV)[5]
$[DDBO]_4[Si_8O_{20}].32H_2O$	(V)[5]

where,

DMPI = 1,1-dimethylpiperidinium	(VI)
TMPA = 1,1,4,4-tetramethylpiperazinium	(VII)
DDBO = 1,4-dimethyl-1,4-diazoniabicyclo[2.2.2]octane	(VIII)
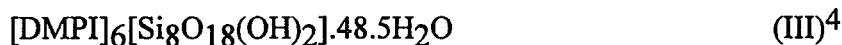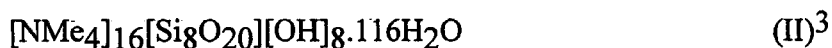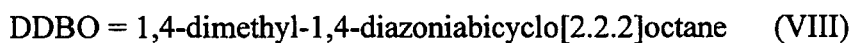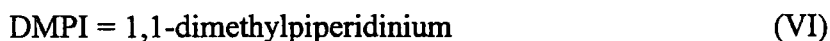
Clearly I, II and III contain singly-charged cations, whereas IV and V have doubly-charged cations. However, in all cases a stable host-guest network is obtained.

5A. Synthesis and structural analysis of a crystalline silicate, [HMBTP]$_2$[Si$_8$O$_{18}$(OH)$_2$].41H$_2$O, involving solid-state high-resolution NMR and X-ray diffraction

As part of an ongoing investigation into the synthesis of novel zeolites, it was aimed to produce a silicate clathrate hydrate containing the cubic octameric silicate anion with triply-charged cations. The interesting organic cation which has been used in this study is HMBTP (IX), where HMBTP is: (2,3,4,5,6,7,8,9-octahydro-2,2,5,5,8,8-hexamethyl-2H-benzo(1,2-c:3,4-c':5,6-c-")tripyrrolium^{+++}).

$$R = CH_3$$

(IX)
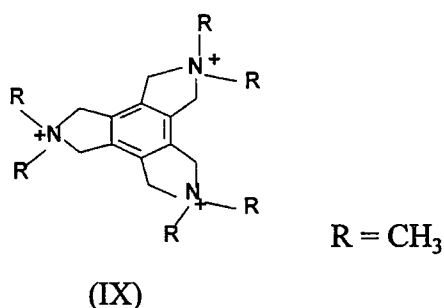
We have succeeded in crystallising a novel product with molecular formula:

$$[HMBTP]_2[Si_8O_{18}(OH)_2].41H_2O \quad (X)$$
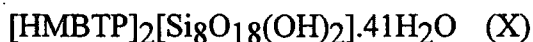
The synthesis of HMBTP tribromide and the crystal structure of the tribromide dihydrate have been described[6,7]. The cation has been used in the synthesis of zeolites ZSM-18[8] and SUZ-9[9].

5A.1. Experimental

Synthesis. A clear solution with a molar ratio HMBTP:SiO$_2$ of 1:4 was prepared at ca. 60°C (with standing for 2 days) from HMBTP hydroxide, silica and deionized water. This solution was examined by NMR at several temperatures. The water contained 15 wt% D$_2$O to give a ^{2}H field/frequency lock signal. Crystals of [HMBTP]$_2$[Si$_8$O$_{18}$(OH)$_2$].41H$_2$O were obtained by cooling the solution to ca. 15°C. Since the crystals dehydrated/decomposed in air, they were stored under the mother liquor in a polyethylene container.

Diffraction Measurements. An appropriate single crystal of approximate size 0.4 × 0.3 × 0.2 mm was mounted on a RIGAKU AFC6S diffractometer at 150K with graphite-crystal monochromatized Mo-Kα radiation (λ=0.71073 Å). A total of 6362 independent reflections were used. The structure was solved by direct methods and refined by the full-matrix least-squares procedure including the observed reflections.

NMR measurements. High-resolution ^{29}Si, ^{13}C and ^{1}H NMR spectra were obtained of the powdered polycrystalline solid at a magnetic field strength of 7.05 T, using a spectrometer operating at 59.83, 75.43 and 299.945 MHz for ^{29}Si, ^{13}C and ^{1}H respectively under conditions of cross-polarization and magic-angle spinning (CPMAS) at 233K. The crystals were first dried between filter papers and packed into a 7.5 mm o.d. pencil rotor. A Varian Unity Plus 300 spectrometer was used.

Spectra for the precursor solution and of the mother liquor after crystallisation were recorded at ca. 323K and at ambient probe temperature (ca. 298K), respectively, using a Bruker AC250 spectrometer (5.86 T) operating at 49.69 and 62.90 MHz for ^{29}Si and ^{13}C respectively.

5A.2. Results and discussion

5A.2.1. Crystal structure. The crystal structure of $[HMBTP]_2[Si_8O_{18}(OH)_2].41H_2O$ was determined by X-ray diffraction methods. The crystal data and the relevant experimental parameters are listed in table 1. The compound crystallises in the triclinic space group $P\bar{1}$ (as does I), in contrast to II and III, which are trigonal, and IV and V which are monoclinic. Clearly there is little common morphology among these structures, which all appear to contain different numbers of water molecules per octameric silicate anion. The unit cell of X contains two HMBTP cations and one anionic octamer. The refined coordinates of the Si, O and N atoms are listed in Table 2. The asymmetric unit of X contains one HMBTP cation and half a cubic silicate octamer, together with 21 water oxygen atoms. For the cations and anions this is similar to the situation for IV and V. However, for X the best refinement model indicates that four of the water molecules are positionally disordered. Thus O(62), O(63) and O(64) show 3:1 site occupancy per asymmetric unit.

Table 3 gives the bond distances for the cations and anions, while Table 4 lists the relevant bond angles. Table 5 gives some additional geometry data in condensed form. The crystalline compound is clearly a host/guest system, as for the related molecules I-V. The anionic host structure is a three-dimensional network of hydrogen-bonded octameric silicate units and water molecules. Figure 1 shows the local environment of the octameric silicate ion, which is centrosymmetric and contains 22 water molecules, in contrast to IV and V which have 24 water molecules, possibly because X contains $[Si_8O_{18}(OH)_2]^{6-}$ anions (while IV and V have $[Si_8O_{20}]^{8-}$ anions) or possibly because of the size of the HMBTP cation. This situation breaks the "24

water molecule" rule suggested in ref. 5. Each external Si-O oxygen is linked to others, intramolecularly, via two water molecules. However, whereas four of the terminal oxygens participate in three of these bridges, the other four (which are near to the cations) are only involved in two such links. Furthermore, of the latter four, two are bonded to only two water molecules, whereas the other two link to three. This is reflected in the Si-O distances, which are notably shorter (1.573 -1.581Å) for those terminal oxygens hydrogen-bonded to three water molecules than for those linked to two (1.623Å). The internal Si-O distances are mostly in the region 1.621-1.643Å, but with those involving the silicon atoms whose terminal oxygen atoms participate in only two hydrogen bonds distinctly shorter (1.606 - 1.607). It is tempting to suppose that these silicon atoms are those with OH groups, but we have no direct evidence of this, and presumably the H-bonding network can in principle delocalise the charges. For V and VI all Si-O bond lengths lie in the range 1.612-1.628Å.

Figure 2 shows the complex hydrogen-bonded network linking silicate anions. Each structure of this type so far examined in detail contains a different number of water molecules, presumably to accommodate the different cation shapes within a stable framework. Table 5 gives some data for the hydrogen-bonded O-O distances for X, which show an anticipated range of values. The framework shown in Figure 2 reveals large irregular cage-like cavities, which contain the guest HMBTP cations. Figure 3 reveals the guest cation HMBTP within a large polyhedral cavity built up by silicate anions and framework water. The high charge but large size of these cations means there are fewer but more substantial breaks in the host framework than is the case for structures I-V. The cations are almost planar (apart from the methyl groups).
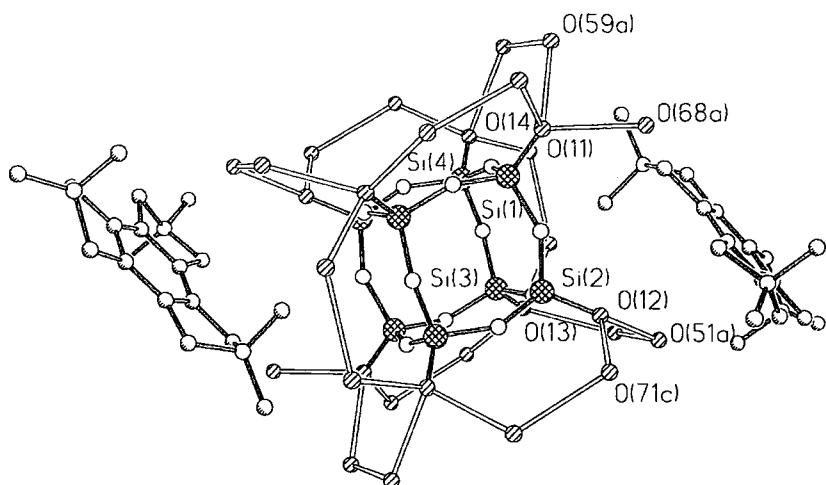
Figure 1. The environment of the octameric silicate unit $[Si_8O_{18}(OH)_2]^{-6}$ in the crystal structure of compound X. The 22 water oxygen atoms neighbouring the silicate terminal oxygens are indicated.
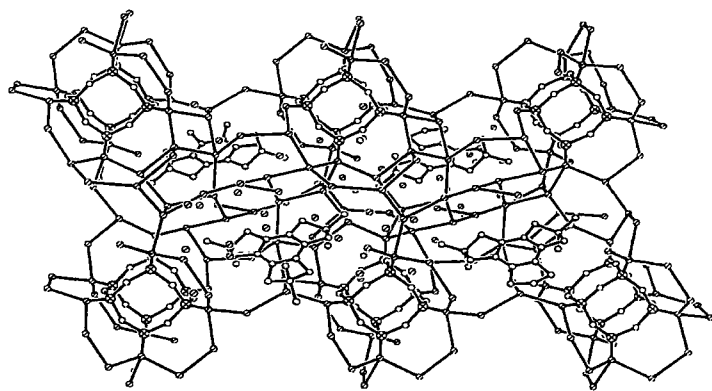
Figure 2 . The host-guest framework structure of compound X.
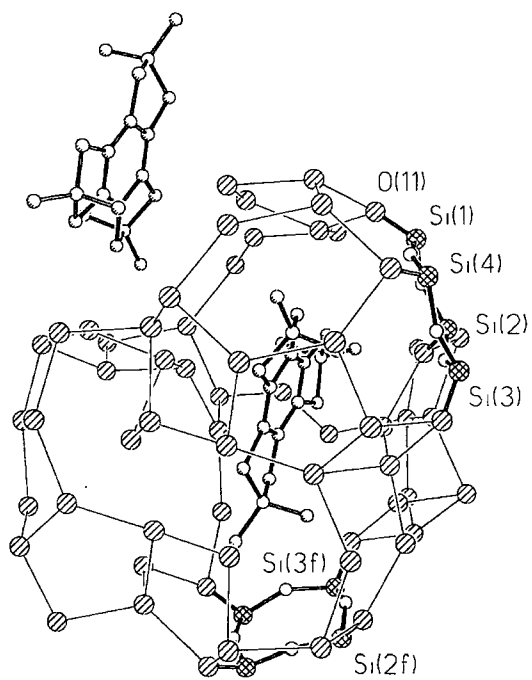
Figure 3. Cage-like void with the enclosed HMBTP cation as a guest. The cavity is built up by silicate anions and the water framework as a host.

Table 1. Crystal data and structure refinement for X.

Chemical formula	$(C_{18}H_{30}N_3)_2.[Si_8O_{18}(OH)_2].41H_2O$
Formula weight	1862.28
Temperature	150(2) K
Wavelength	0.71073 Å
Crystal system	Triclinic
Space group	$P\bar{1}$
Unit cell dimensions	$a = 12.910(6)$ Å $\quad \alpha = 100.76(4)°$
	$b = 13.699(6)$ Å $\quad \beta = 114.77(4)°.$
	$c = 13.945(7)$ Å $\quad \gamma = 94.55(5)°.$
Volume	2165(2) Å^3
Z	1
Number of reflections used	20
Crystal description	Block
Crystal colour	Colourless
Density (calculated)	440 Mg/m^3
Absorption coefficient	0.236 mm^{-1}
F(000)	1010
Crystal size	0.7 x 0.5 x 0.4 mm
θ range for data collection	2.52 to 24.97 °
Index ranges	$5 \leq h \leq 15, 0 \leq k \leq 14, -16 \leq l \leq 16$
Experiment device	Rigaku AFC6S
Experiment methods	ω
Number of standard reflections	3
Interval Counts	150
Reflections collected	6712
Independent reflections	6362 [R(int) = 0.0198]
Absorption correction	ψ-scan
Refinement method	Full-matrix least-squares on F^2
Data / restraints / parameters	6362 / 0 / 543
Goodness-of-fit on F^2	1.036
Final R indices [I>2σ (I)]	R1 = 0.0423, wR2 = 0.1078
R indices (all data)	R1 = 0.0743, wR2 = 0.1241

Largest diff. peak and hole $\qquad$ 1.019 and -.429 e.Å^{-3}

Table 2. Fractional coordinates ($\times 10^4$) and equivalent isotropic displacement parameters Ueq (Å$^2 \times 10^3$) for compound X

Ueq = 1/3 Σi ΣjUijaiaja*ia*j

	x	y	z	Ueq
Si(1)	6988(1)	1420(1)	6147(1)	14(1)
Si(2)	6288(1)	-104(1)	3935(1)	14(1)
Si(3)	3755(1)	353(1)	3002(1)	13(1)
Si(4)	4427(1)	1882(1)	5238(1)	13(1)
O(1)	6883(2)	649(2)	6871(2)	23(1)
O(2)	6992(2)	752(2)	5048(2)	25(1)
O(3)	5066(2)	177(2)	3197(2)	22(1)
O(4)	3883(2)	1306(2)	3953(2)	21(1)
O(5)	5821(2)	1916(2)	5761(2)	24(1)
O(6)	3892(2)	1186(2)	5814(2)	26(1)
O(11)	8107(2)	2256(2)	6805(2)	20(1)
O(12)	7070(2)	-180(2)	3275(2)	21(1)
O(13)	3068(2)	540(2)	1833(2)	19(1)
O(14)	4131(2)	2981(2)	5405(2)	18(1)
N(1)	6427(2)	2492(2)	-583(2)	18(1)
N(2)	6730(2)	3529(2)	3777(2)	18(1)
N(3)	10093(2)	1153(2)	3002(2)	21(1)
C(1)	7853(3)	2296(3)	1076(3)	19(1)
C(2)	7221(3)	3003(3)	1326(3)	17(1)
C(3)	7293(3)	3262(3)	2363(3)	17(1)
C(4)	8011(3)	2817(3)	3170(3)	16(1)
C(5)	8656(3)	2136(3)	2931(3)	17(1)
C(6)	8578(3)	1869(3)	1879(3)	19(1)

C(11)	5453(3)	1659(3)	-837(3)	24(1)
C(12)	6223(3)	2822(3)	-1607(3)	27(1)
C(13)	6655(3)	4309(3)	4649(3)	29(1)
C(14)	5762(3)	2649(3)	3375(3)	25(1)
C(15)	11153(3)	1924(3)	3323(3)	29(1)
C(16)	10467(4)	171(3)	3225(3)	32(1)
C(21)	7583(3)	2116(3)	-107(3)	22(1)
C(22)	6499(3)	3347(3)	324(3)	20(1)
C(23)	6679(3)	3950(3)	2825(3)	21(1)
C(24)	7888(3)	3163(3)	4193(3)	20(1)
C(25)	9431(3)	1537(3)	3637(3)	23(1)
C(26)	9270(3)	1053(3)	1809(3)	25(1)
O(51)	3694(2)	9639(2)	8600(2)	30(1)
O(52)	4103(3)	798(2)	622(2)	35(1)
O(53)	3403(3)	3813(2)	3690(2)	42(1)
O(54)	2611(2)	2406(2)	1734(2)	29(1)
O(55)	4235(2)	5443(2)	3160(2)	30(1)
O(56)	433(3)	2872(3)	964(3)	51(1)
O(57)	799(2)	9667(2)	796(3)	45(1)
O(58)	234(2)	7922(2)	1288(2)	40(1)
O(59)	2009(2)	5840(2)	2492(2)	36(1)
O(510)	8458(3)	8372(2)	3638(3)	47(1)
O(61)	6322(3)	6121(3)	1573(3)	56(1)
* O(62A)	8183(4)	-1766(7)	1484(4)	47(2)
*O(62B)	8292(11)	-2401(17)	1368(10)	31(4)
*O(63A)	1135(5)	5478(8)	248(4)	73(3)
*O(63B)	1141(11)	4748(17)	325(10)	44(5)
*O(64A)	8409(7)	5525(4)	1522(8)	67(3)
*O(64B)	8152(17)	5875(20)	889(19)	93(9)
*O(67A)	9444(14)	5370(14)	3290(13)	56(4)
*O(67B)	8897(18)	5491(16)	2732(18)	59(6)
O(65)	470(4)	4395(3)	2661(3)	81(1)
O(66)	754(4	4242(3)	4786(4)	88(1)

O(68)	148(3)	7230(3)	3656(4)	77(1)
O(69)	4330(3)	4852(2)	1152(2)	46(1)
O(610)	3689(2)	2769(2)	474(2)	35(1)
O(70)	7401(2)	6658(2)	3844(2)	35(1)

* O(62A) occup. 75%, O(62B) occup. 25%;

O(63A) occup. 75%, O(63B) occup. 25%;

O(64A) occup. 75%, O(64B) ocup. 25%;

O(67A) occup. 27%, O(67B) occup. 23%;

Table 3. Bond lengths (in Å) for the anions and cations of compound X.

Si(1)-O(11)	1.573(3)
Si(1)-O(5)	1.625(3)
Si(1)-O(1)	1.626(3)
Si(1)-O(2)	1.634(3)
Si(2)-O(2)	1.606(3)
Si(2)-O(3)	1.606(3)
Si(2)-O(6)#1	1.607(3)
Si(2)-O(12)	1.623(2)
Si(3)-O(13)	1.578(3)
Si(3)-O(4)	1.621(3)
Si(3)-O(1)#1	1.621(3)
Si(3)-O(3)	1.643(3)
Si(4)-O(14)	1.581(3)
Si(4)-O(5)	1.627(3)
Si(4)-O(4)	1.630(3)
Si(4)-O(6)	1.637(3)
O(1)-Si(3)#1	1.621(3)
O(6)-Si(2)#1	1.607(3)
N(1)-C(11)	1.503(5)
N(1)-C(12)	1.503(5)
N(1)-C(22)	1.520(4)
N(1)-C(21)	1.534(4)
N(2)-C(14)	1.501(5)

N(2)-C(13)	1.503(5)
N(2)-C(23)	1.522(4)
N(2)-C(24)	1.525(4)
N(3)-C(16)	1.507(5)
N(3)-C(15)	1.508(5)
N(3)-C(25)	1.523(4)
N(3)-C(26)	1.525(5)
C(1)-C(6)	1.387(5)
C(1)-C(2)	1.401(5)
C(1)-C(21)	1.502(5)
C(2)-C(3)	1.384(5)
C(2)-C(22)	1.506(5)
C(3)-C(4)	1.404(5)
C(3)-C(23)	1.501(5)
C(4)-C(5)	1.384(5)
C(4)-C(24)	1.494(5)
C(5)-C(6)	1.403(5)
C(5)-C(25)	1.500(5)
C(6)-C(26)	1.498(5)

#Symmetry transformation used to generate equivalent atoms: -x+1, -y, -z=1.

Table 4. Bond angles (in degrees) for the anions and cations of compound X.

O(11)-Si(1)-O(5)	111.31(14)
O(11)-Si(1)-O(1)	111.54(14)
O(5)-Si(1)-O(1)	107.70(14)
O(11)-Si(1)-O(2)	111.27(14)
O(5)-Si(1)-O(2)	107.04(14)
O(1)-Si(1)-O(2)	107.77(14)
O(2)-Si(2)-O(3)	111.1(2)
O(2)-Si(2)-O(6)#1	110.6(2)
O(3)-Si(2)-O(6)#1	110.9(2)
O(2)-Si(2)-O(12)	107.69(14)
O(3)-Si(2)-O(12)	109.19(13)
O(6)#1-Si(2)-O(12)	107.19(14)

O(13)-Si(3)-O(4)	111.67(14)
O(13)-Si(3)-O(1)#1	110.92(14)
O(4)-Si(3)-O(1)#1	108.88(14)
O(13)-Si(3)-O(3)	110.01(13)
O(4)-Si(3)-O(3)	107.74(14)
O(1)#1-Si(3)-O(3)	107.47(14)
O(14)-Si(4)-O(5)	111.10(14)
O(14)-Si(4)-O(4)	111.80(13)
O(5)-Si(4)-O(4)	107.64(14)
O(14)-Si(4)-O(6)	110.78(13)
O(5)-Si(4)-O(6)	108.29(14)
O(4)-Si(4)-O(6)	107.1(2)
Si(3)#1-O(1)-Si(1)	151.2(2)
Si(2)-O(2)-Si(1)	147.0(2)
Si(2)-O(3)-Si(3)	149.8(2)
Si(3)-O(4)-Si(4)	150.2(2)
Si(1)-O(5)-Si(4)	154.4(2)
Si(2)#1-O(6)-Si(4)	147.6(2)
C(11)-N(1)-C(12)	108.7(3)
C(11)-N(1)-C(22)	109.1(3)
C(12)-N(1)-C(22)	112.7(3)
C(11)-N(1)-C(21)	109.3(3)
C(12)-N(1)-C(21)	112.1(3)
C(22)-N(1)-C(21)	104.9(3)
C(14)-N(2)-C(13)	109.4(3)
C(14)-N(2)-C(23)	109.6(3)
C(13)-N(2)-C(23)	112.3(3)
C(14)-N(2)-C(24)	109.5(3)
C(13)-N(2)-C(24)	111.7(3)
C(23)-N(2)-C(24)	104.2(3)
C(16)-N(3)-C(15)	108.8(3)
C(16)-N(3)-C(25)	111.3(3)
C(15)-N(3)-C(25)	109.6(3)

C(16)-N(3)-C(26)	112.8(3)
C(15)-N(3)-C(26)	108.9(3)
C(25)-N(3)-C(26)	105.4(3)
C(6)-C(1)-C(2)	119.9(3)
C(6)-C(1)-C(21)	130.2(3)
C(2)-C(1)-C(21)	109.9(3)
C(3)-C(2)-C(1)	120.5(3)
C(3)-C(2)-C(22)	129.7(3)
C(1)-C(2)-C(22)	109.8(3)
C(2)-C(3)-C(4)	119.6(3)
C(2)-C(3)-C(23)	131.1(3)
C(4)-C(3)-C(23)	109.2(3)
C(5)-C(4)-C(3)	119.9(3)
C(5)-C(4)-C(24)	130.2(3)
C(3)-C(4)-C(24)	109.8(3)
C(4)-C(5)-C(6)	120.4(3)
C(4)-C(5)-C(25)	129.3(3)
C(6)-C(5)-C(25)	110.1(3)
C(1)-C(6)-C(5)	119.6(3)
C(1)-C(6)-C(26)	130.4(3)
C(5)-C(6)-C(26)	109.7(3)
C(1)-C(21)-N(1)	101.9(3)
C(2)-C(22)-N(1)	102.0(3)
C(3)-C(23)-N(2)	102.0(3)
C(4)-C(24)-N(2)	102.2(3)
C(5)-C(25)-N(3)	102.5(3)
C(6)-C(26)-N(3)	102.4(3)

\# Symmetry transformation used to generate equivalent atoms: -x+1, -y, -z + 1

Table 5. Geometry data for compound X (bond distances in Å and bond angles in degrees).

	Average value	Range of values
Si-Obr	1.622(3)	1.606(3)-1.643(3) Å
Si-O$term$	1.589(3)	1.573(3)-1.623(3) Å

O-Si-Obr	108.5(1)	107.04(14)-111.1(2)°
Obr-Si-O$term$	110.37(14)	107.19(14)-111.80(13)°
Si-Obr-Si	150.0(2)	147.0(2)-154.4(2)°
O$_w$····O$_{term}$	2.676(5)	2.609(4)-2.756(5)Å
O$_w$·····O$_w$	2.72(2)	2.26(2)-2.92(3)Å

5A.2.2. NMR studies of the compound X. Silicon-29 NMR spectra of the precursor solution at ca. 323K and of the mother liquor (i.e. saturated solution after crystallisation) at ca. 298K are shown in Figure 4. They were recorded using a substantial recycle delay (50 s) to obtain quantitative data. It can be seen that a wide range of silicon environments is present in both cases. This contrasts with the situation reported in ref. 5. As usual for alkaline silicate signals, separate bands are visible in Fig. 5 for Q^0, Q^1, Q^2_Δ, Q^2/Q^3_Δ and Q^3 sites, where the superscript gives the number of siloxane bridges and the subscript triangle refers to three-membered $(SiO)_3$ rings. Peaks assignable to the individual species Q^0, Q^1_2, Q^3_2, Q^3_6 and Q^3_8 (known as the monomer, dimer, cyclic trimer, prismatic hexamer and cubic octamer respectively) are of substantial intensity. In general the spectrum of the mother liquor contains less intensity arising from condensed units, as expected because of the lower total concentration of silicate. The spectrum of the precursor solution is not as well resolved as that for the mother liquor. The crystalline material was later melted and the ^{29}Si spectrum obtained at ca. 355K (Figure 5). This liquid has a high silica-to-water molar ratio of 8:41 (the latter figure including the hydroxyl groups) and a silica-to-cation ratio of 4:1 (identical to that of the precursor solution). The spectrum shows many species are present, with broad lines (indicating relatively facile exchange) except for the Q^3_6 and Q^3_8 peaks (which demonstrates their stability). Evidently a distribution of species is rapidly regained on melting.

Figure 6 displays the 59.83 MHz CPMAS ^{29}Si spectrum of the powdered solid X at 233K. Three distinct peaks can be seen at chemical shifts -98.6, -99.5 and -100.1 ppm from the signal for TMS. The shifts for the cubic octamer in the spectra of the precursor solution and the mother liquor are -98.5 and -98.9 ppm respectively, so there is little overall change on crystallisation, which is not surprising as the dominant environment consists of water molecules in both solid and solution states. It seems the
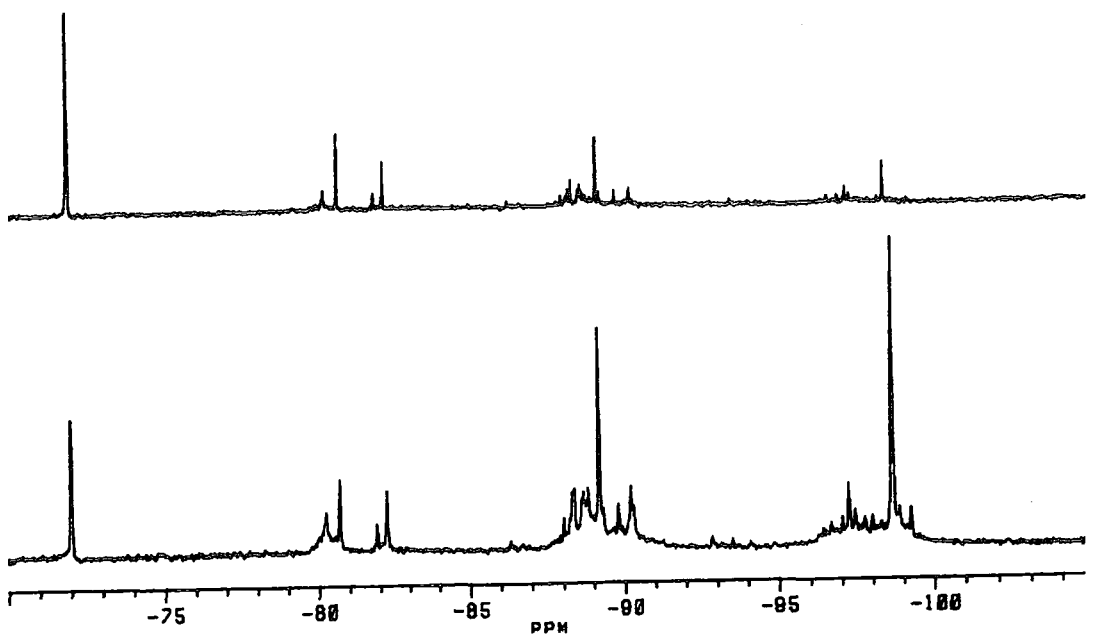
Figure 4. The 49.69 MHz ^{29}Si NMR spectra of HMBTP silicate solutions. The lower trace shows the silicate solution prior to crystallisation at ca. 323K with 1300 transients. The upper trace shows the mother liquor at ca. 298K after crystallisation with 1424 transients. The two spectra were recorded under similar spectral conditions which were as follows: 50 s recycle delay; 4950 Hz total spectral width; 16384 data points. They are plotted on the same scale and at absolute intensity.
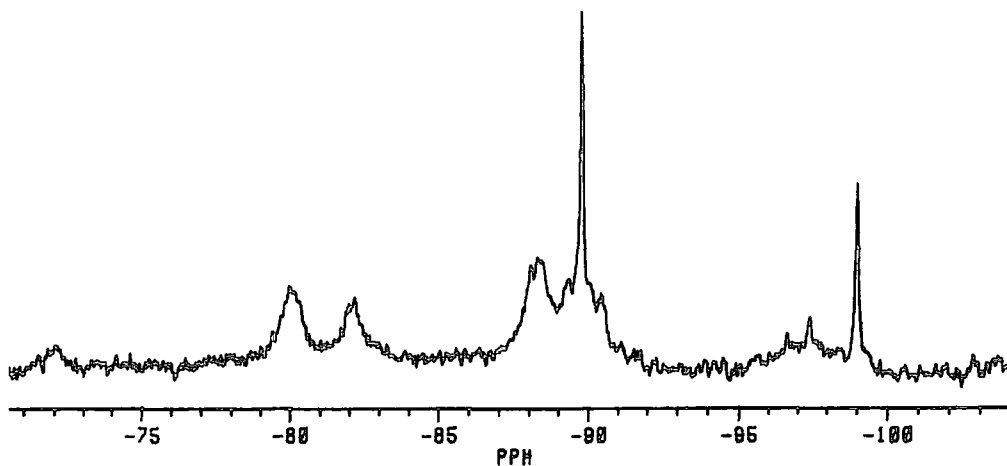
Figure 5. The 49.69 MHz ^{29}Si NMR spectrum of the melted [HMBTP]$_2$[Si$_8$O$_{18}$(OH)$_2$].41 H$_2$O at ca. 355K. Spectral parameters: 50 s recycle delay; 1320 transients; 4950 Hz total spectral width and 16384 data points.
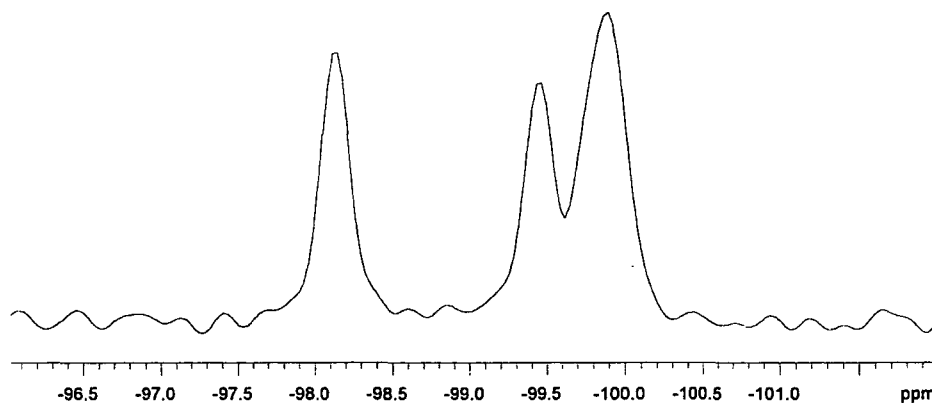
Figure 6. The 59.83 MHz CPMAS ^{29}Si NMR spectrum of compound X at 233K. Spectral parameters : 5 s recycle delay; 320 transients; 5 ms contact time 30007.5 Hz total spectral width; 32768 data points and 2350 Hz spin-rate.

signal at ca. -100 ppm arises from the overlap of two peaks, i.e. from two silicon sites which have similar magnetic environments. Evidently distortions in the cubic octamer cage in the solid state cause chemical shifts sufficient to distinguish at least three sites in the asymmetric unit. A recycle delay of 5 s and a contact time of 5 ms may not allow a fully quantitative spectrum to be obtained.

Figure 7 shows the 75.43 MHz CPMAS ^{13}C spectrum of powdered X. Three major bands are seen, as expected, at chemical shifts 55.5, 70.2 and 130.9 ppm, assignable to the CH_3, CH_2 and quaternary carbon nuclei respectively. Data from Table 2, which gives atomic coordinates of the compound X, indicate there are six different crystallographic sites for each group of carbon atoms (i.e. methyl, methylene and quaternary), while means the environments of the carbons with the same chemical group are different. However, all the peaks show evidence of shoulders and splitting arising from different crystallographic sites. Once again, this is consistent with the crystal structure, which would indicate all 18 carbons are in non-equivalent sites. It is, of course, not to be expected that resolution would suffice to enable these to be clearly distinguished. Carbon-13 spectra of silicate solutions corresponding to X (e.g. after melting the solid) show sharp peaks at shifts of 53.5, 69.1 and 130.8 ppm. Evidently there are no substantial changes in shift on crystallisation, presumably because both in solution and in the solid sate the immediate environment of the HMBTP cation is composed of water molecules.

Figure 8 displays the ^{1}H MAS NMR spectrum of X at 233K, showing two distinct peaks at shifts of 3.6 and 5.2 ppm assignable to the CH_3 and CH_2 protns of the HMBTP cation. Figure 8 does not give any evidence to distinguish the hydrogens of O_{term}-H····O_w and O_w-H····O_w, but shows only one broad peak in the shift range of 4-8 ppm. This might be expected since data from table 5 reveal that the range of values of O_w···O_w is 2.26-2.92, while that for the O_{term}-H····O_w is 2.61-2.76, which indicates that the latter values are within the range for the former. Therefore it can be realised that signals arising from the hydrogen atoms of O_{term}-H····O_w overlap those from O_w-H····O_w and consequently can not be resolved as two separate peaks (this fact will be discussed further in the next section about another new crystal)
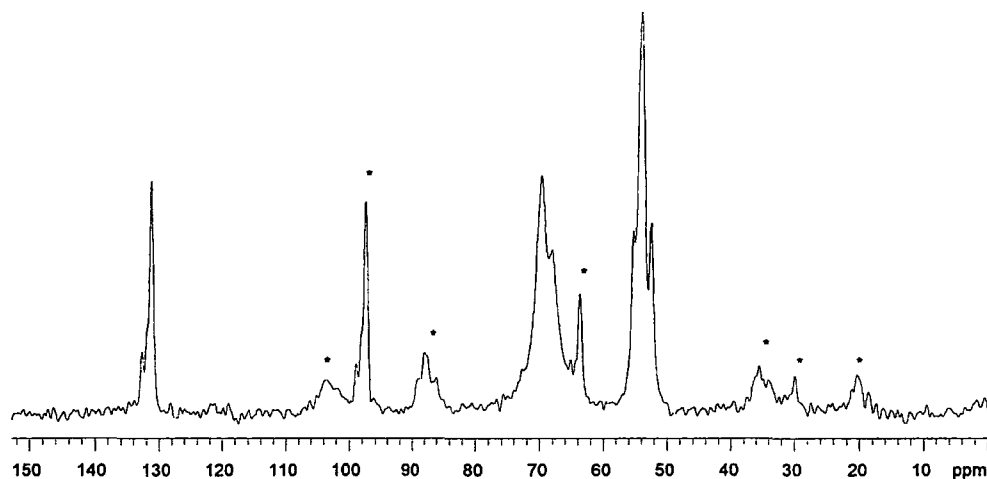
Figure 7. The 75.43 CPMAS ^{13}C NMR spectrum of solid X at 233K. Spectral parameters :5 s recycle delay; 340 transients; 5 ms contact time; 30007.5 Hz total spectral width; 65536 data points and 2540 Hz spin-rate.
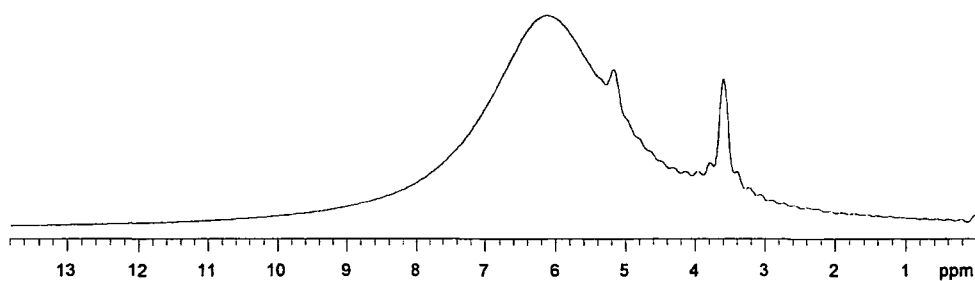

Figure 8. The 299.95 MHz MAS ^{1}H NMR spectrum of solid X at 233K. Spectral parameters: 5 s recycle delay; 100 transients; 100 kHz total spectral width; 2200 Hz spin-rate.

5B. Synthesis and structural analysis of a crystalline silicate, $[HMBTP]_2[TEA]_2[Si_8O_{20}].70H_2O$, involving solid-state high-resolution NMR and X-ray diffraction.

In the previous section a novel silicate crystal $[HMBTP]_2[Si_8O_{18}(OH)_2].41H_2O$ (X) was described and explained as a host-guest compound with a three-dimensional, mixed silicate-water host framework (heteronetwork clathrate), which provides a link between zeolite-type and clathrate hydrate-type materials[1].

In this study another new crystalline silicate hydrate was synthesised by using two quaternary ammonium bases simultaneously, i.e. $HMBTP(OH)_3$ (HMBTP= 2,3,4,5,6,7,8,9-octahydro-2,2,5,5,8,8-hexamethyl-2H-benzo(1,2-c:3,4-c':5,6-c") tripyrrolium^{+++}, (IX)) and TEA(OH) (TEA =tetraethyl ammonium).

5B.1. Experimental

The silicate crystal of $[HMBTP]_2[TEA]_2[Si_8O_{20}].70H_2O$ (XI) was obtained by crystallisation at ca. 285K from an aqueous HMBTP-TEA silicate solution with a Si/cation molar ratio of 1 and HMBTP:TEA molar ratio of 1:6. The water contained 15 wt% of D_2O to give a ^2H field/frequency lock signal. Since the crystals dehydrated/decomposed in air, they were stored under the mother liquor in a polyethylene container.

Diffraction measurements. An appropriate single crystal of approximate size $0.40 \times 0.25 \times 0.20$ mm was mounted on a RIGAKU AFC6S diffractometer at 150 K with graphite-crystal monchromatized Cu-Kα radiation(λ=1.54178 Å). The structure was initially solved by direct methods (SHELXL-86) and completed by full-matrix least-squares refinenment with F^2_0 (SHELXL-93) and Fourier difference synthesis. A total of 12242 independent reflections was used. Further details of the structure analysis are listed in Table 6.

NMR measurements. Solid-state ^{13}C and ^{29}Si CPMAS NMR spectra of XI were recorded using a Varian Unity Plus spectrometer (7.05 T) at resonance frequencies of 75.43 (^{13}C) and 59.83 (^{29}Si) MHz, with spinning rates of 2.45 (^{13}C) and 2.50 (^{29}Si) kHz. Also, ^{13}C MAS NMR were recorded with direct polarisation by applying single pulse excitation. The ^1H MAS NMR spectrum at 299.95 MHz and 2.6 KHz spin rate was also recorded with single pulse excitation. Chemical shifts of all nuclei are referred

to tetramethylsilane (TMS). The crystals were first dried between filter papers and packed into a 7.5 mm o.d. pencil rotor.

Spectra for the precursor solution and of the mother liquor after crystallisation were recorded at ca. 353K and at ambient probe temperature (ca. 298K), respectively, using a Bruker AC250 spectrometer (5.86 T) operating at 49.69 and 62.90 MHz for ^{29}Si and ^{13}C respectively.

5B.2. Results and discussion

5B.2.1. Crystal structure : Compound XI crystallises in the monoclinic system, with space group C2/c. The asymmetric unit of the structure comprises one TEA and one HMBTP cation (both in general positions), part of an anion, i.e. four silicon atoms, four terminal oxygen atoms and seven bridging oxygen atoms (two of which lie on a twofold symetry axis), 34 water molecules in general positions and two on twofold axes, thus giving four formula units of [HMBTP]$_2$[TEA]$_2$[Si$_8$O$_{20}$].70H$_2$O per unit cell. According to the previous discussion of the silicate crystal of compound X, it can be deduced that the crystal structure of XI may also be described as a host-guest compound. The description of the host framework is best started from an idealised three-dimensional, four-connected tetrahedral network in which the tetrahedral positions are occupied by the Si and O$_{term}$ atoms of the double-ring anions and water oxygen atoms (O$_w$), while the oxygen bridge (O$_{br}$) atoms are two co-ordinate.

Crystal data are listed in Table 6, atomic coordinates in Table 7, bond lengths and bond angles for the cations and anions are given in Table 8 and Table 9 respectively, while selected interatomic distances and angles are shown in Table 10.

Table 6. Crystal data and structure refinement for compound XI.

Chemical formula	$(C_{18}H_{30}N_3)_2(C_8H_{20}N)_2[Si_8O_{20}].70H_2O$
Formula weight	2643.24
Temperature	150(2) K
Wavelength	1.54178 Å
Crystal system	Monoclinic
Space group	C2/c
Unit cell dimensions	$a = 23.730(5)$ Å $\quad \alpha = 90°$.
	$b = 26.280(5)$ Å $\quad \beta = 111.39(3)°$.
	$c = 23.570(5)$ Å $\quad \gamma = 90°$.
Volume	13686(5) Å^3
Z	4
Density (calculated)	1.283 g/cm^3
Absorption coefficient	1.676 mm^{-1}
F(000)	5760
Crystal size	0.40 x 0.25 x 0.20 mm
θ range for data collection	3.36 to 75 deg.
Index ranges	$0 \leq h \leq 29, 0 \leq k \leq 32, -29 \leq l \leq 27$
Reflections collected	12567
Independent reflections	12242 [R(int) = 0.0855]
Absorption correction	Semi-empirical from ψ-scans
Max. and min. transmission	1.0000 and 0.8823
Refinement method	Full-matrix least-squares on F^2
Data / restraints / parameters	12191 / 0 / 735
Goodness-of-fit on F^2	1.020
Final R indices [I>2σ(I)]	R1 = 0.0871, wR2 = 0.2287
R indices (all data)	R1 = 0.1886, wR2 = 0.3255
Largest diff. peak and hole	0.797 and -1.288 e.Å^{-3}

Table 7. Atomic coordinates (×10^4) and equivalent isotropic displacement
parameters (Å^4 × 10^4) for compound XI.

$Ueq = 1/3\ \Sigma i\ \Sigma jUijaiaja*ia*j$

	x	y	z	U(eq)
Si(1)	6209(1)	1573(1)	8165(1)	16(1)
Si(2)	5636(1)	1565(1)	6739(1)	16(1)
Si(3)	5272(1)	717(1)	8205(1)	17(1)
Si(4)	5302(1)	2403(1)	8217(1)	16(1)
O(1)	6909(2)	1528(2)	8558(2)	22(1)
O(2)	6105(2)	1600(2)	7440(2)	23(1)
O(3)	5832(2)	1093(2)	8277(2)	28(1)
O(4)	5926(2)	2093(2)	8338(2)	23(1)
O(5)	5998(2)	1592(2)	6291(2)	24(1)
O(6)[a]	5000	522(2)	7500	25(2)
O(7)	5486(2)	246(2)	8654(2)	26(1)
O(8)	5253(2)	1038(2)	6657(2)	24(1)
O(9)	5163(2)	2037(2)	6609(2)	25(1)
O(10)	5451(2)	2903(2)	8629(2)	22(1)
O(11)[a]	5000	2550(2)	7500	23(2)
O(12)	7393(2)	2268(2)	9327(2)	37(1)
O(13)	6623(2)	-31(2)	4319(2)	34(1)
O(14)	5296(2)	3813(2)	8131(3)	37(1)
O(15)	7413(2)	800(2)	9348(2)	32(1)
O(16)	5963(2)	2404(2)	5586(2)	33(1)
O(17)	2836(3)	3806(2)	5534(3)	43(1)
O(18)	5540(3)	2262(2)	4283(3)	43(1)
O(19)	2128(3)	3530(2)	8456(3)	44(2)
O(20)	5798(3)	867(2)	5491(3)	40(1)
O(21)	6555(3)	73(2)	5475(3)	46(2)
O(22)	7186(2)	1407(2)	6752(2)	34(1)
O(23)	5107(2)	-703(2)	8479(3)	36(1)

O(24)	7672(2)	1347(3)	8012(3)	45(2)
O(25)	5170(2)	3146(2)	5691(2)	31(1)
O(26)	5819(3)	1257(2)	4449(3)	46(2)
O(27)	3576(3)	4192(2)	6688(3)	48(2)
O(28)	3451(2)	2905(2)	5520(2)	38(1)
O(29)	4108(3)	2698(2)	11635(3)	45(2)
O(30)	2267(3)	1659(3)	9855(3)	61(2)
O(31)	6344(3)	4723(3)	6712(3)	53(2)
O(32)	1017(3)	3123(2)	7684(3)	42(1)
O(33)	707(3)	2782(3)	6479(3)	53(2)
O(34)	3091(3)	-974(2)	5613(3)	45(2)
O(35)	4685(3)	4142(3)	8868(4)	66(2)
O(36)	1812(5)	494(3)	6227(5)	90(3)
O(37)	2883(3)	2775(3)	9233(3)	52(2)
O(38)	4821(3)	290(3)	5397(3)	64(2)
O(39)	7407(3)	393(2)	6567(3)	49(2)
O(40)	2120(3)	1973(3)	8726(3)	61(2)
O(41)[b]	5000	-1289(3)	7500	42(2)
O(42)	4062(3)	3231(3)	4749(3)	59(2)
O(43)[b]	5000	3287(3)	12500	51(2)
O(44)	4283(4)	4294(5)	4799(6)	130(4)
O(45)	1427(3)	201(3)	7770(3)	50(2)
O(46)	4061(4)	3816(4)	12663(5)	94(3)
O(47)	1277(3)	1863(3)	6499(3)	63(2)
N(1)	1803(3)	1917(2)	2491(3)	24(1)
N(2)	3449(2)	178(2)	2576(3)	25(1)
N(3)	3960(3)	1537(3)	4747(3)	32(2)
C(1)	2509(3)	1237(3)	2795(3)	25(2)
C(2)	2888(3)	836(3)	2822(3)	22(1)
C(3)	3422(3)	775(2)	3323(3)	23(2)
C(4)	3581(3)	1129(3)	3792(3)	23(2)
C(5)	3190(3)	1525(3)	3779(3)	23(1)
C(6)	2652(3)	1575(3)	3279(3)	25(2)

C(7)	2150(3)	1955(3)	3172(3)	27(2)
C(8)	1909(3)	1372(3)	2318(3)	28(2)
C(9)	1144(3)	2022(3)	2324(4)	35(2)
C(10)	2071(4)	2292(3)	2182(4)	38(2)
C(11)	2815(3)	404(3)	2381(3)	26(2)
C(12)	3743(3)	300(3)	3252(3)	25(2)
C(13)	3433(3)	-380(3)	2453(4)	31(2)
C(14)	3797(3)	441(3)	2248(3)	27(2)
C(15)	4141(3)	1170(3)	4345(3)	26(2)
C(16)	3455(3)	1865(3)	4322(3)	29(2)
C(17)	3717(4)	1236(4)	5147(3)	41(2)
C(18)	4488(4)	1854(4)	5132(4)	46(2)
N(4)	877(3)	658(3)	-636(3)	39(2)
C(19)	735(4)	1205(3)	-885(4)	43(2)
C(20)	174(5)	1422(4)	-828(5)	61(3)
C(21)	1473(4)	533(4)	-706(4)	43(2)
C(22)	1760(5)	33(4)	-406(5)	68(3)
C(23)	385(4)	284(4)	-971(4)	49(2)
C(24)	237(4)	265(4)	-1662(4)	52(2)
C(25)	936(5)	638(4)	27(4)	47(2)
C(26)	1413(5)	993(5)	447(4)	60(3)

[a] These bridging oxygen atoms of the anion lie on a crystallographic twofold axis.

[b] These water oxygen atoms lie on a symmetry element.

Table 8. Bond lengths (in Å) for the anions and cations of compound XI.

Si(1)-O(1)	1.584(4)
Si(1)-O(3)	1.623(5)
Si(1)-O(2)	1.636(5)
Si(1)-O(4)	1.638(5)
Si(2)-O(5)	1.586(5)
Si(2)-O(9)	1.624(5)
Si(2)-O(2)	1.624(5)
Si(2)-O(8)	1.628(5)
Si(3)-O(7)	1.588(5)

Si(3)-O(3)	1.613(5)
Si(3)-O(6)	1.630(3)
Si(3)-O(8)#1	1.635(5)
Si(4)-O(10)	1.594(5)
Si(4)-O(4)	1.622(5)
Si(4)-O(11)	1.623(2)
Si(4)-O(9)#1	1.626(5)
N(1)-C(9)	1.491(9)
N(1)-C(10)	1.497(10)
N(1)-C(7)	1.517(8)
N(1)-C(8)	1.535(9)
N(2)-C(14)	1.493(10)
N(2)-C(13)	1.493(9)
N(2)-C(12)	1.522(9)
N(2)-C(11)	1.524(8)
N(3)-C(17)	1.499(11)
N(3)-C(18)	1.502(9)
N(3)-C(16)	1.519(8)
N(3)-C(15)	1.521(10)
C(1)-C(2)	1.372(9)
C(1)-C(6)	1.387(10)
C(1)-C(8)	1.500(8)
C(2)-C(3)	1.392(8)
C(2)-C(11)	1.506(10)
C(3)-C(4)	1.388(10)
C(3)-C(12)	1.504(9)
C(4)-C(5)	1.387(9)
C(4)-C(15)	1.487(9)
C(5)-C(6)	1.393(8)
C(5)-C(16)	1.498(9)
C(6)-C(7)	1.504(9)
N(4)-C(23)	1.510(11)
N(4)-C(25)	1.518(11)

N(4)-C(21)	1.518(11)
N(4)-C(19)	1.542(11)
C(19)-C(20)	1.499(13)
C(21)-C(22)	1.529(13)
C(23)-C(24)	1.536(13)
C(25)-C(26)	1.522(13)

Symmetry transformation used to generate equivalent atoms: -x+1, y, -z+3/2.

Table 9. Bond angles (in degree) for the anions and cations of compound XI.

O(1)-Si(1)-O(3)	111.6(3)
O(1)-Si(1)-O(2)	109.9(3)
O(3)-Si(1)-O(2)	108.7(3)
O(1)-Si(1)-O(4)	110.8(2)
O(3)-Si(1)-O(4)	108.0(3)
O(2)-Si(1)-O(4)	107.8(2)
O(5)-Si(2)-O(9)	110.3(3)
O(5)-Si(2)-O(2)	109.7(2)
O(9)-Si(2)-O(2)	108.6(2)
O(5)-Si(2)-O(8)	111.8(3)
O(9)-Si(2)-O(8)	108.0(2)
O(2)-Si(2)-O(8)	108.2(3)
O(7)-Si(3)-O(3)	110.9(3)
O(7)-Si(3)-O(6)	110.3(3)
O(3)-Si(3)-O(6)	107.8(2)
O(7)-Si(3)-O(8)#1	110.5(3)
O(3)-Si(3)-O(8)#1	108.8(3)
O(6)-Si(3)-O(8)#1	108.6(2)
O(10)-Si(4)-O(4)	108.8(2)
O(10)-Si(4)-O(11)	110.7(3)
O(4)-Si(4)-O(11)	109.3(2)
O(10)-Si(4)-O(9)#1	110.8(3)
O(4)-Si(4)-O(9)#1	108.5(3)

O(11)-Si(4)-O(9)#1	108.7(2)
Si(2)-O(2)-Si(1)	147.8(3)
Si(3)-O(3)-Si(1)	160.0(3)
Si(4)-O(4)-Si(1)	143.7(3)
Si(3)#1-O(6)-Si(3)	143.3(4)
Si(2)-O(8)-Si(3)#1	148.1(3)
Si(2)-O(9)-Si(4)#1	153.0(3)
Si(4)-O(11)-Si(4)#1	152.5(4)
C(9)-N(1)-C(10)	109.8(6)
C(9)-N(1)-C(7)	112.3(6)
C(10)-N(1)-C(7)	107.9(6)
C(9)-N(1)-C(8)	111.1(6)
C(10)-N(1)-C(8)	110.2(6)
C(7)-N(1)-C(8)	105.3(5)
C(14)-N(2)-C(13)	109.5(6)
C(14)-N(2)-C(12)	108.4(5)
C(13)-N(2)-C(12)	112.3(5)
C(14)-N(2)-C(11)	109.7(5)
C(13)-N(2)-C(11)	111.8(5)
C(12)-N(2)-C(11)	105.1(5)
C(17)-N(3)-C(18)	109.9(6)
C(17)-N(3)-C(16)	108.8(6)
C(18)-N(3)-C(16)	111.5(6)
C(17)-N(3)-C(15)	108.6(6)
C(18)-N(3)-C(15)	111.4(6)
C(16)-N(3)-C(15)	106.5(5)
C(2)-C(1)-C(6)	119.6(6)
C(2)-C(1)-C(8)	130.1(6)
C(6)-C(1)-C(8)	110.2(6)
C(1)-C(2)-C(3)	120.4(6)
C(1)-C(2)-C(11)	129.7(6)
C(3)-C(2)-C(11)	109.8(6)
C(4)-C(3)-C(2)	119.8(6)

C(4)-C(3)-C(12)	130.1(6)
C(2)-C(3)-C(12)	110.1(6)
C(5)-C(4)-C(3)	120.0(6)
C(5)-C(4)-C(15)	110.0(6)
C(3)-C(4)-C(15)	129.9(6)
C(4)-C(5)-C(6)	119.3(6)
C(4)-C(5)-C(16)	111.1(6)
C(6)-C(5)-C(16)	129.5(6)
C(1)-C(6)-C(5)	120.6(6)
C(1)-C(6)-C(7)	110.2(5)
C(5)-C(6)-C(7)	129.1(6)
C(6)-C(7)-N(1)	103.0(6)
C(1)-C(8)-N(1)	103.0(5)
C(2)-C(11)-N(2)	103.5(5)
C(3)-C(12)-N(2)	103.5(5)
C(4)-C(15)-N(3)	103.0(5)
C(5)-C(16)-N(3)	102.1(5)
C(23)-N(4)-C(25)	106.2(7)
C(23)-N(4)-C(21)	112.0(7)
C(25)-N(4)-C(21)	111.4(7)
C(23)-N(4)-C(19)	112.8(7)
C(25)-N(4)-C(19)	110.4(7)
C(21)-N(4)-C(19)	104.1(7)
C(20)-C(19)-N(4)	113.5(8)
N(4)-C(21)-C(22)	114.3(8)
N(4)-C(23)-C(24)	114.2(8)
N(4)-C(25)-C(26)	114.6(8)

Symmetry transformations used to generate equivalent atoms: -x+1, y, -z+3/2.

Table 10. Geometry data for compound XI (bond distances in Å and bond angles in deg.).

	Average value	range of values
Si-O*br*	1.626	1.613-1.638
Si-O*term*	1.588	1.584-1.594
O*br*-Si-O*br*	108.2	107.8-109.3
O*br*-Si-O*term*	110.5	108.8-111.8
Si-O*br*-Si	149.8	160.0-143.3
Ow····Ow	2.804	2.677-3.301
Oterm····Ow	2.650	2.596-2.689

The host structure of the heteronetwork clathrate consists of a three-dimensional assembly of oligomeric $[Si_8O_{20}]^{8-}$ anions and H_2O molecules (O_W) which are linked through hydrogen bonds O-H···O. Figure 9 shows the double four-ring of $[Si_8O_{20}]^{8-}$ while Figure 10 presents a view of the silicate anion surrounded by water molecules. Each terminal oxygen is bonded to three water molecules. As shown in Figures 9 and 10, the silicate anions are built up of eight SiO_4 tetrahedra sharing three corners each to form a double four-ring structure[5]. The local environment of a silicate anion within the water framework, together with nearby HMBTP and TEA cations, is shown in figure 11. Figure 12 indicates the crystal structure of XI without the water framework, showing the mole ratio of the two cations is 1:1. Two types of cages are present in the heterogeneous network of $[HMBTP]_2[TEA]_2[Si_8O_{20}].70H_2O$ formed by the host structure. These cages are occupied by HMBTP and TEA cations as guest species, with different orientations, in conformity with the space group (see Figure 12). The approximate positions of the guest cations HMBTP and TEA within the large polyhedral cavities are shown in Figures 13 and 14 respectively, while Figure 15 shows the labelling of both cations. The orientation of the cationic guest species HMBTP and TEA within the different large polyhedral cavities of the compounds under consideration might vary with the composition of the homogeneous/heterogeneous networks, i.e. the orientation of the cations depends on the weak guest-host interactions C-H····O. The ions are

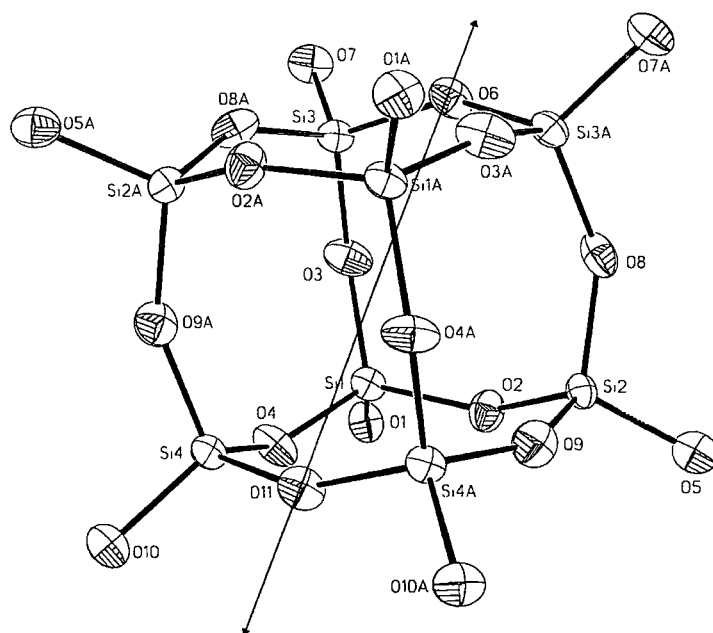Figure 9. Double four-ring $[Si_8O_{20}]^{8-}$ anion in $[HMBTP]_2[TEA]_2[Si_8O_{20}].70H_2O$ at 150K. The twofold axis is indicated.
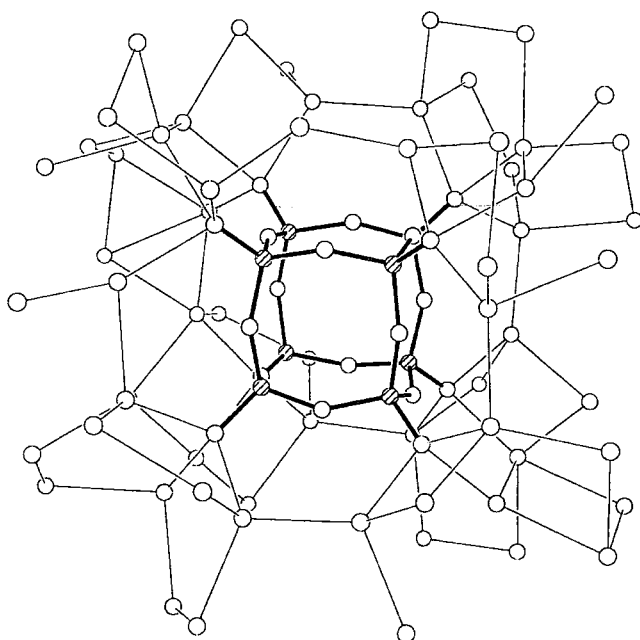

Figure 10. Double four-ring $[Si_8O_{20}]^{8-}$ anion with its local environment. Thick lines represent covalent-ionic bonds Si-O, and thin lines shows contacts between donor and acceptor atoms in hydrogen bonds O-H····O.

arranged approximately into layers, as shown in Figure 12. These are constituted by double four-ring silicate anions, water framework and large cages.

The compound XI is a more water-rich member of the silicate clathrate series than the previous one (compound X) and is closely related to the many clathrate hydrate-type phases which have recently been discovered in the system $TMAOH-H_2O$ (TMAOH = tetramethyl ammonium hydroxide)[10,11].

As shown in Figure 11, the oligomeric, diprotonated $[Si_8O_{20}]^{8-}$ anions in crystalline $[HMBT]_2[TEA]_2[Si_8O_{20}].70H_2O$ contain a cube-shaped double four-ring structure and a local environment formed by HMBTP and TEA cations and by H_2O molecules hydrogen-bonded to the eight terminal oxygen atoms. The geometrical parameters of the silicate anions are typical (Table 10). The double four-ring anions possess a small distortion (site symmetry 2) with regard to the maximum possible point symmetry $m\bar{3}m$ (Oh). Cations surround the silicate anion and are oriented in such a way that methyl groups point approximately to the anion (Figure 11).

The environments of the bridged oxygen atoms (O_{br}) are given in Table 12. As can be seen, values for such O-O distances within the anion lie between 2.616 Å and 2.662 Å. However, four of the listed values are between 3.329 Å and 3.396 Å. These are not O-Si-O distances, but they are distances between bridged oxygen (O_{br}) and water oxygen (Ow) of the framework.

The environments of each terminal oxygen (O_{term}) as well as each water oxygen (O_w) are shown individually in Figures 16 and 17 respectively. The hydrogen bonds of the silicate-water host framework (considered to be for those oxygen-oxygen distances which are less than 3 Å) can be classified in two different categories, O_{term} - H$\cdots O_w$ and O_w -H$\cdots O_w$. The distances of the hydrogen bonds for the former are smaller than those for the latter (Tables 11&13). It is noted that the O_{term} -H$\cdots O_w$ values are very close to each other (i.e. 2.596-2.656) except for oxygen number 5, which has values of 2.599, 2.670 and 2.689 Å, the average of which is 2.650 Å. On the other hand the O_w -H$\cdots O_w$ distances have a wider range of different values (i.e. 2.677-3.301) and the average is 2.804. Table 13 and Figure 17 show the local environments of oxygen atoms in the water framework, including oxygen-oxygen distances up to 3.5 Å.

As mentioned oxygen-oxygen atom distances less than 3 Å can be considered to indicate hydrogen bonds of the water molecules in the crystal framework, there are 2 with two, 12 with three, 22 with four hydrogen bonds, i.e. with oxygen-oxygen
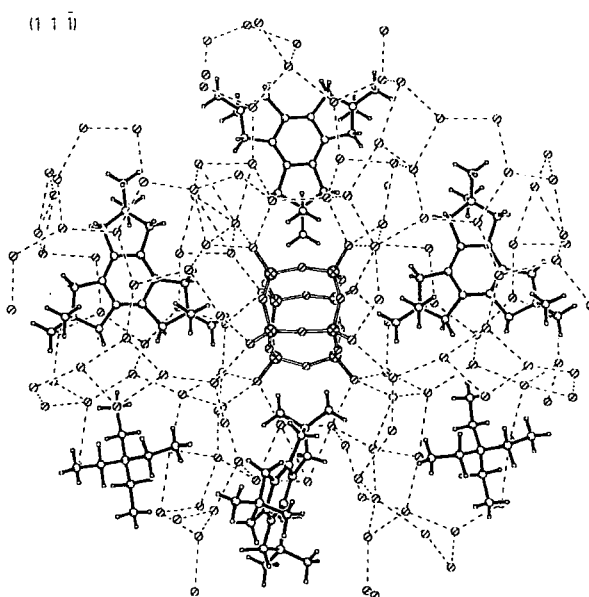
(1 1 Ī)

Figure 11. Double four-ring $[Si_8O_{20}]^{8-}$ anion in $[HMBTP]_2[TEA]_2[Si_8O_{20}].70\ H_2O$ with its local environment. The anion has site symmetry 2. Double lines represent covalent-ionic bonds Si-O, dashed lines show contacts between donor and acceptor atoms in hydrogen bonds O-H····O. The HMBTP and TEA cations are shown with thick lines.
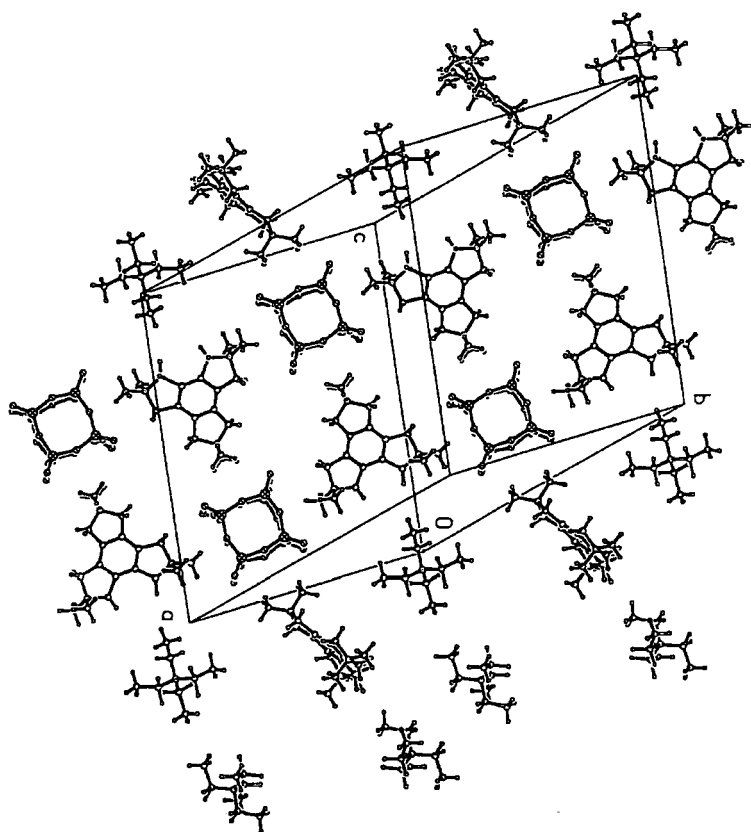
Figure 12. Packing of cations and anions in the crystal structure of XI : projection on the (2 2 $\bar{1}$) plane. Water molecules are omitted for clarity.
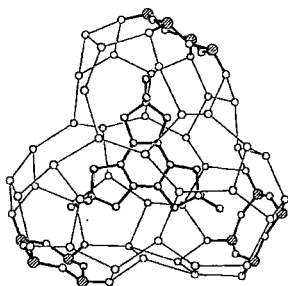
Figure 13. Cage-like void with the enclosed HMBTP cation. The HMBTP is shown with double lines, thick lines represent covalent-ionic bonds Si-O, while thin lines shows contacts between donor and acceptor atoms in hydrogen bonds O-H⋯O.
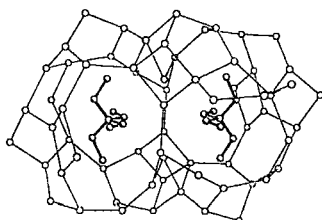

Figure 14. Cage-like void with the two enclosed TEA cations. The TEA is shown with double lines, while thin lines shows contacts between donor and acceptor atoms in hydrogen bonds O-H⋯O.
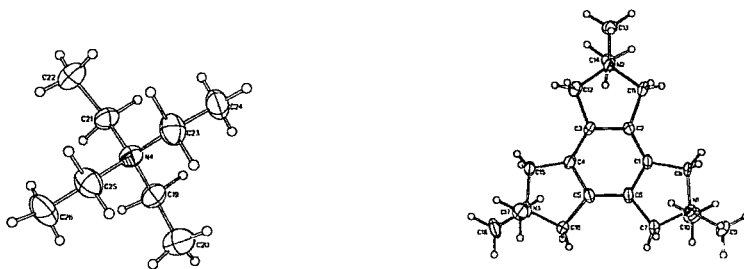

Figure 15. Cation structure with labelling of carbon and nitrogen atoms.Left:TEA cation, and right : HMBTP cation.

Figure 16. Environment of terminal oxygen atoms in compound XI. The numbers of the oxygen atoms are quoted below each picture.

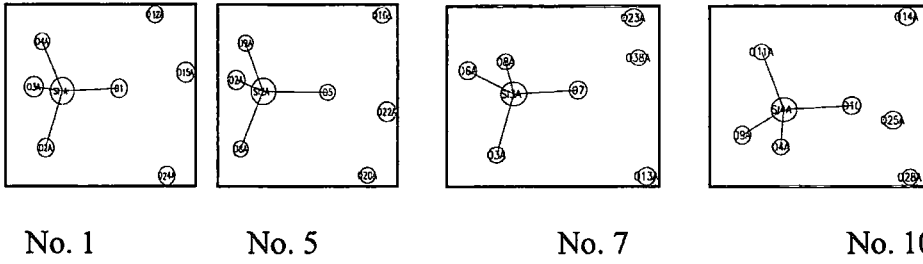No. 1   No. 5   No. 7   No. 10
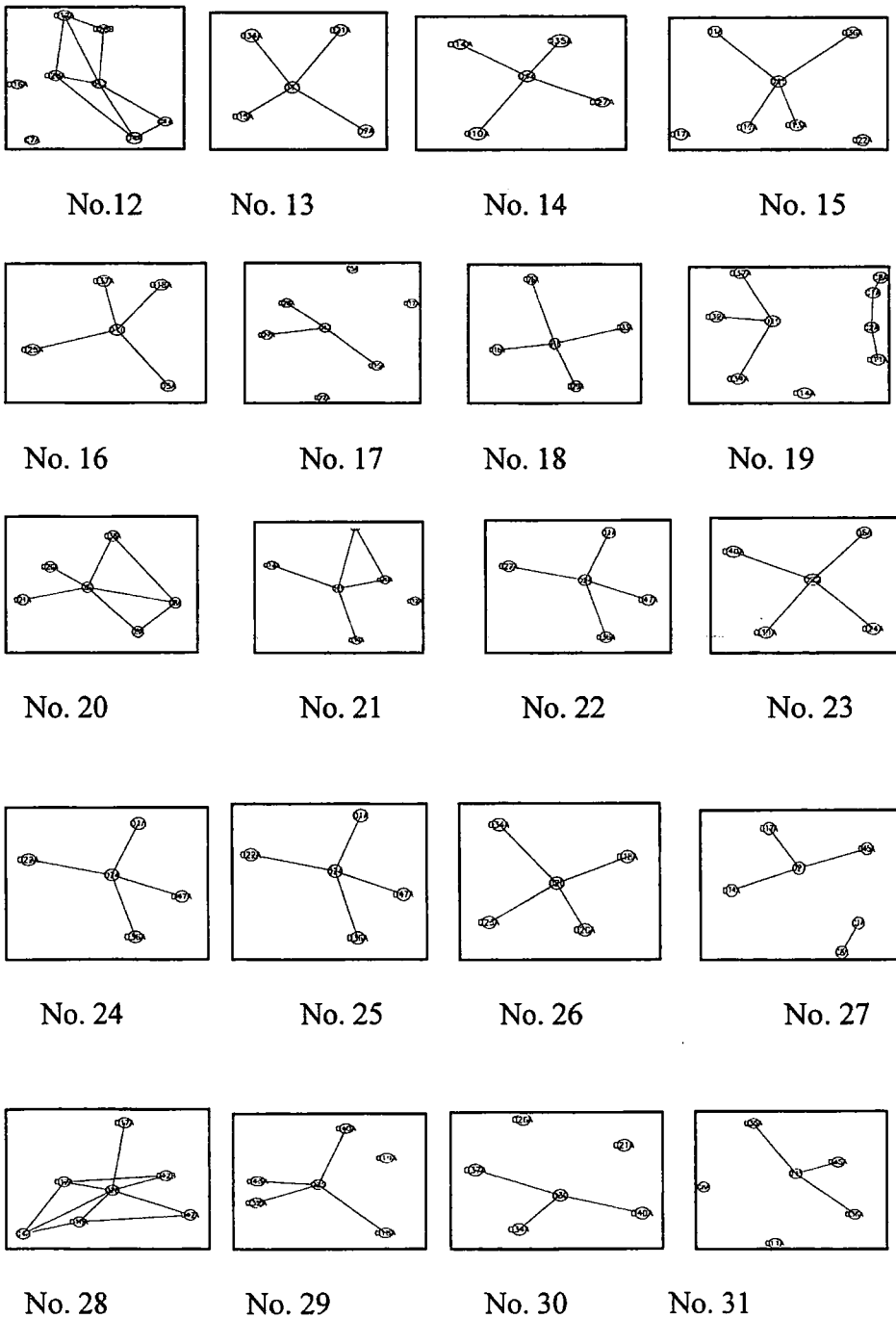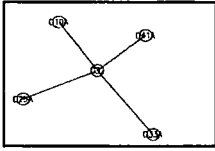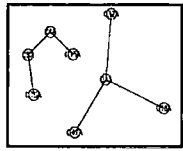
Figure 17. Environment of oxygen atoms in the water framework. The oxygen atom number is quoted below each picture.

No.12   No. 13   No. 14   No. 15
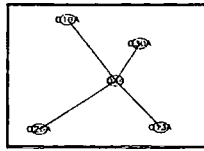
No. 16   No. 17   No. 18   No. 19

No. 20   No. 21   No. 22   No. 23

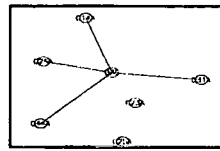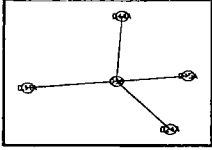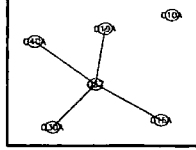No. 24   No. 25   No. 26   No. 27
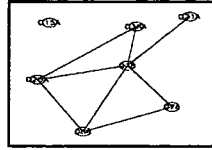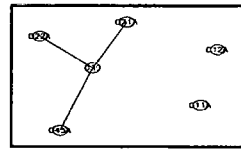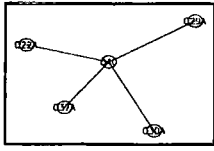
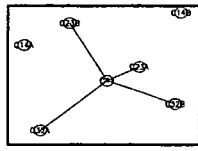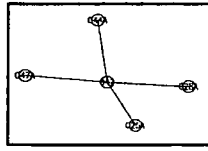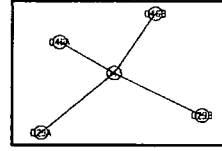No. 28   No. 29   No. 30   No. 31

No. 32 No. 33 No. 34 No. 35

No. 36 No. 37 No. 38 No. 39

No. 40 No. 41 No.42 No. 43
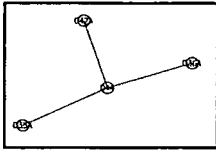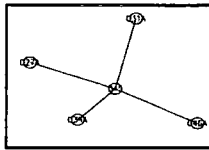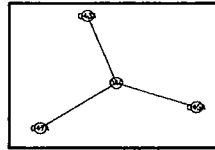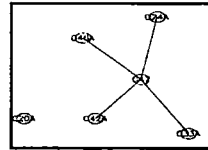
No. 44 No. 45 No. 46 No. 47

distances of less than 3 Å. However, if O⋯O distances of less than 3.5 Å are involved, there are 10 with three, 22 with four, 3 with five and 1 with six neighbouring oxygens, but the longer distances represent weaker interactions than normal hydrogen bonds.

As Figure 16 and Table 11 reveal, within such a finite cluster of composition $[HMBTP]_2[TEA]_2[Si_8O_{20}][H_2O]_{24}$, each terminal O atom ($O_{term}$) accepts three comparatively short, i.e. strong, hydrogen bonds from three H_2O molecules.

As a result, from the crystallographic study of the silicate crystal $[HMBTP]_2[TEA]_2[Si_8O_{20}]\cdot70H_2O$, it can be concluded that crystalline structural links within a heterogeneous network exist between zeolite- and clathrate hydrate-type materials.

Table 11. Environments of terminal oxygen (O_{term}) atoms in compound XI (distances in Å).

Atom O1:

O2A : 2.636(11); O3A : 2.653(10); O4A : 2.651(10); O12A : 2.622(10); O15A : 2.634(10); O24A : 2.620(10)

Atom O5:

O2A : 2.625(10); O8A : 2.662(10); O9A : 2.634(10); O16A : 2.689(10) ; O20A : 2.599(10); O22A : 2.670(10)

Atom O7:

O3A : 2.636(10); O6A : 2.640(10); O23A : 2.634(10); O8A : 2.649(10); O13A : 2.640(10); O38A : 2.596(10)

Atom O10 :

O4A : 2.616(10); O11A : 2.648(10) ; O14A : 2.630(10) ; O9A : 2.650(10) ; O25A : 2.620(10); O28A : 2.646(11)

Table 12. Environments of bridged oxygen (O_{br}) atoms in compound XI (distances in Å).

Atom O2:

O1A : 2.636(11); O3A : 2.648(10) ; O4A : 2.645(10) ;O5A : 2.625(10); O8A : 2.635(10); O9A : 2.638(10) ;

Atom O3:

O1A : 2.653(10); O2A : 2.648(10) ; O4A : 2.639(10); O6A : 2.620(10); O7A : 2.636(10); O8A : 2.641(10)

Atom O4:

O1A : 2.651(10); O2A : 2.645(10); O3A : 2.639(10); O10A : 2.616(10); O11A : 2.647(10); O12A : 3.441(11); O9A : 2.637(10); O28A : 3.329(11)

Atom O6:

O3A : 2.620(10); O7A : 2.640(10); O8A : 2.651(10); O3B : 2.620(10); O7B : 2.640(10); O8B : 2.651(10)

Atom O8:

O2A : 2.635(10) ; O5A : 2.662(10); O6A : 2.651(10); O9A : 2.631(10); O20A : 3.467(11); O38A : 3.395(11); O3A : 2.641(10) ; O7A : 2.649(10)

Atom O9

O2A : 2.638(10); O5A: 2.634(10); O8A : 2.631(10); O11A : 2.639(10) O4A : 2.637(10); O10A : 2.650(10)

Atom O11:

O4A : 2.647(10); O9A : 2.639(10); O10A : 2.648(10); O4B : 2.647(10); O9B : 2.639(10); O10B : 2.648(10)

Table 13. Environment of oxygen of water (O$_W$) atoms in compound XI (distance in Å).

Atom O12 :

O1A : 2.622(10); O4A : 3.441(11); O12A : 3.262(10); O28A : 2.734(10) ; O28B : 3.045(11)

Atom O13:

O21A : 2.803(10) ; O7A : 2.640(10); O15A : 2.739(10); O34A : 2.718(10)

Atom O14:

O10A : 2.630(10) ; O35A : 2.776(10); O14A : 2.788(10); O27A : 2.740(10)

Atom O15:

O1A : 2.634(10); O13A : 2.739(10); O17A : 2.802(10); O36A : 2.773(10)

Atom O16:

O5A : 2.689(10); O18A : 2.888(10); O25A : 2.781(10); O37A : 2.790(10)

Atom O17:

O27A : 2.833(11); O28A : 2.787(10); O15A : 2.802(10);

Atom O18:

O16A : 2.888(10); O26A : 2.716(10); O29A : 2.830(10) ; O33A : 2.850(11)

Atom O19:

O32A : 2.812(11) ; O37A : 2.846(10); O34A : 2.760(10)

Atom O20:

O5A : 2.599(10); O8A : 3.467(11); O21A : 2.763(10); O26A : 2.677(10) ; O38A : 2.712(10)

Atom O21:

O13A : 2.803(10); O20A : 2.763(10); O39A : 2.760(11); O38A : 3.301(11)

Atom O22:

O5A : 2.670(10); O24A : 2.772(10) O39A : 2.780(10) ; O40A : 2.748(10)

Atom O23:

O7A : 2.634(10); O41A : 2.707(10); O26A : 2.719(10)

Atom O24:

O1A : 2.620(10) ; O22A : 2.772(10); O36A : 2.852(10); O47A : 2.700(10)

Atom O25:

O16A : 2.781(10); O42A : 2.764(11); O10A : 2.620(10); O35A : 2.791(10)

Atom O26:

O18A : 2.716(10); O20A : 2.677(10) ; O23A : 2.719(10) ; O34A : 2.745(10)

Atom O27:

O17A : 2.833(11); O14A : 2.740(10) ; O45A : 2.943(10)

Atom O28:

O17A : 2.787(10); O42A : 2.837(10); O4A : 3.329(11); O10A : 2.646(11); O12A : 2.734(10); O12B : 3.045(11)

Atom O29:

O43A : 2.807(11); O18A : 2.830(10); O32A : 2.769(10); O40A : 2.856(10)

Atom O30

O40A : 2.685(10); O34A : 2.774(10); O37A : 2.741(10)

Atom O31:

O35A : 2.779(10); O36A : 2.752(10) ;O45A : 2.734(10)

Atom O32:

O19A : 2.812(11); O33A : 2.810(10); O29A : 2.769(10); O41A : 2.763(10);

Atom O33:

O32A : 2.810(10); O47A : 2.761(10); O18A : 2.850(11)

Atom O34:

O13A : 2.718(10); O19A : 2.760(10); O26A : 2.745(10); O30A : 2.774(10)

Atom O35:

O14A : 2.776(10); O25A : 2.791(10); O31A : 2.779(10); O44A : 3.226(11)

Atom O36:

O15A : 2.773(10); O24A : 2.852(10); O31A : 2.752(10); O44A : 2.886(11)

Atom O37:

O19A : 2.846(10); O40A : 2.749(10); O16A : 2.790(10); O30A : 2.741(10)

Atom O38:

O8A : 3.395(11); O20A : 2.712(10); O7A : 2.596(10); O21A : 3.301(11) ;O38A : 2.773(10)

Atom O39:

O21A : 2.760(11); O22A : 2.780(10); O45A : 2.685(10)

Atom O40:

O30A : 2.685(10); O37A : 2.749(10). O22A : 2.748(10); O29A :2.856(10)

Atom O41

O23A : 2.707(10); O23B : 2.707(10); O32A : 2.763(10) ; O32B : 2.763(10)

Atom O42:

O25A : 2.764(11); O28A : 2.837(10) ; O44A : 2.838(10); O47A : 2.762(10)

Atom O43:

O29A : 2.807(11); O46A : 2.769(10); O29B : 2.807(11); O46B : 2.769(10)

Atom O44:

O42A : 2.838(10); O35A : 3.226(11); O36A : 2.886(11)

Atom O45:

O27A : 2.943(10); O31A : 2.734(10); O39A : 2.685(10); O46A : 2.864(10)

Atom O46:

O43A : 2.769(10); O45A : 2.864(10); O47A : 2.980(10)

Atom O47:

O33A : 2.761(10); O24A : 2.700(10);O42A : 2.762(10); O46A : 2.980(10)

5B.2.2. NMR studies of compound XI

In contrast to diffraction techniques, NMR spectroscopy monitors the local structure around the relevant atom and can be applied to crystalline, amorphous and liquid samples. Within the last decade, solid-state NMR spectroscopy has been developed into an important tool for the structure characterisation of crystalline and non-crystalline silicates[12,13]. In particular, solid-state ^{29}Si NMR has been used to study the structural environment of SiO_4 tetrahedra in solid silicates. On the other hand, liquid-state ^{29}Si NMR studies have provided detailed insights into the constitution of silicate anions in silicate solutions. To understand the precursor solution and the silicate structure of compound XI the ^{29}Si, ^{13}C and ^{1}H NMR were studied.

5B.2.2.1. Solution-state NMR study . Silicon-29 NMR spectra of the precursor solution at ca. 313K and of the mother liquor (i.e.the saturated solution after crystallisation) at ca. 298K are shown in Figure 18. They were recorded using a substantial recycle delay (50 s) to obtain quantitative data. It can be seen that a wide range of silicon environments is present in both cases. As usual for alkaline silicate signals, separate bands are visible in Fig. 18 for Q^0, Q^1, Q^2_Δ,Q^2/Q^3_Δ and Q^3 sites, where the superscripts give the number of siloxane bridges and the subscript triangle refers to three-membered $(SiO)_3$ rings. Peaks assignable to the individual species Q^0, Q^1_2, Q^2_Δ and Q^3_6 (known as the monomer, dimer, cyclic trimer, and prismatic hexamer respectively) are of substantial intensity. The mother liquor of this compound still contains a substantial amount of the TEA cation (as mentioned above, the silicate solution contained a HMBTP:TEA mole ratio of 1:6 , but the silicate crystal involves a HMBTP:TEA mole ratio of 1:1). Since TEA stabilises the prismatic hexamer it can be expected that the peak assigned to this species is dominant in this solution[14,15]. However, it is worth mentioning that the corresponding HMBTP-TEA silicate solution contains little or no cubic octamer anion (peak at ca. -100 ppm) in spite of the fact that HMBTP silicate solutions show an intense peak for this anion (Figure 4). Note that the former solution contains a lower ratio Si/cation (i.e. the Si/cation mole ratio is 1 for the HMBTP-TEA silicate but 4 for HMBTP silicate), which is an important factor for the distribution of the silicate anions in solution. However, this fact is not significant, since it was shown in the previous chapter that for a HMBTP silicate solution with a Si:HMBTP ratio of 1 the Q^3_8 peak is also dominant. Therefore the distribution of

Figure 18. The 49.69 MHz ^{29}Si NMR spectra of HMBTP-TEA silicate solutions. The lower trace shows the silicate solution prior to crystallisation at ca. 313K with 1400 transients. The upper trace shows the mother liquor at ca. 298K after crystallisation with 1300 transients. The two spectra were recorded under similar spectral conditions which were as follows: 50 s recycle delay; 4950 Hz total spectral width and 16384 data points. They are plotted on the same scale and with absolute intensity.

silicate anions in HMBTP-TEA silicate solutions is governed preferably by the TEA cation rather than the HMBTP cation.

It is interesting to consider the silicon-29 NMR spectrum of compound XI after melting. The crystalline material was later melted and the ^{29}Si spectrum obtained at ca. 353K (Figure 19). This liquid has a high silicate : water molar ratio of 4 : 35 and a silica to cation ratio of 2:1 (twice that of the precursor solution). The spectrum shows many species are present, with broad lines (indicating relatively facile exchange) except for the $Q^3{}_6$ and $Q^3{}_8$ peaks (which demonstrates their stability). In spite of ^{29}Si NMR spectra shown in Figure 18, this spectrum shows a substantial signal at the cubic region, indicating the presence of the cubic octamer. This probably arises from the higher molar ratio of Si:cation and high concentration of silica, which factors play an important role for the stabilisation of cage-like species. However, this composition contains a HMBTP:TEA mole ratio of 1:1, which means the concentration of HMBTP is more than in the precursor solution or mother liquor. As pointed out above, HMBTP preferably stabilises $Q^3{}_8$, and therefore the abundance of the $Q^3{}_8$ signal might arise from this factor.

Figure 20 displays the ^{13}C NMR spectra of the mother liquor and precursor silicate solution of compound XI. Five separate signals are observed in the spectrum. Those at chemical shifts of 7.1 and 52.2 ppm may be ascribed to the CH_3 and CH_2 of TEA respectively, while peaks at shifts of 55.4, 69.5 and 131.2 ppm are assigned to the CH_3, CH_2 and quaternary carbons of HMBTP respectively. The recycle delay of 1 s might not be enough for quantitative results. However, both spectra were recorded under the same conditions. In general there is no difference between the two spectra, except that the TEA signals for the mother liquor are relatively enhanced since, as mentioned earlier, the precursor silicate solution contains a HMBTP:TEA mole ratio of 1:6 whereas crystalline compound XI involves the ratio of 1:1, so that the mother liquor should contain more TEA than the precursor solution.

5B.2.2.2. Study by solid-state NMR. Figure 21 displays the 59.83 MHz CPMAS ^{29}Si spectrum of the powdered solid XI at 263K. Two distinct peaks can be seen at chemical shifts -98.86 and -99.06 ppm from the signal for TMS. Although the crystallographic data give four independent silicon sites in the double four-membered ring (Table 7), this spectrum shows only two peaks, indicating that in the double four-ring crystallographic sites within the silicate anion (Table 6) can be grouped into two distinguishable
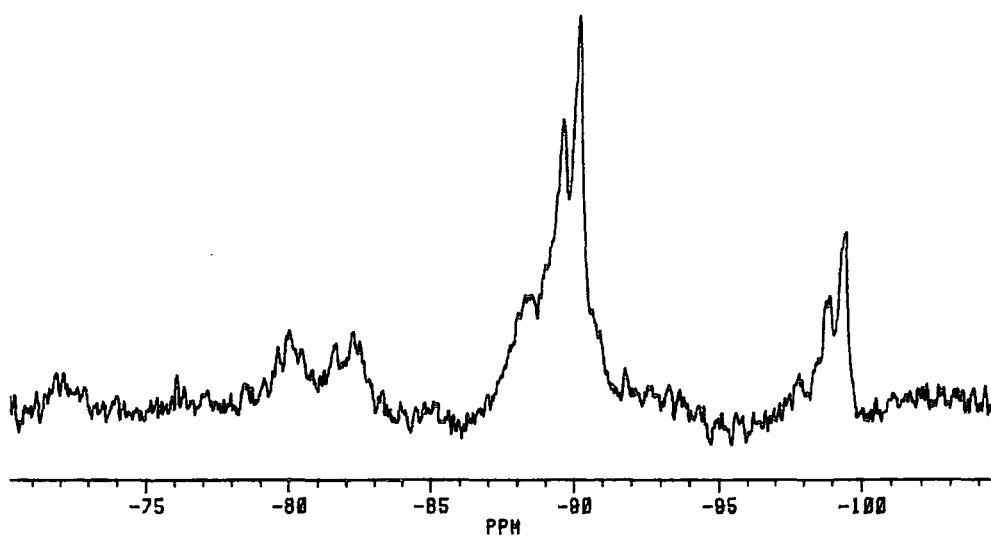
Figure 19. The 49.69 MHz ^{29}Si NMR spectrum of the melted [HABTP]$_2$[TEA]$_2$[Si$_8$O$_{20}$].70 H$_2$O at ca. 353K. Spectral parameters: 45 s recycle delay; 1600 transients; 4950 Hz total spectral width and 16384 data points.
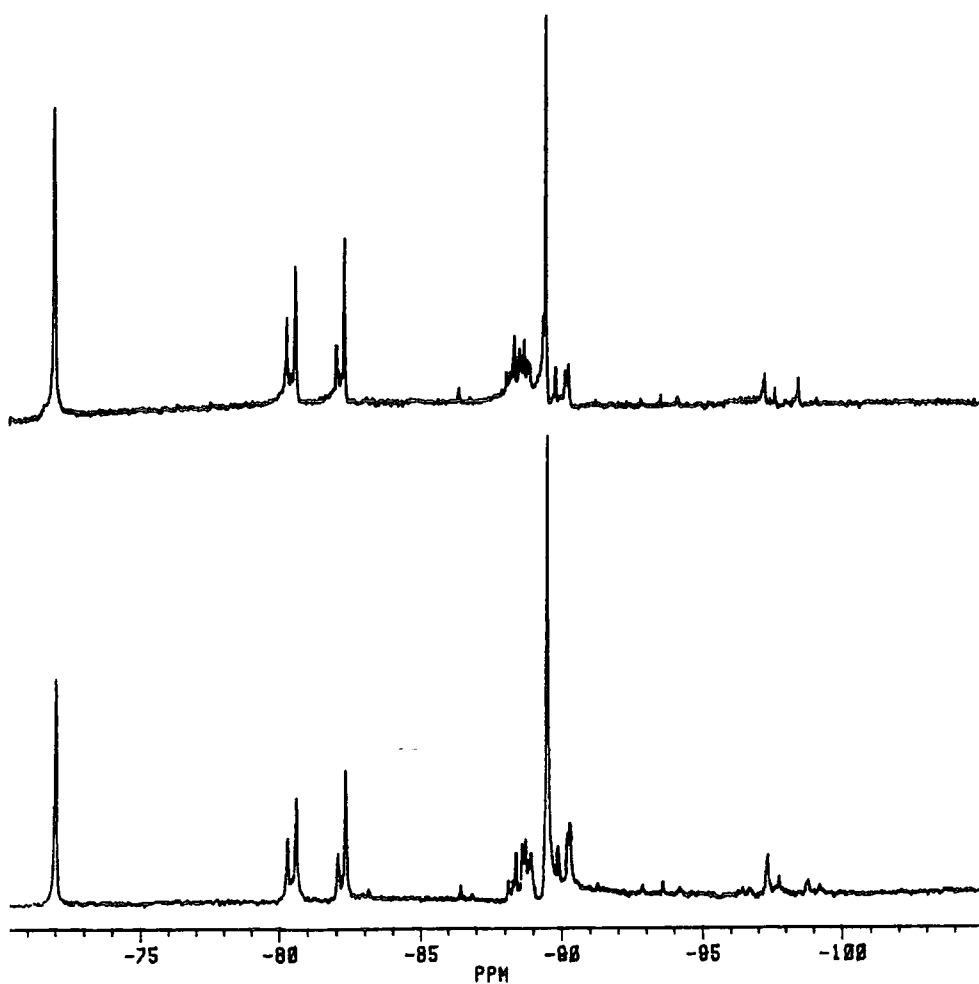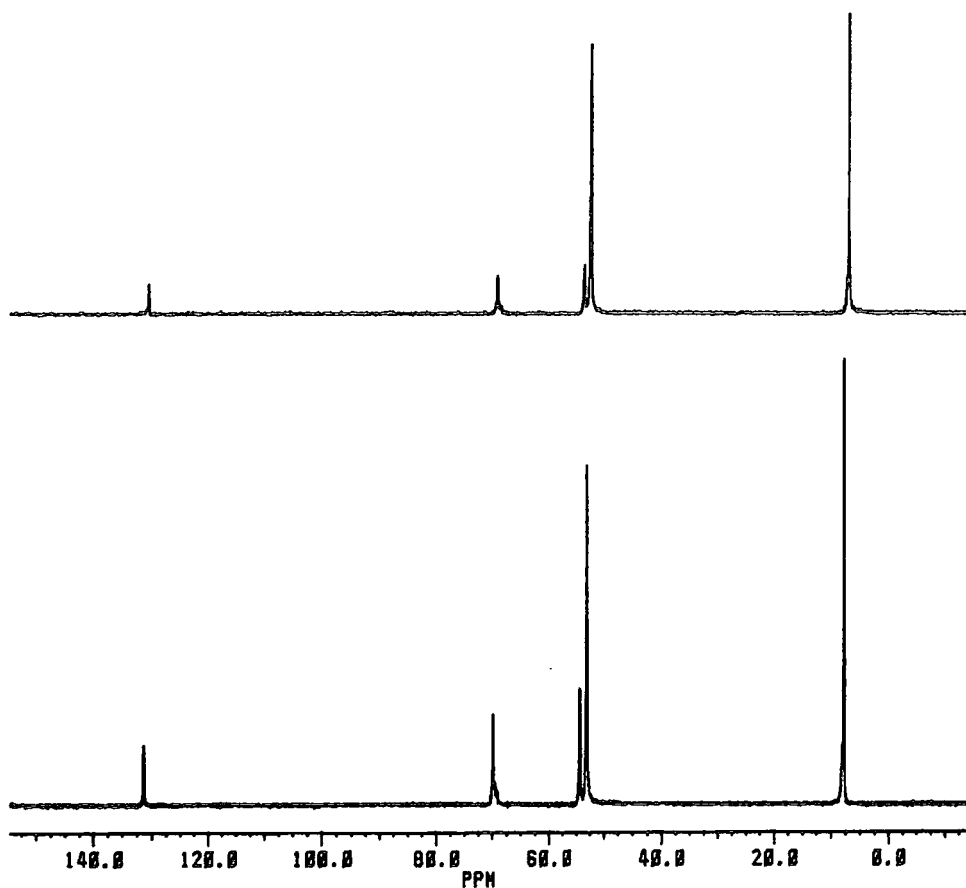
Figure 20. 62.85 MHz ^{13}C NMR spectra of HMBTP-TEA silicate solutions. The lower trace shows the silicate solution prior to crystallisation at ca. 313K. The upper trace shows the mother liquor at ca. 298K after crystallisation. Both spectra were recorded under similar spectral conditions which were as follows: 10 s recycle delay; 19230 Hz total spectral width; 16384 data points and 100 transients for each spectrum . They are plotted at the same scale and absolute intensity.

-96.5   -97.0   -97.5   -98.0   -98.5   -99.0   -99.5   -100.5   -101.5   ppm
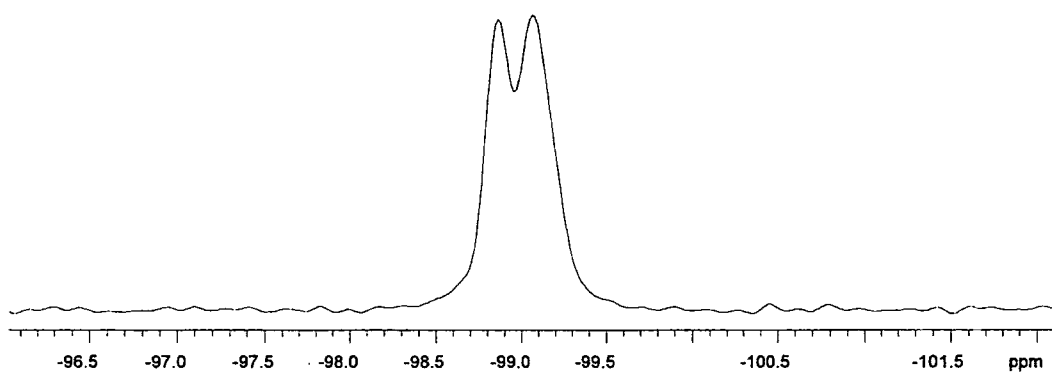
Figure 21. The 59.83 MHz CPMAS ^{29}Si NMR spectrum of solid XI at 263K.
Spectral parameters : 5 s recycle delay; 240 transients; 5 ms contact time; 30007.5 Hz
total spectral width; 32768 data points and 2500 Hz spin-rate.

environments. Although the crystal system is monoclinic and space group of C2/c (Table 7), i.e. not of high symmetry, the magnetic environments of the silicon atoms are very similar, so that it can be said that four silicon crystallographic sites involve only two distinguishable magnetic environments. Although the recycle delay of 5 s might not be enough for the quantitative measurement, it seems that the two sites have the same number of silicon atoms, i.e. each contains four silicon atoms. This crystal system is more symmetric than the previous one (triclinic for compound X), which is consistent with the relatively small shift range. Thus, the crystallographic data and NMR results are consistent. The structure directing property of the organic cation is shown by the silicon-29 NMR spectra of the precursor solution and of the silicate crystal. Although the former shows little or no signal for the cubic octamer (Figure 18), the crystalline material of this composition (compound XI) involves only the double four-membered silicate ring.

Figure 22 shows the 75.43 MHz CPMAS ^{13}C spectrum of powdered XI at 263K. Five major bands are seen, as expected, at shifts of 55.4, 69.5 and 131.2 ppm, assignable to the CH_3, CH_2 and quaternary carbon nuclei of HMBTP respectively, and 7.1 and 52.2 ppm, ascribed to the CH_3 and CH_2 of the TEA carbon nuclei respectively. Data from Table 7, which gives atomic coordinates of compound XI, indicate there are six different crystallographic sites for each group of carbon atoms (i.e. 18 independent carbons) of HMBTP, indicating a difference in environment for all carbon nuclei. However, all peaks show evidence of shoulders and splitting arising from different crystallographic sites.

It is noticeable that, although the crystal structure involves a HMBTP:TEA mole ratio of 1:1, the signal associated with HMBTP (Figure 22) is higher than that of TEA, which indicates that the transfer of magnetization from hydrogen to carbon for the two cations is not the same. To understand this fact, the ^{13}C MAS NMR spectrum of compound XI was carried out with the same conditions except using direct polarisation rather than cross polarisation. Figure 23 displays the ^{13}C MAS NMR spectrum of compound XI with direct polarisation. As can be seen, the peak heights of the carbons associated with the TEA cation are now greater than those of HMBTP. This fact is consistent with the crystallographic data, which reveal that the cages around the disordered cations of HMBTP and TEA are not the same. It seems the TEA is more mobile (Figure 14) than HMBTP (Figure 13). Both spectra (Figs. 22 & 23) display
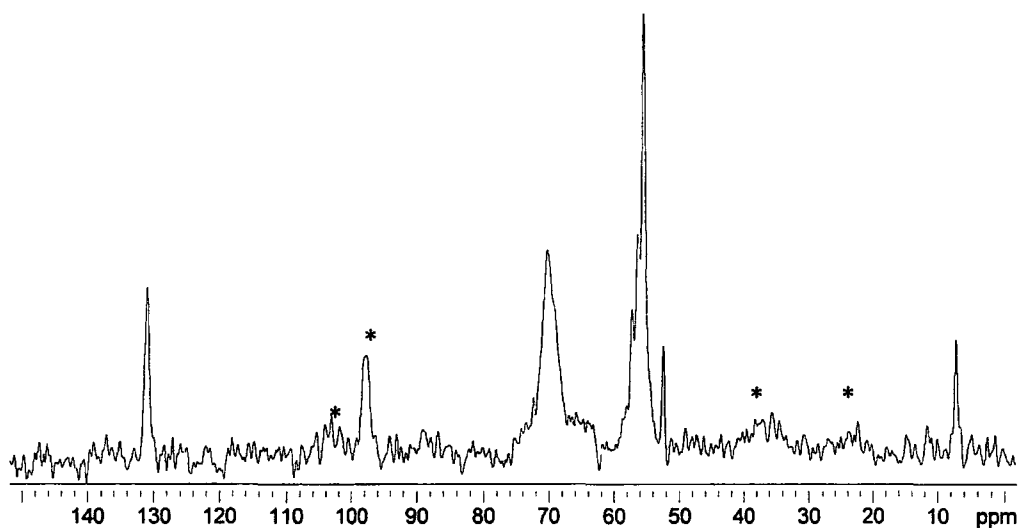
Figure 22. The 75.43 CPMAS ^{13}C NMR spectrum of solid XI at 263K. Spectral parameters : 5 s recycle delay; 340 transients; 5 ms contact time; 30007.5 Hz total spectral width; 65536 data points and 2450 Hz spin-rate. The peaks marked by asterisks are spinning sidebands.
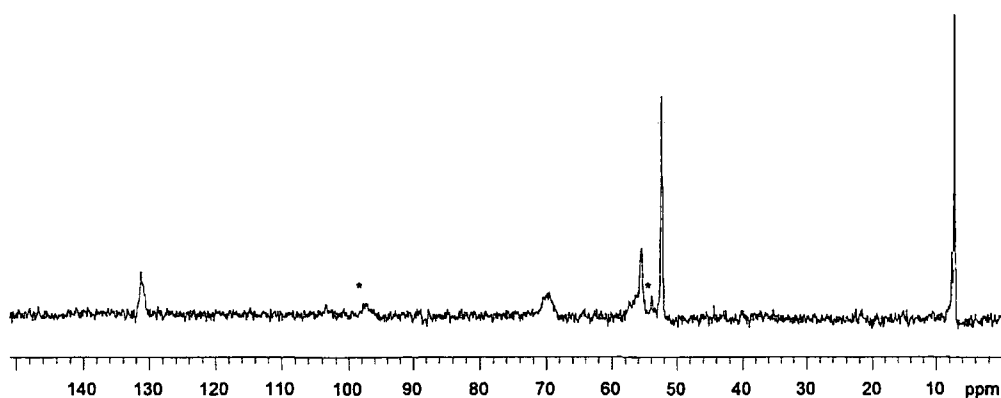
Figure 23 The 75.43 MAS ^{13}C NMR spectrum of solid XI at 263K with direct polarisation. Spectral parameters : 30 s recycle delay; 160 transients; 30007.5 Hz total spectral width; 65536 data points and 2600 Hz spin-rate. The peaks marked by asterisks are spinning sidebands.

carbon signals associated with TEA which are narrower than those for HMBTP, again indicating mobility of TEA cations. The considerable linewidths for the HMBTP cation may, however, arise from dispersion of chemical shifts and illustrate that this cation has lowered symmetry in the crystalline environment and/or it is more rigid than that TEA cation.

The solid-state ^{1}H MAS NMR spectrum of compound XI was obtained at 263K with single-pulse excitation and is shown in Figure 24. This displays peaks at shifts of 1.39 and 3.38 ppm, assignable to the hydrogen nuclei of the methyl and methylene groups of the TEA cation respectively, and peaks at shifts of 3.61 and 5.22 ppm, which are associated with the hydrogen nuclei of the methyl and methylene groups of HMBTP cation respectively. The ^{1}H MAS NMR of compound XI shows a broad peak in the shift range ca. 5 to 7 ppm, but interestingly there is another narrow peak at a shift of 5.65 ppm in this spectrum. Presumably there are two kinds of hydrogen nuclei in the water framework of the crystalline material of $[HMBTP]_2[TEA]_2[Si_8O_{20}].70H_2O$. As explained earlier, the hydrogen bonds to the terminal oxygen, O_{term}, (i.e. O_{term} - O_w) are stronger than those of O_w - O_w (Tables 11 & 12). Moreover, there is a variety of O_w - O_w distances. Consequently, the broad line can arise from the different environments of the hydrogen nuclei and/or the mobility of the hydrogen atoms of the weak hydrogen bond, whereas the narrow peak might arise from the strong hydrogen bonds.

5.2. Comparison of the silicate crystals of compounds X and XI

In aqueous silicate media, HMBTP-silicate solutions preferably stabilise the cubic octamer, but in HMBTP-TEA silicate solution the prismatic hexamer is dominant. In compound X double four-rings occur as $[Si_8O_{18}(OH)_2]^{6-}$ anions whereas in compound XI $[Si_8O_{20}]^{8-}$ anions exist. Crystalline material X is built up with two triply-charged cations (HMBTP) and the charge-balance includes two hydroxide groups, whereas in compound XI the material is formed by two triply-charged cations as well as two singly-charged cations (i.e. HMBTP and TEA respectively). The silicate anions in compounds X & XI are connected to 22 and 24 water molecules respectively. Therefore the hydroxyl groups involved for compound X might be the reason for the reduction in the number of water molecules atached to the silicate anion in X. Also, compounds X & XI differ in the total amount of water X 41 and 70 molecules per octameric silicate unit respectively.
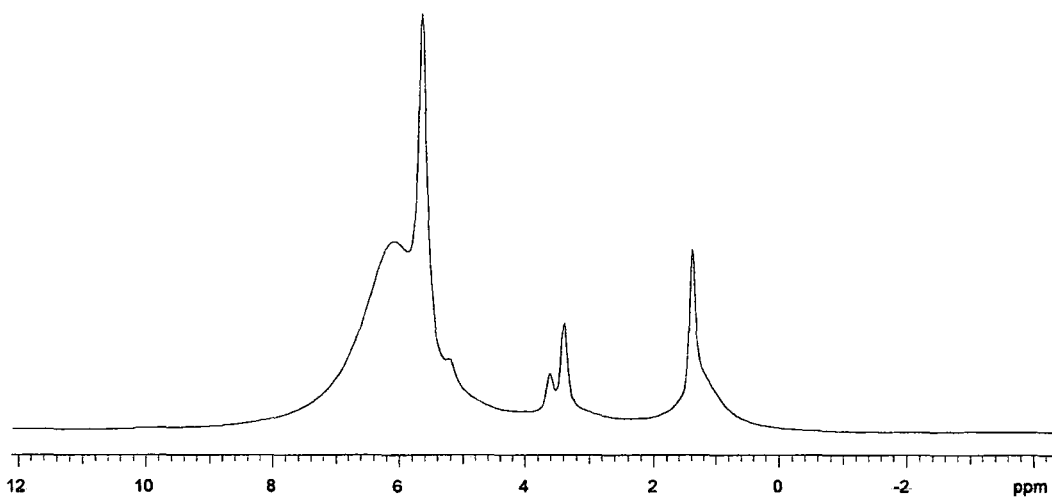
Figure 24 The 299.95 MHz MAS ^{1}H NMR spectrum of solid XI at 233K. Spectral parameters: 5 s recycle delay; 100 transients; 100 kHz total spectral width and 2600 Hz spin-rate.

In the unit cell of compound X there are only one cubic anion and two organic cations (HMBTP) but compound XI contains four cubic anions and sixteen cations (8 HMBTP and 8 TEA). Moreover, the volume of unit cell for compound XI is 13686 $Å^3$ but for that compound X is 2165 $Å^3$ which indicates that the former is about 6 times larger than the latter. Peaks of the ^{29}Si CPMAS NMR spectrum of X lie within a shift range of ca. 2 ppm but are closer (within ca. 1 ppm) for XI, which can be ascribed to the symmetry of the crystal system. This observation is consistent with the crystallography, which is triclinic for X and monoclinc for XI. The ^{1}H NMR of compound XI displays narrow peaks but compound X does not show such a peak, which means that in XI there may be two distinguishable hydrogen bonds.

Powder X-ray diffraction. To compare the crystal systems of compounds X & XI, powder X-ray diffraction patterns were also recorded. The two compounds were dried between filter paper and powder x-ray diffraction carried out at ambient temperature. A Philips PW 1050 diffractometer was used. As can be seen from Figure 25, the two compounds crystallized in a different form. Comparison of the two different patterns reveals that there are substantial differences in the range of about 4 to 17 in $2\theta°$. It should be mentioned that both crystals crystallised under the same conditions except that there were different chemical compositions.

5.3. Conclusion

Silicate anions and water molecules together in the presence of organic cations can organise into extended 3D heteronetworks of various topologies. Such mixed silicate-water networks can create polyhedral voids holding the cations.

The NMR studies of the silicate crystal are highly consistent with the crystallographic data. They confirm that the cation has lowered symmetry and also that the double four-membered ring anion deviates from a perfect cubic octameric shape.

The crystal structure of [HMBTP]$_2$[TEA]$_2$[Si$_8$O$_{20}$].70H$_2$O is the first organic silicate to be reported which has octameric anions and two different organic cations. It supports recent experimental findings for compound X as well as other alkylammonium silicate hydrates, which have important implications for zeolite chemistry. Detailed investigations into the organisation of silicate species, organic cations and H$_2$O molecules are of particular interest with regard to questions concerning the mechanisms of zeolite formation. The variety of silicate-water networks now known for nitrogen-
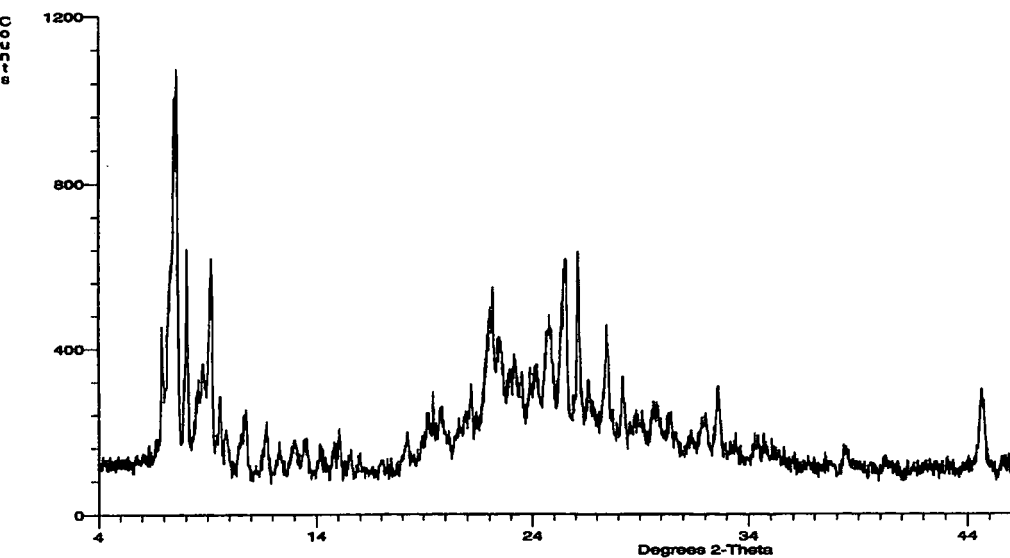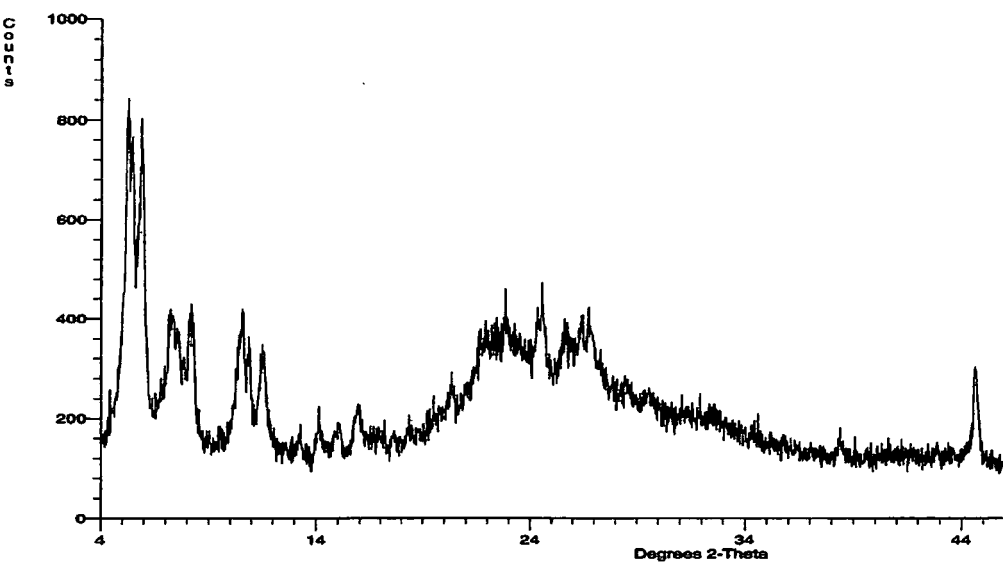
Figure 25. The powder X-ray diffraction profiles for [HMBTP]$_2$[Si$_8$O$_{18}$(OH)$_2$].41H$_2$O (upper trace) and [HMBTP]$_2$[TEA]$_2$[Si$_8$O$_{20}$].70 H$_2$O (lower trace). The two spectra are recorded under the same conditions and at ambient temperature.

containing organic silicates may provide a clue to the existence of so many different zeolite frameworks. At the very least there is a parallel complexity of structure.

It is pertinent to note that discrete double four-ring species are very rare in crystalline metal silicates[16], but have been found to occur in the crystalline silicate hydrates such as XI and X and also in various reported hydrated quaternary alkylammonium silicates[15, 17].

5.4. References

1. Wiebcke, M. *J.C.S. Chem. Commun.* 1507 (1991).

2. Wiebcke, M.; Grube, M.; Koller, H.; Engelhardt, G. and Felsche, J. *Microporous Mater.* 2, 55 (1993).

3. Wiebcke, M. and Hoebbel, D. *J.C.S. Dalton* 2451 (1992).

4. Wiebcke, M.; Emmer, J. and Felsche, J. *J.C.S. Chem. Comm.* 1604 (1993).

5. Wiebcke, M.; Emmer, J.; Felsche, J.; Hoebbel, D. and Engelhardt, G. *Z.Anorg. Allgem. Chem.* 620, 757 (1994).

6. Lawton, S.L.; Ciric, J.; Kokotailo, G.T. and Griffin, G.W. *Acta Cryst.* C41, 1683 (1985).

7. Ciric, J.; Lawton, S.L.; Kokotailo, G.T. and Griffin, G.W. *J. Am. Chem. Soc.* 100, 2173 (1978).

8. Ciric, J. U.S. patent 3 950 496 (1976).

9. W.J. Smith, Eur. Pat. 0 526 252 A1 (1993).

10. Mootz, D. and Siedel, R. *J. Inclusion phenom. Mol. Recognit. Chem.* 8, 139 (1990).

11. Hesse, W. and Jansen, M. *Z. Anorg. Allg. Chem.* 595, 115 (1991).

12. Engelhardt, G. and Michel, D. *High resolution Solid State NMR of Silicates and Zeolites*, Chichester, Wiley 1987.

13. Eckert, H. *Progr. NMR Spectrosc.* 24, 159 (1992).

14. Harris, R.K. and Knight, C.T.G. *J. Mol. Struct.* 78, 273 (1982).

15. Hoebbel, D; Garzo, G.; Engelhardt, G.; Ebert, R.; Lippmaa, E. and Alla, M. *Z. Anorg. Allg. Chem.*, 465, 15 (1980).

16. Bisser, G. and Liebau, F. *Z Kirstallogr.* 179, 359 (1987).

17. Rademacher, O.; Ziemens, O. and Scheler, H. *Z. anorg. allg. Chem.* 519, 165 (1984).

Chapter six

Characterization of zeolite SUZ-9 by studies using liquid- and solid-state ^{29}Si, ^{27}Al, ^{13}C and ^{1}H NMR spectroscopy

# 6.1. Introduction

The name zeolite originates from Cronstedt[1] who more than 200 years ago condensed the Greek word *zeo* (to boil) and *lithos* (stone) to the Swedish word *zeolit*, in order to describe the behaviour of the mineral stilbite, which loses water rapidly on heating and thus seems "to boil". In the past forty years zeolites have stimulated a huge amount of academic and industrial research and impacted on several adsorption and catalytic processes. Throughout this period of time, the discovery of new concepts has been closely related to the discovery of new structure types and compositions. The commercial success of zeolites was due primarily to their unique structure- and composition-controlled properties which permitted the improvement of known processes and the development of new ones. On the other hand, the microporous zeolite frameworks have provided the degree of realization needed for the study of fundamental events in sorption, catalysis, spectroscopy and surface science in general. As an example, from the catalysis point of view, zeolites exhibit appreciable acid activity with shape-selective features which are not available in the compositionally equivalent amorphous catalytically active metals.

Zeolites are microporous and crystalline aluminosilicates with three-dimensional networks. A representative empirical formula for a zeolite is:

$$M_{2/n}.Al_2O_3.xSiO_2.yH_2O$$
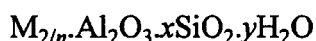
where M represents a cation, generally from group I or II. However, other metal and organic cations may also be used to balance the framework charge, and n represents the cation valence. The value of x is equal to or greater than 2 since Al^{3+} does not occupy adjacent tetrahedral sites due to Loewenstein's rule[2] (i.e. for two tetrahedral sites linked by one oxygen bridge, the centre of only one of them can be occupied by aluminium; the other centre must be occupied by silicon or by another small ion of electrovalency 4 or more, such as phosphorus). The negative charge of the aluminosilicate framework is neutralised by exchangeable cations, M, of valence n, and the void space, which may be more than 50% of the crystal volume, is normally occupied by y molecules of water per unit cell. Depending upon the particular structure of the zeolite, the porosity may consist of one-, two- or three-dimensional networks of interconnected channels and cavities of molecular dimensions[3]. An important attribute of many zeolites, as was first recognised by Weisz et al.[4-6], is their shape selectivity. Because of the dimensions and the geometry

of the channels only certain reactants may, for example, enter and diffuse through crystals (e.g. ZSM-5).

The addition of organic molecules such alkylammonium ions to zeolite synthesis gels can affect the rate at which a particular material is formed or can make new structures or framework chemical compositions accessible. It has been frequently shown that in the presence of these organic species, crystallisation to various structures can be directed. The structure-directing effect was explained in detail previously (chapter 3), but a brief review of the template effect in the crystallization of zeolites is given below.

6.2. Role of templates

The use of organic amines and quaternary ammonium ions in zeolite synthesis, developed first by Barrer in 1961[7], has extended the number of zeolite structures discovered. The use of organic cations in the synthesis of Si-Al zeolites gives rise to highly siliceous materials. It is well accepted that this arises from the large size of these molecules, which limits their number in the zeolite cages[8]. Although many studies indicate a great contribution by the cation for crystallizing individual structures, finding a direct correlation between specific cations and any one structural building unit has been less than satisfactory. A templating theory has been postulated for the role of the cations in stabilizing the formation of structural subunits thought to be precursors of crystalline zeolite species in the reaction mixture. The cations are considered to be a template or crystal-directing agent, and it is supposed that crystallization is induced of a specific zeolite structure that may not be formed in the absence of the agent.

A number of approaches might be considered in the design of templates to induce zeolite formation. The simplest is to design a template that produces the lowest-energy zeolite/template product[9]. This is analogous to the problem in drug design in which one seeks a similar drug/enzyme complex. For enzymes, this may be a correct approach since only conformational changes are needed, but for zeolites it is clearly incorrect since it is the formation of *backbone* bonds themselves that we wish to direct. The exact role of the organic species and the mechanism by which it affects the formation of the product structure remain to be elucidated. However, a fairly correct approach of involving a mechanistic direction of the assembly of building units or rearrangement of gel containing the template is hindered by our lack of knowledge of how these processes occur. Finally, these questions remain to be answered about the template theory: can the structure of the template be correlated with the shape and size

of the pore in the framework of the zeolite? Could large templates produce large pore systems?

6.3. Application of High-resolution Solid-State MAS NMR Spectroscopy for Zeolites

6.3.1. Principles

Thirteen active NMR nuclei have been utilised in obtaining information on structural features of zeolites and silicate containing molecular sieves. These nuclei are listed in table 1. The most directly relevant nucleus in zeolite studies has been ^{29}Si, though other nuclei including ^{27}Al, ^{1}H, ^{13}C, and ^{129}Xe may also provide framework or structural information about the zeolite and molecular sieves.

Table 1. The properties of selected active NMR nuclei[10].

Isotope	Spin	Natural abundance	Relative sensitivity	NMR freq.[a]
^{1}H	1/2	99.98	1.00	100.00
^{2}H	1	1.5×10^{-2}	9.65×10^{-3}	15.351
^{7}Li	3/2	92.58	0.29	38.863
^{11}B	3/2	80.42	0.17	32.084
^{13}C	1/2	1.108	1.59×10^{-2}	25.144
^{15}N	1/2	0.365	1.04×10^{-3}	10.133
^{17}O	5/2	3.7×10^{-2}	$2.91\times^{-2}$	13.557
^{19}F	1/2	100.00	0.83	94.077
^{23}Na	3/2	100.00	9.25×10^{-2}	26.451
^{27}Al	5/2	100.00	0.21	26.057
^{29}Si	1/2	4.70	7.84×10^{-3}	19.865
^{129}Xe	1/2	26.44	2.12×10^{-2}	27.660
^{205}Tl	1/2	70.50	0.19	57.708

a. In a field of 2.3488 T.

In the last two decades, techniques have been developed which prove NMR spectroscopy to be a powerful method for solutions and solid samples. These have been described elsewhere[11] and here are only briefly reviewed with special emphasis on the aspects relevant to the study of zeolites.

The NMR spectra of abundant nuclei such as ^{1}H in the solid-state are dominated by the direct dipole-dipole interactions between the nuclei resulting in characteristic,

broad, featureless absorption bands. These interactions are orders of magnitude larger than the chemical shift and spin-spin couplings, the observation of which in solution, where the dipolar interactions average to zero, has made high-resolution NMR the most powerful technique for the structural elucidation of soluble chemical species. Although, in principle, it is possible to remove the dipolar interactions in the case of abundant nuclei, the limited efficiency of the experiment coupled with the small range of proton chemical shifts greatly reduce the value of solid-state NMR of protons.

However, in the case of *dilute* nuclei (such as ^{29}Si, ^{13}C), where there is a low concentration of magnetically-active spins of the nucleus of interest in the sample, it has been demonstrated[12-14] that it is possible to obtain spectra of good resolution for a whole range of nuclei in the solid state. The total magnetic interaction, H_t appropriate for a dilute spin 1/2 nucleus such as ^{13}C in the presence of an abundant one such as ^{1}H is given by equation 1:

$$H_t = H_z + H_{H-^{13}C} + H^{13}_{C-^{13}C} + H^{13}_{C(CSA)} \qquad (1)$$

where H_z is the Zeeman effect, $H_{H-^{13}C}$, $H^{13}_{C-^{13}C}$ are ^{1}H-^{13}C and ^{13}C-^{13}C dipolar interactions respectively and $H^{13}_{C(CSA)}$ is chemical shift. The ^{1}H-^{13}C dipolar interactions involve different nuclear species and can be removed by a powerful dipolar decoupling field applied at the proton resonance frequency. The ^{13}C-^{13}C dipolar term involves interactions between nuclei of the same spin; but because of the rare spin of ^{13}C in the sample caused by the low natural abundance of ^{13}C (1.1%), this term is negligible. The only remaining line broadening contribution is the chemical shift anisotropy, i.e. $H^{13}_{C(CSA)}$, which results from the different shielding of nuclei in different orientations to the magnetic field. In solution, the random motion of the molecules produces an average (isotropic) value of this shielding; but in the solid a broad band characteristic of the orientation-dependence of the chemical environment of the nucleus results. This remaining interaction may be averaged to the zero, i.e. giving only isotropic chemical shifts in a high-resolution spectrum, by mechanical spinning of the sample about an axis at the so-called magic angle of 54° 44' to the magnetic field vector, as first introduced by Andrew et al.[15] and Lowe[16]. The spinning frequency must be comparable to the frequency spread of the signal for the static sample. Spinning at frequencies less than the frequency spread of the shift anisotropy pattern yields a spectrum consisting of a central peak at the isotropic chemical shift of the same linewidth as for fast spinning but flanked by a series of spinning sidebands separated by the spinning frequency and with

intensities that approximate (at low speeds) to the profile of the shift anisotropy pattern. A combination of high-power proton decoupling and magic-angle spinning (MAS) produces a spectrum of moderate resolution, the signals of which occur at the isotropic shift values similar to those in solution.

The intensity of the signals arising from the rare spin in the system may be substantially enhanced from the magnetization of the abundant nuclei (usually protons) in the sample by use of the *cross-polarization* (CP) pulse sequence which was first implemented by Pines, Gibby and Waugh[17]. It should be noticed that the CP technique does not affect the widths of the signals and therefore the resolution of the experiment, but that the resulting intensities may be quite different for chemically different nuclei, producing spectra which are not normally quantitatively reliable. It should be mentioned that the experiment is equally applicable to a whole range of rare-spin nuclei such as silicon-29.

6.3.2. Notation

In silicate systems the Q-unit is used to indicate the different silicate species (this notation was described in detail in Chapter 3). However, this is not sufficient to describe the basic building units in the zeolite or aluminosilicate frameworks. Since zeolite frameworks consist exclusively of three-dimensionally connected SiO_4 and AlO_4 tetrahedral, only five local silicon environments $Si(OSi)_{4-n}(OAl)_n$ with n = 0 - 4 and one local $Al(OSi)_4$ environment are of interest. Therefore, in the zeolite system, the Q-unit is always the Q^4, where each silicate is surrounded by four silicates or aluminates. Thus, in the zeolites there are five possibilities, described by:

$$Q^4(n\text{Al}, (4-n)\text{Si}) \qquad \text{where n} = 0,1,2,3,4$$

For simplicity, and to be consistent with most of the literature of the NMR of zeolites[18], the Si-centred units will be designated by $Si(n\text{Al})$ instead of $Q^4(n\text{Al})$, indicating that each silicon atom is linked through oxygen to n aluminium and 4-n silicon neighbours, i.e. $Si(0\text{Al})$ represents $Si(OSi)_4$; $Si(1\text{Al})$ represents $Si(OSi)_3(OAl)$; $Si(2\text{Al})$ represents $Si(OSi)_2(OAl)_2$; $Si(3\text{Al})$ represents $Si(OSi)(OAl)_3$, and $Si(4\text{Al})$ represents $Si(OAl)_4$. When one or more Si atoms at a Q^4 position are replaced by Al atoms, a shift in the Si chemical shift occurs. In general, for every aluminium substituting one of the OSi neighbours of the Q^4 unit, i.e. in the the second co-ordination sphere of the silicon atoms, the ^{29}Si peaks are shifted about 5 ppm to higher frequency. The general range for the $Si(n\text{Al})$ chemical shifts for n=0 to 4 is presented in Table 2[19].

Table 2. Chemical shift ranges for ^{29}Si NMR of aluminosilicates[*].

Si(nAl)	Chemical shift (ppm)
4	-80 to -87
3	-88 to -94
2	-93 to -99
1	-97 to -105
0	-103 to -114

[*] Chemical shift are referenced to the TMS signal.

6.3.3. Structural analysis of zeolites by ^{29}Si NMR spectroscopy

In addition to studies of silicate systems (silicate and aluminosilicate solutions), NMR techniques have been applied to the identification of framework features in the crystalline aluminosilicate zeolites. Silicon-29 MAS NMR has already proved to be an extremely valuable technique for the investigation of zeolites. High-resolution solid-state ^{29}Si NMR with magic-angle spinning (MAS NMR) is capable of distinguishing between the five possible Si(OAl)$_n$(OSi)$_{4-n}$ structural building blocks in zeolitic frameworks. The first application of this technique to the investigation of zeolites was made by Lippmaa et al.[18], who showed clearly that up to five peaks could be observed for ^{29}Si NMR spectra of zeolites.

The simplest but essential feature of zeolite frameworks that has been extensively studied by ^{29}Si NMR and ^{27}Al NMR is the atomic ratio of Si and Al in tetrahedral sites. The method is applied as follows:

Careful analysis of the individual chemical shifts and peak intensities is needed. This spectral analysis is complicated when the silicons in certain Si(nAl) environment occupy different crystallography non-equivalent, framework sites. This may lead to additional splitting and partial, overlap of the Si(Al) peaks, which renders the spectral assignment difficult. If the immediate neighbourhood of every Al tetrahedral site is Al(OSi)$_4$ then each Si–O–Al linkage in a Si(nAl) structural unit incorporates 1/4Al atom. It follows[20-22], therefore, that the quantitative ratio of tetrahedral Si to Al in the zeolite framework , i.e. the Si/Al ratio, can be directly calculated from the Si(nAl) peak intensities, according to equation 2.

$$(Si/Al)NMR = \sum_{n=0}^{4} I_{Si(nAl)} / \sum_{n=0}^{4} 0.25n \, I_{Si(nAl)} \qquad (2)$$

where I is the intensity of the NMR signal of the Si(nAl) unit. This equation is structure-independent and so can be applied to any zeolite, and represents a powerful quantitative method of determining framework Si/Al ratios, provided no Al–O–Al linkages are present. The limitation of this equation is the SiO_2/Al_2O_3 range over which accuracy can be maintained. Above a SiO_2/Al_2O_3 ratio of 20, the ^{29}Si NMR is dominated by the Si(OSi)$_4$ signal, and the composition estimation becomes inaccurate (e.g. in zeolite Omega)[20,22].

6.4. Experimental

The templates used by Smith[23] for the synthesis of the new zeolite SUZ-9, were either template I alone or template I and the tetraethylammonium ion. Until the discovery of SUZ-9, ZSM-18 was the only zeolite whose crystallization was induced by template I. The reason very few zeolite preparations have used I as a template may be the difficulty of synthesis of I[24]. (It should be noted that very recently Schmitt[25] synthesised a zeolite with template II and, by comparison of the XRD diffraction pattern, he claimed this is also SUZ-9).

R = CH$_3$
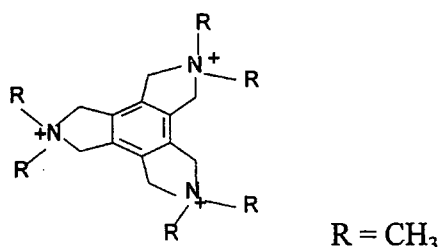
2,3,4,5,6,7,8,9-octahydro-2,2,5,5,8,8-hexamethyl-2H-benzo(1,2-c:3,4-c':5,6-c'')tripyrrolium cation (HMBTP), (I)
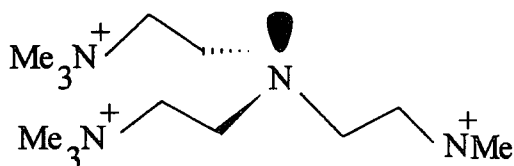
2,2',2''-nitrilotris[N,N,N-trimethylethaneaminium cation (II)

In the present study, SUZ-9 was synthesised on the basis of Smith's procedure[23], using HMBTP and TEA as templates. The HMBTP (I) was prepared by the method of US 3950496 patent[26]. Powder X-ray diffraction (XRD) data were collected on a Philips PW 1050 diffractometer from 4 to 60° 2θ. (see Figure 1).

High-resolution solid-state ^{29}Si, ^{27}Al, ^{13}C and ^{1}H NMR spectra were obtained of the zeolite at a magnetic field strength of 7.05 T, using a spectrometer operating at

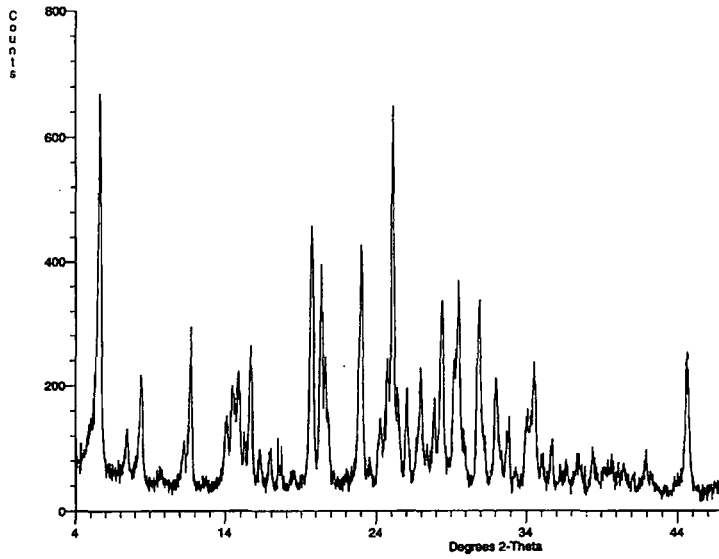Figure 1. Powder X-ray diffraction pattern at $4° \leq 2\theta \leq 60°$ for as-synthesized SUZ-9.

59.83, 78.16, 75.43 and 299.96 MHz respectively under conditions of cross-polarization and magic-angle spinning (CPMAS) at ambient probe temperature (ca. 294K). The zeolite was packed into a 7.5 mm o.d. pencil rotor. A Varian Unity Plus 300 MHz spectrometer was used.

^{29}Si, ^{13}C and ^{1}H liquid-type NMR spectra for the precursor gel and the liquid components isolated from the zeolite were recorded at ambient probe temperature (ca. 298K), using a Bruker AC250 spectrometer (5.86 T) operating at 49.69, 62.90 and 250.00 MHz for ^{29}Si, ^{13}C and ^{1}H respectively.

6.5. Results and discussion

6.5.1. Solution-state NMR study. Silicon-29 NMR spectra of the precursor gel and mother liquor (liquid component isolated from the solid i.e after crystallization of zeolite) were obtained at ambient probe temperature ca. 298K and are shown in Figure 2. They were recorded using a substantial recycle delay (50 s) to obtain quantitative data. It can be seen that a wide range of silicon environments is present in both cases, i.e. the two silicate solutions contain a variety of silicate anions. Generally, separate bands are visible in Figure 2 for Q^0, Q^1, Q^2_Δ, Q^2/Q^3_Δ, and Q^3 sites, (as mentioned earlier, the superscripts give the number of silioxane bridges and the subscript triangle refers to three-membered $(SiO)_3$ rings). Peaks assignable to the individual species Q^0, Q^1, Q^2_Δ and Q^3_6 (known as the monomer, dimer, cyclic trimer, and prismatic hexamer respectively) are of substantial intensity. The ^{29}Si NMR spectrum of the precursor gel shows broad peaks due to the viscosity of the system. However, the mobility of the silicate species is enough to obtain a reasonable spectrum. Although the gel contains a higher concentration of silica than the mother liquor, the silicon-29 spectra of the two solutions closely resemble one another. The ^{29}Si NMR spectrum of the gel shows a significant distribution of silicate species in the cubic octamer region (ca. -96 to -99 ppm) indicating extensive polymerization of the silicate species in the gel compound. However, the two spectra both display a substantial signal for the prismatic hexamer (ca. -89 ppm) and it seems no signal can be observed at a shift of ca. -100 ppm as would be assigned to be cubic octamer itself. Since TEA stabilises the prismatic hexamer[27-29], it can be concluded that the observed distribution of the silicate anions is preferentially directed by TEA rather than by HMBTP.

It is pertinent to consider the silicon-29 NMR spectrum of the HMBTP-TEA silicate solution with the same HMBTP:TEA mole ratio as the gel component but
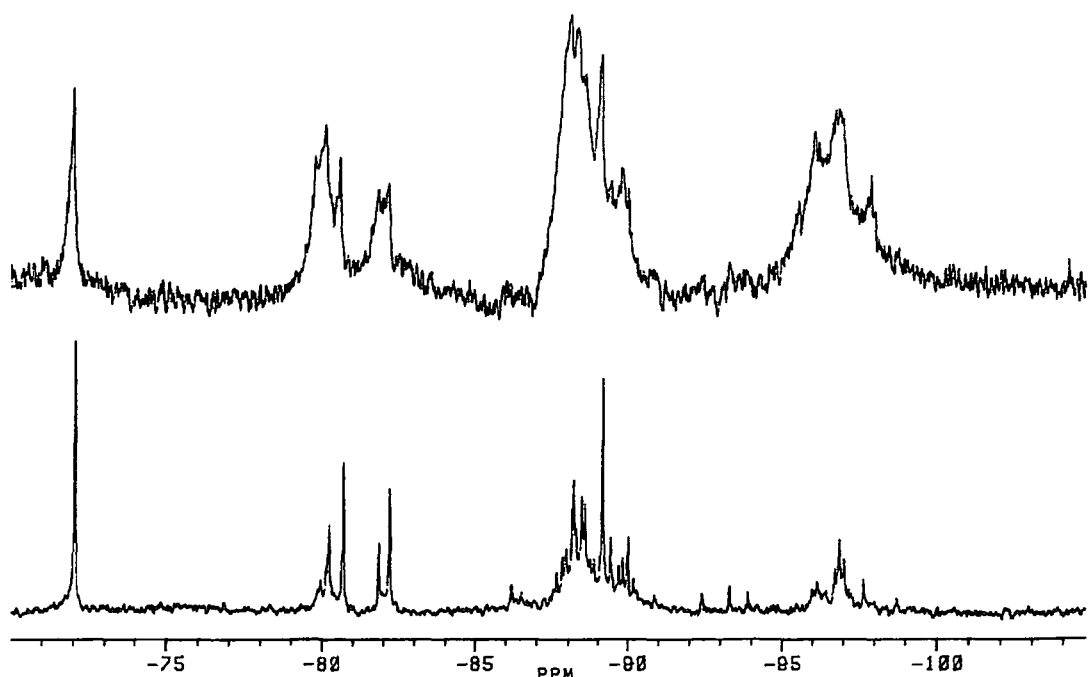
Figure 2. Liquid-state 49.69 MHz ^{29}Si NMR spectra. The upper trace shows the spectrum of the silicate gel precursor at ca. 298K with 1400 transients. The lower trace shows that of the mother liquor at ca. 298K with 1100 transients. The two spectra were recorded under similar spectral conditions which were as follows: 50 s recycle delay; 4950 Hz total spectral width; 16384 data points. They are plotted on the same scale and at absolute intensity.
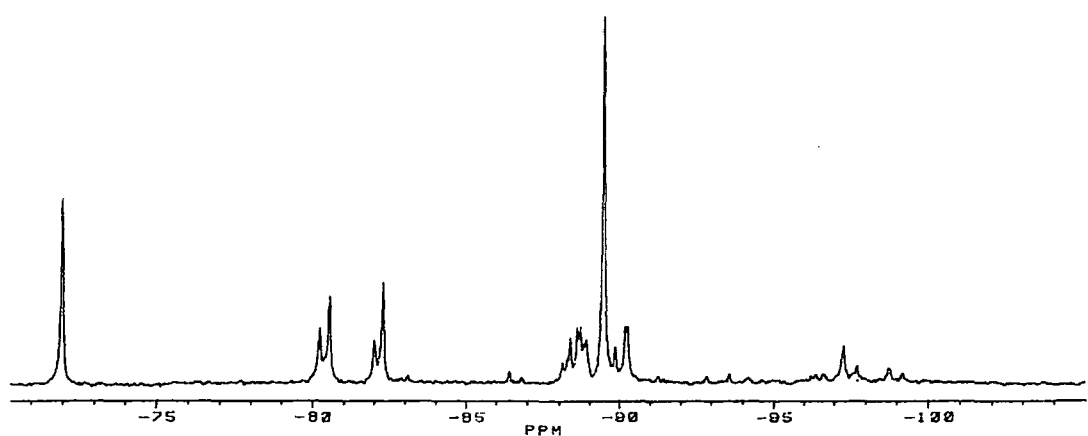
Figure 3. The 49.69 MHz ^{29}Si NMR spectra of a HMBTP-TEA silicate solution at a HMBTP:TEA ratio of 1:6 and Si/cation ratio of 1.0 with SiO_2 concentration of 5.78 wt% at ambient probe temperature (ca. 298 K). Spectral conditions: 50 s recycle delay; 1000 transients; 4950 Hz total spectral width; 16384 data points.

without aluminium and, moreover, (in order to make a clear solution) with a different silica concentration from the gel. Figure 3 shows that the distribution of the silicate species is similar to that of previous silicate solutions (i.e. gel and mother liquor), and clearly demonstrates that the prismatic hexamer is dominant in the silicate solution, indicating the strong role of TEA on the distribution.

Figure 4 displays ^{13}C NMR spectra of the mother liquor solution and gel silicate. The spectrum of the mother liquor (Fig.4 lower trace) displays five separate signals. Those at chemical shifts of 7.1 and 52.2 ppm may be ascribed to the CH_3 and CH_2 of TEA respectively, while peaks at shifts of 55.4, 69.5 and 131.2 ppm are assigned to the CH_3, CH_2 and quaternary carbons of HMBTP respectively. However, some small signals can also be observed that maybe arise from decomposition of the templates. The recycle delay of 10 s might not be enough for quantitative results. Moreover, the two spectra were recorded under the same conditions. The ^{13}C NMR spectrum of the gel displays only four distinguishable signals, and, as expected, has broad lines due to the viscosity of the system. Since there is clear evidence for the presence of HMBTP in the gel (i.e. signals at shifts of ca. 70 ppm and 130 ppm assignable to the CH_2 and quaternary carbon atoms of HMBTP respectively), the shoulder at the left hand side of the peak at about 55 ppm can be recognised and ascribed to the methyl carbon atoms of HMBTP.

Figure 5 shows the ^{13}C NMR spectrum of the HMBTP-TEA silicate solution with the same mole ratio of HMBTP:TEA as the gel composition. It displays five separate signals. The assignment of peaks is the same as for the previous one, i.e. the signals at shifts of 7.1 and 52.2 ppm are ascribed to the CH_3 and CH_2 of TEA respectively, and peaks at shifts of 55.4, 69.5 and 131.2 ppm are assigned to the CH_3, CH_2 and quaternary carbons of HMBTP respectively. However, it does not show any further peaks such as are observed in the mother liquor, supporting the suggestion that the traces in the latter are due to the decomposition of the templates (HMBTP & TEA). However, it is clear that substantial amounts of the template remain in the solution (i.e. in the mother liquor) without decomposition during the heating time as the SUZ-9 zeolite is formed.

The liquid-type ^{1}H NMR spectrum of the mother liquor and gel precursor of the SUZ-9 zeolite were recorded at ambient probe temperature and are shown in Figure 6. The two spectra were scaled vertically (the signals for the protons of water molecules are cut off in both spectra). The lower trace of Figure 6 displays the spectrum of the

Figure 4. Liquid-type 62.85 MHz ^{13}C NMR spectra. The upper trace shows that of the silicate gel precursor at ca. 298K. The lower trace shows the spectrum of the mother liquor at ca. 298K. The two spectra were recorded under similar spectral conditions, which were as follows: 10 s recycle delay; 19230 Hz total spectral width; 16384 data points and 100 transients for each spectrum . They are plotted on the same scale and with absolute intensity.
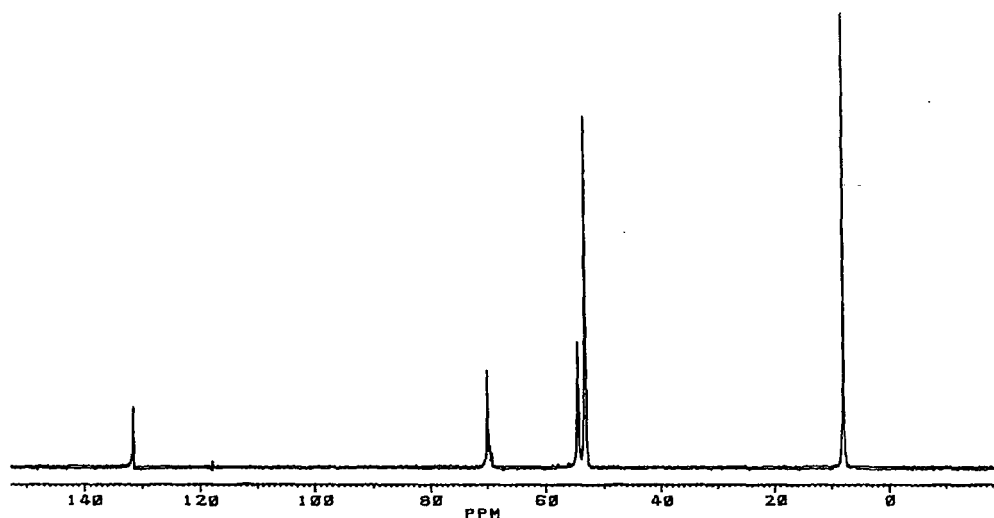
Figure 5. 62.85 MHz ^{13}C NMR spectrum of HMBTP-TEA silicate solution at a HMBTP:TEA ratio of 1:6 and Si/cation ratio of 1.0 with SiO_2 concentration of 5.78 wt% at ambient probe temperature (ca. 298K). Spectral conditions: 10 s recycle delay; 19230 Hz total spectral width; 16384 data points and 100 transients for each spectrum.

mother liquor. Signals at shifts of 0.5 and 2.4 ppm (i.e. triplet and quartet respectively) can be associated with protons of the methyl and methylene groups of TEA. However, there are two signals at shifts of about 2.6 ppm, of which one may be assigned to the hydrogen atoms of the methyl groups of HMBTP. However, the proton signal of the methylene groups of HMBTP may be overlapped by the broad line (ca. 4.5 ppm) from those water molecules. The signal at the right hand side of the broad peak might belong to the protons of the methylene group of HMBTP. However, as can be seen, there are some other signals (i.e. ca. 1.4, 1.7 and 3.2 ppm) that probably arise from decomposition of the templates. The ^{1}H NMR spectrum of the precursor gel composition carried out by liquid-state NMR is shown in the upper trace of Figure 6. As mentioned earlier, the gel system is mobile enough to provide a spectrum with liquid-state NMR. The assignments of the signals are the same as for the mother liquor, but the broad line at a shift of ca. 2.6 ppm (assignable to the hydrogen atoms of HMBTP methyl groups) indicates the low mobility of the HMBTP in this system.

Figure 7 displays the ^{1}H NMR spectrum of TEA-HMBTP silicate solution (the same as used in the case of ^{29}Si and ^{13}C NMR). As expected, two signals located at 0.46 and 2.46 ppm belong to the TEA protons of CH_3 and CH_2 groups respectively, and the ^{1}H of methyl groups of HMBTP appear at a shift of 2.52 ppm, but the signal for HMBTP methylene groups is overlapped by that for the protons of water molecules (ca. 4.5 ppm). This spectrum does not show further signals, indicating that the small peak in the ^{1}H NMR spectrum of the mother liquor (Figure 6, lower trace) arises from decomposition of the organic molecules.

6.5.2. Study by solid-state NMR. Figure 8 displays the 59.83 MHz CPMAS ^{29}Si spectrum of the zeolite SUZ-9 at ambient probe temperature (ca. 295K). Three distinct peaks can be seen at chemical shifts -97.2, -102.1 and -107.2 ppm from the signal for TMS. In addition, the spectrum shows evidence of a shoulder at the high frequency side of the spectrum. Deconvolution of this spectrum reveals that there are five different silicon sites, i.e. for Si(nAl) where n=0 - 4 (Figure 9). The chemical shifts and the peak areas were calculated by using peaks of Gaussian line-shape[22] and are given in table 3. As described earlier, substitution of aluminium in the second co-ordination sphere of silicon (i.e. with respect to Si(4OSi)) changes the chemical shift of the silicon atoms by about 5 ppm to higher frequency. This is consistent with the ^{29}Si NMR spectrum of the SUZ-9 zeolite (in Table 3).
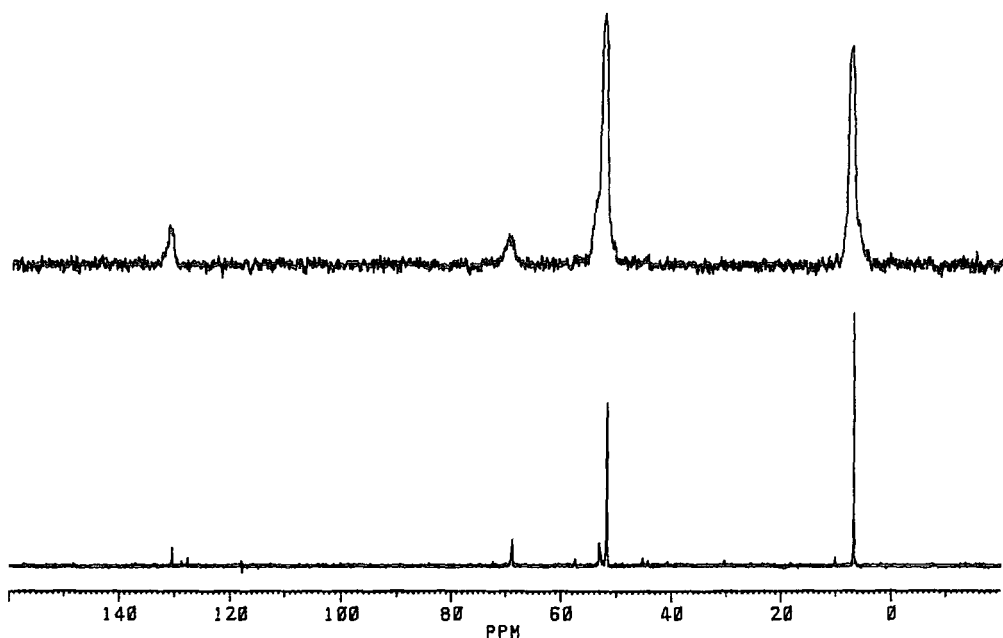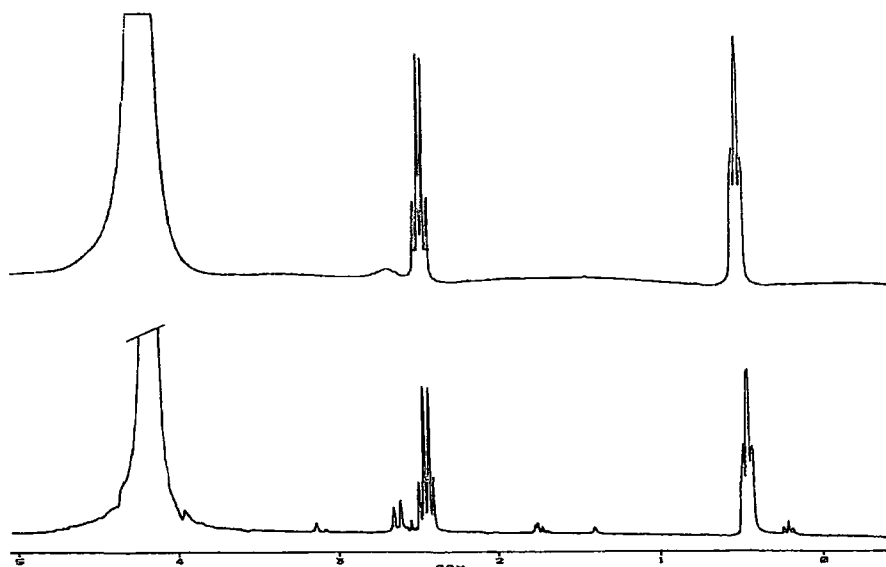
Figure 6. The liquid-type 250 MHz ^{1}H NMR spectra. The upper trace shows the spectrum of silicate gel precursor at ca. 298K. The lower trace shows that of the mother liquor, also at ca. 298K. The two spectra were recorded under similar spectral conditions, which were as follows: 1 s recycle delay; 3246 Hz total spectral width; 16384 data points and 6 transients for each spectrum. They are plotted on the same scale.
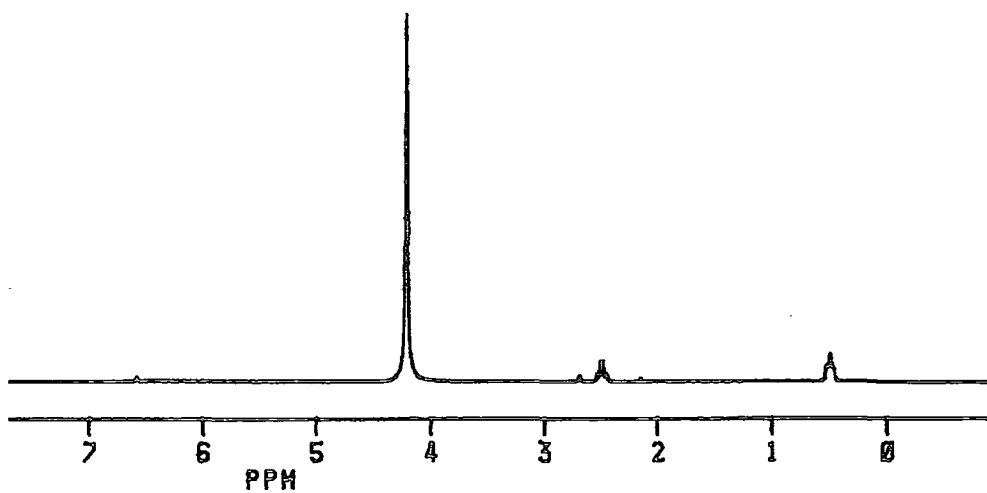
Figure 7. ^{1}H NMR spectrum of the HMBTP-TEA silicate solution at a HMBTP:TEA ratio of 1:6 and Si/cation ratio of 1.0 with SiO_2 concentration of 5.78 wt% at ambient probe temperature (ca. 298K). Spectral conditions: 1 s recycle delay; 3246 Hz total spectral width; 16384 data points and 6 transients for each spectrum.
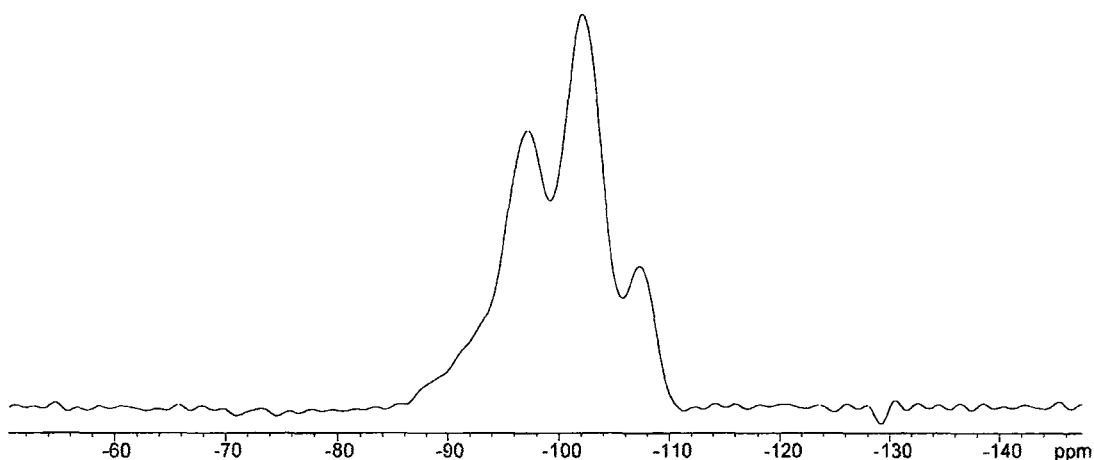
Figure 8. The 59.83 MHz CPMAS ^{29}Si NMR spectrum of zeolite SUZ-9 at ambient probe temperature (ca. 295K). Spectral parameters : 1 s recycle delay; 4000 transients; 7.5 ms contact time; 30007.5 Hz total spectral width; 32768 data points and 4500 Hz spin-rate.
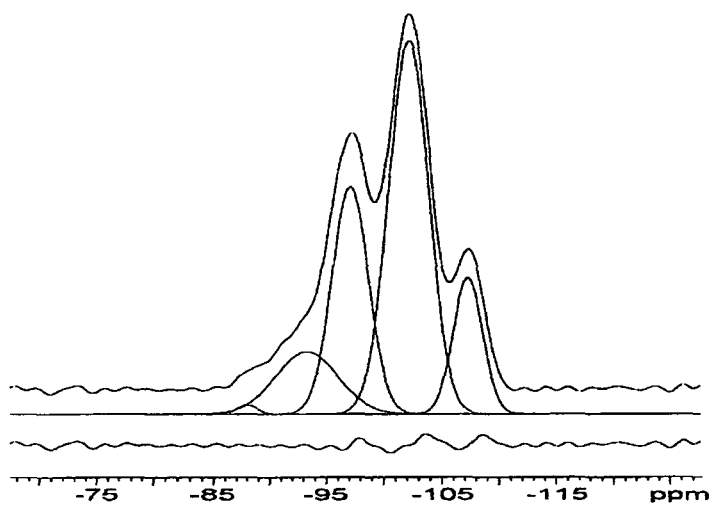
Figure 9. Deconvolution of the CPMAS ^{29}Si NMR spectrum of SUZ-9 zeolite.

Table 3. Data of chemical shifts and intensities of Si(nAl) for SUZ-9 zeolite

Sample	Chemical shift (ppm)	Intensity (area %)
Si(4Al)	-88.3	0.6
Si(3Al)	-93.0	9.9
Si(2Al)	-97.1	28.4
Si(1Al)	-102.2	47.7
Si(0Al)	-107.4	13.3

Use of equation 2 and the data of table 3 gives the ratio Si/Al of 2.9. However, this value is not consistent with that reported by Smith[23] from this particular composition of SUZ-9 zeolite (i.e. Si/Al =3.7). There are some possible reasons for this discrepancy. Firstly from the NMR point of view: the recycle delay of 1 s may be not long enough to obtain an accurate quantitative result, and the deconvolution procedure subject to an unquantifiable error. Secondly: The value of Si/ Al reported by Smith was obtained from an analytical method (i.e. atomic absorbtion) which may be not exactly correct since in zeolite SUZ-9 there is an alkaline metal (i.e. potassium). This can interfere with the silicon signal and therefore affect the intensity (i.e. giving more than the true value). Also, the atomization of aluminum may not have been complete, again resulting in a value of Si/Al which is more than that the actual one. Although both samples (i.e. Smith's and the one used in this study) were prepared from the same composition gel, they were made at different times and are not necessarily identical.

Figure 10 shows the 75.43 MHz CPMAS ^{13}C spectrum of SUZ-9 zeolite. Interestingly, only three major bands are seen, at shifts of 54.5, 69.9 and 130.1 ppm, assignable to the CH_3, CH_2 and quaternary carbon nuclei of HMBTP respectively, but there is no evidence for signals to be assigned to the methyl and methylene carbons of the TEA cation (these should appear at shifts of ca. 7 and 52 ppm respectively (see Figure 5)). The shoulder on the right hand side of the methyl and methylene carbon resonances (Figure 10) may be due to differences in the van der Waals interactions between those groups and the silicate framework in the straight and sinusoidal channels[30]. However, the chemical shifts of those carbons was not changed substantially relative to that of HMBTP-TEA silicate solution (Figure 5).

Figure 10. The 75.43 CPMAS ^{13}C NMR spectrum of zeolite SUZ-9 at ambient probe temperature (ca. 295K). Spectral parameters : 0.5 s recycle delay; 1300 transients; 1 ms contact time; 30007.5 Hz total spectral width; 65536 data points and 5000 Hz spin-rate. The peak marked by an asterisk is a spinning sideband.
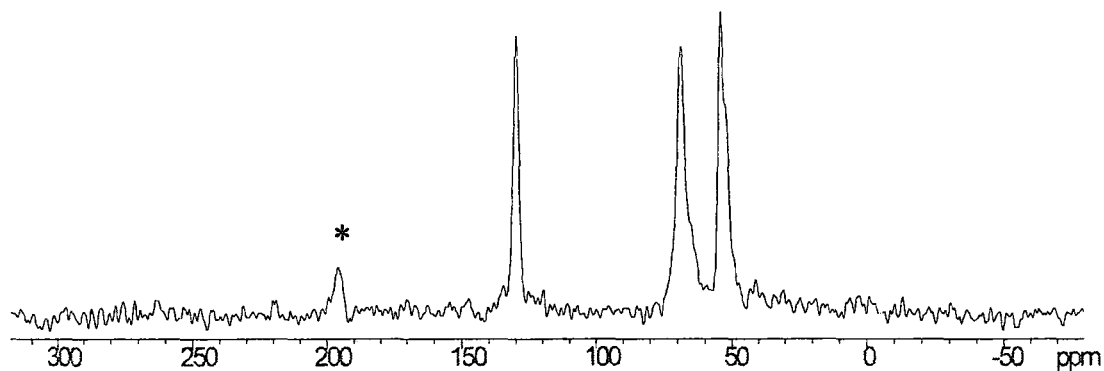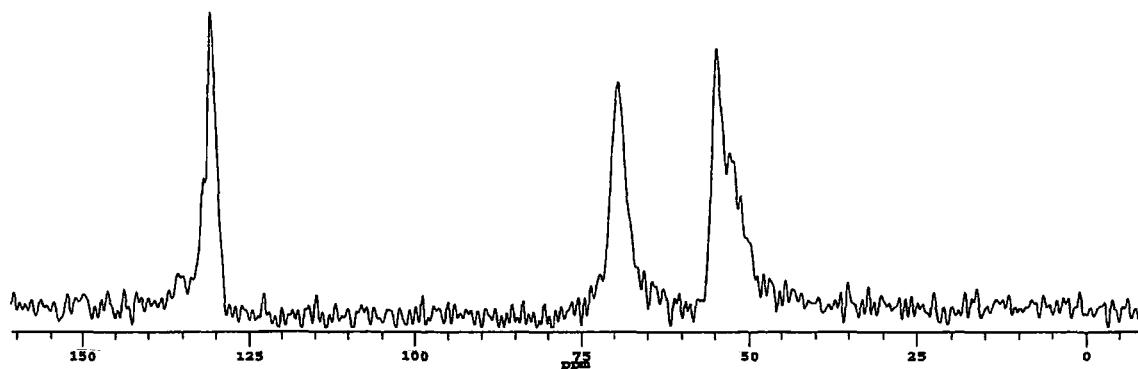

Figure 11. The 50.32 CPMAS ^{13}C NMR spectrum of zeolite SUZ-9 at ambient probe temperature (ca. 295K). Spectral parameters : 1 s recycle delay; 1300 transients; 1 ms contact time; 20.0 kHz total spectral width and 4040 Hz spin-rate.

To clarify whether or not absence of the carbon resonances associated with the TEA cation arises from the mobility of the cation (Figure 10), ^{1}H-^{13}C CPMAS NMR spectra were carried out with the same conditions but at different contact times as follows (in this case the 200 MHz (4.7 T) Chemagnetics spectrometer was used).

(I) 1 ms contact time (Figure 11)

(II) 10 ms contact time (Figure 12)

Figures 11 and 12 show that the efficiency of the polarization transfer is nearly the same for the two cases, and once again no line can be observed which is associated with the carbon resonances of TEA (i.e. at least there is no signal at a chemical shift of ca. 7 ppm, where the carbons of the methyl group of TEA are expected (Figure 5)). Moreover, the ^{13}C MAS NMR spectrum of this sample was carried out under similar conditions to the above but with direct polarization and a substantial recycle delay 30 s (Figure 13). Although the signal-to-noise is rather poor, there is no evidence for the signals of the carbons for TEA, and once again only three signals can be observed.

By considering the above evidence it can be said with confidence that no TEA is included in the crystalline SUZ-9 zeolite; in other words the SUZ-9 is crystalline with occlusion of the HMBTP template only although the mole ratio of HMBTP:TEA is 1:6 in the gel components. However, it is difficult to understand why this phenomenon occurs during the crystallization of the zeolite, and the matter requires further investigation.

The solid-state ^{1}H MAS NMR spectrum of the zeolite SUZ-9 was obtained at ambient probe temperature with single-pulse excitation. Resolution enhancement was applied and the spectrum is shown in Figure 14. Two distinct peaks can be observed at chemical shifts of 1.5 and 2.4 ppm and a shoulder is seen at the low-frequency side of a broad line in the spectrum. By comparison with the spectrum shown in Figures 6-8, it should be possible to say whether TEA is occluded in the zeolite, in which case a line at a shift of ca. 0.5 ppm (ascribed to the protons of methyl groups of TEA) should be observed. However, solid-sate ^{13}C NMR (as mentioned earlier) showed there is no TEA occluded in the crystalline SUZ-9 zeolite. To further investigate this question and to obtain better resolution, it was decided to remove water from the zeolite. To perform that, the sample was kept under vacuum for a few days.

Figure 15 displays the ^{1}H NMR spectrum of the SUZ-9 after drying. A sharp signal is observed at the position of the shoulder of the spectrum shown in Figure 14 (i.e. of
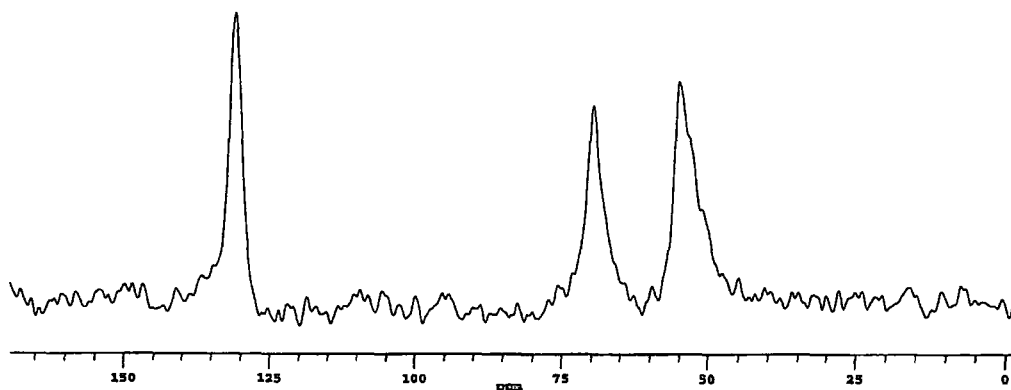
Figure 12. The 50.32 CPMAS ^{13}C NMR spectrum of zeolite SUZ-9 at ambient probe temperature (ca. 295K). Spectral parameters : 1 s recycle delay; 1300 transients; 10 ms contact time; 20.0 kHz total spectral width and 4040 Hz spin-rate.
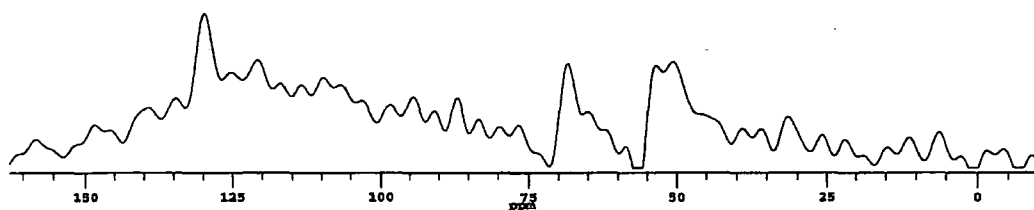
Figure 13. The 50.32 ^{13}C NMR spectrum of zeolite SUZ-9 at ambient probe temperature (ca. 295K) with direct polarization. Spectral parameters : 30 s recycle delay; 42 transients; 20.0 kHz total spectral width and 4040 Hz spin-rate.

Figure 14. The 299.95 MHz MAS ^{1}H NMR spectrum of zeolite SUZ-9 at ambient probe temperature (ca. 295K) before drying. Spectral parameters: 1 s recycle delay; 100 transients; 100.0 kHz total spectral width and 4000 Hz spin-rate.

Figure 15. The 299.95 MHz MAS ^{1}H NMR spectrum of zeolite SUZ-9 at ambient probe temperature (ca. 295K) after drying. Spectral parameters: 0.5 s recycle delay; 100 transients; 100.0 kHz total spectral width and 6000 Hz spin-rate.
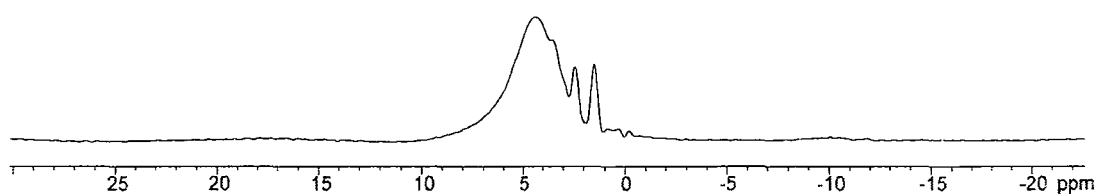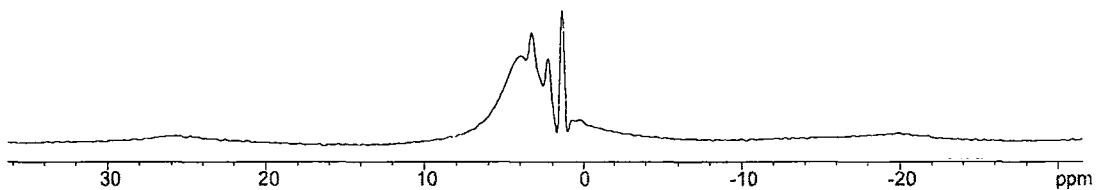
the sample before drying). The peak at a chemical shift of 1.5 ppm is probably due to *terminal* SiOH groups at the crystal surface. The two other sharp peaks, which lie at chemical shifts of 2.3 and 3.3 ppm, can be associated with the protons of the methyl and methylene groups of HMBTP respectively. The broad line (ca. 4 ppm) arises from the protons of water molecules. Signals from protons due to the acidic sites in the zeolite (i.e. bridging Si(OH)Al) may be located in the region of the broad line (i.e ca 4 - 5.5 ppm) but they are not observed separately since such protons are probably in rapid exchange with water protons. The solid-state ^{1}H NMR spectrum of an empty rotor was obtained under comparable conditions, and it indicated that no substantial signal comes from the rotor (or probe) in the region of the spectrum discussed here. Therefore it can be said unambiguously that the peaks mentioned here are real.

^{27}Al NMR study of SUZ-9 zeolite. Unlike ^{1}H, ^{13}C and ^{29}Si, which have a nuclear spin I=1/2, ^{27}Al has I=5/2 and therefore a nuclear quadrupole moment, which gives additional complications at the experimental and theoretical level. The characteristics of quadrupolar nuclei and their implications in solid-state NMR have been described elsewhere[11]. However, there are two features which make ^{27}Al a very favourable nucleus for NMR investigation: 100% natural abundance and fast relaxation. Therefore short pulse delays can be applied, and ^{27}Al NMR spectrum of good quality with high signal-to-noise can be obtained, but usually with somewhat broadened lines.

As explained earlier, different sites of aluminium in aluminosilicate species can be identified by the characteristics of their ^{27}Al NMR spectra. The tetrahedral site of AlO_4^{5-} has a shift of ca. 80 ppm (relative to the aluminium signal for aqueous $AlCl_3.6H_2O$), addition of each silicon to the second sphere co-ordination to the aluminium (i.e. formation of a siloxane bridge) causing about 5 ppm shift to lower frequency.

Figure 16 displays the ^{27}Al MAS NMR spectrum of SUZ-9 zeolite, and shows only one peak. The chemical shift is about 60 ppm, confirming the known tetrahedral geometry in this sample, where the apparent chemical shift value is close to the correct one[35,36] The ^{27}Al linewidth is about 10 ppm, which is less informative about local environmental effects than the corresponding ^{29}Si spectrum (Figures 9 & 10). However, there is apparently only one kind of aluminium site. It should be noted that Loewenstein's Rule implies that each aluminium atom will be completely surrounded by silicons in the first co-ordination sphere, giving them a common local environment.
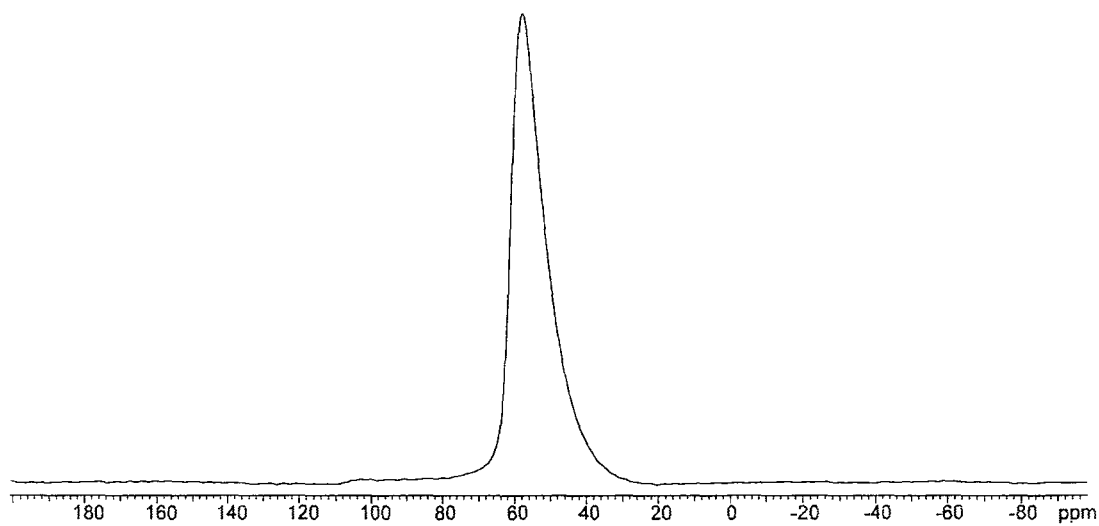
Figure 16. The 78.158 MHz MAS ^{27}Al NMR spectrum of zeolite SUZ-9 at ambient probe temperature (ca. 295K). Spectral parameters: 0.5 s recycle delay; 1000 transients; 100.0 kHz total spectral width and 11200 Hz spin-rate.

As a result, it can be expected that there is only one kind of aluminium geometry (i.e. tetrahedral) in the SUZ-9 zeolite. However, it should be mentioned that no aluminium can be detected in the mother liquor by ^{27}Al NMR, even using a 600 MHz spectrometer (i.e. operating at 156.3 MHz for ^{27}Al NMR).

6.6. Conclusions

By employing ^{29}Si, ^{27}Al, ^{13}C and ^{1}H NMR spectroscopy, the characteristics of SUZ-9 zeolite have been found and the main results obtained from this study are summarized as follows:

The ^{29}Si NMR spectrum shown by the precursor gel indicates that there is a variety of silicate anions of Q^0 to Q^3 type, with dominance of the prismatic hexamer, Q^3_6, while the ^{29}Si MAS NMR spectrum of the SUZ-9 zeolite contains signals from five different Q^4 sites of Si(nAl), and the mother liquor of the SUZ-9 zeolite still contains a number of silicate species.

The ^{27}Al MAS NMR spectrum of the zeolite confirms that there is only one kind of tetrahedral geometry for aluminium in the sample.

The ^{13}C MAS NMR, with different techniques, verifies that from two templates TEA and HMBTP present in the precursor gel, only HMBTP is occluded in SUZ-9 zeolite, while ^{13}C liquid-state NMR indicates that the mother liquor of the zeolite contains a substantial amount of both TEA and HMBTP.

^{1}H NMR at high magnetic field provides a powerful means of identifying different proton sites of the template and the zeolite framework and of characterizing their distribution in the zeolite structure. The ^{1}H MAS NMR spectrum shows a sharp signal for the protons of *terminal* SiOH groups in the zeolite, and confirm that there is no TEA left in SUZ-9 zeolite.

6.7. References

1. Cronstedt, A. F.; *Kongl. Svenska Vetenskaps Acdemiens Handilngar Stockholm, 17,* 120 (1756).

2. Loewenstein, W. *Am. Mineral., 39,* 92 (1954).

3. Fyfe, C. A.; Thomas, J. M.; Klinowski, J. and Gobbi, G. C. *Angew. Chem. Int. Ed. Engl. 22,* 259 (1983).

4. Weisz, P. B. and Frilette, V. J. *J. Phys. Chem.* **64,** 382 (1960)

5. Weisz, P. B.; Frilette, V. J.; Maatman, R. W. and Mower, E. G. *J. Catal.* **1,** 307 (1962).

6. Weisz, P. B. *Chemtech* **3,** 498 (1973).

7. Barrer, R. M. and Denny, P. J. *J.Chem. Soc.* 971 (1961).

8. Vomscheid, R.; Briend, M.; Peltre, M. J. Man, P. P. and Barthomeuf, D. *J. Phys. Chem.* **98,** 9614 (1994).

9. Schmitt, K. D. and Kennedy, G. J. *Zeolites,* **14,** 635 (1994).

10. Klinowski, J. *Prog. NMR Spectros.* **16,** 237 (1984).

11. See for example: (a) Andrew, E.R. *Int. Rev. Phys. Chem.* **1,** 195 (1981); (b) Mehring, M. "High Resolution NMR Spectroscopy in Solids"; (c) Fyfe, C. A. "Solid State NMR for Chemistry" and (d) Engelhardt, G. and Michel, D. "High-Resolution Solid-State NMR of Silicates and Zeolites", Wiley , New York, 1987.

12. Harris, R. K.; Packer, K. J. *Eur. Spectrosc. News* **21,** 37 (1978).

13. Schaefer, J. Stejskal, E. O. *Top.Carbon-13 NMR Spectrosc.* **3,** 283 (1979).

14. Harris, R. K.; Packer, K. J.; Say B. J. and Tanner, S. F. *Philos. Trans. R. Soc. London A 299,* 665 (1981).

15. Andrew, E. R.; Bradbury, A. and Eades, R. G. *Nature (London)* **182,** 1659 (1958).

16. Lowe, I. J. *Phys. Rev. Lett.* **2** 285 (1959).

17. Pines, A.; Gibby, M. G. and Waugh J. S. *Chem. Phys. Lett.* **15,** 273 (1972).

18. Lippmaa, E.; Mägi, M.; Samson, A.; Engelhardt, G. and Grimmer, A. R. *J. Am. Chem. Soc.* **102,** 4889 (1980).

19. Lippmaa, E.; Mägi, M.; Samson, A.; Tarmak, M. and Engelhardt, G. *J. Am. Chem. Soc.* **103,** 4992 (1981).

20. Engelhardt, G.; Lohse, U.; Lippmaa, E.; Tarmak, M and Mägi, M. *Z. Anorg. Allg. Chem.* **482,** 49 (1981).

6.7. References

1. Cronstedt, A. F.; *Kongl. Svenska Vetenskaps Acdemiens Handilngar Stockholm*, 17, 120 (1756).

2. Loewenstein, W. *Am. Mineral.*, 39, 92 (1954).

3. Fyfe, C. A.; Thomas, J. M.; Klinowski, J. and Gobbi, G. C. *Angew. Chem. Int. Ed. Engl.* 22, 259 (1983).

4. Weisz, P. B. and Frilette, V. J. *J. Phys. Chem.* 64, 382 (1960)

5. Weisz, P. B.; Frilette, V. J.; Maatman, R. W. and Mower, E. G. *J. Catal.* 1, 307 (1962).

6. Weisz, P. B. *Chemtech* 3, 498 (1973).

7. Barrer, R. M. and Denny, P. J. *J.Chem. Soc.* 971 (1961).

8. Vomscheid, R.; Briend, M.; Peltre, M. J. Man, P. P. and Barthomeuf, D. *J. Phys. Chem.* 98, 9614 (1994).

9. Schmitt, K. D. and Kennedy, G. J. *Zeolites*, 14, 635 (1994).

10. Klinowski, J. *Prog. NMR Spectros.* 16, 237 (1984).

11. See for example: (a) Andrew, E.R. *Int. Rev. Phys. Chem.* 1, 195 (1981); (b) Stejskal, E.O. and Memory, J.O. "High Resolution NMR in the Solid state"; Oxford university press, Oxford, 1994; (c) Fyfe, C. A. "Solid State NMR for Chemistry" C.F.C. press Ontario, 1983 and (d) Engelhardt, G. and Michel, D. "High-Resolution Solid-State NMR of Silicates and Zeolites", Wiley , New York, 1987.

12. Harris, R. K.; Packer, K. J. *Eur. Spectrosc. News* 21, 37 (1978).

13. Schaefer, J. Stejskal, E. O. *Top.Carbon-13 NMR Spectrosc.* 3, 283 (1979).

14. Harris, R. K.; Packer, K. J.; Say B. J. and Tanner, S. F. *Philos. Trans. R. Soc. London A 299*, 665 (1981).

15. Andrew, E. R.; Bradbury, A. and Eades, R. G. *Nature (London)* 182, 1659 (1958).

16. Lowe, I. J. *Phys. Rev. Lett.* 2 285 (1959).

17. Pines, A.; Gibby, M. G. and Waugh J. S. *Chem. Phys. Lett.* 15, 273 (1972).

18. Lippmaa, E.; Mägi, M.; Samson, A.; Engelhardt, G. and Grimmer, A. R. *J. Am. Chem. Soc.* 102, 4889 (1980).

19. Lippmaa, E.; Mägi, M.; Samson, A.; Tarmak, M. and Engelhardt, G. *J. Am. Chem. Soc.* 103, 4992 (1981).

20. Engelhardt, G.; Lohse, U.; Lippmaa, E.; Tarmak, M and Mägi, M. *Z. Anorg. Allg. Chem.* 482, 49 (1981).

21. Thomas, J. M.; Fyfe, C. A. Ramdas, S. Klinowski, J. and Gobbi, G. C. *J. Phys. Chem.* 86 86, 3061 (1982).

22. Klinowski, J.; Ramdas, S.; Thomas, J. M.; Fyfe, C. A. and Hartman, J. S. *J. Chem. Soc. Faraday Trans. II* 78, 1025 (1982).

23. Smith, W. J. Eur. Pat. 0 526 252 A1 (1993).

24. Ciric. J.; Lawton, S. L.; Kokotailo, G. T. and Griffin, G.W. *J. Am. Chem. Soc.* 100, 2173 (1978).

25. Schmitt, K. D. *Zeolites*, 15, 315 (1995).

26. Ciric. J. US Pat. 3950496 (1976).

27. Harris, R.K. and Knight, C.T.G. *J. Mol. Struct.* 78, 273 (1982).

28. Hoebbel, D; Garzo, G.; Engelhardt, G.; Ebert, R.; Lippmaa, E. and Alla, M. *Z. Anorg. Allg. Chem.*,465, 15 (1980).

29. Hoebbel, D; A. Vargha; Fahlke B. and Engelhardt Z. *Anorg. Allg. Chem.*, 521, 61 (1985).

30. Burkett, S.L. and Davis, M. E. *Chem. Mater,* 7, 920 (1995).

31. Boxhoorn, G.; van Santen, R. A.; van Erp, W.A.; Hays, G. R.; Huis, R. and Clague, D. *J. Chem. Soc. Chem. Commun.* 264 (1982).

32. Nagy, J. B.; Gabelica, Z.; Derouane, E. G. *Zeolite,* 3, 43 (1983).

33. Gabelica, Z.; Nagy, J. B.; Bodart, P.; Dewaele, N. Nastro, A. *Zeolites* 7, 67 (1987).

34. Engelhardt, G.; H. -G. Jerschkewitz; Lohse, U.; Sarv, P.; Samoson, A. and Lippmaa, E. *Zeolites,*.7, 291 (1987).

35. Fyfe, C. A.; Gobbi, G. C; Hartman, J. S.; Klinowski, J. and. Thomas, J.M. *J. Phys. Chem.* 86, 1247 (1982).

36. Fyfe, C. A.; Gobbi, G. C.; Hartman, J. S.; Lenkinski, R. E.; O'Brien, J. H.; Beange, E. R. and Smith, M. A. R. *J. Mag. Res.* 47, 168 (1982).

Research Conferences Attended

17th Annual Meeting of the British Zeolite Association, Loughborough, 28-30th March, 1994.

12th International NMR Meeting , UMIST, Manchester, 2-7th July 1995.

British Radiofrequency Spectroscopy Group, King's College ,London, 21st September, 1994.

Oral Presentation

Studies of Silicate Solutions as Precursors of Zeolite Synthesis. *the first seminar of Iranian post graduate students Chemistry & Chemical Engineering*, UMIST, Manchester, 28th May, 1994.

Study of Silicate and Aluminosilicate Solutions as Precursors of the Synthesis of Zeolites. *Durham University Third Year Graduate Colloquia*, 12 July 1995.

Posters Presented

Study of Silicate of a Triply-Charged Cation by Solution and Solid-State NMR, *12th International NMR Meeting*, UMIST, Manchester, 2-7th July 1995,

Publications

1. **A New Silicate Clathrate : An X-ray Diffraction and Nuclear Magnetic Resonance Study of a System with Octameric Silicate Anions and Trivalent Cations.**

Harris, R. K.; Howard, J. A. K.; Samadi-Maybodi, A.; Yao, J. W. and Smith, W. *J. Solid State Chem.* **120,** 231 (1995).

2.**Exchange Reactions in Aluminosilicate Solutions.**

Harris, R. K.; Parkinson, J.; Samadi-Maybodi, A. and Smith, W.. *Chem. Soc. Chem. Commun. in press.* (1996).

3. **X-ray Diffraction and Solid-State NMR Study of a Silicate Containing Two Different Nitrogenous Cations**

Harris, R. K. and Samadi-Maybodi, A. *in preparation.*

Colloquia, Lectures and Seminars Given by Invited Speakers

An asterisk denotes attendance by the author.

1992

October 20   Dr. H.E. Bryndza, Du Pomt Central Research

Synthesis, Reactions and Thermochemistry of Metal (Alkyl) Cyanide

Complexes and Their impact on Olefin Hydrocyanation Catalysis

*October 22   Prof. A. Davies, University College London

The Ingold-Albert Lecture. The Behaviour of Hydrogen as a

Pseudometal

*October 28   Dr. J. K. Cockcroft, University of Durham

Recent Developments in Powder Diffraction

October 29   Dr. J. Emsley, Imperial College London

the Shocking History of Phosphorus

November 4   Dr. T. P. Kee, University of Leeds

Synthesis and Co-ordination Chemistry of Silylated Phosphites

November 5   Dr. C. J. Ludman, University of Durham

Explosions, A Demonstration Lecture

November 11 Prof. D. Robins, Glasgow University

Pyrrolizidine Alkaloids: Biological Activity, Biosynthesis and Benefits

*November 12 Prof. M. R. Truter, University college, London

Luck and Logic in Host-Guest Chemistry

*November 18 Dr. R. Nix, Queen Mary College, London

Characterisation of Heterogeneous Catalysts

November 25 Prof. Y. Vallee, Univerity of Caen

Reactive thiocarbonyl Compounds

November 25 Prof. L. D. Quin, University of Massachusetts, Amherst

Fragmentation of Phosphorus Heterocycles as a Route to Phosphoryl

Species with Uncommon Bonding

November 26 Dr. D. Humber, Glaxo Greenford

AIDS- The Development of a Novel Series of Inhibitors of HIV

December 2 Prof. A. F. Hegarty, University College Dublin

Highly Reactive Enols Stabilised by Steric Protection

December 2 Dr. R. A. Aitken, University of St. Andrews

The Versatile Cycloaddition of $Bu_3P.CS_2$

*December 3 Prof. P Edwards, Birmingham University

The SCI Lecture: What is Metal?

December 9 Dr. A. N. Burgess, ICI Runcorn

The structure of Perfluorinated Ionomer Membranes

1993

*January 20 Dr. D. C. Clary, University of Cambridge

Energy Flow in Chemical Reactions

January 21 Prof. L. Hall, Cambridge

NMR- Window to the Human Body

January 27 Dr. W. Kerr, University of Strathclyde

Development of the Pauson-Khand Annulation Reaction:

Organocobalt Mediated Synthesis of Natural and Unnatural Products

January 28	Prof. J. Mann, University of Reading
	Murder, Magic and Medicine
February 3	Prof. M. S. Roberts, University of Exeter
	Enzymes in Organic Synthesis
*February 10	Dr. D. Gillies, University of Surrey
	NMR and Molecular Motion in Solution
February 11	Prof. S. Knox, Bristol University
	The Tiden Lecture: Organic Chemistry at Polynuclear Metal Centres
February 17	Dr. W. R. Kemmitt, University of Leicester
	Oxatrimethylenemethane Metal Complexes
February 18	Dr. I. Fraser, ICI Wilton
	Reactive Processing of Composite Materials
*February 22	Prof. D. M. Grant, Universityof Utah
	Single Crystals, Molecular Structure and Chemical-Shift Anisotropy
February 24	Prof. C. J. M. Stirling, University of Sheffield
	Chemistry on the Flat. Reactivity of Ordered Systems
*March 10	Dr. P. K. Baker, University College of North Wales, Bangor
	'Chemistry of Highly Versatile 7-Coordinate Complexes
March 11	Dr. R. A. Y. Jones, University of East Anglia
	The Chemistry of Wine Making
*March 17	Dr. R. J. K. Taylor, University of East Anglia
	Adventures in Natural Product Synthesis

March 24   Prof. I. O. Sutherland, University of Liverpool
            Chromogenic Reagents for Cations

*May 13   Prof. J. A. Pople, Carnegie-Mellon University, Pittsburgh, USA
            The Boys-Rahman Lecture: Applications of Molecular Orbital Theory

May 21   Prof. L. Weber, University of Bielefeld
            Metallo-phospha Alkenes as Synthons in Organometallic Chemistry

June 1   Prof. J. P. Konopelski, University of California Santa Cruz
            Synthetic Adventures with Enantiomerically Pure Acetals

June 2   Prof. F. Ciardelli, University of Pisa
            Chiral Discrimination in the Stereospecific Polymerisation of Alpha
                        Olefins

June 7   Prof. R. S. Stein, University of Massachusetts
            Scattering Studies of Crystalline and Liquid Crystalline Polymers

*June 16   Prof A. K. Covington, University of Newcastle
            Use of Ion Selective Electrodes as Detectors in Ion Chromatography

*June 17   Prof. O. F. Nielsen, H. C. Ørsted Institute, University of Copenhagen
            Low-Frequency IR- and Raman Studies of Hydrogen Bonded Liquids

September 13 Dr A. D. Schluter, Freie Universitat, Berlin, Germany
            Synthesis and Characterisation of Molecular Rods and Ribbons

September 13 Dr. K. J. Wynne, Office of Naval Research, Washington, USA
            Polymer Surface Design for Minimal Adhesion

September 14 Prof. J. M. DeSimone, University of North Carolina, Chapel Hill, USA
            Homogeneous and Heterogeneous Polymerisations in Environmentally
                        Responsible Carbon Dioxide

September 28 Prof. H. Ila, North Eastern Hill University, India

Synthetic Strategies for Cyclopentanoids via Oxoketene Duithioacetals

*October 4 Prof. F. J. Feher, University of California, Irvine, USA

Bridging the Gap Between Surfaces and Solution with Sessilquioxanes

October 14 Dr. P. Hubberstey, University of Nottingham

Alkali Metals: Alchemist's Nightmare, Biochemist's Puzzle and Technologist's Dream

*October 20 Dr. P. Quayle, University of Manchester

Aspects of aqueous ROMP Chemistry

October 23 Prof. R. Adams, University of South Carolina, USA

Chemistry of Metal Carbonyl Cluster Complexes: Development of Cluster Based Alkyne Hydrogenation Catalysts

*October 27 Dr. R. A. L. Jones, Cavendish Laboratory, Cambridge

Perambulating Polymers

November 10 Prof. M. N. R. Ashfold, University of Bristol

High Resolution Photofragment Translational Spectroscopy: A New Way to Watch Photodissociation

November 17 Dr. A. Parker, Rutherford Appleton Laboratory, Didcot

Applications of Time Resolved Resonance Raman Spectroscopy to Chemical and Biochemical Problems

*November 24 Dr P. G. Bruce, University of St. Andrews

Structure and Properties of Inorganic Solids and Polymers

November 25 Dr. R. P. Wayne, University of Oxford

The Origin and Evolution of the Atmosphere

December 1   Prof. M. A. McKervey, Queen's University, Belfast

Synthesis and Applications of Chemically Modified Calixarenes

*December 8 Prof. O. Meth-Cohn, University of Sunderland

Friedel's Folly Revisited- A Super Way to Fused Pyridines

December 16 Prof. R. F. Hudson, University of Kent

Close Encounters of the Second Kind

1994

January 26   Prof. J. Evans, University of Southampton

Shining Light on Catalysts

February 2   Dr. A. Masters, University of Manchester

Modelling Water Without Using Pair Potentials

*February 9   Prof. D. Young, University of Sussex

Chemical and Biological Studies on the Coenzyme Tetrahydrofolic

Acid

February 16   Prof. K. P. Theopold, University of Delaware, USA

Paramagnetic Chromium Alkyls: Synthesis and Reactivity

February 23   Prof. P. M. Maitlis, University of Sheffield

Across the Border: From Homogeneous to Heterogeneous Catalysis

March 2   Dr. C. Hunter, University of Sheffield

Noncovalent Interaction between Aromatic Molecules

March 9   Prof. R. Wilkinson, Loughborough University of Technology

Nanosecond and Picosecond Laser Flash Photolysis

March 10   Prof. S. V. Ley, University of Cambridge

New Methods for Organic Synthesis

*March 25   Dr. J. Dilworth, University of Essex

Technetium and Rhenium Compounds with Applications as Imaging

Agents

April 28   Prof. R. J. Gillespie, McMaster University, Canada

The Molecular Structure of some Metal Fluorides and Oxofluorides:

Apparent Exceptions to the VSEPR Model

May 12   Prof. D. A. Humphreys, McMaster University, Canada

Bringing Knowledge to Life

*October 5   Prof N. L. Owen, Brigham Young University, Utah, USA

Determining Molecular Stuctrure-The INADEQUATE NMR Way

October 19   Professor N. Bartlett, University of California

Some Aspects of (AgII) and (AgIII) Chemistry.

October 26   Dr. G. Rumbles, Imperial College

Real or Imaginary 3rd Order Non-Linear Optical Materials.

November 2   Dr. P. G. Edwards, University of Wales, Cardiff

The Manipulation of Electronic and Structural Diversity in Metal

Complexes - New Ligands for New Properties.

*November 9 Dr. G. Hogarth, University College, London

New Vistas in Metal Imido Chemistry.

November 16 Professor M. Page, University of Huddersfield

Four Membered Rings and B-Lactamase.

November 23   Dr. J. Williams, University of Loughborough
              New Approaches to Asymmetric Catalysis.

November 30   Professor P. Parsons, University of Reading
              Applications of Tandem Reactions in Organic Synthesis.

*December 7   Professor D. Briggs, ICI and University of Durham
              Surface Mass Spectrometry.

1995

January 25   Dr. D. A. Roberts, Zeneca Pharmaceuticals
              The Design and Synthesis of Inhibitors of the Renin-Angiotensin
              System.

February 1   Dr. T. Cosgrove, Bristol University
              Polymers do it at Interfaces.

February 8   Dr. D. O'Hare, Oxford University
              Synthesis and Solid State Properties of Poly- Oligo- and Multidecker
              Metallocenes.

February 15   Professor W. Motherwell, University College, London
              New Reactions for Organic Synthesis.

*February 22 Professor E. Schaumann, University of Clausthal
              Silicon- and Sulphur-mediated Ring-opening Reactions of Epoxide.

March 1   Dr. M. Rosseinsky, Oxford University
              Fullerene Intercalation Chemistry.

April 26   Dr. M. Schroder, University of Edinburgh

Redox Active Macrocyclic Complexes: Rings, Stacks and Liquid
Crystals.

*May 24   Dr. P. Beer, Oxford University
            Anion Complexation Chemistry.